

UNCLASSIFIED

AD NUMBER

ADB013256

LIMITATION CHANGES

TO:

Approved for public release; distribution is unlimited.

FROM:

Distribution authorized to U.S. Gov't. agencies only; Test and Evaluation; JAN 1976. Other requests shall be referred to Air Force Flight Dynamics Laboratory, FGL, Wright-Patterson AFB, OH 45433.

AUTHORITY

AFWAL LTR 16 FEB 1982

THIS PAGE IS UNCLASSIFIED

76
35
U1

AD-Bo13256

~~Classified Ref.~~

AFFDL-TR-76-35
Volume I

**FLIGHT CONTROL REQUIREMENTS FOR
WEAPON DELIVERY**
**Volume I - Development of the Terminal
Aerial Weapon Delivery Simulation
(TAWDS) Programs and Their Use in
Formulating Flying Qualities Guidelines
for Manually Coupled Aircraft Weapon
Delivery Systems**

MCDONNELL DOUGLAS CORPORATION

MARCH 1976

TECHNICAL REPORT AFFDL-TR-76-35, Volume I
FINAL REPORT FOR PERIOD JUNE 1973 - SEPTEMBER 1975

~~D. 82~~
~~Distribution limited to U.S. Government agencies only; test and
evaluation statement applied January 1976. Other requests for this
document must be referred to Air Force Flight Dynamics
Laboratory (FGL), Wright-Patterson Air Force Base, Ohio 45433~~

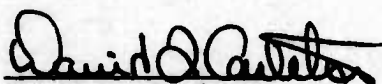
This document has been approved
for public release and sale; its
distribution is unlimited.

AIR FORCE FLIGHT DYNAMICS LABORATORY
AIR FORCE WRIGHT AERONAUTICAL LABORATORIES
AIR FORCE SYSTEMS COMMAND
WRIGHT-PATTERSON AIR FORCE BASE, OHIO 45433

NOTICES

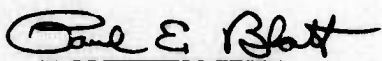
When Government drawings, specifications, or other data are used for any purpose other than in connection with a definitely related Government procurement operation, the United States Government thereby incurs no responsibility nor any obligation whatsoever; and the fact that the government may have formulated, furnished, or in any way supplied the said drawings, specifications, or other data, is not to be regarded by implication or otherwise as in any manner licensing the holder or any other person or corporation, or conveying any rights or permission to manufacture, use, or sell any patented invention that may in any way be related thereto.

This report has been reviewed and is approved for publication.



David L. Carleton
Project Engineer

FOR THE COMMANDER



Paul E. Blatt
Chief
Control Systems Development Branch
Flight Control Division

Copies of this report should not be returned unless return is required by security considerations, contractual obligations, or notice on a specific document.

UNCLASSIFIED

SECURITY CLASSIFICATION OF THIS PAGE (When Data Entered)

REPORT DOCUMENTATION PAGE		READ INSTRUCTIONS BEFORE COMPLETING FORM
1. REPORT NUMBER AFFDL-TR-76-35, Volume I	2. GOVT ACCESSION NO.	3. RECIPIENT'S CATALOG NUMBER
4. TITLE (and Subtitle) FLIGHT CONTROL REQUIREMENTS FOR WEAPON DELIVERY Volume I - Development of the Terminal Aerial Weapon Delivery Simulation (TAWDS) Programs and Their Use in Formulating Flying Qualities Guidelines for Manually Coupled Aircraft Weapon Delivery Systems	5. TYPE OF REPORT & PERIOD COVERED Final Technical Report 6/29/73 - 9/30/75	
	6. PERFORMING ORG. REPORT NUMBER N/A	
7. AUTHOR(s) J. B. Berger R. P. Meyer D. B. Groll	8. CONTRACT OR GRANT NUMBER(s) F33615-73-C-3122	
	10. PROGRAM ELEMENT, PROJECT, TASK AREA & WORK UNIT NUMBERS Project No. 1987 Task No. 01	
9. PERFORMING ORGANIZATION NAME AND ADDRESS McDonnell Aircraft Company P. O. Box 516 St. Louis, Missouri 63166	11. CONTROLLING OFFICE NAME AND ADDRESS Air Force Flight Dynamics Laboratory Air Force Systems Command Wright-Patterson AFB, Ohio 45433	
14. MONITORING AGENCY NAME & ADDRESS (if different from Controlling Office)	12. REPORT DATE March 1976	
	13. NUMBER OF PAGES 272	
	15. SECURITY CLASS. (of this report) Unclassified	
	15a. DECLASSIFICATION/DOWNGRADING SCHEDULE	
16. DISTRIBUTION STATEMENT (of this Report) Distribution limited to U.S. Government agencies only; test and evaluation; statement applied Jan 1976. Other requests for this document must be referred to Air Force Flight Dynamics Laboratory (FGL), Wright-Patterson AFB, Ohio 45433		
17. DISTRIBUTION STATEMENT (of the abstract entered in Block 20, if different from Report)		
18. SUPPLEMENTARY NOTES		
19. KEY WORDS (Continue on reverse side if necessary and identify by block number)		
Air-to-Air Gunnery	Deterministic Simulation	Simulation
Air-to-Ground Gunnery	Fire Control	Stochastic Simulation
Bombing	Flight Control	Weapon Delivery
Military Specifications	Gunnery	Weapon Delivery
Pilot Modeling	Flying Qualities	Sensitivity
20. ABSTRACT (Continue on reverse side if necessary and identify by block number)		
<p>The objectives of this research were to (1) develop man-machine multi-axis analytical models for predicting weapon delivery accuracy for piloted aircraft and (2) use the analytical models, the Terminal Aerial Weapon Delivery Simulation (TAWDS) computer programs, to determine the effects of aircraft flying qualities on air-to-air gunnery and air-to-ground gunnery and bombing effectiveness. The TAWDS programs enable a digital simulation to be performed on various closed loop weapon delivery systems under manual tracking control</p>		

This document has been approved for public release and its distribution is unlimited.

UNCLASSIFIED

SECURITY CLASSIFICATION OF THIS PAGE(When Data Entered)

20. ABSTRACT

for predicting and evaluating weapon delivery accuracy. The TAWDS method of determining and establishing flight control system requirements for weapon delivery has been demonstrated.

A set of flying qualities characteristics which provides improved tracking capability and increased weapon delivery effectiveness for fighter aircraft was determined using the TAWDS analysis programs. This set of flying qualities is recommended for inclusion into MIL-F-8785B as a guideline for design of fighter aircraft flying qualities characteristics to assure a high probability of kill for these aircraft performing tactical weapon delivery.

It is also recommended that the TAWDS methodology, which computes probability of kill (a direct function of weapon impact error statistics and target vulnerability), be considered for MIL-F-8785B as an evaluation measure of merit for determining weapon effectiveness of fighter aircraft performing weapon delivery.

UNCLASSIFIED

SECURITY CLASSIFICATION OF THIS PAGE(When Data Entered)

FOREWORD

This report was prepared for the United States Air Force by the McDonnell Aircraft Company (MCAIR), a division of the McDonnell Douglas Corporation, P. O. Box 516, St. Louis, Mo., 63166, and covers the work performed under Air Force Contract F33615-73-C-3122, Project 1987, Task 01. The work was performed from 29 June 1973 to 30 September 1975.

The studies described in this report were performed by MCAIR under the direction of Dr. John B. Berger. Dr. Berger is a member of the Guidance and Control Mechanics (G&CM) department of MCAIR reporting to Mr. Fred M. Krachmalnick, Chief Guidance and Control Mechanics Engineer. Other principal contributors to this report were Mr. Darin B. Groll (G&CM) and Dr. Roland P. Meyer. Dr. Meyer is a member of MCAIR's Electronic Systems Technology (EST) department. The authors wish to acknowledge the contributions of Mr. Roger A. Ahrens of MCAIR's Operations Analysis department, Dr. Roger L. Berger (G&CM), Dr. Robert J. Landy (G&CM), Mr. Robert L. Berg (EST), and Mr. Dennis T. Rybarczyk of MCAIR's Flight Simulation Laboratory. The timely and notable contributions of the Air Force project engineer, Mr. David L. Carleton, AFFDL/FGL, are also acknowledged. This report was submitted by the authors in February, 1976. An interim report of the same title bearing the number AFFDL-TR-74-119 has already been printed.

TABLE OF CONTENTS

<u>Section</u>	<u>Title</u>	<u>Page</u>
1	INTRODUCTION	1
2	THE TAWDS PROGRAMS	4
2.1	Functional Description of TAWDS(AA), the Air-to-Air Program	6
2.1.1	Structure of TAWDS(AA).	9
2.1.2	The Major Subroutines of TAWDS(AA)	10
2.2	Functional Description of TAWDS(AG), the Air-to-Ground Program	26
2.2.1	Structure of TAWDS(AG)	33
2.2.2	TAWDS, the Main Subroutine of TAWDS(AG)	33
2.2.3	Subroutine DATAIN	33
2.2.4	Generation of the Nominal Trajectory	34
2.2.5	Generation of the Linear Model	36
2.2.6	Performance: Sensitivities and Ensemble Statistics	37
2.3	Weapon Delivery Ensemble Impact Error Statistics	38
2.3.1	Ensemble Burst Statistics	39
2.3.2	Calculation of Pass Statistics for Air-to-Air Gunnery	42
2.3.3	Monte Carlo Verification of the TAWDS(AG) Covariance Model	45
3	MANNED AIR COMBAT SIMULATION STUDY	49
3.1	Description of Simulation Study	49
3.2	Pilot Evaluation of Aircraft Flying Qualities for Air-to-Air and Air-to-Ground Weapon Delivery Tasks	57
3.2.1	Pilot Evaluation of Longitudinal Flying Qualities	57
3.2.2	Pilot Evaluation of Lateral-Directional Flying Qualities	59
3.3	Comparison of TAWDS Generated Impact Error Distribution with Impact Errors Measured from Manned Simulation Studies	61
4	MULTI-AXIS PILOT MODEL DEVELOPMENT AND VALIDATION	65
4.1	The Precision Tracking Task	66
4.2	Pilot Tracking Error Characteristics	66
4.3	Pilot Models	69
4.3.1	Longitudinal Pilot Model	71
4.3.2	Lateral-Directional Pilot Model	74
4.4	Pilot Model Validation	77
4.4.1	Representative Air-to-Air Gunnery Tracking Responses	79
4.4.2	Representative Air-to-Ground Gunnery Tracking Responses	95
4.4.3	Representative Air-to-Ground Bombing Tracking Responses	101
4.5	TWeaD Flight Test Results	116

TV blank

TABLE OF CONTENTS

<u>Section</u>	<u>Title</u>	<u>Page</u>
5	TAWDS ANALYSES OF AIRCRAFT FLYING QUALITIES	120
5.1	Description of TAWDS Flying Qualities Evaluation Study .	120
5.2	TAWDS Flying Qualities Analyses	145
5.2.1	TAWDS Analyses of Longitudinal Flying Qualities for Air-to-Ground Weapon Delivery Tasks	149
5.2.2	TAWDS Analyses of Lateral-Directional Flying Qualities for Air-to-Ground Weapon Delivery . . .	149
5.2.3	Multiple Burst Criteria for Air-to-Air Gunnery Tasks	156
5.2.4	TAWDS Analyses of Longitudinal Flying Qualities for Air-to-Air Gunnery	169
5.2.5	TAWDS Analyses of Lateral-Directional Flying Qualities for Air-to-Air Gunnery	175
6	WEAPON DELIVERY CRITERIA CONSIDERATIONS	
6.1	Formulation of Aircraft Flying Qualities Guidelines for Weapon Delivery	182
6.2	Merit Functions for Weapon Delivery	185
6.2.1	Use of Ensemble Burst Statistics	185
6.2.2	Effect of Round-to-Round Correlation on Kill Probability	190
6.3	Recommended Weapon Delivery Criteria Consideration . . .	191
7	CONCLUSIONS AND RECOMMENDATIONS	196
	REFERENCES	199
	APPENDIX I - Nonlinear Aircraft Equations for the TAWDS(AA) Program	201
	APPENDIX II - Weapon Fire Control Systems	212
	APPENDIX III - Error Sources and Sensitivities for Weapon Delivery Sights	226
	APPENDIX IV - Development of Modified Vacuum Trajectory Equations .	242
	APPENDIX V - Air-to-Ground Dynamic Formulation for the TAWDS(AG) Program	249
	APPENDIX VI - Burst Statistics for Air-to-Ground Weapon Delivery . .	264
	APPENDIX VII - Description of Frequency Response Analysis Computer Programs	270

LIST OF ILLUSTRATIONS

<u>Figure No.</u>		<u>Page</u>
1	Block Diagram of Weapon Delivery Terminal Tracking Task	5
2	Typical Attack Sequence with Director Sight	7
3	Typical Attack Sequence with LCOSS Sight	8
4	Flow Diagram of TAWDS(AA) Executive Subroutine	11
5	Performance Logic in TAWDS(AA) Executive Subroutine	13
6	Flow Diagram of Data Input Subroutine	14
7	Initial Lead Angle Perturbation Quantities	16
8	TAWDS(AA) Encounter Parameter Matrix	16
9	Summary of Target Initialization	20
10	Target Heading and Climb Angle Initialization	20
11	Target Bank Angle Initialization	21
12	Target Thrust and Angle of Attack Initialization	21
13	Geometry of Gun Error Computation	24
14	Block Diagram of the Bullet Integration Subroutine	24
15	Definition of Bullet Drag, and Position and Velocity Update	25
16	Air-to-Ground Gunnery Attack Sequence	28
17	Profile View of FIP Bombing Attack	29
18	Along-Track Stationary Source Errors for Air-to-Ground Weapon Delivery	31
19	Cross-Track Stationary Source Errors for Air-to-Ground Weapon Delivery	
20	Structure of the TAWDS(AG) Program	34
21	Subroutine Sequence for Nominal Trajectory	35
22	Uncoupled Aircraft Tracking Error Geometry Perturbation Equations for Wings Level Weapon Delivery Tasks	35
23	Subroutine Sequence for Linear Time Histories	37
24	Subroutine Sequence of Performance Subroutines	37
25	Equivalent Salvo Distribution for Impact Errors	40
26	Gun Firing Regions Defined by Tracking Error Constraints	43
27	Comparison of Monte Carlo and Covariance Model Round-to-Round Correlations	47
28	Comparison of Ensemble Burst Statistics Generated by the TAWDS(AG) Monte Carlo and Covariance Models	48
29	Aircraft/Pilot/Weapon System Configurations for Manned Simulation Study	50
30	Manned Air Combat Simulator Layout	50

LIST OF ILLUSTRATIONS (Cont'd)

<u>Figure No.</u>		<u>Page</u>
31	Generic TWeaD Longitudinal Flight Control System	52
32	Generic TWeaD Lateral-Directional Flight Control System	53
33	Longitudinal and Lateral-Directional Flying Qualities Variations for Aircraft Simulated in Manned Simulation Studies	53
34	Description of Aerial Gunnery Encounter and Pilot Tracking Instructions for Manned Simulation Study	55
35	Air-to-Air Head Up Display for Generic Director and LCOSS Sights	55
36	Air-to-Ground Gunnery Head-Up Display	56
37	Pilot Evaluation of Longitudinal Short-Period Frequency and Damping Variations for Air-to-Ground Weapon Delivery Tasks	58
38	Pilot Evaluation of Longitudinal Short-Period Frequency and Damping Variations for Air-to-Air Gunnery Tasks	58
39	Pilot Evaluation of Longitudinal Stick Force Per G Variations for Air-to-Ground and Air-to-Air Weapon Delivery Tasks	59
40	Pilot Evaluation of Lateral-Directional Dutch Roll Damping for Air-to-Ground and Air-to-Air Weapon Delivery Tasks	60
41	Pilot Evaluation of Lateral-Directional Proverse/Adverse Yaw Variations for Air-to-Ground and Air-to-Air Weapon Delivery Tasks	60
42	Pilot Evaluation of Lateral-Directional Commanded Roll Rate Response Variations for Air-to-Ground and Air-to-Air Weapon Delivery Tasks	61
43	Comparison of TAWDS(AG) Generated Bomb Impact Error One Sigma Distribution	63
44	Comparison of TAWDS(AA) Generated Pass Mean Impact Error One Sigma Distribution	63
45	Comparison of TAWDS(AA) Generated Round-to-Round Impact Error One Sigma Distribution	64
46	Director Air-to-Air Gunnery Tracking Error and Aircraft Command Time Histories for Aircraft Configuration with Short-Period Damping = 0.50 and Frequency = 3.0 Rad/Sec	67
47	Director Air-to-Air Gunnery Tracking Error and Aircraft Command Time Histories for Aircraft Configuration with Short-Period Damping = 0.70 and Frequency = 5.0 Rad/Sec	68
48	Multi-Axis Pilot Model Structure for Air-to-Air and Air-to-Ground Weapon Delivery Tasks	70
49	Variation in Longitudinal Pilot Model Transfer Function Zeros with Low-Pass Filter Gain, K_L	72
50	Recommended Values for Longitudinal Pilot Model Parameters in Terms of the Aircraft Dynamics and Weapon Delivery Task	73
51	Typical Root Locus for Elevation Tracking Error	73

LIST OF ILLUSTRATIONS (Cont'd)

<u>Figure No.</u>		<u>Page</u>
52	Recommended Range of Values for Traverse Pilot Model Parameters for Different Weapon Delivery Tasks	76
53	Summary of Pilot Model Parameter Values Used With F-4 TWeaD Aircraft Simulation	78
54	Director Air-to-Air Gunnery Tracking Error and Aircraft Command Time Histories for F-4 TWeaD Aircraft Configuration	80
55	Longitudinal Frequency Responses for Air-to-Air Gunnery Tasks with Director Sight and F-4 TWeaD Aircraft Configuration	84
56	Longitudinal Spectral Responses for Air-to-Air Gunnery Tasks with Director Sight and F-4 TWeaD Aircraft Configuration	85
57	Lateral Frequency Responses for Air-to-Air Gunnery Tasks with Director Sight and F-4 TWeaD Aircraft Configuration	86
58	Lateral Spectral Responses for Air-to-Air Gunnery Tasks with Director Sight and F-4 TWeaD Aircraft Configuration	87
59	LCOSS Air-to-Air Gunnery Tracking Error and Aircraft Command Time Histories for F-4 TWeaD Aircraft Configuration	88
60	Longitudinal Frequency Responses for Air-to-Air Gunnery Tasks with LCOSS Sight and F-4 TWeaD Aircraft Configuration	91
61	Longitudinal Spectral Responses for Air-to-Air Gunnery Tasks with LCOSS Sight and F-4 TWeaD Aircraft Configuration	92
62	Lateral Frequency Responses for Air-to-Air Gunnery Tasks with LCOSS Sight and F-4 TWeaD Aircraft Configuration	93
63	Lateral Spectral Responses for Air-to-Air Gunnery Tasks with LCOSS Sight and F-4 TWeaD Aircraft Configuration	94
64	CCIP Air-to-Ground Gunnery Tracking Error and Aircraft Commanded Time Histories for F-4 TWeaD Aircraft Configuration	96
65	Longitudinal Frequency Responses for Air-to-Ground Gunnery Tasks with CCIP Sight and F-4 TWeaD Aircraft Configuration	99
66	Longitudinal Spectral Responses for Air-to-Ground Gunnery Tasks with CCIP Sight and F-4 TWeaD Aircraft Configurations	100
67	Lateral Frequency Responses for Air-to-Ground Gunnery Tasks with CCIP Sight and F-4 TWeaD Aircraft Configuration	102
68	Lateral Spectral Responses for Air-to-Ground Gunnery Tasks with CCIP Sight and F-4 TWeaD Aircraft Configuration	103
69	FDR Air-to-Ground Gunnery Tracking Error and Aircraft Command Time Histories for F-4 TWeaD Aircraft Configuration	104
70	Longitudinal Frequency Responses for Air-to-Ground Gunnery Tasks with FDR Sight and F-4 TWeaD Aircraft Configuration	106
71	Longitudinal Spectral Responses for Air-to-Ground Gunnery Tasks with FDR Sight and F-4 TWeaD Aircraft Configuration	107
72	Lateral and Directional Frequency Responses for Air-to-Ground Gunnery Tasks with FDR Sight and F-4 TWeaD Aircraft Configuration	108

LIST OF ILLUSTRATIONS (Cont'd)

<u>Figure No.</u>		<u>Page</u>
73	Lateral and Directional Responses for Air-to-Ground Gunnery Tasks with FDR Sight and F-4 TWeaD Aircraft Configuration	109
74	FIP Air-to-Ground Bombing Tracking Error and Aircraft Command Time Histories for F-4 TWeaD Aircraft Configuration	110
75	Longitudinal Frequency Responses for Air-to-Ground Bombing Tasks with FIP Sight and F-4 TWeaD Aircraft Configuration	113
76	Longitudinal Spectral Responses for Air-to-Ground Bombing Tasks with FIP Sight and F-4 TWeaD Aircraft Configuration	114
77	Lateral Frequency Responses for Air-to-Ground Bombing Tasks with FIP Sight and F-4 TWeaD Aircraft Configuration	115
78	Lateral Spectral Responses for Air-to-Ground Bombing Tasks with FIP Sight and F-4 TWeaD Aircraft Configuration	117
79	Flight Test Air-to-Air Gunnery Tracking Responses	118
80	Flight Test Air-to-Ground Bombing Tracking Response	118
81	Functional Block Diagram of Weapon Delivery Effectiveness Model	121
82	Longitudinal Flight Control System Configurations for Aircraft Weapon Delivery Tasks	124
83	Lateral-Directional Flight Control System Configurations for Aircraft Weapon Delivery Tasks	125
84	Generic Longitudinal TWeaD Flight Control System	126
85	Generic Lateral-Directional TWeaD Flight Control System	127
86	Longitudinal Responses Due to Unit Step Longitudinal Stick Command for Various Longitudinal Aircraft Configurations	128
87	Longitudinal Responses Due to Unit Step Longitudinal Stick Command for Various Longitudinal Aircraft Configurations	131
88	Lateral-Directional Responses Due to Unit Step Lateral Stick Command for Various Lateral-Directional Aircraft Configurations	134
89	Lateral-Directional Responses Due to Unit Step Lateral Stick Command for Various Lateral-Directional Aircraft Configurations	137
90	Sample Stationary Source Error Standard Deviations for the Air-to-Ground Gunnery Fixed Depressed Reticle Sight (Altitude Option)	140
91	Sample Stationary Source Error Standard Deviations for the Air-to-Ground Gunnery Continuously Computed Impact Point Sight	141
92	Sample Stationary Source Error Standard Deviations for the Air-to-Ground Bombing Future Impact Point Sight	142
93	Sample Dynamic Source Errors	143
94	Sample Stationary Source Error Standard Deviations for the Air-to-Air Gunnery with Director Sight	144

LIST OF ILLUSTRATIONS (Cont'd)

<u>Figure No.</u>		<u>Page</u>
95	Sample Stationary Source Error Standard Deviations for the Air-to-Air Gunnery with LCOSS Sight	144
96	Multiaxis Pilot Model Structure for Air-to-Air Gunnery Task	146
97	Longitudinal Pilot Gain Variations for Air-to-Air Gunnery Tasks	146
98	Linear Multi-Axis Pilot Model Structure for Air-to-Ground Weapon Delivery Tasks	147
99	Pilot Gain Variations for Air-to-Ground Weapon Delivery Tasks	148
100	Effects of Longitudinal Short-Period Frequency and Damping Variations on Air-to-Ground Gunnery Task for F-4 TWeaD Aircraft Configured with FDR Sight	150
101	Effects of Longitudinal Short-Period Frequency and Damping Variations on Air-to-Ground Gunnery Task for F-4 TWeaD Aircraft Configured with CCIP Sight	151
102	Effects of Longitudinal Short-Period Frequency and Damping Variations on Air-to-Ground Bombing Task for F-4 TWeaD Aircraft Configured with FIP Sight	152
103	Effects of Longitudinal Stick Force Per G Variations on Air-to-Ground Gunnery Task for F-4 TWeaD Aircraft Configured with FDR Sight	153
104	Effects of Longitudinal Stick Force Per G Variations on Air-to-Ground Gunnery Task for F-4 TWeaD Aircraft Configured with CCIP Sight	154
105	Effects of Longitudinal Stick Force Per G Variations on Air-to-Ground Bombing Task for F-4 TWeaD Aircraft Configured with FIP Sight	155
106	Effects of Dutch Roll Mode Damping Variations on Air-to-Ground Gunnery Task for F-4 TWeaD Aircraft Configured with FDR Sight	157
107	Effects of Dutch Roll Mode Damping Variations on Air-to-Ground Gunnery Task for F-4 TWeaD Aircraft Configured with CCIP Sight	158
108	Effects of Dutch Roll Mode Damping Variations on Air-to-Ground Bombing Task for F-4 TWeaD Aircraft Configured with FIP Sight	158
109	Effects of Proverse/Adverse Yaw Variations on Air-to-Ground Gunnery Task for F-4 TWeaD Aircraft Configured with FDR Sight	159
110	Effects of Proverse/Adverse Yaw Variations on Air-to-Ground Gunnery Task for F-4 TWeaD Aircraft Configured with CCIP Sight	161
111	Effects of Proverse/Adverse Yaw Variations on Air-to-Ground Bombing Task for F-4 TWeaD Aircraft Configured with FIP Sight	162
112	Effects of Commanded Roll Rate Sensitivity Variations on Air-to-Ground Gunnery Task for F-4 TWeaD Aircraft Configured with FDR Sight	163
113	Effects of Commanded Roll Rate Sensitivity Variations on Air-to-Ground Gunnery Task for F-4 TWeaD Aircraft Configured with CCIP Sight	164

LIST OF ILLUSTRATIONS (Cont'd)

<u>Figure No.</u>		<u>Page</u>
114	Effects of Commanded Roll Rate Sensitivity Variations on Air-to-Ground Bombing Task for F-4 TWeaD Aircraft Configured with FIP Sight	165
115	Gunfire Durations for Pilot During Air-to-Air Gunnery Director Tracking Task	166
116	Weapon Delivery Accuracy Statistics	167
117	Effects of Longitudinal Short-Period Variations on Air-to-Air Gunnery Task for F-4 TWeaD Aircraft Configured with LCOSS Sight	168
118	Effects of Longitudinal Short-Period Frequency Variations on Air-to-Air Gunnery Task for F-4 TWeaD Aircraft Configured with LCOSS Sight	170
119	Effects of Longitudinal Stick Force per G Variations on Air-to-Air Gunnery Task for F-4 TWeaD Aircraft Configured with LCOSS Sight	171
120	Effects of Longitudinal Short-Period Damping Variations on Air-to-Air Gunnery Task for F-4 TWeaD Aircraft Configured with Director Sight	172
121	Effects of Longitudinal Short-Period Frequency Variations on Air-to-Air Gunnery Task for F-4 TWeaD Aircraft Configured with Director Sight	173
122	Effects of Longitudinal Stick Force per G Variations on Air-to-Air Gunnery Task for F-4 TWeaD Aircraft Configured with Director Sight	174
123	Effects of Dutch Roll Mode Damping Variations on Air-to-Air Gunnery Task for F-4 TWeaD Aircraft Configured with Director Sight	176
124	Effects of Dutch Roll Mode Damping Variations on Air-to-Air Gunnery Task for F-4 TWeaD Aircraft Configured with LCOSS Sight	177
125	Effects of Proverse/Adverse Yaw Variations on Air-to-Air Gunnery Task for F-4 TWeaD Aircraft Configured with Director Sight	178
126	Effects of Proverse/Adverse Yaw Variations on Air-to-Air Gunnery Task for F-4 TWeaD Aircraft Configured with LCOSS Sight	179
127	Effects of Commanded Roll Rate Sensitivity Variations on Air-to-Air Gunnery Task for F-4 TWeaD Aircraft Configured with Director Sight	180
128	Effects of Commanded Roll Rate Sensitivity Variations on Air-to-Air Gunnery Task for F-4 TWeaD Aircraft Configured with LCOSS Sight	181
129	Comparison of Most Desired Sets of Aircraft Flying Qualities Obtained by Manned Simulation Evaluation and TAWDS Analyses for Air-to-Ground Weapon Delivery Tasks	183

LIST OF ILLUSTRATIONS (Cont'd)

<u>Figure No.</u>		<u>Page</u>
130	Comparison of Most Desired Sets of Aircraft Flying Qualities Obtained by Manned Simulation Evaluation and TAWDS Analyses for Air-to-Air Gunnery Tasks	184
131	Impace Error Dispersion Patterns	187
132	Ensemble Expected Hits on an Offset Circular Target	189
133	Ensemble Expected Hits on an Offset Rectangular Target	189
134	Weapon Delivery Accuracy Statistics for Unity Round-to-Round Correlation	192
135	Weapon Delivery Accuracy Statistics for Gauss Markov Round-to-Round Correlation	193
I-1	The Geometry of the Airframe Simulation	202
I-2	Generic Longitudinal Flight Control System for Air-to-Air Gunnery TAWDS Program	209
I-3	Generic Lateral-Directional Flight Control System for Air-to-Air Gunnery TAWDS Program	210
II-1	Generic Sight Systems for Weapon Delivery Tasks	213
II-2	Basic Principles of the Time-of-Flight Computation Used in LCOSS and Director Sights	214
II-3	Functional Flow Diagram of Generic Lead Computing Optical Sight System (LCOSS)	215
II-4	Functional Flow Diagram of Director Sight	217
II-5	Profile View of Representative FIP Bombing Attack	218
II-6	Summary of Bomb Component Equations at Bomb Release Signal in Ground Track Velocity Coordinates	220
II-7	Sequence of Computations for FIP Bombing Sight	221
II-8	Estimating Altitude Lost During Dive Recovery for 4G Pullup	221
II-9	Summary of Bullet Component Equations in Ground Track Velocity Coordinates	223
II-10	Sequence of Computations for CCIP Gunnery Sight	224
III-1	Summary of Error Sources for Air-to-Air LCOSS and Director Sights	227
III-2	Summary of Along-Track and Cross-Track Error Sources for FIP Bombing Sight	229
III-3	Summary of Along-Track Error Sensitivity Equations for FIP Bombing Sight	230
III-4	Summary of Cross-Track Error Sensitivity Equations for FIP Bombing Sight	231
III-5	Dynamic Tracking Error Model for FIP Bombing Sight	232
III-6	Summary of Error Sources for Fixed Depressed Reticle Gun Sight	234
III-7	Summary of Error Sources for CCIP Gunnery Sight	235
III-8	Summary of Along-Track Error Sensitivity Equations for Air-to-Ground Gunnery	236

LIST OF ILLUSTRATIONS (Cont'd)

<u>Figure No.</u>		<u>Page</u>
III-9	Summary of Cross-Track Error Sensitivity Equations for Air-to-Ground Gunnery	237
III-10	Dynamic Tracking Error Models for Fixed Depressed Reticle Gunnery Sight	237
III-11	Dynamic Tracking Error Models for CCIP Gunnery Sight	238
IV-1	Modified Vacuum Trajectory Equations	243
IV-2	Derivation of Bomb Retardation Factor from Bomb Tables	243
IV-3	Maximum Bomb Ground Range Prediction Error Due to Approximation of the Bomb Retardation Factor C_B	245
IV-4	Bullet Ground Range Error Due to C_B Approximation Against a Sea Level Target	246
IV-5	Variation in Bomb Ground Range with Altitude of Target Above Sea Level	247
IV-6	Bullet Impact Error Due to C_B Approximation Without Target Altitude Compensation	247
IV-7	Bullet Impact Error Due to C_B Approximation with Target Altitude Compensation	248
V-1	Generic Longitudinal Flight Control System for Air-to-Ground TAWDS(AG) Program	253
V-2	Block Diagram of the Linearized Longitudinal Pilot Models	254
V-3	Block Diagram of the Linearized Lateral-Directional Flight Control System	260
V-4	Block Diagram of the Linearized Lateral Pilot Model	261
V-5	Block Diagram of the Linearized Directional Pilot Model	261

LIST OF ABBREVIATIONS AND SYMBOLS

ABBREVIATION

ARI	Aileron-to-Rudder Interconnect
BMPI	Burst Mean Point of Impact
CCIP	Continuously Computed Impact Point
CEP	Circular Error Probability
DIP	Displayed Impact Point
EMPI	Ensemble Mean Point of Impact
FCRWD	Flight Control Requirements for Weapon Delivery
FDR	Fixed Depressed Reticle
FIP	Future Impact Point
FOV	Field of View
HUD	Head Up Display
LCOSS	Lead Computing Optical Sight System
LOS	Line of Sight
MACS	Manned Air Combat Simulator
MCAIR	McDonnell Aircraft Company
MPI	Mean Point of Impact
SFCS	Survivable Flight Control System
TAWDS	Terminal Aerial Weapon Delivery Simulation
TAWDS(AA)	Air-to-Air-TAWDS Simulation
TAWDS(AG)	Air-to-Ground TAWDS Simulation
TWeaD	Tactical Weapon Delivery

SYMBOLS

a_i	Impact error of the i th round of the burst
a_{ij}	Impact point of the j th bullet fired during the i th pass
$A(t)$	$n \times n$ time varying matrix of coefficients for the set of differential equations describing the dynamics of the air-to-ground weapon delivery tasks
A_p	Target presented area, line of sight approach aspect
A_v	Target vulnerable area corresponding to A_p
ABW	TAWDS(AG) subroutine that computes elements of dynamic matrices associated with Dryden wind gust model
AC	TAWDS(AG) subroutine that computes state derivatives
AMAT	TAWDS(AG) subroutine that computes elements of aircraft's dynamic matrices for selected flight control system
$B(t)$	$m \times n$ time varying matrix of coefficients for the stochastic disturbance vector
B	Aircraft bank angle
\bar{b}	Ensemble mean impact error
b_e	Burst bias impact point, elevation component
\bar{b}_e	Ensemble mean impact point, elevation component
\bar{b}_i	Average value of impact point with respect to target during i th pass
b_t	Burst bias impact point, traverse component
\bar{b}_t	Ensemble mean impact point, traverse component
$c(t)$	$k \times n$ time varying matrix of coefficients for the deterministic disturbance vector
C_D	Aircraft drag coefficient
C_L	Aircraft lift coefficient
CDIP	TAWDS(AG) subroutine that computes CCIP pipper setting
CORREL	TAWDS(AG) subroutine that computes bullet autocorrelation matrices
COVARI	TAWDS(AG) subroutine that computes weapon delivery impact error statistics due to stationary errors
DZ_{eE}	Pilot dead zone parameter for elevation error rate
DZ_{eT}	Pilot dead zone parameter for traverse error rate
DZ_{ϕ}	Pilot dead zone parameter for relative bank angle

E[]	Expected value of []
E_H	Expected number of hits for a burst of n rounds
E _L	Elevation coordinate
F_{DIR}	Rudder pedal force
F_{LAT}	Lateral stick force
F_{LON}	Longitudinal stick force
F_S/G	Stick force per g
FCT	TAWDS(AG) subroutine that updates coefficients describing aircraft's dynamic matrices
FIXRS	TAWDS(AG) subroutine that computes Fixed Depressed Reticule sight data for the firing burst midpoint
FIPRAT	TAWDS(AG) subroutine that computes sensitivities for FIP pipper elevation setting
g	Acceleration of gravity constant
h	Aircraft altitude
K_{AIL}	Lateral pilot gain parameter
K_{ARI}	Aileron-to-rudder-interconnect gain parameter
K_{co}	K_{PE} crossover gain value for elevation tracking error task
K_D	Ballistic constant
K_E	Gain of prefilter network compensating longitudinal stick force
K_I	Gain of integral controller for longitudinal flight control system
K_L	Pilot longitudinal low pass filter gain parameter
K_M	Mechanical linkage gain relating elevator actuator to longitudinal stick force
K_{mc}	Mechanical linkage gain relating aileron actuator to lateral stick force
K_{me}	Gain of prefilter network compensating lateral stick force
K_{ny}	Lateral acceleration feedback gain
K_{nz}	Normal acceleration feedback gain
K_{PE}	Longitudinal pilot model gain parameter
K_R	Pilot elevation error rate gain parameter
K_{RL}	Controller gain for longitudinal flight control system

K_{rr}	Computed sideslip rate feedback gain
K_{RTR}	Pilot traverse error rate gain parameter
K_{RUD}	Pilot rudder gain parameter
$K_{\dot{\theta}}$	Pitch rate feedback gain
K_{ϕ}	Pilot bank angle gain parameter
M	Mach
MR	Milliradians
N_i	Number of bullets fired during the i^{th} pass
OUTCOV	TAWDS(AG) output subroutine
$P(b_e, b_t)$	Probability density function of the burst or pass bias impact point
P_H	Single-shot kill probability
$P_{H/b}$	Probability that an individual round within the burst or pass impacts within the presented area of target
P_K	Probability of kill
$P_{K/BURST}$	Probability of kill per burst
$P_{K/H}$	Single round probability of target kill given a hit on its presented area
PERF	TAWDS(AG) subroutine that computes ensemble weapon statistics data
PIPRAT	TAWDS(AG) subroutine that computes elevation sensitivities for CCIP piper setting
$Q(t)$	Variance of white noise process
R	Range
RKI	TAWDS(AG) Runge-Kutta integration subroutine
S	Laplace operator
SENTIV	TAWDS(AG) subroutine that computes weapon impact error sensitivity matrices
t	time
TH	Aircraft thrust
T_F	Projectile time of flight
Tr.	Traverse coordinate
TRIM	TAWDS(AG) subroutine that computes aircraft's initial state and profile geometry
U_c	Deterministic disturbance vector

U_v	Stochastic state vector assumed to be white noise
WEAPON	TAWDS(AG) subroutine that computes bullet or bomb trajectories
WPNINT	TAWDS(AG) subroutine that initializes bullet or bomb trajectories
x	State variable vector
α	Aircraft angle of attack (rad)
β	Aircraft sideslip angle
β_2	Sideslip at 2 seconds due to lateral step stick force
γ	Flight path angle
γ^2	Multiple coherence function for lateral stick force
F_{LAT}	
γ^2	Multiple coherence function for longitudinal stick force
F_{LON}	
γ^2	Multiple coherence function for rudder pedal force
F_{DIR}	
ϵ_{EL}	Elevation tracking error
ϵ_{TR}	Traverse tracking error
ρ	Round-to-round correlation coefficient
$\rho_d(1,j)$	Dynamic individual round-to-round correlation coefficient for rounds 1 and j
$\rho_E(t,o)$	Round-to-round correlation between bullets fired at t second intervals, elevation component
$\rho_T(t,o)$	Round-to-round correlation between bullets fired at t second intervals, traverse component
$\Phi(t_i,t_j)$	Transition matrix for the weapon delivery task's state vector
ω_D	Dutch roll mode natural frequency
ω_{sp}	Short-period mode natural frequency
ω_n	Natural frequency of pilot's low pass filter representation
σ_{be}^2	Variance of bias impact point, elevation component
σ_{bt}^2	Variance of bias impact point, traverse component
σ_d^2	Impact error variance due to dynamic source errors
σ_{re}^2	Variance of individual impact points with respect to their burst or pass mean point of impact, elevation component
σ_{ri}^2	Variance of impact points within a pass about the pass mean point of impact

σ_{rt}^2	Variance of individual impact points with respect to their burst or pass mean point of impact, traverse component
σ_s^2	Impact error variance due to stationary source errors
μ	Average individual round-to-round correlation for all pairs of individual rounds in the burst
τ_E	Pilot's ability to smooth observed elevation tracking error
τ_R	Time to attain 50% of commanded roll rate
τ_T	Pilot's ability to smooth observed traverse error
θ_{EC}	Pilot's elevation error gunfire boundary constraint
θ_{TC}	Pilot's traverse error gunfire boundary constraint
θ_{RC}	Pilot's radial error gunfire boundary constraint
ζ_D	Dutch roll mode damping ratio
ζ_n	Damping ratio of pilot's low pass filter representation
ζ_s	Aircraft short-period damping ratio
.	Derivative with respect to time, d/dt

SUMMARY

The Flight Control Requirements for Weapon Delivery program developed a methodology for evaluating weapon delivery accuracy and establishing accuracy requirements for manually coupled integrated tactical aircraft weapon system configurations. Man-machine multi-axis analytical models were developed for predicting weapon delivery accuracy of fighter aircraft. These analytical models, called the "Terminal Aerial Weapon Delivery Simulation" (TAWDS) computer programs, are unique tools for relating the dynamics of manually integrated aircraft weapon systems to weapon delivery impact error statistics. The TAWDS programs simulate weapon delivery tasks for air-to-air gunnery, air-to-ground gunnery, and bombing.

Analytical multi-axis pilot models, which realistically transform weapon delivery tracking errors into aircraft steering commands, were developed. Tracking performance results, acquired from analytical pilot simulations, were compared with those obtained from the manned simulations and the Tactical Weapon Delivery (TWeaD) flight test evaluation programs. These comparisons indicate that the TAWDS programs in conjunction with manned simulation studies provide a very cost-effective approach for designing, developing, and optimizing advanced aircraft weapon delivery systems. Background information on development of pilot models for use in evaluating manually coupled aircraft weapon delivery systems is contained in Volume II.

The TAWDS analyses also show that flying qualities for fighter aircraft performing weapon delivery tasks can be evaluated in terms of weapon system effectiveness (probability of kill). A set of flying qualities which provides optimized tracking capability as well as weapon delivery effectiveness for fighter aircraft was determined by the TAWDS analyses. This same set of flying qualities also compared very favorably with the set of flying qualities selected by pilots in a manned simulation study to be best for weapon delivery tracking tasks. Based on these study results, it is recommended that the TAWDS set of flying qualities be considered for inclusion into MIL-F-8785B as a guideline for the design of fighter aircraft flying qualities characteristics to assure a high probability of kill for these aircraft performing weapon delivery. These flying qualities characteristics can readily be achieved through judicious design of active feedback flight control systems in future fighter aircraft.

The TAWDS methodology computes a set of impact error statistics which is transformed into a probability of kill measure of merit by using a target vulnerability model. This capability provides a useful analytical tool for comparing and evaluating competitive fighter aircraft weapon system designs. It is therefore recommended that the TAWDS methodology also be considered for MIL-F-8785B as an evaluation procedure for determining weapon effectiveness of fighter aircraft performing weapon delivery.

SECTION 1
INTRODUCTION

During the past few years considerable USAF and industry efforts have been directed to developing tactical aircraft flight control systems which improve weapon delivery accuracy. These efforts, which included analytical studies and weapon delivery testing, have generated weapon delivery math models and pilot models, developed flight control systems for improving weapon delivery, and established flight test techniques for assessing aircraft maneuverability and the combat potential of new weapon systems. The wealth of data generated by these efforts has provided a basis for establishing a methodology to determine flight control criteria for weapon delivery.

The goals of this program were (1) to use the results of these previous efforts for developing an analytical model capable of predicting weapon delivery accuracy for piloted tactical aircraft, and (2) to use this analytical model as a design tool in generating performance specifications for highly maneuverable air superiority fighters and attack aircraft.

The best analytical procedures of previous efforts have been combined in this study to develop two advanced Terminal Aerial Weapon Delivery Simulation (TAWDS) digital computer programs, one for air-to-air gunnery and the other for air-to-ground gunnery and bombing. These programs enable digital simulations of various closed loop weapon delivery systems under manual control to be performed. Weapon delivery accuracy can thus be predicted and evaluated in the presence of probabilistic disturbances.

The air-to-air gunnery TAWDS program uses Monte Carlo statistical procedures to evaluate the dynamic characteristics of various integrated aircraft weapon system configurations in terms of bullet impact error ensemble statistics. The air-to-ground weapon delivery TAWDS program uses the state space statistical covariance method to determine the effects of various integrated aircraft weapon systems' dynamic characteristics on weapon delivery accuracy.

During the development of the TAWDS programs, it was necessary to show that the TAWDS programs realistically simulate weapon delivery and can be used as a design tool in generating performance specifications for highly maneuvering fighter aircraft. The conclusions drawn from a literature survey on pilot modeling were (1) additional pilot model development for simulating weapon delivery was necessary to provide the TAWDS programs with the capability to realistically simulate weapon delivery, and (2) the TAWDS flying qualities

results should be similar to those determined by pilot evaluation. Consequently, pilot-in-the-loop weapon delivery studies were performed to establish the credibility of the TAWDS programs.

In these manned simulation studies, aircraft weapon system configurations which exhibited different longitudinal and lateral-directional flying qualities were flown by two USAF pilots for air-to-air and air-to-ground weapon delivery tasks. These parametric simulation studies provided (1) a pilot evaluation of aircraft flying qualities characteristics for air-to-air and air-to-ground weapon delivery, (2) weapon delivery impact error measurements which were used to compare with the TAWDS analytical statistical measures, and (3) aircraft tracking data which were used for developing and validating analytical multi-axis pilot models.

The pilot models were developed by varying steering laws and the analytical pilot's gain parameters until the tracking error response characteristics of the analytical pilot compared closely with those obtained from the piloted "man-in-the-loop" simulation of the same task. Validation of the analytical pilot models was accomplished by measuring and comparing the frequency response characteristics of the human and analytical pilots. These analytical pilot models in the TAWDS programs were further verified by comparing the weapon delivery accuracy computed by the TAWDS programs (using the validated analytical pilot models) with measured weapon impact errors obtained from the piloted simulations of air-to-air and air-to-ground weapon delivery. Additional verification was obtained by comparing tracking responses (for similar tracking tasks) obtained from pilot-in-the-loop simulations, from the TAWDS pilot model analytical simulations, and from pilots actually flying the Tactical Weapon Delivery (TWeaD) F-4C aircraft during the flight test evaluation program at Edwards AFB.

After establishing that the TAWDS programs using the multi-axis analytical pilot models realistically simulate fighter aircraft performing weapon delivery, these programs were used to analyze the effects of aircraft flying qualities on weapon delivery effectiveness. These analyses demonstrated that the TAWDS computer programs can be used to evaluate longitudinal and lateral-directional flying qualities characteristics for weapon delivery and to produce a set of flying qualities which provided optimized weapon delivery effectiveness. This TAWDS derived set of flying qualities also compared favorably with a set of flying qualities selected by the simulator pilots to be best for weapon delivery tracking tasks. Consequently, this set of flying qualities was formulated as a proposed guideline for design of tactical fighter

aircraft flying qualities to attain a high probability of kill for these aircraft performing weapon delivery.

The developed TAWDS methodology computes a set of impact error statistics which are transformed into a probability of kill measure of merit by a target vulnerability model. The TAWDS analyses demonstrated that probability of kill is a desirable measure for evaluating the effectiveness of fighter aircraft performing weapon delivery. Therefore, it is recommended that the TAWDS methodology be used by the industry as an analytical procedure for evaluating competitive weapon delivery system designs for fighter aircraft.

Section 2 of this report discusses the features and capabilities of the TAWDS programs. Section 3 discusses the weapon delivery manned simulation studies which were performed to (1) evaluate flying qualities during weapon delivery, (2) provide a data base for developing the analytical pilot models, and (3) validate the weapon delivery ensemble impact error statistics generated by the TAWDS programs. Section 4 describes the development and validation of the analytical multi-axis pilot models. Additional pilot model development analysis results, which show how the multi-axis pilot models can be used for performing manual closures and weapon delivery tasks in an all-digital simulation with different aircraft weapon system configurations, are presented in Volume II of the Flight Control Requirements for Weapon Delivery Background Information Report. Section 5 presents results from the TAWDS weapon delivery effectiveness analyses. Section 6 discusses the TAWDS methodology and appropriate weapon delivery criteria considerations. Finally, Section 7 contains a summary of the results and conclusions emanating from this research study program.

SECTION 2
THE TAWDS PROGRAMS

The TAWDS computer programs enable the digital simulation of contemporary closed loop weapon delivery systems under manual tracking control to be performed. A typical fighter weapon system shown in Figure 1 consists of a pilot and a fighter aircraft with its integrated flight control, sight, and weapon delivery systems. The TAWDS simulation capability is a very valuable design tool for predicting and evaluating weapon delivery accuracy. The development of the TAWDS programs is the most significant accomplishment of this Flight Control Requirements for Weapon Delivery program.

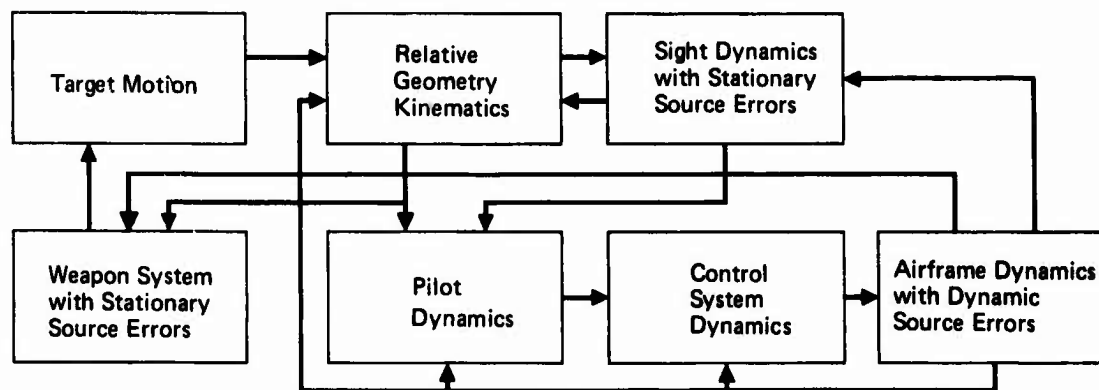
The TAWDS programs propagate stationary and dynamic source errors associated with each weapon delivery task into statistical impact error distributions. Stationary source errors considered stem from the flight profile and system mechanization errors. Dynamic source errors are those due to atmospheric disturbances, weapon release forces, and pilot steering tasks.

The TAWDS programs express the accuracy expected from the fighter weapon system in terms of impact error. Impact error is the distance from an ideal projectile's impact point to the target center, measured in the plane normal to the line of sight and passing through the target. The impact error is printed in the statistical terms of means and variances. The air-to-air statistics are labeled "ensemble pass statistics," and the air-to-ground statistics are labeled "ensemble burst statistics."

The programs simulate three weapon delivery tasks:

- o Air-to-air gunnery
- o Air-to-ground gunnery
- o Air-to-ground bombing

The stochastic procedures most suitable for the modeling of the air-to-air and air-to-ground weapon delivery tasks were chosen. The air-to-air TAWDS program uses the Monte Carlo procedure for computing ensemble pass statistics. The air-to-ground TAWDS program contains both the Monte Carlo and covariance stochastic procedures for computing ensemble burst statistics. State space equations for modeling air-to-ground weapon delivery have been implemented for the covariance procedure because the simulation of air-to-ground wings level weapon delivery tasks can be accurately described by a set of linear time varying equations. The TAWDS programs are unique analytical tools for evaluating the weapon delivery performance of aircraft weapon systems under manual tracking control in terms of weapon impact errors.



GP75-0864-379

Figure 1. Block Diagram of Weapon Delivery Terminal Tracking Tasks

Since the air-to-air and air-to-ground simulations require different equation implementations, TAWDS consists of two separate programs: one for air-to-air, called "TAWDS(AA)" and one for air-to-ground, called "TAWDS(AG)". The descriptions of TAWDS(AA) and TAWDS(AG), and verification of the TAWDS(AG) covariance procedure are presented in this section.

2.1 Functional Description of TAWDS(AA), the Air-to-Air Program

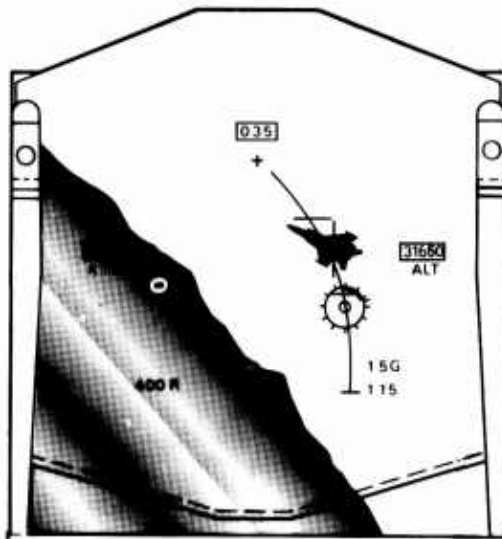
TAWDS(AA) provides a digital simulation and analysis tool for evaluating aim error and bullet impact error in the terminal phase of air-to-air gunnery. The program has provisions for including the effects of

- o Aircraft dynamics
- o Control system characteristics and dynamics
- o Gunsight system characteristics and dynamics
- o Pilot control characteristics and dynamics
- o Attacker-to-target geometry
- o Target maneuvering capability
- o Gun orientation, location, rate of fire, and recoil forces
- o Bullet trajectory characteristics
- o Random wind gusts
- o Stationary source errors

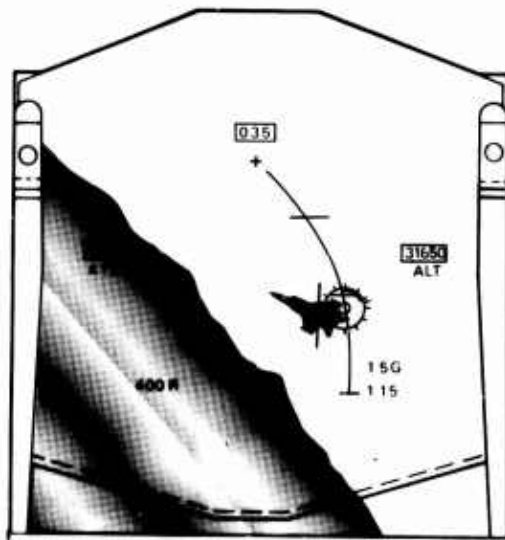
The program models a tracking encounter in either a deterministic mode or a stochastic mode. Typical attack sequences for air-to-air Director and Lead Computing Optical Sight System (LCOSS) gunnery are shown in Figures 2 and 3.

TAWDS(AA) has a deterministic nonlinear six-degree-of-freedom simulation capability. It runs independently of the stochastic simulation, giving nominal time histories of the fighter weapon system. With this deterministic procedure, bullet miss distance can be used to assess system performance. Likewise, the stochastic simulation runs independently of the deterministic simulation, using the Monte Carlo method to determine ensemble pass statistics. Although this method has the disadvantage that many passes are generally required before the ensemble pass statistics converge, it does have the advantage that it accommodates the dynamic coupling between the longitudinal and the lateral-directional control axes. This multi-axis coupling is necessary to simulate air-to-air encounters between highly maneuvering attackers and targets.

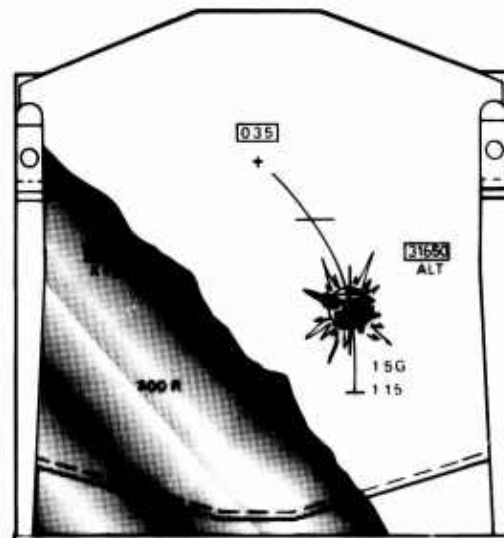
The deterministic mode uses nonlinear time-varying equations to simulate a six-degree-of-freedom attacking aircraft tracking and firing at a five-degree-of-freedom maneuvering target. For the target aircraft, sideslip (β) and β were considered zero during the maneuver. The attacker's aerodynamic coefficients,



1. Maneuver to Move Pipper Slowly Toward Target



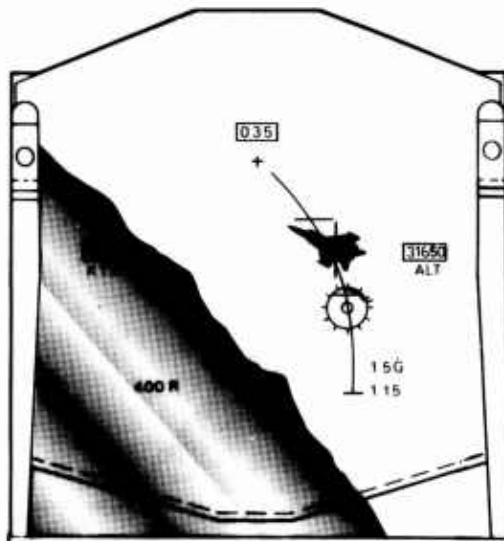
2. Fire When Pipper Reaches Target



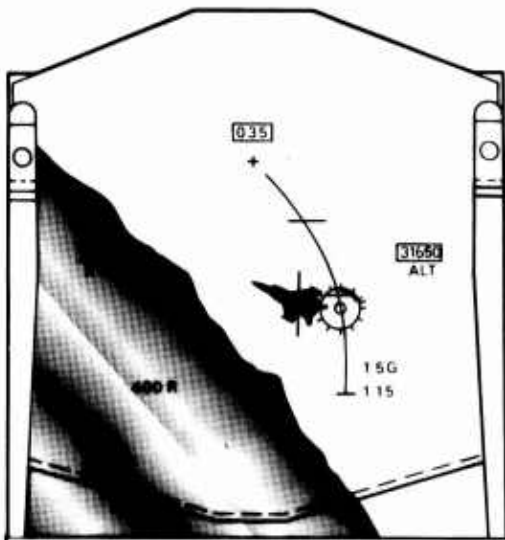
3. Pipper and Bullet Reach Target at Impact

Figure 2. Typical Attack Sequence with Director Sight

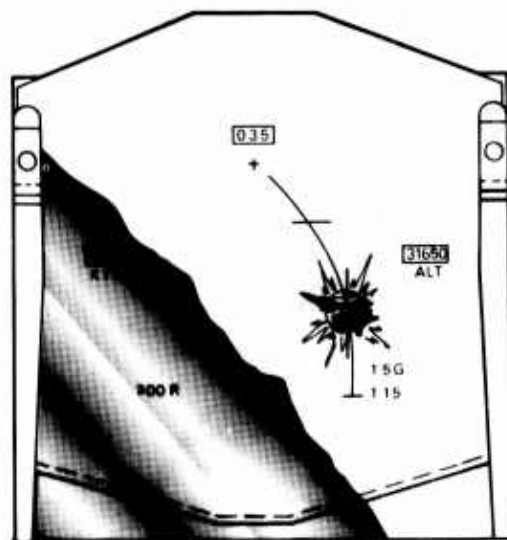
GP75-0884-372



1. Maneuver to Move Pipper Slowly Toward Target



2. Fire t_f Seconds Before Pipper Reaches Target



3. Pipper and Bullet Reach Target at Impact

Figure 3. Typical Attack Sequence with LCOSS Sight

GP 78-0864-371

which are time-varying, are calculated by table look-up. Two sight systems are available: LCOSS and Director. The program output is a set of time histories describing the state of the attacking piloted aircraft, the target aircraft, the resulting tracking error, and bullet trajectories. With this deterministic procedure, system performance can be measured and various combinations of pilot control laws, flight control systems, and fire control systems can be compared in terms of bullet miss distance.

The stochastic mode is a Monte Carlo simulation. Stationary and dynamic source errors are introduced into the deterministic mode in each pass to obtain random aim errors and random bullet miss distances. The stationary errors are introduced at time zero of each pass. They are obtained by sampling from a Gaussian random number generator. Each error has a zero mean and a variance (input). These stationary source errors, which represent measurement or estimation errors, are used in the sight and bullet trajectory calculations. Throughout each pass the dynamic source error of random wind gust perturbs the weapon system simulation. In addition, the dynamic source error of correlated line-of-sight rate measurement noise affects the Director sight model. Gun recoil forces also affect the aim error and bullet miss distance, but because these forces are deterministic, they affect only the means of these performance measures.

After each pass, the performance measures (means and variances) are calculated for the aim error and bullet miss distance. When the ensemble of passes has been made, the performance measures (called ensemble pass statistics) are determined for the ensemble. A large ensemble of passes should be made to guarantee convergence of the ensemble pass statistics. A detailed description of ensemble pass statistics is found in Section 2.3.2.

For a deterministic simulation, only one pass is made per case. For a stochastic simulation, the time histories of only the first pass are printed and plotted. The individual pass statistics of each pass are printed, however, as well as the ensemble pass statistics. TAWDS(AA) has the capability of executing any combination of deterministic and stochastic cases in tandem.

2.1.1 Structure of TAWDS(AA) - The execution of TAWDS(AA) is controlled by the Executive subroutine. This subroutine enables the user to determine whether a deterministic or a stochastic case is to be run, initializes the program at the start of a case, initializes each Monte Carlo pass for a stochastic case, keeps track of each pass, maintains the sequence of subroutine calls, and

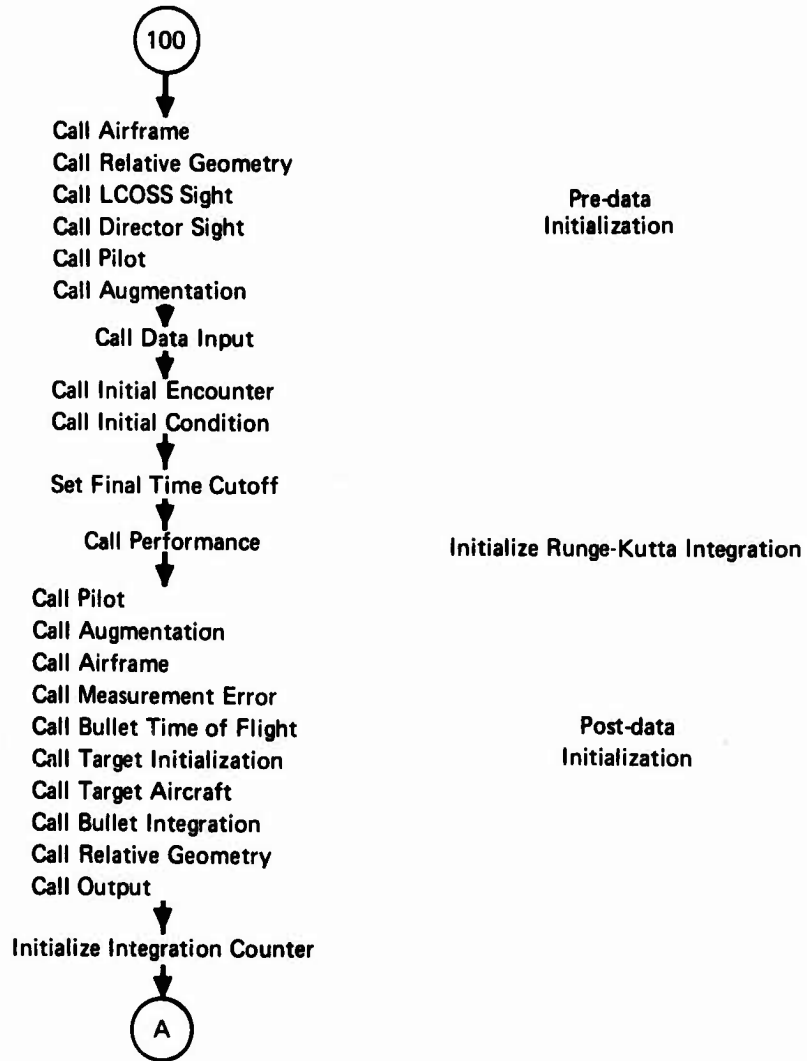
controls output. For a stochastic case, it also controls the tallying of the performance statistics for each pass and for the ensemble. After a case has been executed, it can execute subsequent cases if input data has been provided. The Executive subroutine also contains the logic which determines when the pilot model is to fire a burst. This logic is discussed in Section 2.3.2.

Figure 4 is a flow diagram showing the order in which the Executive subroutine calls the major TAWDS(AA) subroutines associated with the nonlinear six-degree-of-freedom air-to-air terminal tracking task. The logic for tallying the impact error performance statistics is shown in Figure 5.

2.1.2 The Major Subroutines of TAWDS(AA) - The major subroutines called by the Executive subroutine to describe the air-to-air terminal weapon delivery task are the Data Input, Initial Encounter, Initial Condition, Measurement Error, Airframe, Augmentation, Pilot, Target Initialization, Target Aircraft, Relative Geometry, Bullet Time of Flight, LCOSS Sight, Director Sight, Bullet Integration, Performance, Runge-Kutta Integration, and Output Subroutines. These subroutines perform both deterministic and stochastic operations. Data is passed between the subroutines through common blocks.

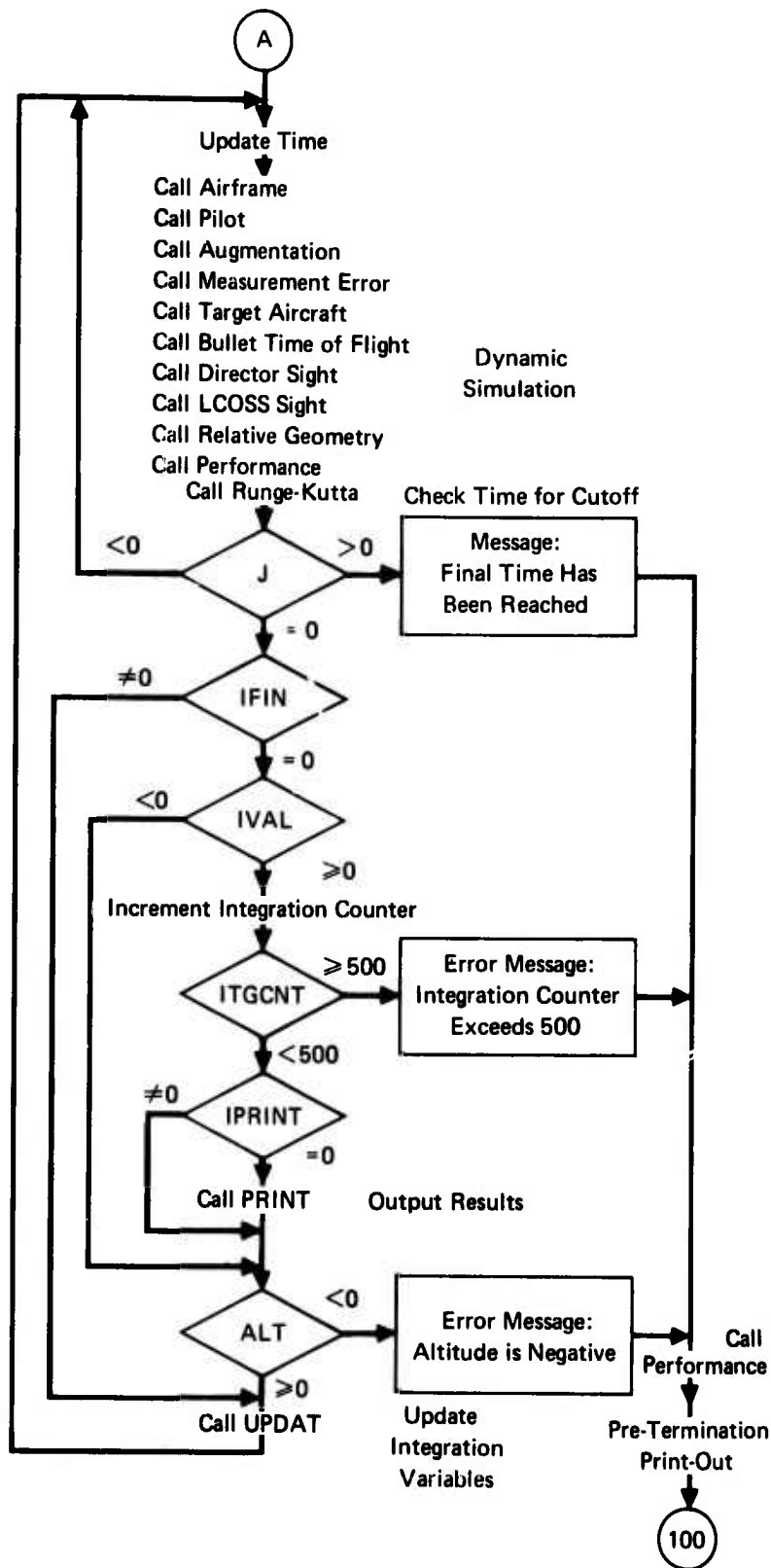
2.1.2.1 Data Input Subroutine - The principal input subroutine is Data Input. A flow diagram describing this subroutine is given in Figure 6. As shown, Data Input calls five subroutines to read the input data. These subroutines are Control Namelist, Integration Namelist, Weapon Task Namelist, Augmentation Namelist, and Airframe Namelist. Subroutine Control Namelist reads the program control parameters which establish a nominal case or which merge subsequent data sets with the nominal case. The Integration Namelist reads data pertaining to the integration routine. The Weapon Task Namelist reads data describing the aircraft in its weapon delivery task. This data pertains to airframe, pilot, relative geometry, target, sight parameters, ballistics, stationary and dynamic source errors, and Monte Carlo execution. It does not include the flight control system, or airframe aerodynamic tables. The Augmentation Namelist subroutine reads data describing the flight control system. The Airframe Namelist subroutine reads the tables of data that define the nonlinear force and moment aerodynamic coefficients in the equations of motion of the attacker. When all data has been read, Data Input converts certain angular variables from degrees to radians.

2.1.2.2 Initial Encounter Subroutine - Initial Encounter allows the user to select various combinations of predetermined initial encounter conditions. The user selects the desired encounter by entering a coded nine digit integer variable. The digits reading from the left to the right sequentially represent:



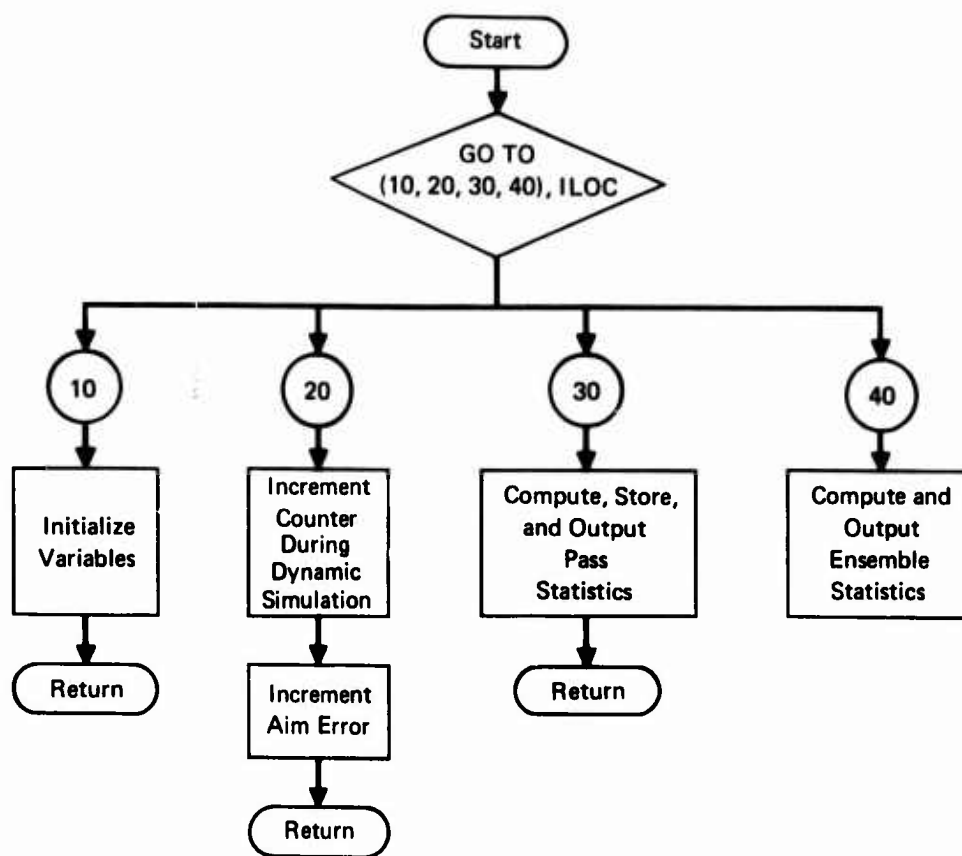
GP75-0864-85

Figure 4. Flow Diagram of TAWDS(AA) Executive Subroutine



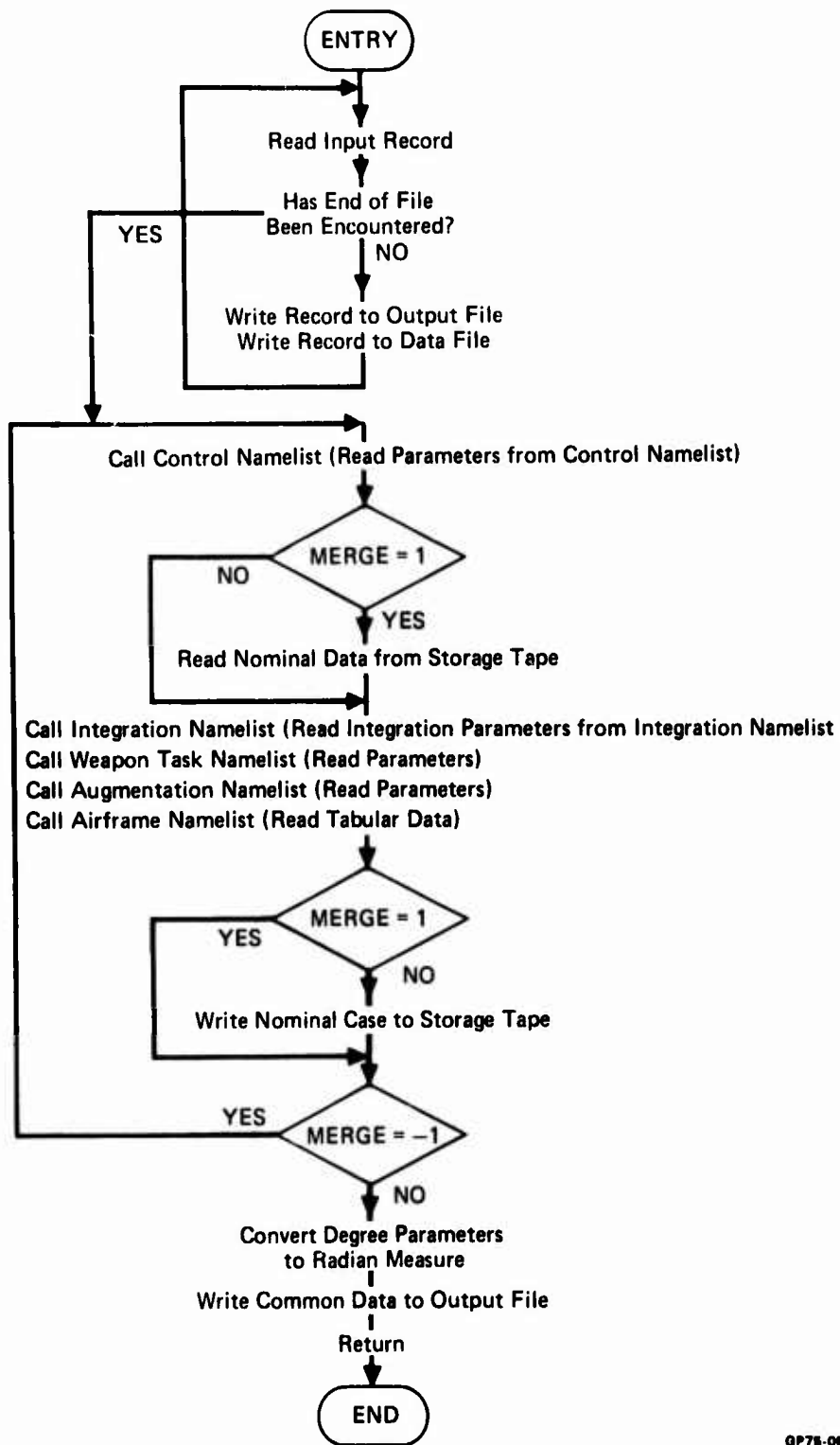
GP78-0884-112

Figure 4. Flow Diagram of TAWDS(AA) Executive Subroutine (Concluded)



GP75-0864-84

Figure 5. Performance Logic in TAWDS(AA) Executive Subroutine



GP75-0864-113

Figure 6. Flow Diagram of Data Input Subroutine

- o K_L - factor to perturb the magnitude of the initial lead angle (see Figure 7)
- o θ_L - angle of rotation of the lead angle plane, used to perturb the orientation of the initial lead angle (see Figure 7)
- c θ_A - attacker pitch angle
- o ϕ_A - attacker roll angle
- o α_A - attacker body angle of attack
- o M_A - attacker Mach number
- o h_A - attacker altitude
- o R - range
- o \dot{R} - range rate

Figure 8 shows a nine-by-nine matrix which is the key for a user-selected set of initial encounter conditions. If the user desires some other initial encounter condition, the control logic in Initial Encounter will have to be modified.

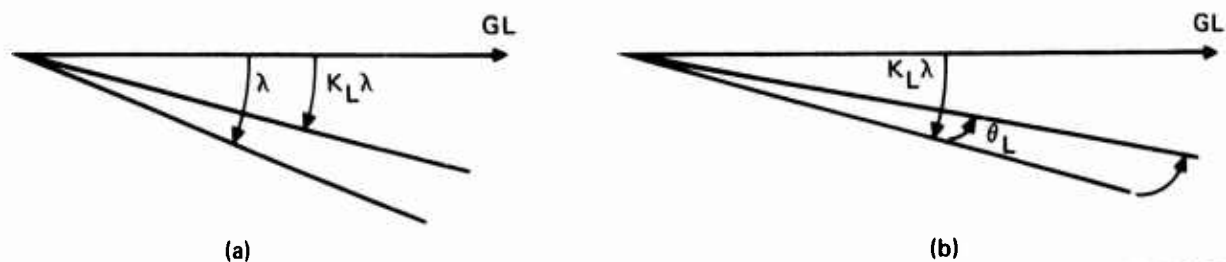
Initial Encounter also contains many combinations of predetermined target maneuvers. In TAWDS(AA), an encounter can be broken into as many as ten separate target maneuvers. Each maneuver is specified by the time at which it begins and by the values of the maneuvering variables. (A maneuver ends when the next maneuver begins.) Each maneuver is specified by a coded, user-selected four-digit integer variable. These digits sequentially represent:

- o t - time at which the maneuver begins
- o \dot{B}_T - commanded target bank rate
- o $\dot{\alpha}_T$ - commanded target angle of attack rate
- o \dot{TH}_T - commanded target thrust rate

Figure 8 also shows a nine-by-four matrix which is the key for a user-selected set of target maneuvers. If the user desires some other target maneuvers, the Initial Encounter subroutine's control logic will have to be modified.

2.1.2.3 Initial Condition Subroutine - Initial Condition generates the initial values for the pitch, roll, and yaw rates and the stabilator deflection of the attacking aircraft. The subroutine is called by Executive subroutine after the call to Data Input and Initial Encounter at the start of a new case, or, for a stochastic case, at the start of each pass. In this subroutine, the lift and pitch angular acceleration equations from the general six-degree-of-freedom equations of motion are solved for the pitch rate and stabilator deflection of the attacking aircraft. The computation of these variables is based on the attacker's initial velocity, altitude, and angle of attack, which

λ : Lead Angle
 K_L : Lead Angle Magnitude Factor for Initial Perturbation
 θ_L : Lead Angle Plane Rotation for Initial Perturbation



GP75-0864-94

Figure 7. Initial Lead Angle Perturbation Quantities

index Number	Initial Conditions									Target Maneuvers			
	K_L	θ_L (deg)	γ (deg)	B (deg)	α (deg)	M	h (K ft)	R (ft)	\dot{R} (ft/sec)	(t) (sec)	\dot{B} (deg/sec)	$\dot{\alpha}$ (deg/sec)	\dot{TH} (K lb/sec)
0	0.5	-20	-60	-135	3	0.5	5	500	-250	0	-90	-3	0
1	0.6	-15	-30	-75	4	0.6	10	1000	-200	4	-60	-2	0.5
2	0.7	-10	-20	-60	5	0.7	15	1500	-150	6	-30	-1	1.0
3	0.8	-5	-10	-45	6	0.8	20	2000	-100	8	-10	-0.5	1.5
4	0.9	0	-5	0	7	0.9	25	2500	-50	10	0	0	2.0
5	1.0	5	0	45	8	1.0	30	3000	0	12	10	1	2.5
6	1.1	10	10	60	9	1.1	35	3500	50	14.5	30	1.5	3.0
7	1.2	15	20	75	10	1.2	40	4000	100	17	60	2.0	3.5
8	1.3	20	30	135	12	1.3	45	4500	150	20	90	3	4.0
9	1.4	25	60	160	16	1.4	50	5000	200	22.5	180	4	4.5

GP75-0864-211

Figure 8. TAWDS(AA) Encounter Parameter Matrix

are determined in the Initial Encounter subroutine. The attacker's initial roll and yaw body rates are determined by the effect of gravity, with the aileron and rudder surface deflections set to zero. These initializations result in small initial tracking error transients. Initial Condition also initializes the attacker's body attitude direction cosine matrix with respect to the earth and the attacker's position and velocity integration arrays.

2.1.2.4 The Measurement Error Subroutine - Measurement Error calculates the stationary errors that initialize each stochastic simulation pass. It also calculates the filter that models the dynamic error for the Line Of Sight (LOS) rate measurement for use in the Director Sight subroutine. Measurement Error is called by the Executive subroutine after the call to Initial Condition. Stationary errors can occur in:

- o Air speed
- o Angle of attack
- o Sideslip angle
- o Altitude
- o Line of sight range
- o Line of sight range rate
- o Muzzle velocity
- o Elevation gunline orientation
- o Traverse gunline orientation
- o Elevation HUD orientation
- o Traverse HUD orientation

These errors are calculated by sampling from a Gaussian random number generator. Each error has a zero mean and a variance obtained from input data. These errors represent measurement errors, or deviations from nominal, of those parameters used in the sight or bullet integration equations. For example, the attacker air speed is measured, while the muzzle velocity of a bullet to be fired is the nominal value plus its deviation. The errors are programmed as biases, since sensor errors are usually biases over time intervals of several seconds. They are treated as stationary errors because TAWDS(AA) simulates a fighter weapon delivery task in its terminal phase, where the error sources are assumed to be in steady state.

The Measurement Error subroutine also sets up the dynamic source error filter that is provided in the Director Sight subroutine. In Director Sight, correlated noise, representative of the dynamics associated with estimating radar LOS angle rates, is added to the correct LOS angle rate. This correlated

noise is obtained by passing white noise, whose standard deviation is referenced to a range of 1500 feet, through a second-order low-pass filter. This filter is calculated in the Measurement Error subroutine by using input parameters that describe its damping and bandwidth. The filter is programmed in discrete form, using the state transition matrix approach. As programmed, the same filter parameters are used in the elevation and traverse axes; however, there is a separate standard deviation for each axis.

2.1.2.5 The Airframe Subroutine - The Airframe subroutine defines generalized six-degree-of-freedom airframe equations of motion. These equations model the attacker aircraft's forward acceleration and wind angle rates, the body axis angular acceleration, the Euler angle rates, and the velocity components in earth coordinates. These variables are integrated by the Runge-Kutta Integration subroutine. The subroutine also calculates the aircraft's accelerometer measurements. The airframe equations include gun recoil forces and vertical and lateral wind gusts. The airframe coefficients can be in either the stability or body axis system.

Significant features of this airframe mechanization are provisions for additional longitudinal control surfaces, the capability of simulating aircraft moments with a shifted center of gravity, and the representation of flexibility effects on the aircraft. The equations programmed in the Airframe subroutine are presented in Appendix I.

The nonlinear aerodynamic derivatives used by the airframe equations of motion are in tabular form. The independent variables in the tables have been selected to represent the variation of the coefficient with changes in Mach number, angle of attack, and in some cases stabilator surface deflection, rudder surface deflection, or sideslip angle.

2.1.2.6 The Augmentation Subroutine - The Augmentation subroutine simulates the flight control system of the attacking aircraft. It calculates surface deflections for split vertical stabilizers (differential tail), ailerons, spoilers, rudder, horizontal stabilizer (stabilator), and horizontal canard. These flight control system models can be used to mathematically describe a variety of contemporary fighter flight control systems such as the flight control laws developed in the Tactical Weapon Delivery (TWeAD) Program (References 1-5), the Survivable Flight Control System (SFCS) Program (References 6-8), the Multimode Program (References 9-10), and other current fighter and attack aircraft. The structure of the TAWDS(AA) model allows for decoupling design techniques to enable the mechanization of longitudinal direct force

modes for precise attitude or flight path control. This subroutine includes not only feedback control laws but also interconnects, which couple pilot command inputs. A description of the generic flight control system model for the TAWDS(AA) program is given in Appendix I.

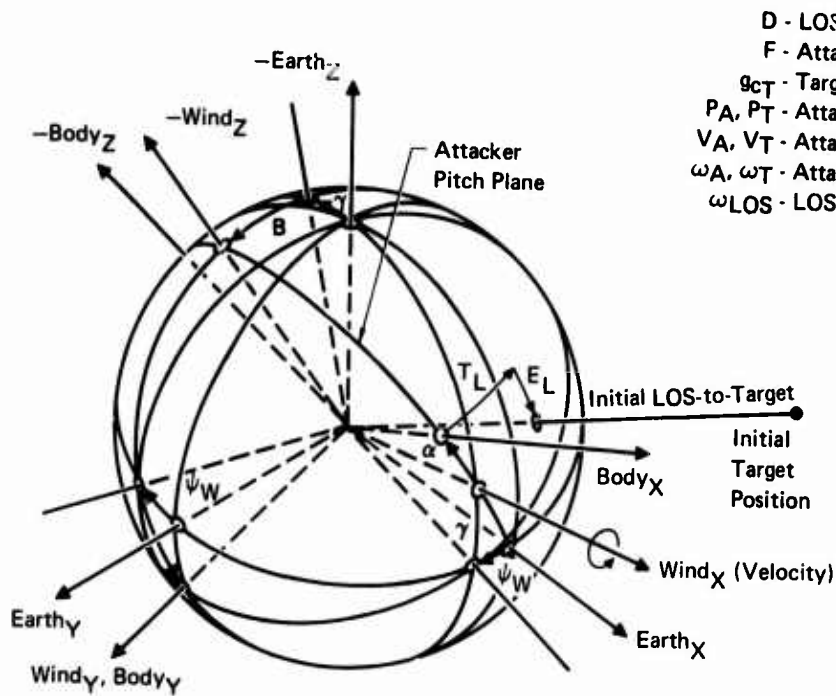
2.1.2.7 The Pilot Subroutine - Using the elevation and traverse tracking errors along with the relative bank angle between the target and the attacking aircraft, the Pilot subroutine generates an input to the longitudinal control system for nulling the elevation error and inputs to the lateral-directional control system for nulling the traverse error. The multi-axis pilot models, developed in this study program, are discussed in Section 4.

2.1.2.8 The Target Initialization Subroutine - The Target Initialization subroutine initializes the inertial quantities of the target at time zero to satisfy the selected encounter geometry. It initializes the target so that the relative geometry between the attacker and target is in steady state. The target inertial quantities, which are initialized, are earth axis position, earth axis velocity, flight path angle, wind axis angular rates, turning plane, and turning g. The encounter is initialized in the terminal phase with the target and pipper coincident or with a selected number of degrees of perturbation. To find the tracking error angle, pipper angle, and lead angle, a special call is made to the selected sight system subroutine. The geometry and associated equations on which the target initialization is based are shown in Figure 9.

2.1.2.9 The Target Aircraft Subroutine - The Target Aircraft subroutine simulates the target aircraft. Target Aircraft has only one entry, but it is divided into two parts. The first part initializes the non-inertial quantities of the target after the call to Target Initialization. This part is skipped after initialization of a pass. The second part contains the dynamic equations that simulate the target. The target model employs simplified five-degree-of-freedom equations of motion (zero sideslip is assumed).

In Target Initialization, the target's inertial earth axis position, earth axis velocity, and wind axis angular rates are computed at time zero. Using these inputs, the Target Aircraft subroutine at time zero computes the target's thrust, angle of attack, attitude, and load factor. The geometry and associated equations used in this initialization are described in Figures 10 through 12.

After initialization, the Target Aircraft subroutine generates the target position, velocity, and attitude in earth coordinates at each time interval throughout the simulation. Target maneuvers are specified by the time at which the maneuver takes place and by the values of the maneuvering variables:



D - LOS Range
 F - Attacker Inertial Force Vector
 g_{cT} - Target Centripetal Acceleration Vector
 P_A, P_T - Attacker, Target Position Vectors
 V_A, V_T - Attacker, Target Velocity Vectors
 ω_A, ω_T - Attacker, Target Angular Rate
 ω_{LOS} - LOS Angular Rate

Attacker

$$\bar{\omega}_A = \frac{\bar{V}_A \times \frac{\bar{F}}{m}}{|\bar{V}_A|^2}$$

Target

$$\bar{P}_T = \bar{P}_A + D \cdot \hat{1}_{LOS}$$

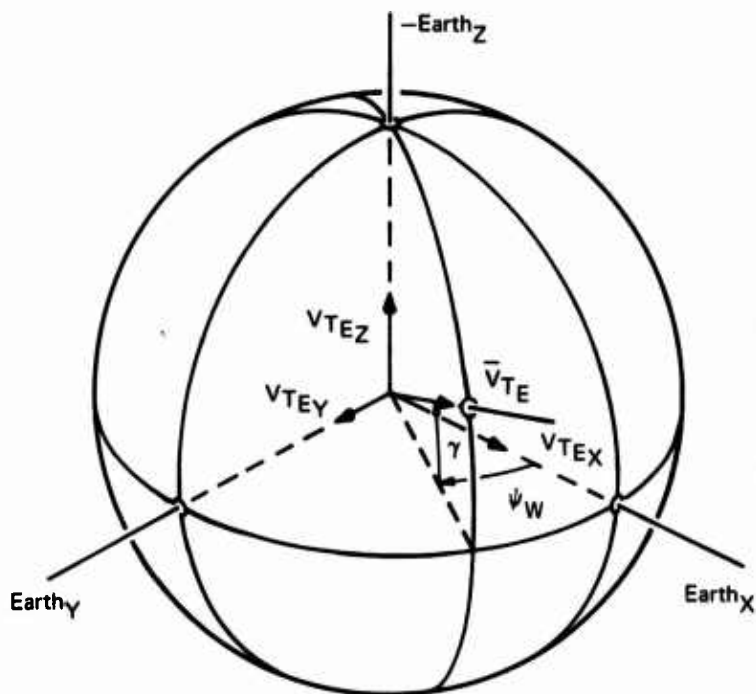
$$\bar{V}_T = \bar{V}_A + \bar{\omega}_{LOS} \times \bar{D} + \dot{\bar{D}}$$

$$\omega_T = \omega_A + \dot{T}_L + \dot{E}_L$$

$$g_{cT} = \frac{\bar{\omega}_{LOS} \times \bar{V}_T}{g}$$

Figure 9. Summary of Target Initialization

GP75-0864-100



$$\psi_W = \tan^{-1} \left(\frac{V_{TEY}}{V_{TEX}} \right)$$

$$\gamma = \tan^{-1} \left(\frac{-V_{TEZ}}{\sqrt{V_{TEX}^2 + V_{TEY}^2}} \right)$$

V_T - Target Velocity Vector
 ψ_W - Target Heading Angle
 γ - Target Climb (Flight Path) Angle

Figure 10. Target Heading and Climb Angle Initialization

GP75-0864-101

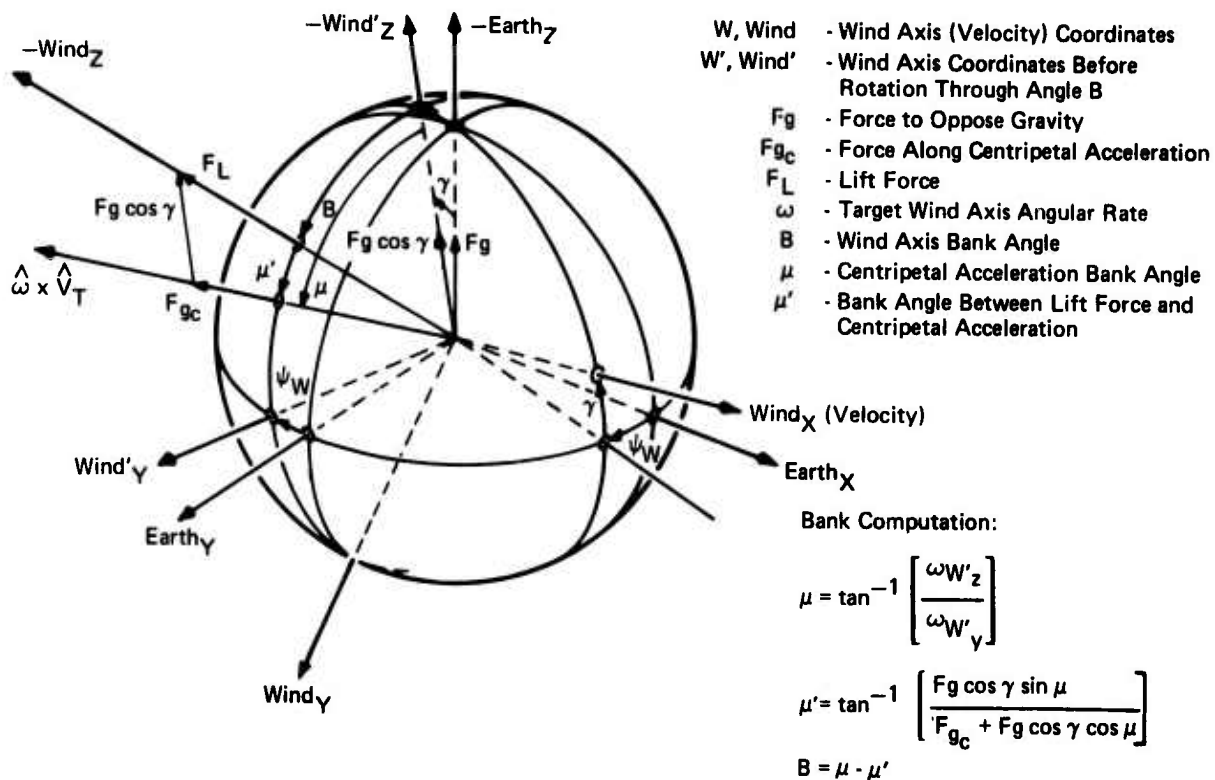


Figure 11. Target Bank Angle Initialization

C_L, C_D - Lift, Drag Aero Coefficients
α - Body Angle of Attack
α_T - Thrust Angle of Attack

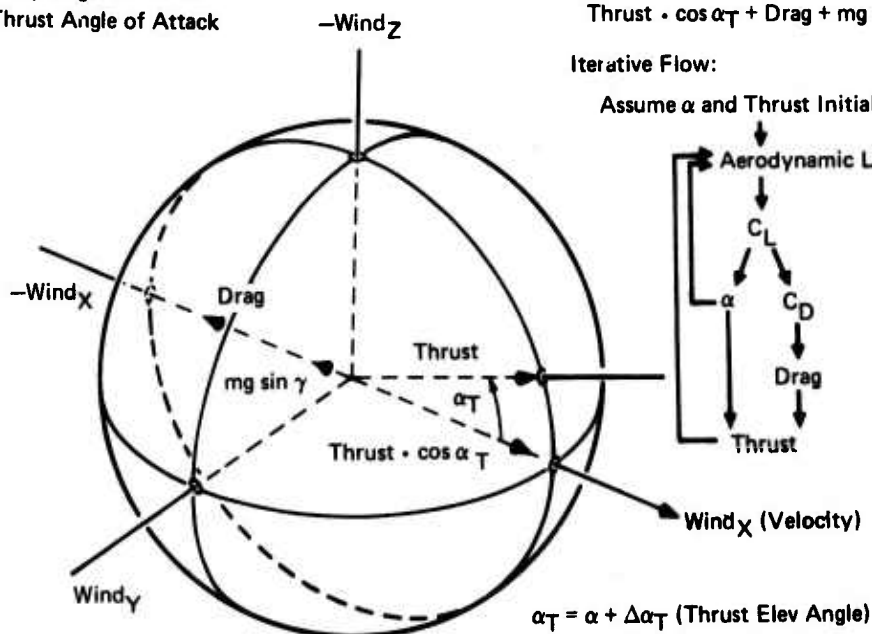


Figure 12. Target Thrust and Angle of Attack Initialization

GP75-0864-97

(1) commanded target bank rate, (2) commanded target angle of attack rate, and (3) commanded target thrust rate. The target flies at constant thrust unless it is modified by a commanded thrust rate.

Lift and drag characteristics used in the target airframe force equations are derived from tabular data as functions of Mach number, angle of attack, and altitude. These data yield trimmed (C_M equal zero) lift coefficients and the corresponding drag coefficients. The tabular data is contained in one of Target Aircraft's subroutines. At present this data represents the F-4E aircraft.

The target trajectory is computed two seconds into the future and stored in data arrays. This data is used in computing the projectile time of flight, gun aiming error, and bullet miss distance.

2.1.2.10 The Relative Geometry Subroutine - The Relative Geometry subroutine computes the elevation and traverse tracking errors throughout an encounter. For a stochastic case, it also records these tracking errors during each encounter, and calculates their means and variances for each pass and for the ensemble of passes. It does not calculate the miss distance statistics, which is done in the Performance subroutine.

2.1.2.11 The Bullet Time of Flight Subroutine - This subroutine calculates the bullet time of flight for use in the sight subroutines. It uses a method that approximates integrating the bullet to the target range but is much faster. When a bullet is actually fired, the correct bullet time of flight is calculated by integrating the bullet to target range in the Bullet Integration subroutine. Appendix II discusses the time of flight computations in detail.

2.1.2.12 The LCOSS Sight Subroutine - The LCOSS Sight subroutine simulates the Lead Computing Optical Sight System and computes the sight lead angle with respect to the attacking aircraft gunline. It contains the basic characteristics associated with advanced LCOSS or damped predictive tracer sights. These characteristics include the use of (1) ownship body rates, (2) ownship load factor as an estimate of target acceleration, and (3) attacker angle of attack and airspeed to account for ballistic curvature. Appendix II presents the LCOSS sight equations.

2.1.2.13 The Director Sight Subroutine - The Director Sight subroutine simulates the Director sight system and computes the sight lead angle with respect to the attacking aircraft gunline. The primary difference of the Director sight from an LCOSS sight is the use of Line Of Sight (LOS) angle

rates instead of ownship body rates in computing lead angle. The equations for modeling the Director sight are presented in Appendix II.

2.1.2.14 The Bullet Integration Subroutine - This subroutine computes the inertial trajectory of a bullet. After the bullet trajectory has been computed, the Bullet Integration subroutine determines: (1) the bullet miss distance when the bullet and the target ranges from the attacker are equal, and (2) the time of flight required for the projectile to reach the target range. These two calculations are made by using the projected target position, which has been stored two seconds ahead.

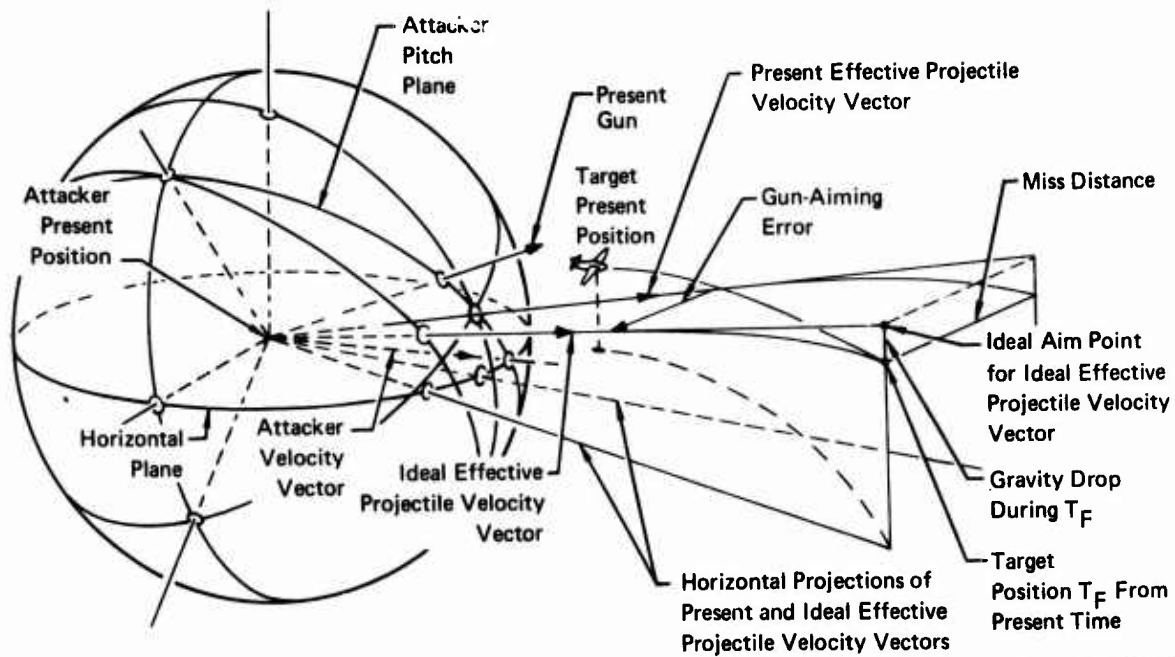
The bullet miss distance (depicted in Figure 13) is determined in feet, and then also calculated in milliradians by using the bullet range. It is printed out in attacker gun coordinates.

Since a maximum of 40 target positions are stored, the bullet is integrated through a maximum of 40 intervals (which corresponds to 2 seconds for an integration interval of 0.05 seconds). If the bullet does not reach the future target position within the 40 integration intervals, a miss distance of 999 feet is printed.

A block diagram of Bullet Integration is shown in Figure 14. The bullet's initial position and velocity are computed in the Bullet Initialization subroutine. The "BULLET VELOCITY UPDATE" and "BULLET POSITION UPDATE" blocks are defined by equations given in Figure 15. This figure also defines the bullet drag constants K_D and C_D . The K_D equation is a curve fit to the data presented for 20 mm projectiles in Armament Memorandum Report 65-30, Ballistic Division, Eglin Air Force Base.

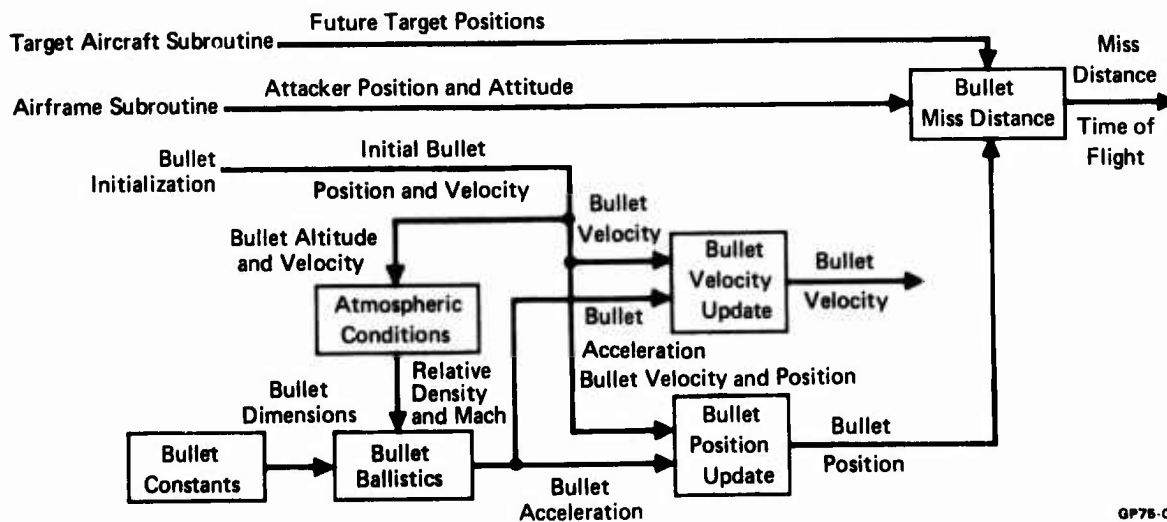
Bullet Integration is called by the Executive subroutine at time zero, to initialize the bullet miss distance. When the Executive subroutine has determined that the attacker has fired a bullet, it again calls Bullet Integration to integrate the bullet to the target range and to calculate the bullet miss distance and time of flight.

2.1.2.15 The Performance Subroutine - The Performance subroutine, which is called during a stochastic simulation, records the bullet miss distance calculated in Bullet Integration and computes the miss distance statistics at the end of each pass and at the end of the ensemble of passes. The Executive subroutine calls Performance at each pass initialization to zero the bullet miss distance accumulators. Every time a bullet is fired, the Executive subroutine calls Performance to add the longitudinal and lateral miss distances to their accumulators. At the end of each pass, Executive again calls Performance to calculate the miss distance statistics. Then, at the end of the



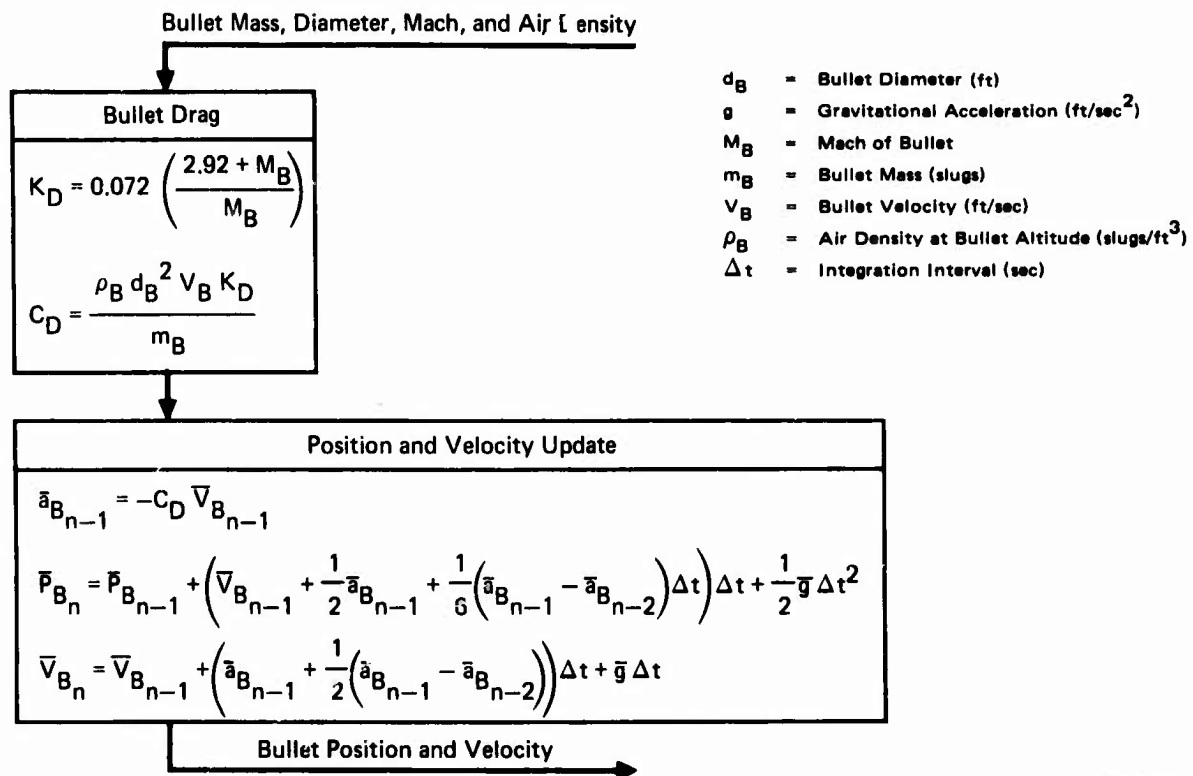
GP75-0864-98

Figure 13. Geometry of Gun Error Computation



GP75-0864-99

Figure 14. Block Diagram of the Bullet Integration Subroutine



GP76-0864-80

Figure 15. Definition of Bullet Drag, and Position and Velocity Update

ensemble of passes, Executive calls the Performance subroutine to determine the bullet miss distance ensemble statistics. (The tracking error ensemble pass statistics are calculated in the Relative Geometry subroutine.)

2.1.2.16 The Runge-Kutta Integration Subroutine - This integration subroutine determines the solution to an arbitrary set of simultaneous ordinary differential equations using a fixed step fourth-order Runge-Kutta technique.

2.1.2.17 The Output Subroutine - The output of TAWDS(AA) consists of:

- 1) A card image copy of the input
- 2) Six statements which tell what data is being read for a case
- 3) Dumps from common blocks and subroutines at the start of a case
- 4) Time histories of attacker and target positions in earth coordinates
- 5) Time histories of attacker aircraft variables
- 6) Time histories of pilot aircraft commands
- 7) Time histories of bullet trajectories and sight and geometry variables
- 8) Time history plots of attacker aircraft and tracking error variables
- 9) Stationary source errors for each pass
- 10) Tracking error statistics for each pass and for the ensemble of passes
- 11) Miss distance statistics for each pass and for the ensemble of passes.

2.2 Functional Description of TAWDS(AG), The Air-to-Ground Program

The TAWDS(AA) program with its Monte Carlo statistical procedure was developed for maneuvering flight associated with aerial combat. In this section the TAWDS(AG) program with its principal stochastic procedure, the covariance method, was developed for wings level air-to-ground weapon delivery. TAWDS(AG) provides a digital simulation and analysis tool for evaluating the tracking error and weapon impact error of an attacking aircraft in the terminal phase of its air-to-ground weaponry task. This analysis program, similar to TAWDS(AA), includes the effects of:

- o Aircraft dynamics
- o Aircraft control system characteristics and dynamics
- o Sight system characteristics and dynamics
- o Pilot control characteristics and dynamics
- o Pilot remnant for linearized pilot models
- o Attacker-to-target geometry dynamics
- o Weapon orientation, location, and release forces
- o Gun rate of fire
- o Weapon trajectory characteristics
- o Random wind gust, discrete gust, and wind shear
- o Stationary source errors.

TAWDS(AG) simulates air-to-ground gunnery with Continuously Computed Impact Point (CCIP) or Fixed Depressed Reticule (FDR) gunsights, and air-to-ground bombing with the Future Impact Point (FIP) bombsight. The air-to-ground gunnery attack sequence is illustrated in Figure 16. In such an attack with an FDR sight system, the pilot tracks the target and fires when the aircraft simultaneously achieves the most attainable set of speed, flight path, and altitude or range conditions corresponding to the FDR setting. The tracking task for the CCIP gunnery sight differs from that with the FDR sight in that the gunfire solution is continuous so long as the pilot can maintain the reticle on the target.

For air-to-ground bombing a derivative CCIP sight system (FIP) is implemented. In FIP bombing, a reticle is continuously displayed on the HUD to indicate where the bomb will impact when it is automatically dropped at the future release conditions if present flight conditions are maintained. The pilot's task is to continually maintain the FIP reticle on the target until bomb release occurs. Another symbol, the Displayed Impact Point (DIP) cross, indicates the impact point for an immediately released bomb. When it becomes coincident with the FIP reticle, the bomb is released. The profile and HUD presentations for this system are shown in Figure 17.

TAWDS(AG) treats the air-to-ground terminal weaponry problem as a Gauss Markov random process, using the covariance method to determine ensemble statistics. This method has the advantage of using only one pass to obtain performance statistics, but it does require linear equations. As discussed in Reference 11, linear equations can simulate an attacker realistically, even in high g maneuvers. These linear equations are generated by perturbing nominal nonlinear equations. To effect this method for air-to-ground weapon delivery, two simulations are run concurrently: a nominal nonlinear deterministic simulation and a linear stochastic simulation. Because the nominal traverse error is zero for fixed forward-firing guns and for bombs, only the elevation channel is modeled deterministically. The stochastic simulation consists of integrating the mean and covariance matrix equations derived from the linearized equations. (The mean equations are actually deterministic.) For gunnery it is also necessary to simulate the bullet round-to-round autocorrelation matrix.

The stochastic simulation includes both the elevation and the traverse channels. Because the complexity of the covariance technique increases by the square of the number of states, it is desirable to keep the system small. For

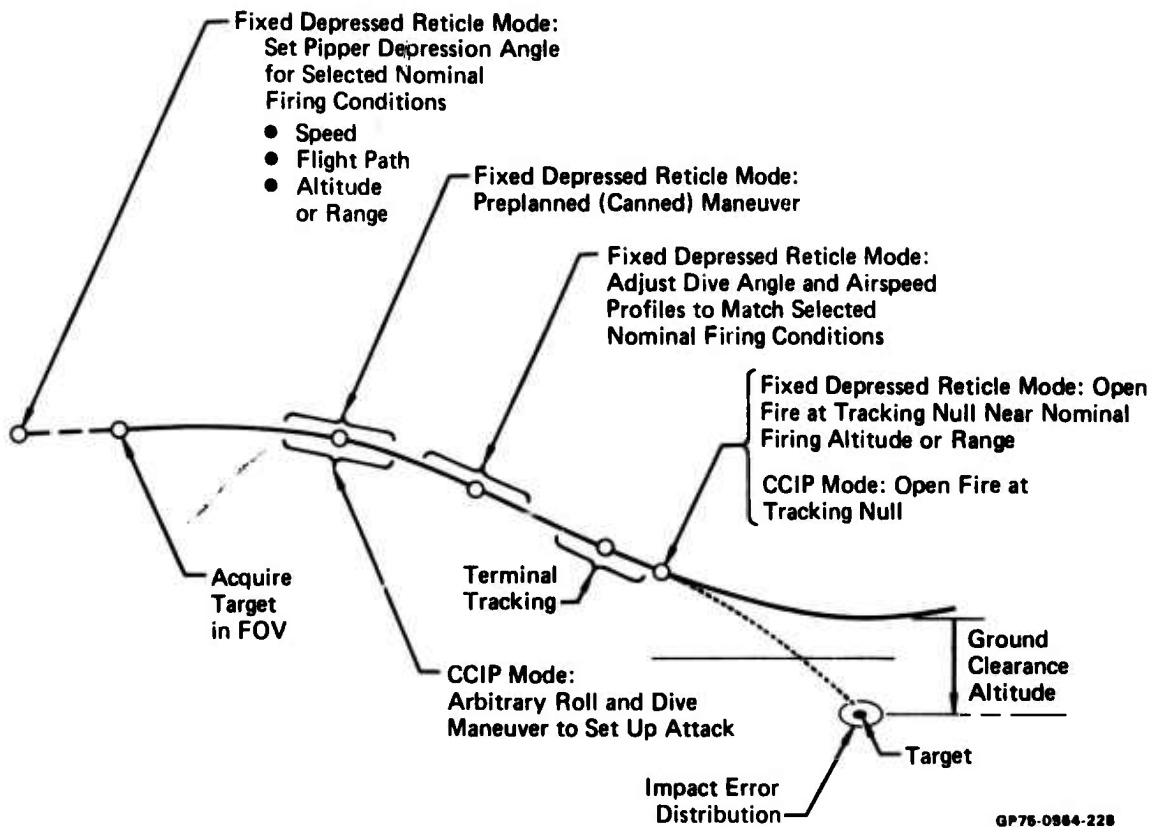
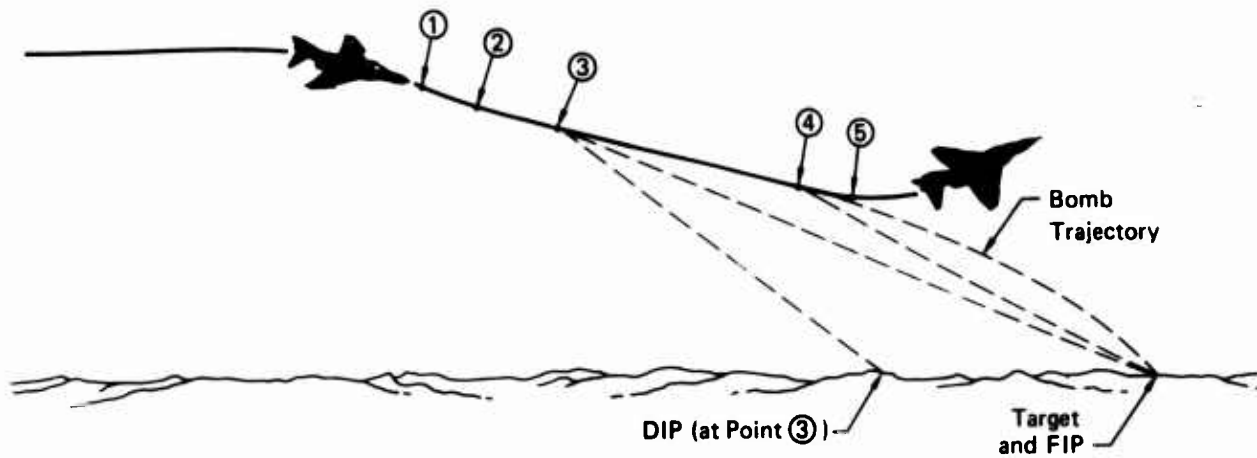
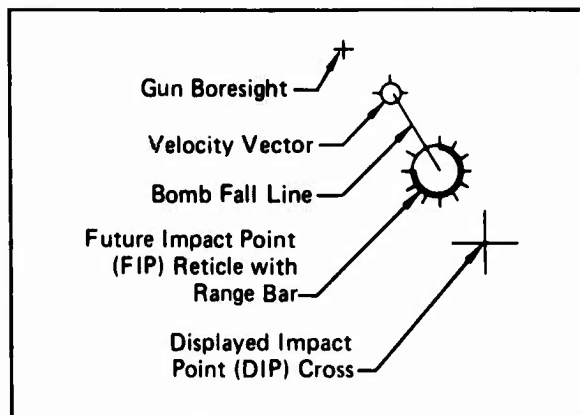


Figure 16. Air-to-Ground Gunnery Attack Sequence



- ① Air-to-Ground Delivery Mode Entered
- ② Aircraft Maneuvered to Place FIP on Target
- ③ FIP on Target
- ④ DIP Moves into Coincidence with Target- Bombs Automatically Released
- ⑤ Start of Pull-up Maneuver

Head-Up Display



GP75-0084-230

Figure 17. Profile View of FIP Bombing Attack

the air-to-ground system, the equations can be decoupled into two smaller systems: one for elevation and one for traverse. TAWDS(AG) simulates these two 22 state systems rather than one coupled 44 state system.

To determine the round-to-round correlation between every pair of gunnery rounds is prohibitive in terms of computer core and time. Therefore, TAWDS(AG) computes the correlation between the initial round of the burst and subsequent rounds. To calculate the other round-to-round correlations, stationarity is assumed; it is assumed that the correlation between rounds is only a function of the time interval between them and not a function of their actual firing times. This assumption has yielded results which compare favorably to those obtained by Monte Carlo simulation.

The nominal nonlinear deterministic simulation includes a three-degree-of-freedom aircraft (forward velocity, normal velocity, and pitch rate), a generic longitudinal control system, a choice of three sight systems (Fixed Depressed Reticule (FDR) and CCIP for gunnery, and FIP for bombing), a linear fourth order pilot, and a weapon (bullets or a bomb). The stochastic simulation linearizes the above and incorporates the traverse channel, with the aircraft having six degrees-of-freedom. It also adds pilot remnant and random wind gust to the covariance equations, and gun recoil forces, wind shear, and discrete gust (all three treated deterministically) to the mean equations.

Besides the dynamic source errors (gun recoil forces, wind shear, discrete gust, pilot remnant, and random wind gust), stationary source errors also affect the aim error (tracking error plus stationary source error effects) and are included in the stochastic model. The stationary source errors originating in the sight systems are listed in Figures 18 and 19. They include measurement, equipment misalignment, and sight mechanization errors. Appendix III discusses stationary source errors in detail. In TAWDS(AG) the mean of each stationary source error is assumed zero over an ensemble of passes. Consequently, the stationary source errors affect only the variance.

The mean and covariance equations model the states of the attacker aircraft, the control system, the sight system, the pilot, and geometry, but they do not model the actual release of the weapon at firing time. Therefore, the means and variances of the weapon impact errors are not a direct calculation of the above linear equations. To determine the means and variances of the impact error, time-varying sensitivity matrices are calculated when a weapon is released. These sensitivity equations propagate the means and variances of

CCIP Sight	Fixed Depressed Reticle Sight	Future Impact Point Sight
True Airspeed	True Airspeed	True Airspeed
Pitch Angle	Pitch Angle	Pitch Angle
Pipper Elevation Positioning	Pipper Elevation Positioning	Pipper Elevation Positioning
Range	Range	Range
Radar Elevation Positioning		Radar Elevation Positioning
Muzzle Velocity	Muzzle Velocity	Fiection Velocity
Gun Elevation Boresight	Gun Elevation Boresight	Rack Release Time Delay
Along-Track Velocity	Aircraft Weight Estimation	Along-Track Velocity
Vertical Velocity	Pilot Timing	Vertical Velocity
	Angle-of-Attack	

GP75-0864-421

Figure 18. Along-Track Stationary Source Errors for Air-to-Ground Weapon Delivery

CCIP Sight	Fixed Depressed Reticle Sight	Future Impact Point Sight
Sideslip Angle	Sideslip Angle	Sideslip Angle
Pipper Positioning	Pipper Positioning	Pipper Positioning
Gun Boresight	Gun Boresight	
Cross-Track Velocity	Bank Angle	Cross-Track Velocity
Heading Angle		Heading Angle

GP75-0864-376

Figure 19. Cross-Track Stationary Source Errors for Air-to-Ground Weapon Delivery

the tracking errors to the target to get the impact error statistics. The source error variances, which are input data, are also propagated by the sensitivity matrices to contribute to the impact error variances. There is a sensitivity matrix for each channel: elevation and traverse. Appendix III discusses these sensitivities.

Computation of the impact statistics is restricted to zero initial conditions in the covariance matrices. In general, the user can exercise TAWDS(AG) by initializing the tracking error components of the elevation and traverse matrices and then can note the tracking error component responses as affected by the dynamics of the selected flight control system and sight configuration. For impact statistics, however, it is unrealistic to assume that a randomly selected weaponry pass will match all nominal delivery conditions except for the initial tracking error. Other components, including off-diagonal components of the covariance matrices, must also be initialized to realistically represent initial conditions for an ensemble of passes. A general rule for initializing the full covariance matrices for all state variables is not presently formulated.

For runs in which the only dynamic inputs (other than gun recoil, wind shear and discrete gust) are pilot remnant and random wind gust, experience has shown that the variance and covariance states of the covariance matrices reach a near steady state condition after an initialization period of approximately two seconds. Therefore, the problem of choosing appropriate initial conditions for the covariance matrices can be circumvented by using an appropriate initialization period before weapon firing. To exercise the TAWDS(AG) option of generating impact statistics, the user must zero the covariance matrix, read in pilot remnant and wind components, and run the program for a user specified initialization period.

The TAWDS(AG) user can select one of three options to analyze the tracking and the impact errors of a selected weaponry system:

- ° Covariance Option - mean state equations are integrated in the presence of initial state errors, with or without wind shear, discrete gust, and gun recoil effects. Covariance state equations are integrated in the presence of initial state variances, with or without random wind gust, and pilot remnant. Ensemble impact statistics are calculated only if the covariance states are initialized to zero.
- ° Mean Option - mean state equations only are integrated. The calculations are all deterministic.

- Monte Carlo Option - a series of Monte Carlo runs is executed using the mean state equations. This option is available only for gunnery. Random initial state errors for each run are determined from state variances which are entered by the user. Random wind gust disturbances are also generated for each run.

2.2.1 Structure of TAWDS(AG) - The structure of TAWDS(AG) is illustrated in Figure 20. The program can be divided into five major sections:

- o A main section which controls the program
- o A data input section
- o A nonlinear section which generates the nominal attacker aircraft profile and the nominal weapon trajectory
- o A section which simulates the linear mean and covariance state equations
- o A section which computes the performance statistics including the sensitivity matrices.

2.2.2 TAWDS, The Main Subroutine of TAWDS(AG) - The air-to-ground TAWDS(AG) program is controlled by the main routine, called TAWDS. This routine calls the DATAIN routine to read most of the input data. After the call to DATAIN, TAWDS reads the initial values of the mean and covariance states, the random wind gust magnitudes, and the stationary source error standard deviations. It then calls the subroutine TRIM to initialize the deterministic simulation and calls the subroutine AMAT to calculate the plant matrices for the stochastic simulation. To integrate the deterministic and the stochastic simulations through time, it calls the subroutine RKI, which in turn calls the subroutine FCT to evaluate the simulation's derivatives.

After the profile initialization time period, TAWDS calls various subroutines that concern weapon firing. It calls SENTIV to generate impact error sensitivity matrices, CORREL to calculate round-to-round correlation for gunnery, and PERF to gather and calculate weapon statistics. Also, if the Monte Carlo option is selected, it controls the subroutine calls to execute the number of passes specified by the user.

2.2.3 Subroutine DATAIN - DATAIN reads most of the data required to execute a case. The remainder of the data is read by the main routine. The input to DATAIN consists of aircraft parameters, the flight control system, the sight system, pilot parameters, the flight profile, wind shear and discrete gust data, and program control variables.

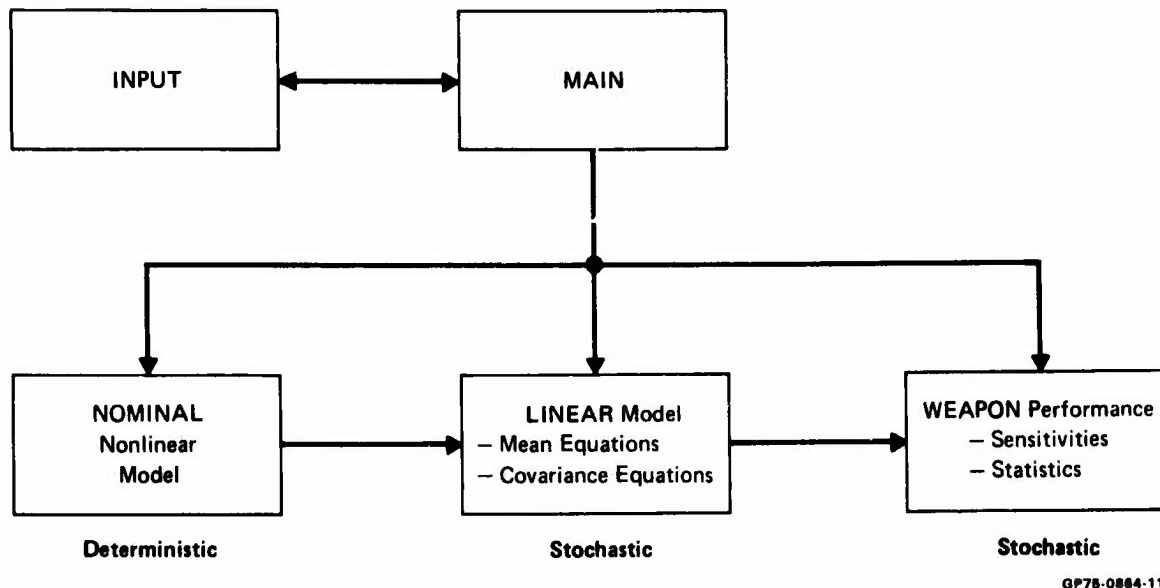


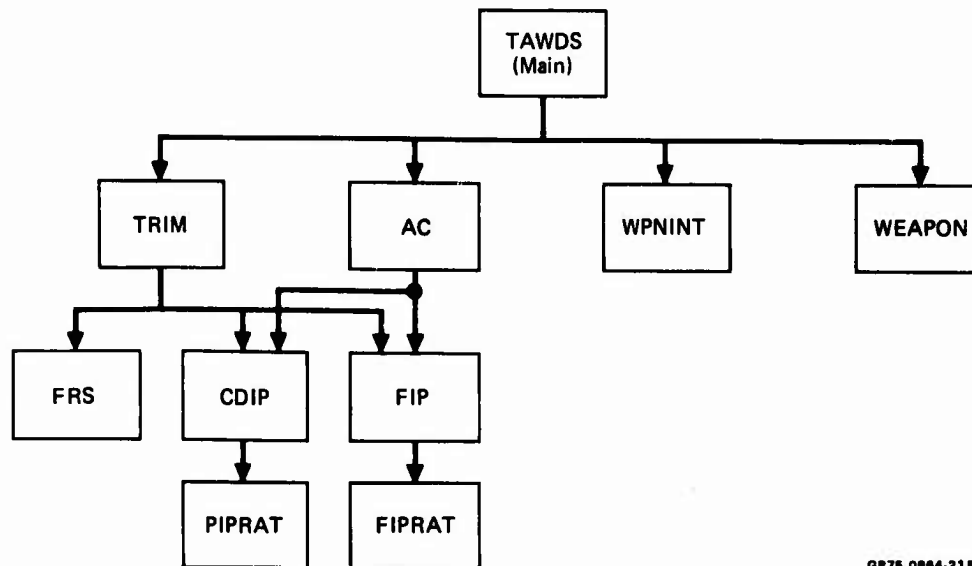
Figure 20. Structure of the TAWDS(AG) Program

2.2.4 Generation of the Nominal Trajectory - Illustrated in Figure 21 are the subroutines required to generate the nominal aircraft profile and associated nominal bullet and sight data. These subroutines are TRIM, AC, FIP, FIPRAT, FRS, CDIP, PIPRAT, WPNINT, AND WEAPON.

2.2.4.1 Subroutine TRIM - TRIM computes the initial profile geometry and aircraft state. The purpose of subroutine TRIM is to initialize the aircraft in a trimmed condition with the sight in solution; that is, papper on target. In addition, the aircraft state is constrained such that the initial tracking error rate is zero. Initial velocity, altitude, and flight path angle are chosen so that the desired quantities at bomb release or burst mid-point are obtained.

2.2.4.2 Subroutine AC - AC computes the nominal longitudinal aircraft trajectory and associated tracking error. The initial aircraft state is determined by subroutine TRIM. Subroutine AC determines the state derivatives for the piloted aircraft performing air-to-ground weapon delivery. These state derivatives illustrated in Figure 22 are integrated by the Runge-Kutta integration subroutine.

Note that the nominal lateral aircraft trajectory is trivial for bombs or fixed, forward-firing guns. Note also that "nominal" refers to a condition of zero initial tracking error, zero initial tracking error rate, and the absence of wind.



GP75-0864-215

Figure 21. Subroutine Sequence for Nominal Trajectory

$$\begin{bmatrix} \dot{X}_1 \\ \dot{X}_2 \end{bmatrix} = \begin{bmatrix} A_{11}(t) & 0 \\ 0 & A_{22}(t) \end{bmatrix} \begin{bmatrix} X_1 \\ X_2 \end{bmatrix} + \begin{bmatrix} B_{11}(t) & 0 \\ 0 & B_{22}(t) \end{bmatrix} \begin{bmatrix} U_{v1} \\ U_{v2} \end{bmatrix} + \begin{bmatrix} C_{11}(t) & 0 \\ 0 & C_{22}(t) \end{bmatrix} \begin{bmatrix} U_{c1} \\ U_{c2} \end{bmatrix}$$

X_1 - Longitudinal Aircraft and Elevation Tracking State Vector
 X_2 - Lateral-Directional Aircraft and Traverse Tracking State Vector

U_{v1}, U_{c1} - Longitudinal Aircraft and Elevation Tracking Disturbance Vectors
 U_{v2}, U_{c2} - Lateral-Directional Aircraft and Traverse Tracking Disturbance Vectors

GP75-0864-63

Figure 22. Uncoupled Aircraft Tracking Error Geometry Perturbation Equations for Wings Level Weapon Delivery Tasks

2.2.4.3 Subroutine FIP - Subroutine FIP computes the Future Impact Point (FIP) pipper setting for bombing. A modified vacuum trajectory approach, as described in Appendix IV, is used to determine the impact point.

2.2.4.4 Subroutine FIPRAT - FIPRAT computes the sensitivities of the FIP pipper elevation setting to perturbations in the aircraft and profile geometry states. This information is required by the linear perturbation model. FIPRAT also computes the pipper elevation rate, which is used by TRIM to obtain a zero tracking error rate at initialization.

2.2.4.5 Subroutine FRS - FRS computes the Fixed Depressed Reticule sight data for the firing burst midpoint, including the nominal elevation setting if desired. The user can also input the reticle setting directly, bypassing the reticle setting computations.

2.2.4.6 Subroutine CDIP - Subroutine CDIP computes the Continuously Computed Impact Point (CCIP) pipper setting. A modified vacuum trajectory approach, as described in Appendix IV, is used to determine the impact point.

2.2.4.7 Subroutine PIPRAT - Subroutine PIPRAT computes the elevation sensitivities of the CCIP pipper setting to perturbations in the aircraft and profile. This information is required by the linear perturbation model. PIPRAT also computes the pipper elevation rate, which is used by TRIM to obtain a zero tracking error rate at initialization.

2.2.4.8 Subroutine WPNINT - WPNINT computes the initial weapon position and velocity at bomb release or bullet firing. WPNINT is called by the main routine TAWDS and the subroutines FIP, FRS, and CDIP.

2.2.4.9 Subroutine WEAPON - WEAPON integrates a bomb or bullet to ground impact. The impact parameters of the weapon are used in determining the sensitivity coefficients. The weapon impact error associated with the nominal aircraft trajectory is determined from the computed impact position in earth coordinates.

2.2.5 Generation of the Linear Model: Mean and Covariance State Equations - Illustrated in Figure 23 are the subroutines required to generate the linear dynamic model for the air-to-ground attack system, discussed in Appendix V. This includes integration of the covariance and/or mean state equations. The major subroutines involved in this process are RKI, FCT, AMAT, ABW, or OUTCOV.

2.2.5.1 Subroutine RKI - RKI is a fourth-order Runge-Kutta integration routine used in conjunction with subroutine FCT to integrate the state variables of the gunnery profile. RKI also integrates the nominal simulation.

2.2.5.2 Subroutine FCT - Subroutine FCT updates time-varying elements of the longitudinal and lateral-directional system dynamics matrices for the selected flight control system and sight configuration. The gun recoil input and discrete gust disturbance vectors are computed for use by the mean state equations. Both longitudinal and lateral-directional covariance and mean state variable derivatives are computed as required by the selected program option for the Runge-Kutta integration. For the covariance option, the autocorrelation matrix derivatives are computed as required for generating burst statistics.

2.2.5.3 Subroutine AMAT - Subroutine AMAT computes elements of the longitudinal and lateral-directional system dynamics matrices for the selected flight control system. In addition, AMAT will compute the aircraft linear coefficients (used in the airframe equations of motion) from the input stability derivatives and the profile midpoint altitude and velocity if desired. Otherwise, the input values of the linear coefficients are used.

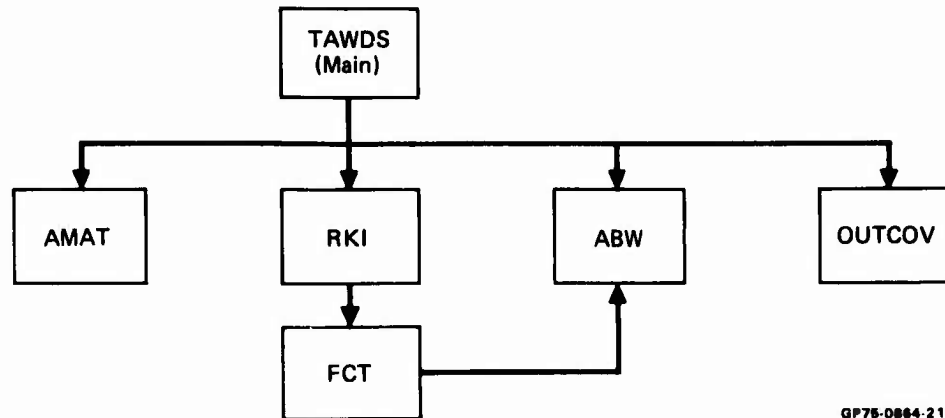


Figure 23. Subroutine Sequence for Linear Time Histories

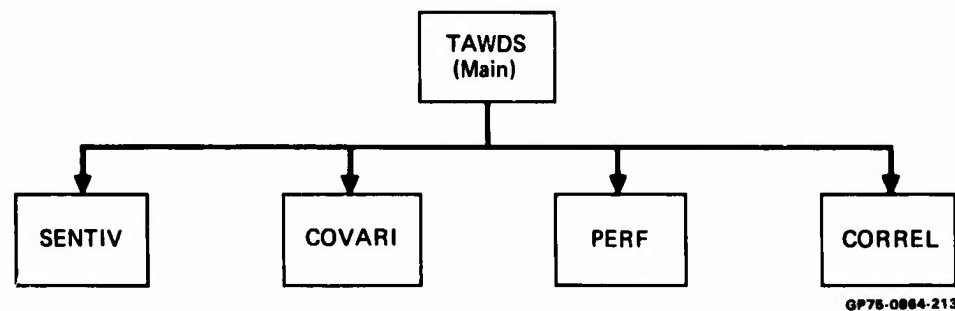


Figure 24. Subroutine Sequence of Performance Subroutines

2.2.5.4 Subroutine ABW - Subroutine ABW computes those elements of the longitudinal and lateral-directional system dynamics matrices associated with the Dryden wind gust model. The wind gust input covariance matrix is also computed, if required.

ABW is called initially by the main program. It is also called by FCT at each integration interval whenever aircraft altitude goes below 1000 feet, to update the wind gust elements as required by the Dryden model.

2.2.5.5 Subroutine OUTCOV - Subroutine OUTCOV outputs the longitudinal and lateral covariance and/or mean state variables of the linear model at the selected interval over the gunnery profile.

2.2.6 Performance: Sensitivities and Ensemble Statistics - Illustrated in Figure 24 are the subroutines involved in generating bullet and bomb performance data. These subroutines are SENTIV, COVARI, PERF, and CORREL.

2.2.6.1 Subroutine SENTIV - SENTIV computes the along-track and cross-track weapon impact error sensitivity matrices in both ground plane and line of sight coordinates for the selected sight configuration.

2.2.6.2 Subroutine COVARI - In conjunction with the covariance option COVARI computes the impact error variances, standard deviations, and CEPs (Circular Error Probability) for the selected sight mode and for the stationary, dynamic (nonstationary), and total (stationary plus nonstationary) source error configurations. For the Monte Carlo option, only the stationary source error statistics are computed. For gunnery, these computations occur at the selected interval during the burst.

The stationary impact errors are determined from the sensitivities computed in subroutine SENTIV and the applicable input stationary source errors. The nonstationary impact errors are computed from the sensitivities and the nonstationary error values contained in the longitudinal and lateral state variable covariance matrices of the linear system models.

2.2.6.3 Subroutine PERF - Subroutine PERF computes the weapon statistics data. For gunnery, PERF is called at the selected interval during the burst to store sample bullet data and at the end of the burst to compute and output the burst statistics. Computation of the ensemble statistics is a user option which can be exercised in conjunction with the covariance or Monte Carlo options where the only dynamic inputs (other than gun recoil, wind shear, and discrete gust) are random wind gust and pilot remnant.

2.2.6.4 Subroutine CORREL - Subroutine CORREL (in conjunction with the covariance option only) computes the bullet impact error autocorrelation from the input autocorrelation and sensitivity matrices. The impact error autocorrelation values are then used by the main program to compute the round-to-round correlation values. The impact error statistics that the PERF and CORREL subroutines compute are discussed in the next section.

2.3 Weapon Delivery Ensemble Impact Error Statistics

There are major differences in the pilots' performing air-to-air and air-to-ground weapon delivery. During air-to-ground weapon delivery the target is stationary, or nearly so; for air-to-air gunnery, the target is not only moving, but is performing evasive maneuvers. During air-to-ground weapon delivery, once the pilot achieves solution for an acceptable weapon delivery envelope, he fires a continuous burst of rounds or releases his bomb. But, in an air-to-air gunnery pass, the attacking aircraft can have limited but yet multiple firing

opportunities as the target maneuvers, even though the attacker maintains his position of relative advantage throughout an encounter. Thus, opportunities for many short firing bursts can occur in a single pass.

The ensemble impact error statistical distributions for air-to-ground and air-to-air weapon delivery tasks are similar, but these distributions are computed by accumulating the impact error measures in a different manner. The air-to-ground statistics are referred to as ensemble burst statistics, to reflect the fact that there is only one gunfiring burst, or bomb release, per pass and the statistical properties are summarized for the burst. The air-to-air gunnery statistics are referred to as ensemble pass statistics, since a single pass may consist of a number of short bursts, and the statistical properties are summarized for the pass as a whole. The ensemble for air-to-ground gunnery is a collection of bursts under identical encounter conditions whereas the ensemble for air-to-air gunnery is a collection of passes under identical encounter conditions.

2.3.1 Ensemble Burst Statistics - It has been shown in Reference 12 that the use of ensemble burst statistics allows the bias for the burst to be isolated from variations within a burst. This permits calculation of two separate, statistically independent, bivariate Gaussian distributions. These describe the distribution of bias impact points, and the distribution of individual impact points within each burst with respect to the mean point of impact for each individual burst as depicted in Figure 25. The accuracy of a set of weapon delivery bursts is summarized in Figure 25 by three sets of parameters:

- o (\bar{b}_e, \bar{b}_t) - The Ensemble Mean Point of Impact (EMPI) in elevation and traverse coordinates relative to the target; that is, the overall average of all the individual Burst Mean Points of Impact (BMPI) for all passes made during an encounter. The BMPI is the centroid of impact points resulting from a particular burst fired during one given weapon delivery pass. Numerous weapon delivery passes are simulated to account for how different sample sets of source errors affect weapon impact errors.
- o $(\sigma_{b_e}^2, \sigma_{b_t}^2)$ - The variance of the centroid of all the impact points made for individual BMPI's in elevation and traverse coordinates with respect to the EMPI. (For the air-to-ground bombing mode, the weapon burst may be one round or a bomb.) This one sigma bivariate distribution defines the ellipsoidal area with the EMPI at its center, in which 39.3 percent of the BMPI lie.

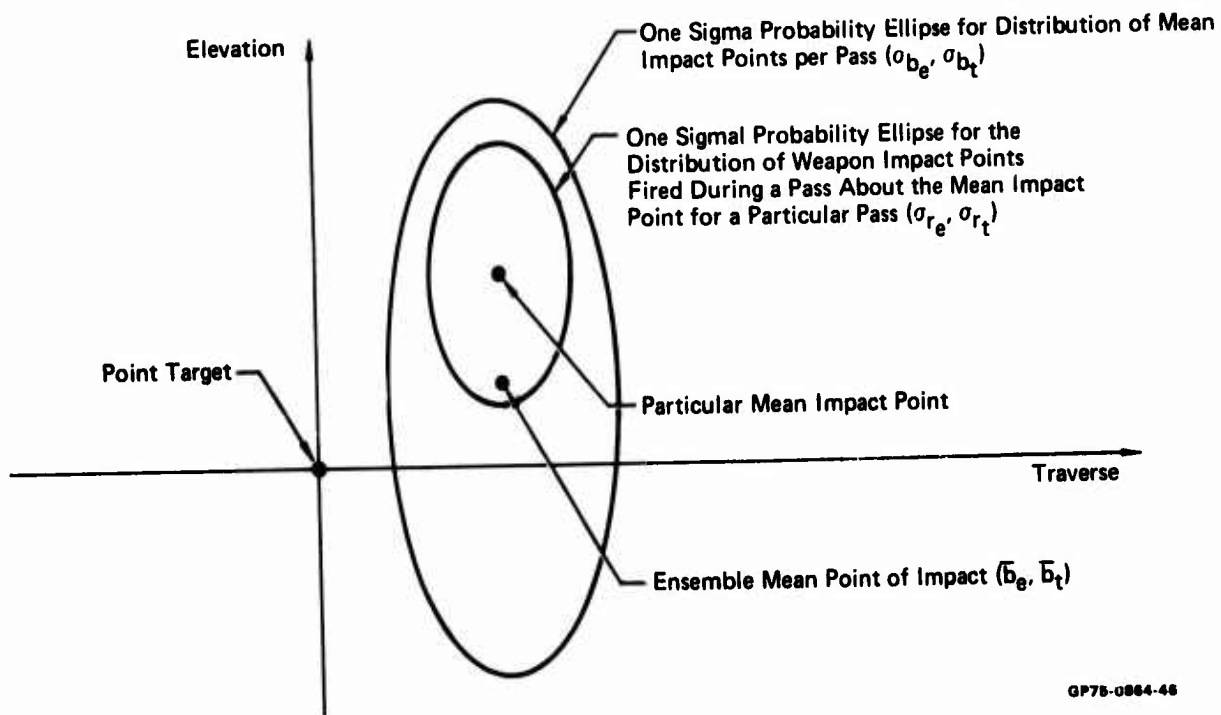


Figure 25. Equivalent Salvo Distribution for Impact Errors

- o $(\sigma_{r_e}^2, \sigma_{r_t}^2)$ - The variance of individual impact points in elevation and traverse coordinates with respect to their BMPI. This one sigma bivariate distribution defines the ellipsoidal area with the BMPI (for a given pass) at its center, in which 39.3 percent of bullets fired in the given pass impact.

The covariance procedure for computing these two bivariate distributions is presented in Appendix VI.

This model with these sets of statistical parameters extends previous models in three major ways:

- o It analytically computes both elevation and traverse components of these three accuracy parameters, using the dynamic response characteristics of particular aircraft. Individual weapon dispersion variances due to the effects of ejection variations and manufacturing anomalies can be combined readily with the variances of individual impact points with respect to their BMPI.
- o It calculates the individual round-to-round autocorrelation functions by separately representing the elevation and traverse components of aim wander as Gauss Markov processes, taking into account the aircraft tracking response characteristics.
- o It does not require the assumption that the ensemble mean impact error is zero, thus permitting explicit consideration of both stationary aim errors, which show up as a systematic or bias error within a burst, and the deterministic aim walk in elevation, which is characteristic of fixed reticle sights.

Considering only one component of the EMPI and BMPI distributions and omitting for convenience the component subscript, the variances of these two bivariate distributions have the form:

$$\sigma_b^2 = \mu \sigma_d^2 + \sigma_s^2 \quad (1)$$

$$\sigma_r^2 = (1 - \mu) \sigma_d^2 \quad (2)$$

where the subscripts "d" and "s" refer to the effects of dynamic (nonstationary) and stationary source errors, respectively.

Error sources are classified as being "stationary" if their correlation time constant is long compared to the duration of the weapon burst, while "nonstationary" or "dynamic" error sources are the short-term effects. In other words, the effect of stationary source errors is to yield a bias impact

error throughout the burst, while the effect of dynamic source errors is to yield a time-varying impact error (aim wander) within the burst.

The parameter μ is the average individual round-to-round correlation for all pairs of individual rounds in the burst. If the weapon dispersion variance were included, it would be added to σ_r^2 in Equation 2.

2.3.2 Calculation of Pass Statistics for Air-to-Air Gunnery - In air-to-air gunnery a firing burst occurs when the pilot decides that the gun is within a gunfiring region. For the pilot using a Director sight, the bursts are fired whenever the elevation and traverse tracking errors, ϵ_{EL} and ϵ_{TR} , simultaneously satisfy the following tracking error boundary constraints:

$$\text{Elevation error constraint: } |\epsilon_{EL}| \leq \theta_{Ec} \quad (3)$$

$$\text{Traverse error constraint: } |\epsilon_{TR}| \leq \theta_{Tc} \quad (4)$$

$$\text{Radial error constraint: } \sqrt{\epsilon_{EL}^2 + \epsilon_{TR}^2} \leq \theta_{Rc} \quad (5)$$

For the pilot using the LCOSS sight, the firing conditions occur when the elevation and traverse tracking errors, projected a bullet's time of flight, (T_f), in the future, satisfy the following tracking error boundary conditions

$$\text{Elevation error constraint: } |\epsilon_{EL} + T_f \dot{\epsilon}_{EL}| \leq \theta_{Ec} \quad (6)$$

$$\text{Traverse error constraint: } |\epsilon_{TR} + T_f \dot{\epsilon}_{TR}| \leq \theta_{Tc} \quad (7)$$

$$\text{Radial error constraint: } \sqrt{(\epsilon_{EL} + T_f \dot{\epsilon}_{EL})^2 + (\epsilon_{TR} + T_f \dot{\epsilon}_{TR})^2} \leq \theta_{Rc} \quad (8)$$

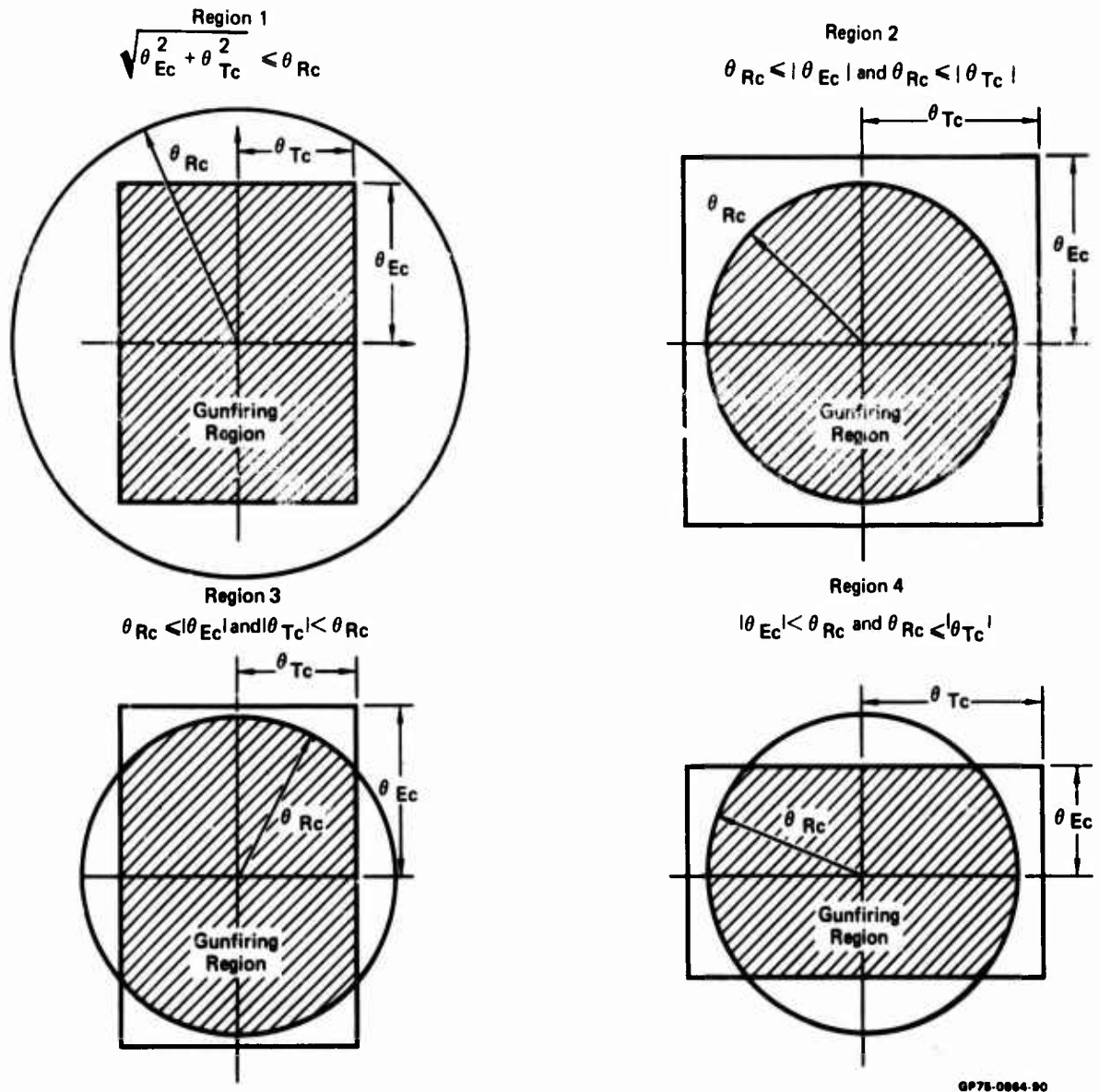
Figure 26 shows the four types of gunfiring regions specified by these tracking error constraints.

With these constraints, more than one firing burst can occur for a given Monte Carlo pass, and the number of bullets fired for each pass will not be equal. Consequently, the statistical measures needed for calculating the ensemble statistics for Monte Carlo runs are:

- o Pass Mean Point of Impact (MPI), $E[a_{ij}]$ - For any individual Monte Carlo run (pass), multiple bursts of varying durations can occur. The average value of impact points with respect to the target, computed in both elevation and traverse components for all N_i bullets fired during the i^{th} pass, is:

$$\bar{b}_i = E[a_{ij}] = \frac{1}{N_i} \sum_{j=1}^{N_i} a_{ij}$$

where a_{ij} is the impact point of the j^{th} bullet fired during the i^{th} pass.



GP76-0064-90

Figure 26. Gun Firing Regions Defined by Tracking Error Constraints

- o Variance of Impact Points within a Pass about the Pass MPI, $E[(a_{ij} - \bar{b}_i)^2]$
This is the variance of rounds within a pass about the pass MPI as given by

$$\sigma_{r_i}^2 = E[(a_{ij} - \bar{b}_i)^2] = \frac{1}{N_i} \sum_{j=1}^{N_i} a_{ij}^2 - \bar{b}_i^2 \quad (10)$$

The statistical measures for each pass, \bar{b}_i and $\sigma_{r_i}^2$, are used to calculate two independent bivariate Gaussian distributions defined by the following ensemble statistical measures: (1) ensemble mean point of impact, EMPI; (2) the ensemble variance of individual pass MPI about the EMPI; and (3) the unbiased estimate, for all passes, of the ensemble variance of impact points within a pass about the pass MPI. The unbiased estimate of the variance of impact points (rounds) within a pass accounts for the variable number of rounds per pass and the variability of MPI from pass to pass. The ensemble statistics are formulated as follows:

- o Ensemble Mean Point of Impact (EMPI), $E[\bar{b}_i]$ - The EMPI is the average value of the impact point with respect to the target for the total number of bullets fired, NBUL, for NRUN Monte Carlo runs. The EMPI is defined in terms of the MPI for all passes.

$$\bar{b} = E[\bar{b}_i] = \frac{1}{\text{NBUL}} \sum_{i=1}^{\text{NRUN}} N_i \bar{b}_i \quad (11)$$

- o Ensemble Variance of Pass MPI about the EMPI, $E[(\bar{b}_i - \bar{b})^2]$ - This is the variance of pass means about the ensemble mean.

$$\sigma_b^2 = E[(\bar{b}_i - \bar{b})^2] = \frac{1}{\text{NBUL}} \sum_{i=1}^{\text{NRUN}} N_i \bar{b}_i^2 - \bar{b}^2 \quad (12)$$

39.3 percent of the Pass MPI's will lie within this bivariate distribution.

- o Ensemble Variance of Impact Points within a Pass about the Pass MPI, $E[\sigma_{r_i}^2]$

$$\sigma_r^2 = E[\sigma_{r_i}^2] = \frac{1}{(\text{NBUL} - \text{NRUN})} \sum_{i=1}^{\text{NRUN}} N_i \sigma_{r_i}^2 \quad (13)$$

If one burst with the same number of bullets is fired for each weapon delivery pass, these ensemble statistical measures which are computed by collecting pass statistics are equivalent to air-to-ground distributions computed by collecting burst statistics. Figure 25 illustrates the two independent bivariate distributions described by these ensemble statistical measures.

2.3.3 Monte Carlo Verification of the TAWDS(AG) Covariance Model - To validate the covariance analysis techniques of the TAWDS(AG) model, the impact error results obtained from Monte Carlo simulation of a typical gunnery profile were compared with the results obtained by covariance simulation of the same profile. The test case was an F-4 configured with a stability augmentation control system, a Fixed Depressed Reticule sight, and a 20mm M-61 gun (100 rounds per second firing rate). The 3 second gunnery profile consisted of a two-second preburst initialization period followed by a one-second burst. The pertinent geometry variables are listed below:

- o Altitude at burst midpoint: 2500 feet (above target altitude)
- o Target Altitude: 2000 feet (above sea level)
- o Flight path angle (burst midpoint): -30 degrees
- o Airspeed (burst midpoint): 500 knots

A gain network was used to represent an idealized pilot for converting the tracking errors to aircraft commands. The pilot gains are listed below:

- o Pilot stabilator command gain: 2.0
- o Pilot rudder command gain: 33.0
- o Pilot aileron command gain: -7.5
- o Pilot roll attitude perturbation gain: 0.5

This Monte Carlo verification was a comprehensive check of the entire TAWDS(AG) program since generation of the ensemble burst statistics involves nearly all computational aspects of the program. Since the most challenging aspect of the TAWDS(AG) covariance model verification is the dynamic source errors, stationary source error variances were not included. Also, since gun recoil effects are deterministic and would affect each Monte Carlo gunnery pass in exactly the same way, the gun recoil force model was set to zero. These two simplifications reduced the cost of Monte Carlo verification without compromising the result. The dynamic source error excitations were wind gusts of 6 feet per second (one sigma value) in both the elevation and traverse channels.

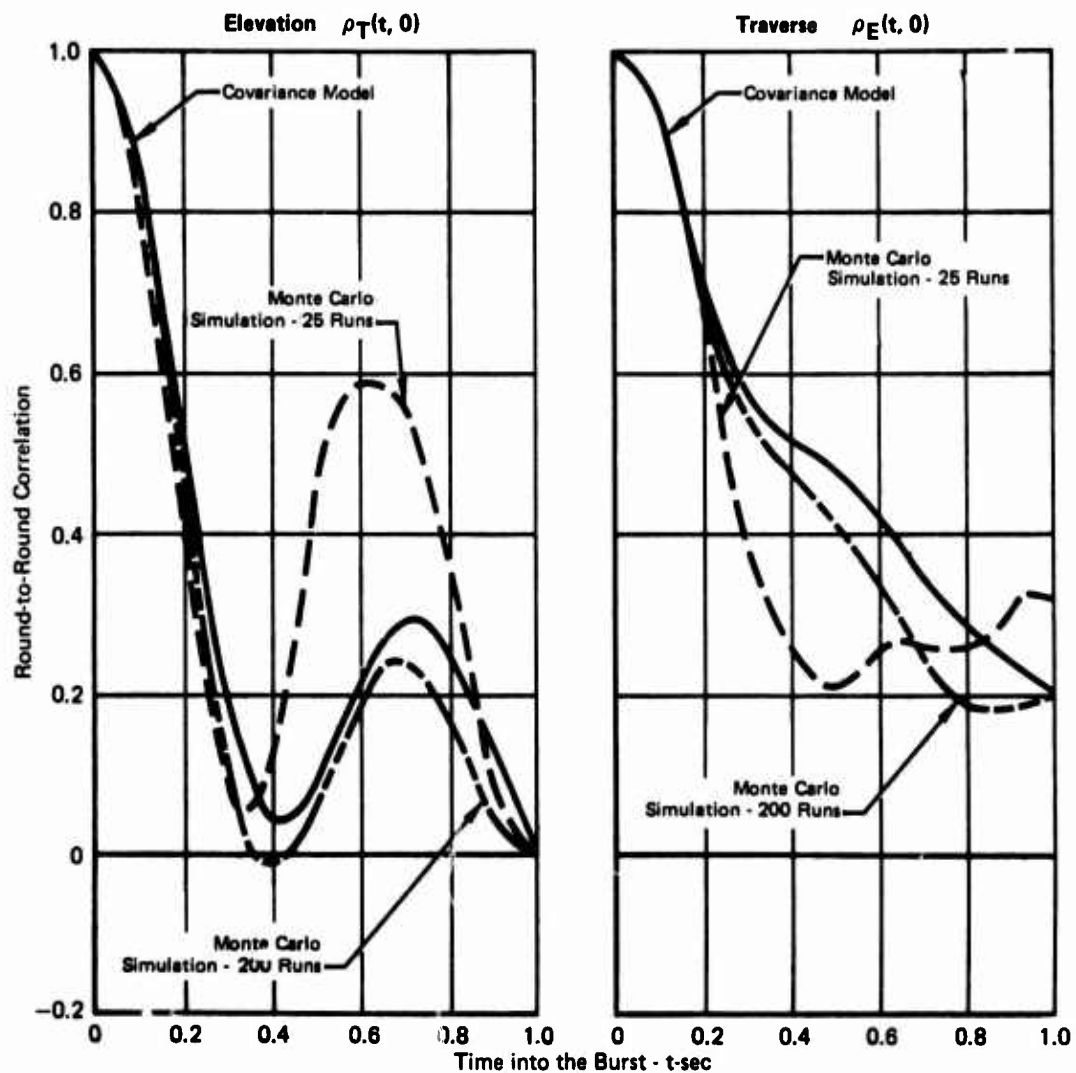
The Monte Carlo simulation exercised the same nominal gunnery profile many times in the presence of different random wind gusts. Two sets of runs, one of 25 sample gunnery passes and the other of 200 sample gunnery passes, were made. The corresponding ensemble burst statistics and round-to-round correlations were computed by the TAWDS(AG) program.

A comparison of the TAWDS(AG)'s Monte Carlo and covariance model round-to-round correlations is presented in Figure 27. The correlations are illustrated as a function of time into the burst, that is, with zero time at burst initiation. For a 100 round per second firing rate (assumed constant), the correlation between round 1 and round 50 would be determined from the figures in terms of their time difference, that is, $\rho(0.5, 0)$. From Figure 27, it can be seen that the Monte Carlo correlation values for 200 runs is a better comparison with the covariance model correlation values than values from the simulation of 25 runs. Increasing the number of Monte Carlo runs should yield results that converge to those of the covariance model.

A comparison of the Monte Carlo and covariance model burst statistics is tabulated in Figure 28. With one exception (the traverse component of ensemble mean aim error), the 200 run Monte Carlo simulation is in closer agreement with the covariance model statistics than the 25 run Monte Carlo simulation. The 200 run Monte Carlo simulation and the covariance model burst statistics compare quite well. Using either statistical description of the aim error in subsequent probability of hit or kill computations would yield very nearly the same results.

There are two basic reasons why one would not expect the 200 run Monte Carlo simulation and the covariance model burst statistics to agree completely. One reason is that the Monte Carlo correlation values did not completely converge to the covariance values. The other reason is that the covariance model assumes that the correlation between round 1 and round 50 is the same as that between round 51 and round 100. The Monte Carlo simulation, which computes its burst statistics from the sample data, permits round-to-round correlations which depend on absolute time in addition to time between rounds. Although the air-to-ground dynamic model is not strictly stationary, the dynamics change so slowly with time that the model can be approximated as a stationary process for the short interval of time corresponding to a firing burst.

The data of Figure 28 does show that the TAWDS(AG) covariance model yields ensemble burst statistics that agree quite well with those obtained from Monte Carlo simulation. In addition, the covariance model overcomes the major disadvantages of Monte Carlo simulation, which require that numbers of runs and adequate data reduction and analysis must be performed to ensure that enough runs have been made to permit confident application of the results.



GP75-0864-367

Figure 27. Comparison of Monte Carlo and Covariance Model Round-to-Round Correlations

The TAWDS(AA) and TAWDS(AG) programs provide an all-digital simulation tool for evaluating aircraft weapon delivery systems in terms of performance and effectiveness. However, to validate the TAWDS programs, it is necessary to compare the weapon delivery statistics, as computed by the TAWDS program with those statistics measured from actual aircraft weapon delivery simulation programs and flight test records. In the following section, weapon delivery accuracy measures which were obtained from measured simulation studies are compared with results obtained using the TAWDS all-digital simulation programs.

		Monte Carlo Simulation - 25 Runs	Monte Carlo Simulation - 200 Runs	Covariance Model
\bar{b} (ft)	El.	10.2	9.1	8.8
	Tr.	-0.1	0.4	0.0
$E [(b - \bar{b})^2]$ (ft ²)	El.	23.8	35.0	35.1
	Tr.	12.4	12.7	14.5
$E \left[\frac{1}{n} \sum_{i=1}^n (a(i) - b)^2 \right]$ (ft ²)	El.	52.4	62.5	64.1
	Tr.	8.7	8.1	8.3

OP75-0064-424

F-4, Stability Augmentation, Fixed Depressed Reticule Sight, M-61 Gun
Error Sources: Elevation and Traverse Wind Gusts (6 fps rms)

Figure 28. Comparison of Ensemble Burst Statistics Generated by the TAWDS(AG) Monte Carlo and Covariance Models

SECTION 3

MANNED AIR COMBAT SIMULATION STUDY

During the development of the TAWDS programs, the Manned Air Combat Simulator was used as (1) a pilot evaluation tool for establishing a most suitable set of aircraft flying qualities for air-to-air and air-to-ground weapon delivery, and (2) the design tool for both developing and validating the analytical pilot models, as well as for validating the TAWDS programs. In this manned simulation study, two USAF pilots flew numerous aircraft weapon system configurations where the aircraft's longitudinal and lateral-directional flying qualities were parametrically altered and the weapon sight systems varied. This manned simulation study was conducted to provide (1) aircraft weapon delivery tracking data for developing and validating an analytical multi-axis pilot model to be incorporated into the TAWDS programs, (2) aircraft weapon delivery impact error performance for comparing with the TAWDS weapon delivery performance results, and (3) pilot evaluation data for comparing with the TAWDS resultant flying qualities criteria for achieving the highest probability of kill. The aircraft weapon delivery performance and pilot evaluation measurements provide a data base for determining whether or not the TAWDS obtained flying qualities results are credible.

The description of the manned simulation study, the pilot evaluations of the effects of longitudinal and lateral-directional flying qualities on tracking performance, and the manned simulation validation of the TAWDS programs are discussed in this section. Because of the extensive development and validation effort that was required for generating and developing multi-axis pilot models, the detailed pilot model analyses are presented and discussed in depth in Section 4.

3.1 Description of Simulation Study

An extensive manned air combat simulation was conducted using two USAF pilots, each with fighter aircraft flying experience greater than 3,000 hours. As summarized in Figure 29, a total of 199 air-to-ground pilot/flight control/sight configurations was investigated, and a total of 137 air-to-air pilot/flight control/sight configurations was studied. Data were recorded on strip charts, video tape and magnetic tape.

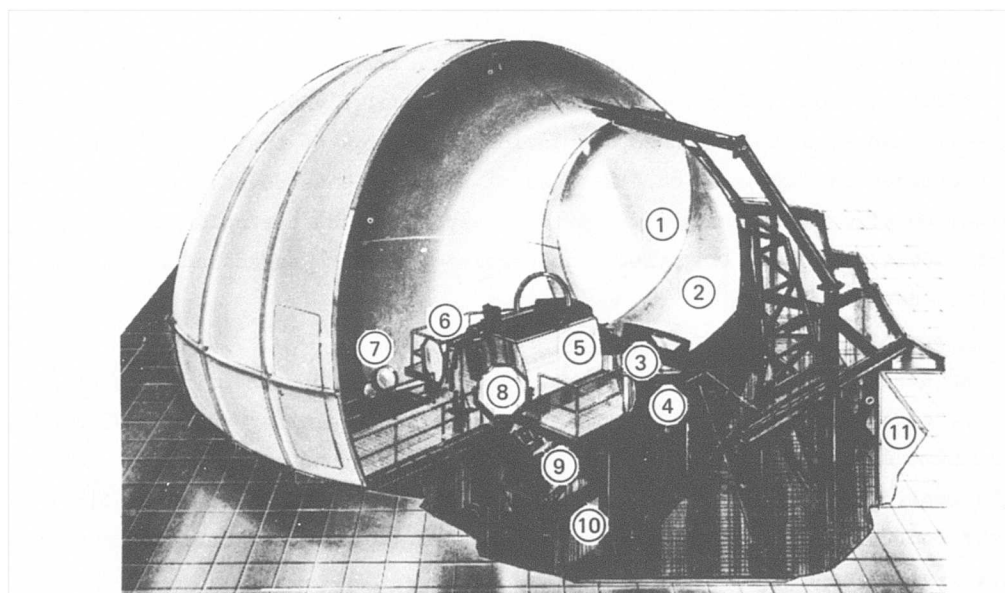
Figure 30 presents a cutaway view of the MCAIR fixed base Manned Air Combat Simulator crew station used in the study. The MACS crew station consists of a fully-instrumented, single-place, fighter-type cockpit at the center of a dome. The projection system displays a horizon and ground target scene.

Pilot		Weapon Delivery Tasks				
		Air-to-Air Gunnery		Air-to-Ground Gunnery		Air-to-Ground Bombing
		Director	LCOSS	CCIP	FDR	FIP
Pilot B	Longitudinal Configurations	16	16	15	16	16
	Runs	30	17	34	31	32
Pilot A	Lateral-Directional Configurations	18	18	14	19	19
	Runs	25	18	28	34	38
Pilot A	Longitudinal Configurations	17	16	15	16	16
	Runs	35	17	30	32	32
Pilot B	Lateral-Directional Configurations	18	18	19	6	18
	Runs	30	19	38	12	32

Total number of aircraft/pilot/weapon system configurations - 326
 Total number of simulations runs - 564

GP75-0864-220

Figure 29. Aircraft/Pilot/Weapon System Configurations for Manned Simulation Study



- | | | |
|--------------------------------|-----------------------------|------------------------------------|
| 1. Beam Splitter | 5. Crew Station | 9. Real Target Projector |
| 2. Spherical Mirror | 6. Real Horizon Projector | 10. Sound and Electronic Equipment |
| 3. Multiplexing Beam Splitter | 7. Real Target Focus Lenses | 11. Pit Area |
| 4. Virtual Image Beam Splitter | 8. Real Target Mirrors | |

GP75-0864-221

Figure 30. Manned Air Combat Simulator Layout

A 360-degree horizon display provides the pilot with realistic cues of the aircraft's motion and attitude in pitch, roll, and yaw. In the MACS, representative fighter aircraft flying qualities and controller characteristics are provided to the pilot along with a full set of flight instruments and other equipment such as head-up displays and weapon sight systems, necessary for the weapon delivery tasks. The MACS crew station is driven through a central computer system and visual generation equipment. The visual equipment generates all-aspect targets, horizon, and terrain map. The central monitoring station is at a single well-oriented location.

The aircraft simulated was an F-4E configured with a Tactical Weapon Delivery (TWeaD) type of flight control system. The TWeaD program, in which a three axis Control Augmentation System was developed for improving air-to-ground weapon delivery, was funded under USAF Contract F33(615)-67-C-1101. Block diagrams of the longitudinal and lateral-directional flight control system dynamics are presented in Figures 31 and 32. The control systems gains were varied to achieve pre-selected combinations of longitudinal and lateral-directional flight control configurations to be evaluated for each weapon delivery task. A variety of longitudinal flying qualities, such as longitudinal short-period frequency and damping characteristics, and stick force per g levels, were simulated by judiciously varying values for the pitch rate feedback gain, normal acceleration feedback gain, and electrical linkage transmission gain. The short-period mode characteristics are the eigenvalue characteristics of the augmented basic airframe short-period mode. Lateral-directional aircraft configurations that exhibited different flying qualities, such as augmented roll rate, proverse/adverse yaw response characteristics, and Dutch roll mode frequency and damping characteristics were simulated. The various roll rate response characteristics due to commanded roll rate were obtained by the proper variation of gain parameters defining (1) the transmission gain of the mechanical linkage between the aileron and lateral stick, (2) the transmission gain of the electrical linkage between the aileron's servo and lateral stick, and (3) the time constant of the prefilter network modifying the electrical roll rate command signal from the lateral stick force transducer. Proverse/adverse yaw configurations were achieved by changing the aileron-to-rudder interconnect gain. The various augmented Dutch roll mode frequency and damping characteristics were obtained by proper combination of computed sideslip rate feedback gain and lateral acceleration feedback gain parameters. The range of each longitudinal and lateral-directional flying quality variation is shown in Figure 33.

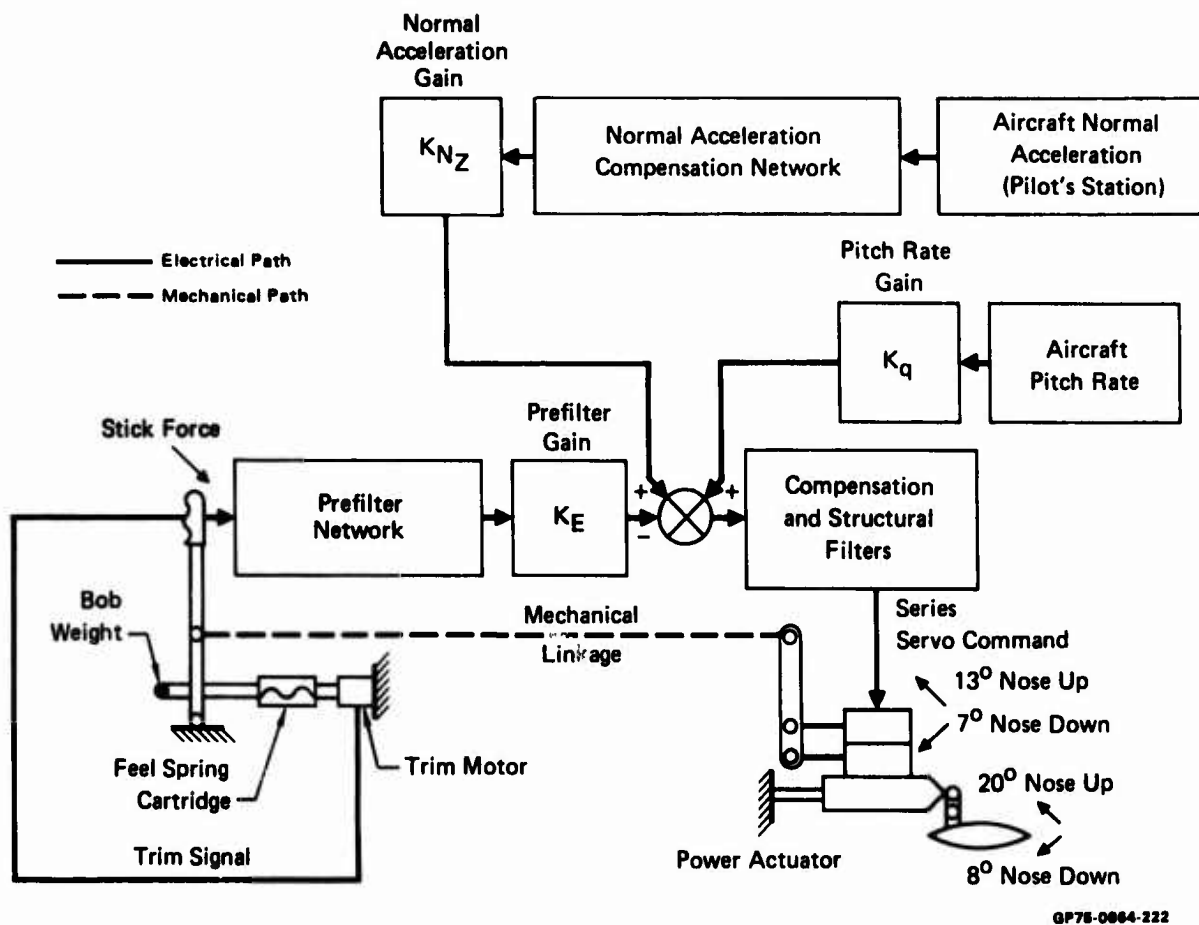
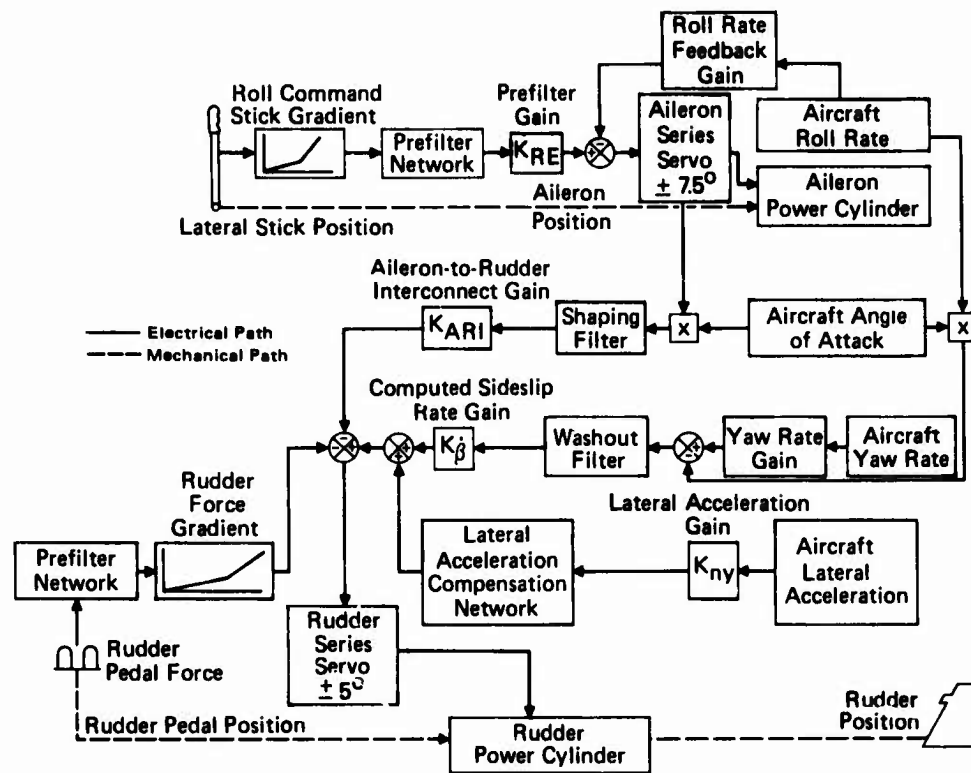


Figure 31. Generic TWeaD Longitudinal Flight Control System



GP78-0864-223

Figure 32. Generic TWed Lateral-Directional Flight Control System

Longitudinal Flying Qualities	
Response Characteristics	Range of Variations
Short-Period Natural Frequency	$3.5 \text{ rad/sec} < \omega_{sp} < 6.7 \text{ rad/sec}$
Short-Period Damping Ratio	$0.3 < \zeta_{sp} < 0.8$
Stick Force per G	$2.0 \text{ lb/G} < F_s/\text{G} < 8.0 \text{ lb/G}$
Lateral-Directional Flying Qualities	
Response Characteristics	Range of Variations
Dutch Roll Mode Natural Frequency	$3.0 \text{ rad/sec} < \omega_D < 3.5 \text{ rad/sec}$
Dutch Roll Mode Damping Ratio	$0.2 < \zeta_D < 0.8$
Augmented Roll Mode Time Constant	$0.25 \text{ sec} < \tau_R < 1.0 \text{ sec}$
Maximum Sideslip (β_2) Excursion within 2 seconds per Step Lateral Stick Command (F_{LAT})	$-1 \text{ deg/lb} < \frac{\beta_2}{F_{LAT}} < 0.4 \text{ deg/lb}$

*Proverse Yaw

GP78-0864-224

Figure 33. Longitudinal and Lateral-Directional Flying Qualities Variations for Aircraft Simulated in Manned Simulation Studies

The sight systems used for air-to-air gunnery were Director and Lead Computing Optical Sight System (LCOSS). For air-to-air gunnery, the pilot was required to track a target aircraft, which was programmed to fly the same pre-recorded maneuvers for all runs. A description of the encounter geometry for the aerial gunnery task is shown in Figure 34. The HUD display used with these sights is shown in Figure 35. These sight definitions are based on work reported in References 13 and 14.

The air-to-ground gunnery sights used were the FDR, and the Continuously Computed Impact Point (CCIP) sights. In all air-to-ground weapon delivery tasks, the aircraft was initialized with an airspeed of 450 kt, in a 30 degree dive, with a target at a range of 19,000 ft in the HUD field-of-view. The air-to-ground gunnery attack sequence is illustrated in Figure 16.

The piloting task for the air-to-ground gunnery mode, using an FDR sight system, was to track the target and to fire when the piloted aircraft simultaneously achieved the most attainable set of speed, flight path, and altitude or range conditions corresponding to the fixed reticle setting. The pilot's tracking task for the CCIP gunnery sight differs from that of the FDR sight. With the CCIP sight, the pilot achieves gunfire solution as long as he can maintain the CCIP reticle on the ground target.

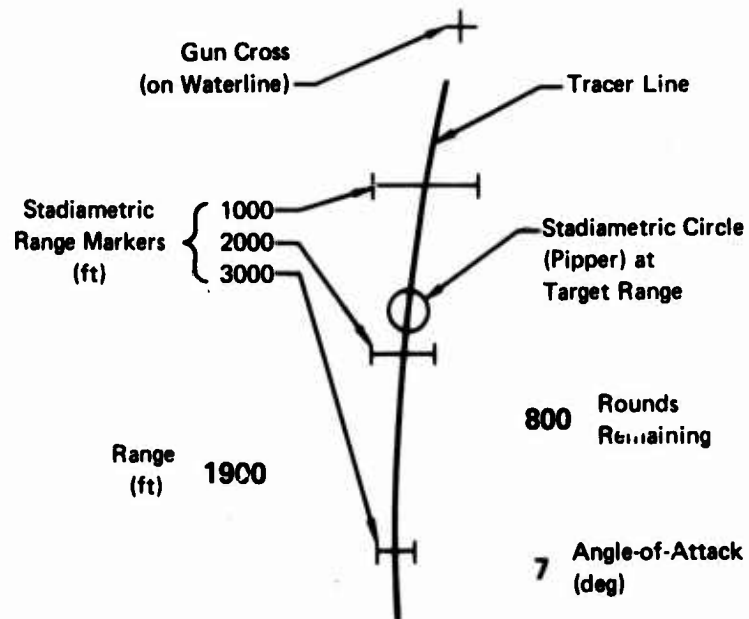
The HUD display used for air-to-ground gunnery is shown in Figure 36. On this display, the maximum gun firing range was based on a three-second bullet time-of-flight (to accommodate computer timing restrictions). The "pull-up" cue was computed based on aircraft ground clearance altitude as a function of flight path angle. This cue was displayed with respect to the ground speed velocity vector and was inertially roll stabilized. The pitch ladder was displayed with respect to the airspeed velocity vector and was inertially roll stabilized.

For the air-to-ground bombing mode, a derivative CCIP sight system called Future Impact Point (FIP) was used. In FIP bombing, a reticle is continuously displayed on the HUD to indicate to the pilot where the bomb will impact when it is dropped at the future release conditions, if present flight conditions are maintained. The pilot's task is to maintain the FIP reticle on the target until bomb release. The release of the bomb occurs when another symbol, a Displayed Impact Point (DIP) cross, which indicates the impact point for an immediately released bomb, comes in coincidence with the FIP reticle. The profile and basic HUD display for this bombing system are depicted in Figure 17. For bombing, the HUD display shown in Figure 36 was modified with both the DIP cross and the bomb fall line between the ground speed velocity vector and

$t_0 = 0$	$(t_0, t_1) = (0, 20) \text{ sec}$	$(t_1, t_2) = (20, 22.5) \text{ sec}$	$(t_2, t_3) = (22.5, 40) \text{ sec}$
Attacker Initial Conditions Angle-of-Attack = $7^\circ (\cong 4 \text{ G})$ Bank Angle = $+75^\circ$ 0.8 Mach Altitude = 10,000 ft Range = 1,900 ft Range Rate = -50 ft/sec	<ul style="list-style-type: none"> ● Pilot Tracks Target with Pipper in Terminal Air-to-Air Gunnery Encounter ● Pilot Fires When He Thinks He Can Score Hits 	Target Maneuver Same Angle-of-Attack and Velocity Bank Angle Changes from $+75^\circ$ to -75° <ul style="list-style-type: none"> ● Pilot Maneuvers to Stay with Target 	<ul style="list-style-type: none"> ● Pilot Maneuvers to Again Track Target with Pipper in Terminal Air-to-Air Gunnery Encounter ● Pilot Fires When He Thinks He Can Score Hits

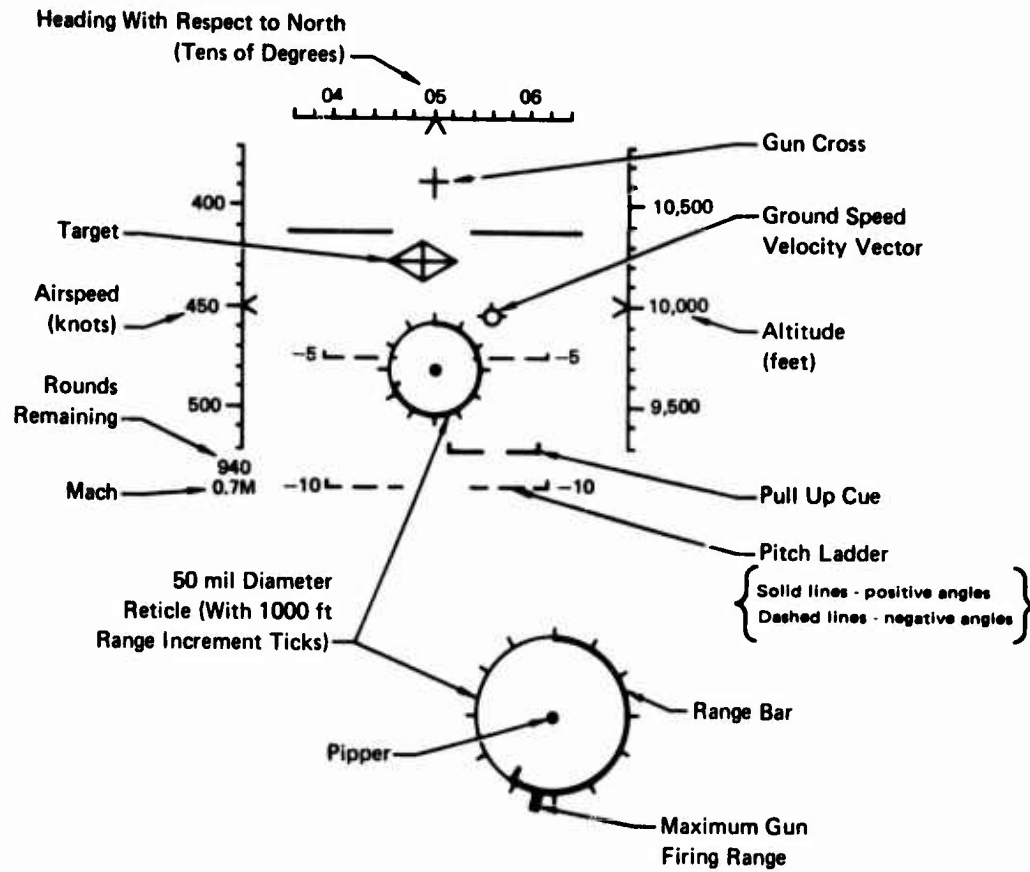
GP75-0064-225

Figure 34. Description of Aerial Gunnery Encounter and Pilot Tracking Instructions for Manned Simulation Study



GP75-0064-227

Figure 35. Air-to-Air Head Up Display for Generic Director and LCOSS Sights



GP75-0864-229

Figure 36. Air-to-Ground Gunnery Head-Up Display

pipper. The FIP reticle computation was based on a bomb release altitude of 2000 feet plus altitude loss during pull up. Detailed descriptions of each sight system used in the manned simulation study are given in Appendix II.

3.2 Pilot Evaluation of Aircraft Flying Qualities for Air-to-Air and Air-to-Ground Weapon Delivery Tasks

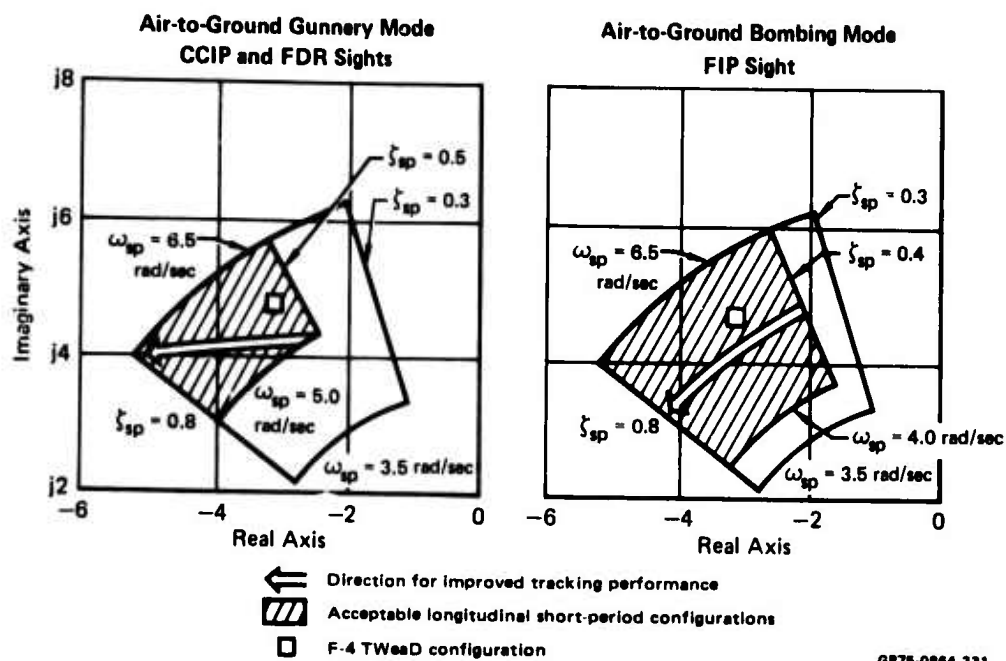
This section summarizes pilot comments on how variations in longitudinal and lateral-directional aircraft flying qualities affected the different weapon delivery tasks. In the precision tracking tasks, the pilots preferred the capability to make desired corrections in aircraft flight path or attitude quickly with minimum overshoot or undershoot in nulling the tracking error.

3.2.1 Pilot Evaluation of Longitudinal Flying Qualities - In Figures 37 and 38, the shaded circular sectors in the negative half of the S-plane depict the ranges of short-period damping and frequency values acceptable to the pilots. The larger circular sectors comprise the ranges of variations for the longitudinal short-period mode aircraft configurations simulated.

As shown in Figure 37, the pilots accepted wider bands of longitudinal short-period mode variations for the FIP bombing task than they did for both the air-to-ground FDR and CCIP gunnery tasks. For the air-to-ground gunnery tasks, simultaneous increase in the short-period damping and frequency values resulted in the most improved tracking performance. Within the pilot's acceptable region for the short-period mode, tracking performance for the FIP bombing task improved as the short-period frequency was increased.

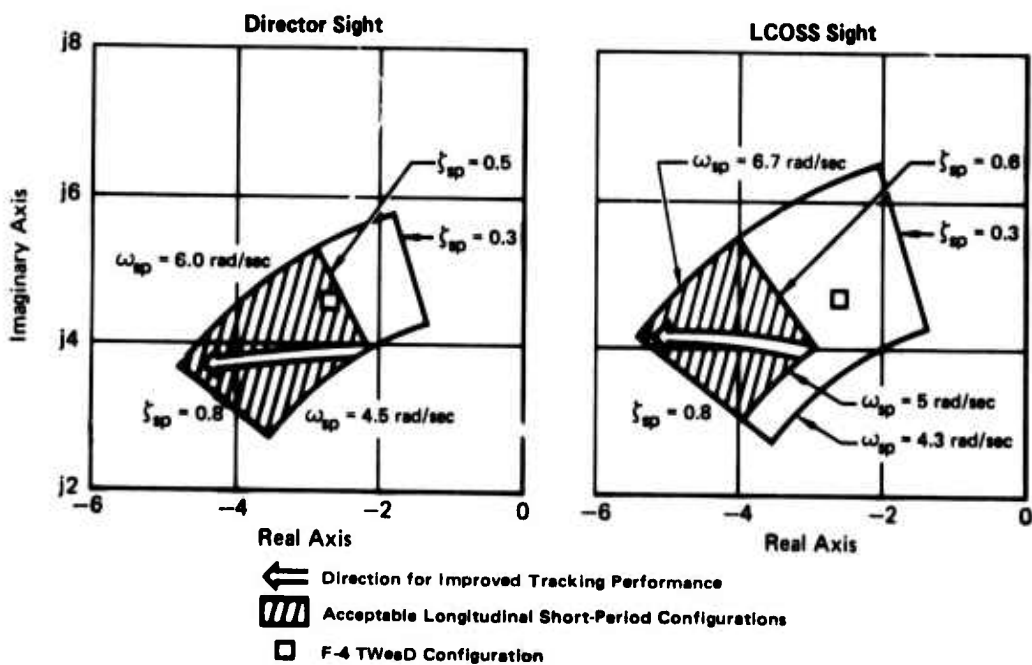
As shown in Figure 38, improved air-to-air gunnery tracking performance for the pilots resulted when both the longitudinal short-period damping and frequency characteristics were increased. The pilots tolerated a wider range of damping variations for the Director tracking tasks than for the LCOSS tracking tasks. Also, the pilots wanted a more responsive aircraft in terms of the short-period frequency characteristics for the LCOSS configuration than for the Director configuration.

Pilot comments concerning different stick-force-per-g variations considered in the precision tracking phase of a weapon delivery task are summarized in Figure 39. Pilot comments indicated a compromise value of around 4 lb/g was probably best for both precision tracking and general aircraft maneuverability. This parameter has an important effect on control harmony. Figure 39 indicates that it has a limited range of acceptable values for gunnery, but a significant range of acceptable values for bombing. The pilots commented that a value of 6 lb/g greatly reduced aircraft pitch sensitivity with the FDR sight. This sensitivity was not as noticeable with the other sights.



GP75-0864-231

Figure 37. Pilot Evaluation of Longitudinal Short-Period Frequency and Damping Variations for Air-to-Ground Weapon Delivery Tasks (F-4 Aircraft Configured with TWeaD Flight Control System)



GP75-0864-232

Figure 38. Pilot Evaluation of Longitudinal Short-Period Frequency and Damping Variations for Air-to-Air Gunnery Tasks (F-4 Aircraft Configured with TWeaD Flight Control System)

Time to Attain 50% of Commanded Roll Rate	Air-To-Ground Gunnery CCIP	Air-To-Ground Gunnery FDR	Air-To-Ground Bombing FIP	Air-To-Air Gunnery Director	Air-To-Air Gunnery LCOSS
0.25 sec**	A*	A*	A*	A*	A*
0.50 sec	D	D	U	A	D
1.0 sec	U	U	U	U	U

A - Acceptable

D - Difficult but Acceptable

U - Unacceptable

* - Most Desired Value

** - F-4 TWeaD Configuration

GP75-0864-226

Figure 42. Pilot Evaluation of Lateral-Directional Commanded Roll Rate Response Variations for Air-to-Ground and Air-to-Air Weapon Delivery Tasks (F-4 Aircraft Configured with TWeaD Flight Control System)

3.3 Comparison of TAWDS Generated Impact Error Distribution with Impact Errors Measured from Manned Simulation Studies

To show credibility for the TAWDS programs, the weapon accuracy computed by the TAWDS programs was compared with measured values from piloted manned simulation of air-to-ground bombing and air-to-air gunnery weapon delivery. The weapon impact error measurements were obtained in the manned simulation study by two USAF pilots, flying the same aircraft configuration for the same flight conditions corresponding to each weapon delivery task. For air-to-ground bombing the aircraft was configured with the baseline Tactical Weapon Delivery (TWeaD) flight control system and the FIP bombsight. For air-to-air gunnery the attack aircraft was configured with the baseline TWeaD flight control system and the Director gunsight. In the manned simulation study, dynamic disturbances, such as wind gust and weapon release forces, were acting upon the aircraft. Stationary source errors associated with sensor measurements were not implemented.

In the TAWDS programs the same dynamic disturbances were modeled and the stationary source errors were set to zero. The tracking errors were initialized in the TAWDS programs with the same values corresponding to those in the manned simulation two seconds before weapon release.

For each weapon delivery mode, a pilot model which reproduced similar tracking error characteristics to those measured and validated on the manned simulator was incorporated into the TAWDS programs. Selection of this pilot model is discussed in Sections 4 and 5.

As shown in Figure 43, bomb impact points were obtained from two different pilots flying the same aircraft weapon delivery task. These impact points are plotted with respect to their average impact point for the 13 runs. Superimposed upon the impact points measured from the manned simulation is the bomb impact error bivariate normal distribution computed by the TAWDS(AG) program. This bivariate normal distribution represents an ellipsoidal area, in which 39.3 percent of the bomb impact points should lie. For this small sample size of thirteen, nine bomb impact points lie within the ellipsoidal area. Thus, Figure 43 shows that the variance of the weapon impact points computed by the covariance air-to-ground TAWDS(AG) program is still fairly representative of the weapon delivery accuracy results obtained from the pilot-in-the-loop simulation of the same weapon delivery tasks. In a sample of 13 passes, there is a .95 probability that three to nine impact errors will lie within the 39.3 percent bounds of the TAWDS(AG) distribution.

For the air-to-air gunnery task, the TAWDS(AA) generated pass mean impact error distribution is compared to the mean impact error per pass measured from two different pilots flying the same aircraft weapon delivery task. Here two pilots flew the same air-to-air gunnery encounter four times. In Figure 44 the resulting impact points are plotted with respect to their average mean impact point. The bivariate normal distribution of the TAWDS(AA) mean impact error per pass which defines the bounds for 39.3 percent of the mean impact points, is superimposed upon the individual mean impact errors per pass. Figure 44 shows that five of the eight mean impact points lie within the TAWDS(AA) generated mean impact error per pass distribution. In a sample of eight passes there is a .90 probability that two to five mean impact errors will lie within the 39.3 percent bounds of the TAWDS(AA) distribution.

The round-to-round impact error one sigma distribution was measured for each manned simulation aerial gunnery pass. These distributions are plotted in Figure 45 along with the round-to-round impact error about the pass mean point of impact distribution, computed by TAWDS(AA). Although the distributions obtained from the manned simulation runs tend to have more dispersion in traverse than in elevation, and the TAWDS(AA) distribution has more dispersion in elevation than in traverse, the results obtained from the simulation agree quite well with those obtained from TAWDS(AA).

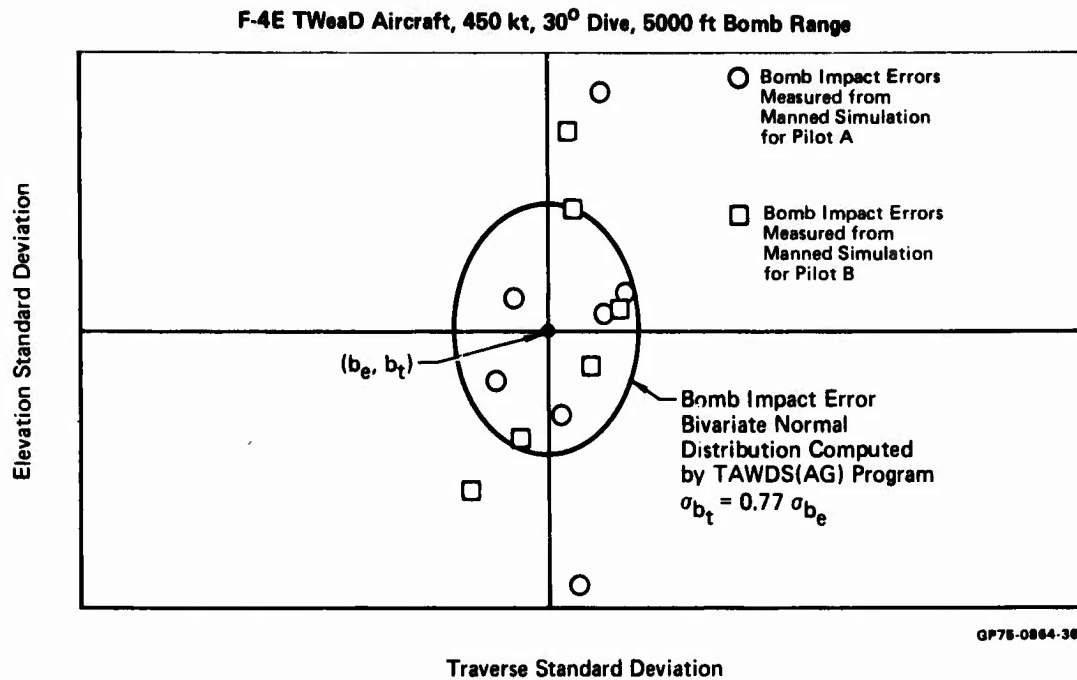


Figure 43. Comparison of TAWDS(AG) Generated Bomb Impact Error One Sigma Distribution (Bomb Impact Errors Measured from Manned Simulation Studies)

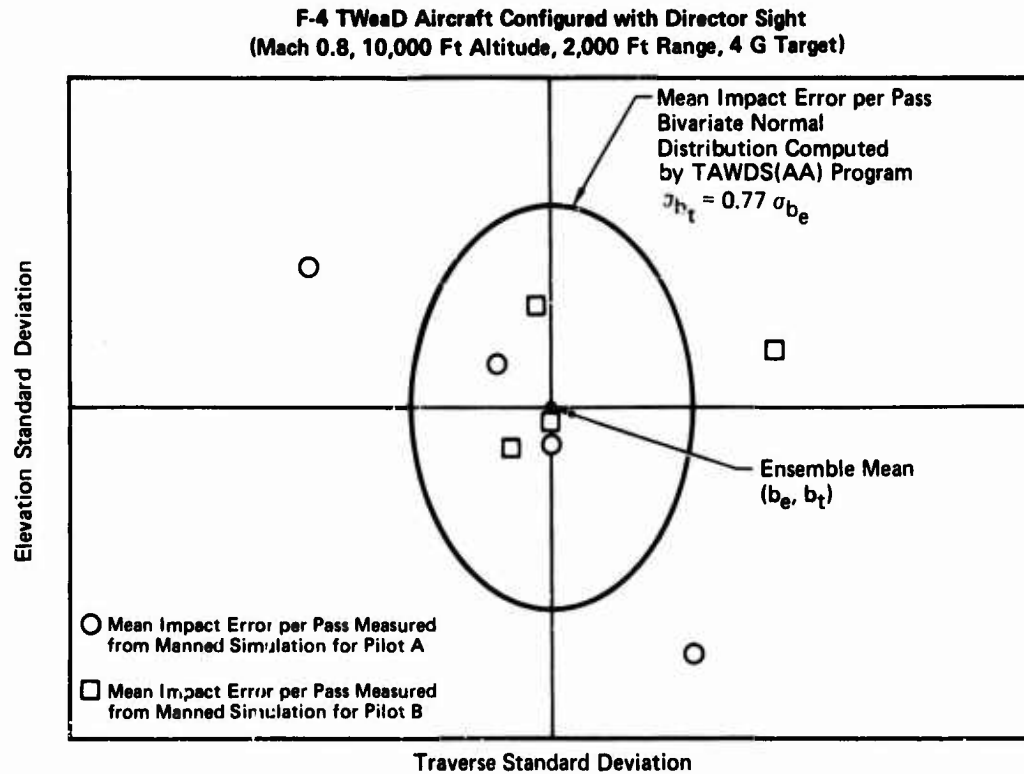


Figure 44. Comparison of TAWDS(AA) Generated Pass Mean Impact Error One Sigma Distribution (Mean Impact Error per Pass Measured from Manned Simulation Studies)

The degree of comparison between the TAWDS computed impact errors and the impact errors measured from the manned simulation runs depends on how well the analytical pilot model simulates the actual pilot tracking task. The development and validation of the multi-axis pilot models used to simulate weapon delivery tracking is discussed in the next section.

F-4E TWaD Aircraft Configured with Director Sight
(Mach 0.8, 10,000 Ft Altitude, 2,000 Ft Range, 4 G Target)

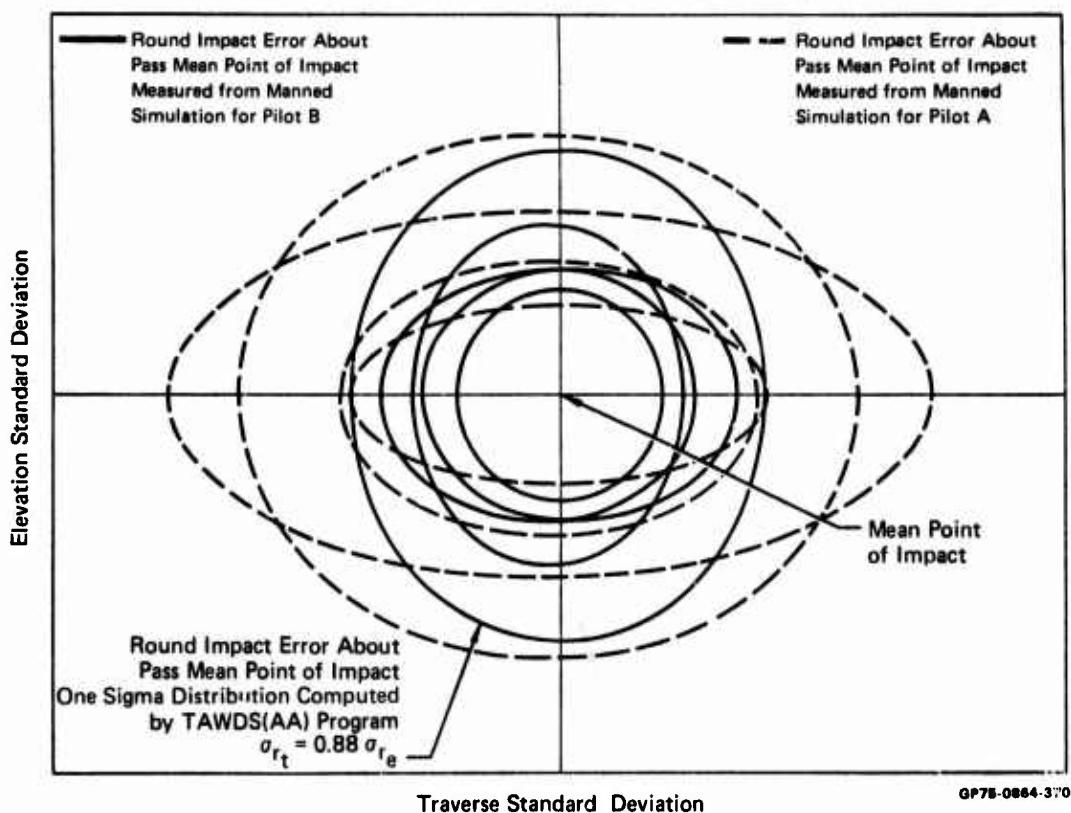


Figure 45. Comparison of TAWDS(AA) Generated Round-to-Round Impact Error One Sigma Distribution
(Round Impact Error per Pass Measured from Manned Simulation Study)

SECTION 4

MULTI-AXIS PILOT MODEL DEVELOPMENT AND VALIDATION

During the development of the TAWDS all-digital computer programs, representative multi-axis analytical pilot models were needed to properly simulate weapon delivery tracking tasks. This section summarizes the development and validation of the multi-axis longitudinal and lateral-directional pilot models used to simulate aerial gunnery and air-to-ground weapon delivery precision tracking tasks. These models have been incorporated into the TAWDS programs. They were developed by analyzing time histories of tracking error obtained from pilot-in-the-loop air combat simulation studies, the criterion being to match these response characteristics as closely as possible. This was accomplished by using the Manned Air Combat Simulator computer program in a batch mode with the human pilot replaced by the pilot model. It was not necessary to model the pilot's stick and rudder pedal motions exactly to satisfy this criterion since the damping and limited bandwidth of the aircraft and flight control system dynamics significantly reduce the effects of these motions.

This criterion is considerably more severe than such statistical criteria as comparing the root-mean-square, mean, or standard deviation of the tracking error. Statistical criteria are easy to satisfy because they do not consider the time-varying characteristics of the tracking error in a particular time history trace.

When pilots fly the same weapon delivery tracking task repeatedly under identical initial conditions, they can reproduce the same time history modal characteristics, but not identical time history traces. Consequently, comparisons between the analytical pilot and human pilot weapon delivery task time histories will show the same correlation. Validation of the analytical pilot models is accomplished by measuring and comparing the describing function characteristics of the human and pilot models in the frequency domain. This frequency response correlation is not dependent on the time phase of the tracking errors and pilot aircraft commands between separate and repetitive runs.

The principal criterion for determining whether the pilot model frequency response matches with human pilot frequency response is the difference in magnitude and phase values for the pilot model compared to the human pilot's gain and phase values at the principal tracking error frequencies. Another standard for validation is to compare the lead characteristics between the pilot model and human pilot over the tracking error's frequency range.

4.1 The Precision Tracking Task

The control task used in developing the pilot models was the nulling of elevation and traverse tracking errors during the terminal tracking phase of a weapon delivery encounter. The precision tracking task considered here is deterministic (as opposed to stochastic), in that the target is either fixed, as in the air-to-ground attack, or is not maneuvering in a random manner relative to the attacker, as in the terminal stage of an air-to-air encounter. As a result, the pilot readily sees the effect of his control inputs and is actively tracking the target. External disturbances, such as wind gusts, do not substantially affect the deterministic nature of the tracking task unless they are very large.

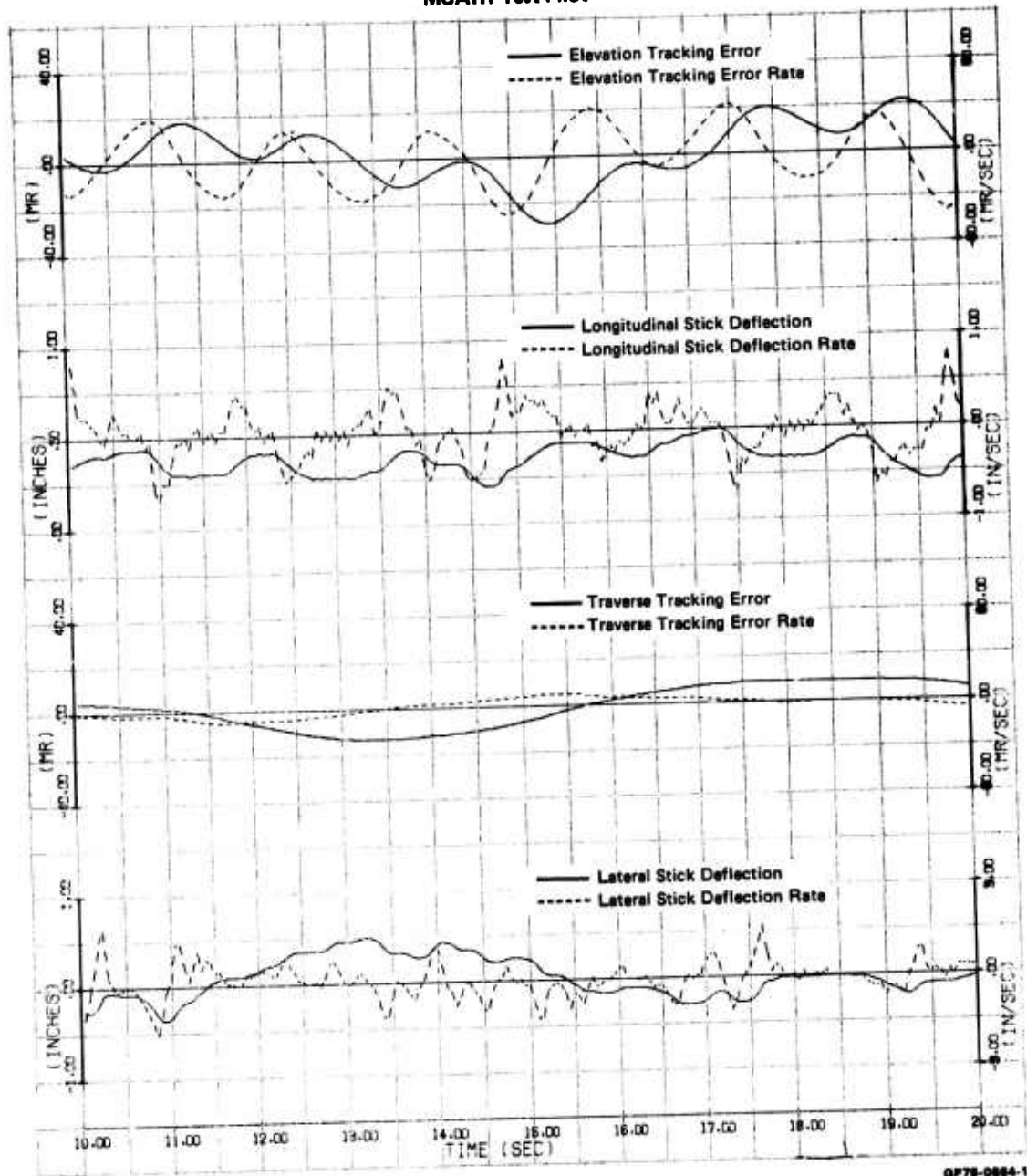
4.2 Pilot Tracking Error Characteristics

Figures 46 and 47 are time histories of the elevation and traverse tracking errors, the pilot's stick commands, and their corresponding rates for two aircraft using the Director gunsight. They describe the time interval from 10 to 20 seconds in an air-to-air gunnery encounter and were taken from the manned simulation study reported in Section 5.4 and Appendix IV of Reference 11. They are representative of the pilot's tracking error responses and were used in developing the pilot model structure. Stick rates are included, because they show the pilot's command response better than stick position alone. It was found that the time history characteristics of the pilot elevation and traverse tracking errors are similar, regardless of the pilot, the weapon delivery task, the aircraft flying qualities, and the sight system characteristics, all of which were varied in the manned simulation studies. Some of these typical tracking error characteristics are also illustrated in Figures 46 and 47 for two different aircraft configurations.

Due to the pilot's interaction with the aircraft short-period dynamics and with the sight/geometry dynamics, the elevation tracking error contains two predominant modal components. Both frequency components exhibit a limit cycle or low damped type of response. This is consistent with the elevation tracking error time history responses obtained in the FCRWD manned simulation study described in Section 3. It can, therefore, be assumed that these characteristics are quite general and apply to many elevation axis precision attitude tracking tasks.

- Aircraft Configuration
- Longitudinal Configuration:
Short Period Damping = 0.5
Short Period Frequency = 3 rad/sec
- Lateral Directional Configuration:
F-4E with Gun on Waterline

MCAIR Test Pilot

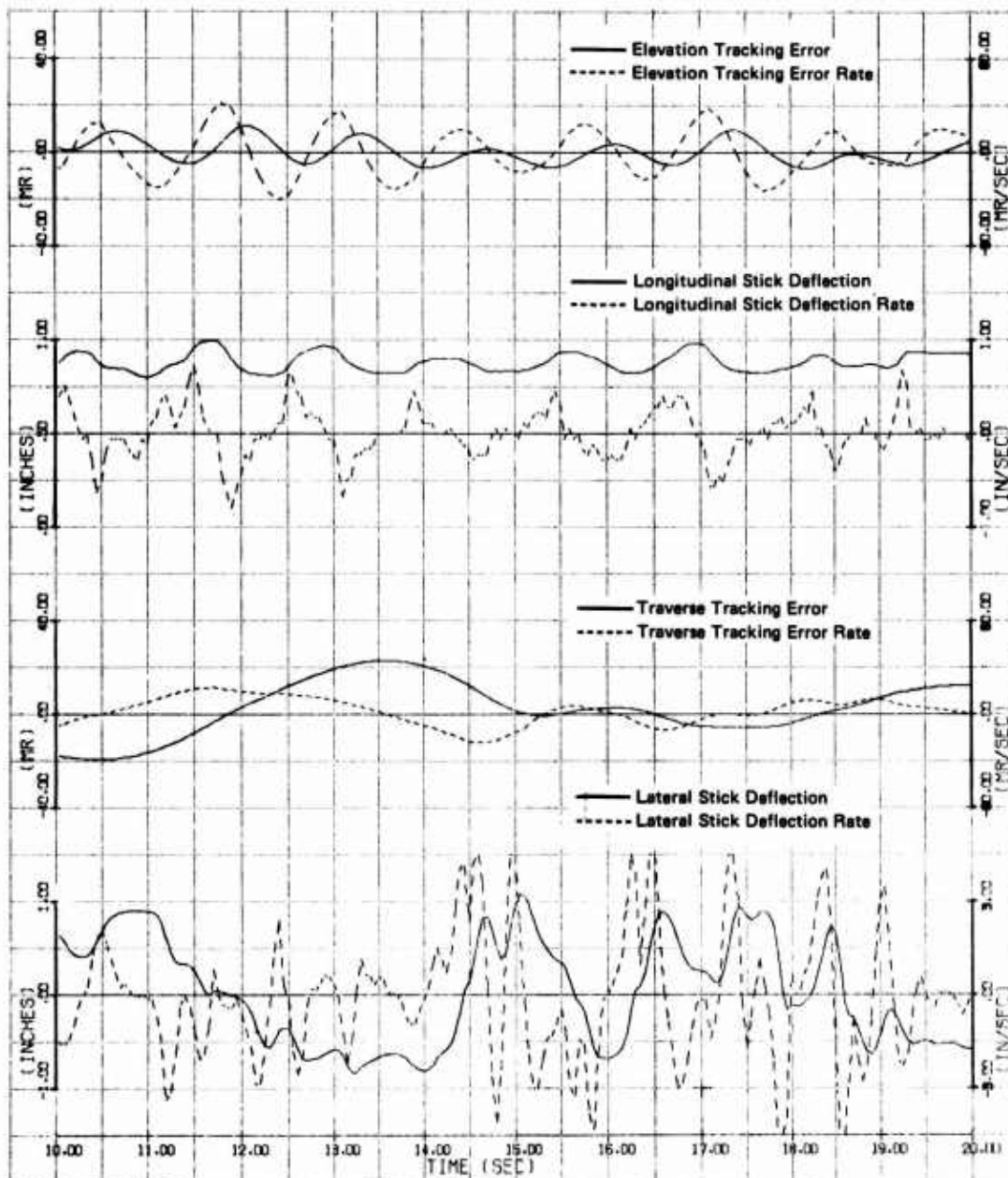


GP78-0864-1

Figure 46. Director Air-to-Air Gunnery Tracking Error and Aircraft Command Time Histories for Aircraft Configuration with Short-Period Damping = 0.50 and Frequency = 3.0 Rad/Sec (Mach 0.8 at 10,000 Ft Altitude, 4 G Target, 1500 Ft < Range < 1900 Ft)

- Aircraft Configuration
- Longitudinal Configuration:
Short-Period Damping = 0.7
Short-Period Frequency = 5 rad/sec
- Lateral-Directional Configuration:
F-4E with Gun on Waterline

MCAIR Test Pilot



OP75-0084-2

Figure 47. Director Air-to-Air Gunnery Tracking Error and Aircraft Command Time Histories for Aircraft Configuration with Short-Period Damping = 0.70 and Frequency = 5.0 Rad/Sec (Mach 0.8 at 10,000 Ft Altitude, 4 G Target, 1500 Ft < Range < 1900 Ft)

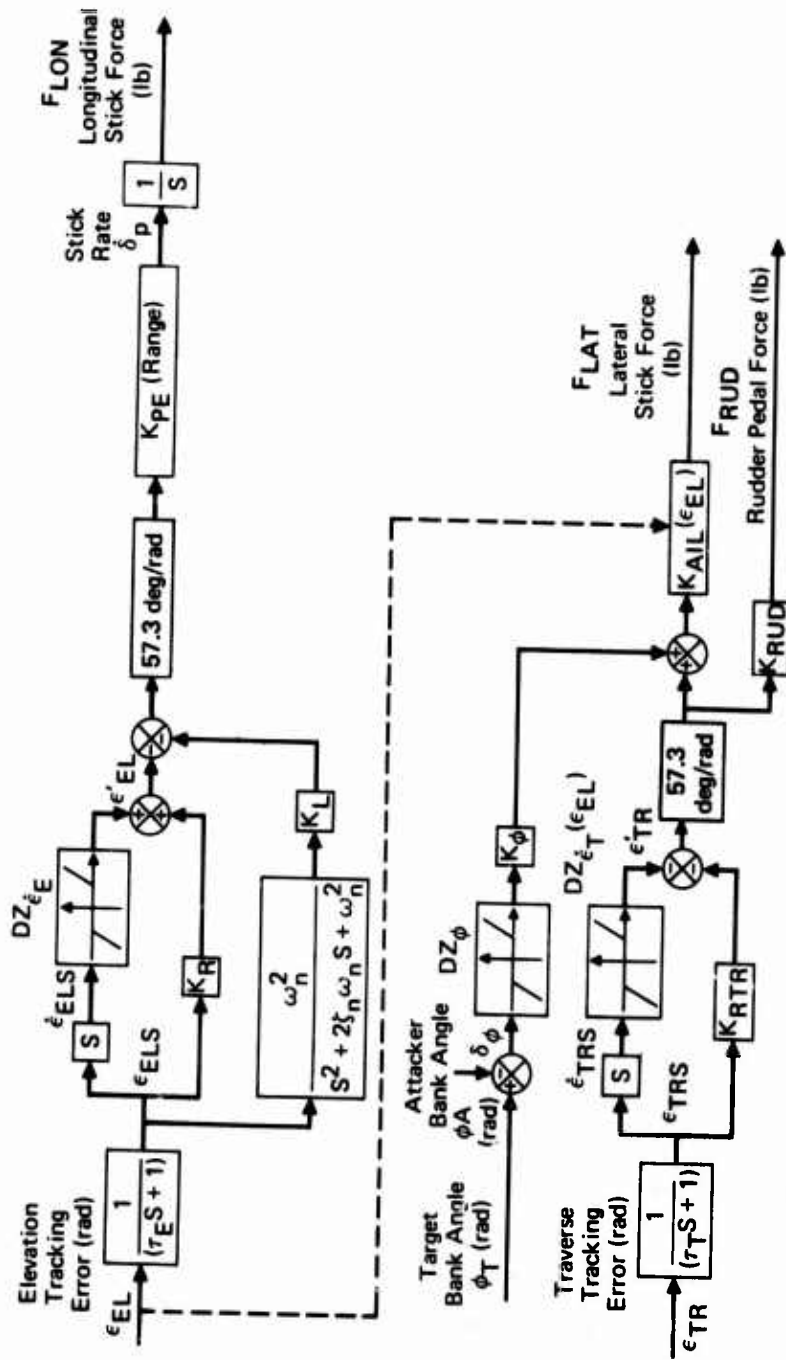
Unlike the elevation tracking error, the traverse tracking error consists primarily of a limit cycle response, with a single frequency and a period ranging from 4 to 8 seconds (Figures 46 and 47). Occasionally, wind gust disturbances or relatively rapid pilot lateral stick action may decrease the period to as low as 2 or 3 seconds. The lower frequency of the traverse tracking error is probably due to the pilot's concentrating more on reducing the elevation tracking error, and to the pilot technique of generating bank angle rate to reduce traverse error by commanding bank angle with stepwise application of lateral stick.

4.3 Pilot Models

The longitudinal and lateral-directional pilot models, developed for terminal weapon delivery precision tracking in the TAWDS programs, are shown in Figure 48. The elevation and traverse tracking error time histories obtained with these models have characteristics like those noted above for the pilot.

The most difficult parameter values to select are the longitudinal and lateral transmission gains K_{PE} and K_{AIL} . From a linear system viewpoint, the damping for the overall pilot/aircraft/geometry/sight system is approximately neutral and these gains are the most critical in attaining this damping level. A negative sign is needed in the pilot models because of the tracking error sign convention. Tracking error is defined here as the piper position with respect to the target, which means the target is taken as the reference.

In Figure 48, the longitudinal gain parameter K_{PE} is shown as a function of tracking range, and the lateral gain parameter K_{AIL} is shown as a function of the elevation tracking error. These variable gains are based on observations and on pilot comments that the longitudinal and lateral-directional axes couple during weapon delivery precision tracking. Figures 46 and 47, and other figures in Section 4.4, indicate that the pilot is more likely to coordinate his longitudinal and lateral commands by moving the stick radially. This means that the pilot acts as a radial controller by nulling both elevation and traverse tracking errors simultaneously. As a result, what might be interpreted as inadvertent coupling may actually be intentionally



GP75-0864-106

Figure 48. Multi-Axis Pilot Model Structure for Air-to-Air and Air-to-Ground Weapon Delivery Tasks

coupled (coordinated) commands. The radial controller approach was used in developing the longitudinal and lateral-directional pilot models.

4.3.1 Longitudinal Pilot Model - The longitudinal pilot model treats the pilot as a proportional-plus-derivative observer of the tracking error input, ϵ_{EL} , with a deadzone on the error rate. This results in an effective, or projected, error, ϵ'_{EL} , which is the tracking error projected a time interval into the future. This projected error is then used, along with the output of the low-pass filter, to determine the pilot's rate input to the control stick, which acts as an integrator in the overall tracking loop. If ϵ_{EL} contains noise, or if its frequency is above the pilot's observation bandwidth, he will first smooth ϵ_{EL} . The longitudinal pilot gains K_{PE} and K_R , and the tracking error rate deadzone ($DZ_{\dot{\epsilon}_E}$) are selected to produce the desired high-frequency limit-cycle characteristic in the elevation tracking error.

The low-frequency component in the elevation tracking error was obtained by using a low-pass filter in the longitudinal pilot model to approximate the pilot's averaging of the high-frequency component of the observed tracking error. The frequency of the low-frequency mode is controlled by the low-pass filter parameters and the gain K_L .

A second-order low-pass filter was selected because it is the simplest function that would give the desired pilot model tracking characteristics. A damping (ζ_n) of 0.6 was chosen because it produces an almost "maximally flat" frequency response for this filter. Results presented in the following section indicate that the natural frequency of the low pass filter, ω_n , must be based on the type of weapon delivery sight.

The effect of K_L on the tracking error response in the longitudinal pilot model is described as follows. By assuming the elevation error rate deadzone to be zero, the longitudinal pilot model transfer function from the tracking error (ϵ_{EL}) to the pilot's longitudinal force command (F_{LON}) is given by:

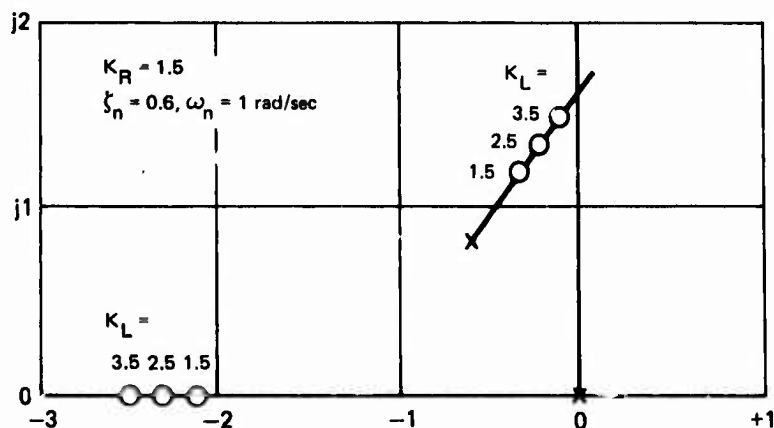
$$\frac{F_{LON}}{\epsilon_{EL}} = \frac{-K_{PE} [s^3 + (2\zeta_n \omega_n + K_R) s^2 + (\omega_n^2 + K_R 2\zeta_n \omega_n) s + (K_L + K_R) \omega_n^2]}{s(s^2 + 2\zeta_n \omega_n s + \omega_n^2) (\tau_E s + 1)} \quad (14)$$

Figure 49 shows how the roots in the numerator of Equation 14 (the zeros of the longitudinal pilot model transfer function) vary as a function of the parameter

K_L . (The values of the other Equation 14 parameters presented in Figure 49 are those used in obtaining the tracking error responses for the Director sight.) The value of K_L thus controls the locations of the complex zeros in the overall longitudinal pilot model transfer function. Poles in the overall aircraft/geometry/pilot tracking loop will be near these complex zeros, since the pilot gain, K_{PE} , will be relatively high to obtain a high-frequency component in ϵ_{EL} . This results in a tracking mode similar to the low-frequency component noted for pilots. Based on results obtained so far, the deadzone does not substantially affect the low-frequency component in the elevation tracking error.

For the various weapon systems considered, a range of values for the longitudinal pilot model's gain parameters has been determined. These are presented in Figure 50. Because these gain values affect the stability of the closed loop tracking task, their recommended values apply specifically only to the aircraft and weapon systems examined in this study. However, they can be used as a guide for other configurations. The parameters are:

- ° τ_E - This prefilter time constant represents the pilot's capability to smooth the observed elevation tracking error.
- ° ζ_n, ω_n - These damping and frequency parameters of the pilot's low pass filtering process represent his interaction with the elevation error's geometry/sight mode.
- ° K_L - This gain parameter is used to adjust the amplitude of the low frequency component in the elevation tracking error.
- ° $DZ_{\dot{\epsilon}_E}$ - This deadzone for the elevation error rate is needed to obtain the limit-cycle type of response in the high frequency



GP78-0884-4

Figure 49. Variation in Longitudinal Pilot Model Transfer Function Zeros with Low-Pass Filter Gain, K_L

Weapon Delivery Task	Longitudinal Pilot Model Parameters					
	K_{PE}	K_R	DZ'_{ϵ_E} (MR/SEC)	K_L	(ω_n, ζ_n)	τ_E
Air-to-Ground Gunnery FDR	$0.5 K_{co} - 0.75 K_{co}$	0.75 - 1.25	5.0	1.0-3.0	(1.0, 0.6)	0.0-0.05
Air-to-Ground Gunnery CCIP	$0.5 K_{co} - 0.75 K_{co}$	0.75 - 1.25	5.0	1.0-3.0	(1.0, 0.6)	0.0-0.05
Air-to-Ground Bombing FIP	$0.5 K_{co} - 0.75 K_{co}$	0.75 - 1.25	5.0	1.0-3.0	(0.5, 0.6)	0.0-0.05
Air-to-Air Gunnery Director	$0.75 K_{co} - 1.2 K_{co}$	0.75 - 1.25	5.0	1.0-3.0	(1.0, 0.6)	0.0-0.05
Air-to-Air Gunnery LCOSS	$0.75 K_{co} - 0.9 K_{co}$	0.75 - 1.25	5.0	1.0-3.0	(1.0, 0.6)	0.0-0.05

K_{co} - Elevation tracking error crossover gains due to aircraft's short-period mode

GP75-0864-5

Figure 50. Recommended Values for Longitudinal Pilot Model Parameters in Terms of the Aircraft Dynamics and Weapon Delivery Task

component. Increasing DZ'_{ϵ_E} usually causes the amplitude to increase and the frequency to decrease.

- ° K_R - This gain parameter affects the amplitude of the high frequency component. With a small K_R it has not been possible to obtain a stable high frequency component.
- ° K_{PE} - The longitudinal pilot model gain, which also affects the amplitude of the high frequency component, has to be determined as a function of the weapon system gain margin stability characteristic. It has to be large enough to excite the high frequency component, but not large enough to cause the tracking to become unstable. Results have shown that this value can be related to the cross-over

gain for the tracking mode, since the cross-over frequency for this mode is closely related to the aircraft's augmented longitudinal short-period frequency. This characteristic is shown by a typical root locus for the elevation tracking error in Figure 51. The integral representation for the pilot's stick command enables the pilot to vary his commands during maneuvering aerial combat flight conditions.

4.3.2 Lateral-Directional Pilot Model - A block diagram of the lateral-directional pilot model that was developed is given in Figure 48. Its traverse tracking error time history responses are similar to those seen in Figures 46 and 47. It has the characteristics of a single frequency, limit cycle response with a period ranging from 4 to 8 seconds.

Like the longitudinal pilot model, the lateral-directional model is based on the assumption that the pilot acts as a proportional-plus-derivative observer of the traverse tracking error, ϵ_{TR} , with a deadzone on the error rate. This results in an effective or projected traverse error signal, ϵ'_{TR} , which the pilot uses to determine his lateral stick and rudder pedal deflection commands for attitude pointing. When ϵ_{TR} contains noise or its frequency is above the pilot's observation bandwidth, he will base ϵ'_{TR} on a smoothed or filtered value of ϵ_{TR} . Then multiplication of ϵ'_{TR} by appropriate gains will give the pilot model's lateral stick and rudder pedal position or force commands.

A review of the pilot's lateral-directional commands during the manned simulation indicates that for the air-to-air terminal gunnery tracking task, his directional (rudder pedal) commands were usually negligible, (except during large maneuvers such as following the target through a snap roll reversal). In addition, the pilot's rudder commands during bombing were usually negligible. Only during air-to-ground gunnery tracking in the presence of wind disturbances were the rudder pedal commands significant.

The rudder commands are assumed to be directly related to the lateral stick commands because the pilot would try to coordinate lateral stick and rudder pedal commands (though not necessarily about the velocity vector).

The lateral-directional pilot model includes the feedback of attacker roll angle relative to the target, which could be used to modify the lateral stick commands based on the traverse tracking error. However, plots of differential bank angle between the target and attacker aircraft indicate that

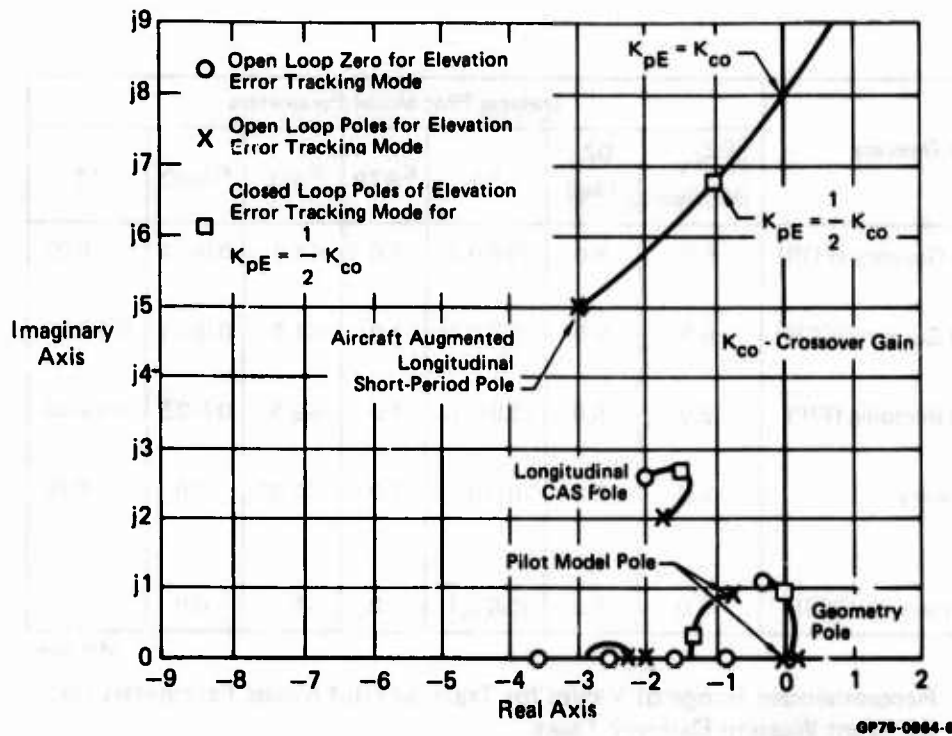


Figure 51. Typical Root Locus for Elevation Tracking Error

the pilot probably does not use this variable as a primary input. It is doubtful that the pilot can accurately detect the differential roll angles typical of precision air-to-air tracking. In air-to-ground tracking the pilot may command significant roll angles to keep the pipper on the target during wind disturbances. As a result, it is felt that the pilot uses the differential roll angle feedback primarily to stabilize excessive wing rocking. On the other hand, during the acquisition phase, this feedback is probably used by the pilot as a primary input. As an example, the target's roll attitude can greatly aid the pilot to get near the target's turning plane in air-to-air combat, which he must do before beginning the terminal tracking phase.

A range of values for the lateral-directional pilot model's gain parameters has been determined for different system configurations. These values are presented in Figure 52.

The gain parameters of the multi-input, multi-output traverse pilot model structure are:

- τ_T - This time constant parameter represents the pilot's capability to smooth the observed traverse tracking error.

Weapon Delivery	Traverse Pilot Model Parameters						
	$DZ_{\dot{\epsilon}_T}$ (MR/sec)	DZ_{ϕ} (deg)	K_{ϕ}	K_{RTR}	K_{AIL}	K_{RUD}	τ_T
Air-to-Ground Gunnery (FDR)	5.0	5.0	(0.0-0.1)	1.0	≤ 1.8	0.0-6.2	0.0-0.05
Air-to-Ground Gunnery (CCIP)	5.0	5.0	(0.0-0.1)	1.0	≤ 1.8	0.0-6.2	0.0-0.05
Air-to-Ground Bombing (FIP)	5.0	5.0	(0.0-0.1)	1.0	≤ 0.9	0.0-3.5	0.0-0.05
Air-to-Air Gunnery (Director)	5.0	5.0	(0.0-0.1)	1.0	≤ 0.36	0.0	0.0-0.05
Air-to-Air Gunnery (LCOSS)	5.0	5.0	(0.0-0.1)	1.0	≤ 0.6	0.0	0.0-0.05

GP78-0884-7

Figure 52. Recommended Range of Values for Traverse Pilot Model Parameters for Different Weapon Delivery Tasks

- $DZ_{\dot{\epsilon}_T}$ - This threshold describes the pilot's ability to perceive traverse error rates.
- K_{RTR} , K_{AIL} - These gain parameters affect the amplitude and frequency of the traverse error. The proper value of these gains, needed to reproduce the 4 to 8 second period traverse error response, can be determined by linear stability analysis.
- K_{RUD} - This gain parameter enables the model to command rudder deflections. It permits the tracking techniques of different pilots to be modeled. A review of manned simulations indicates that for the air-to-air terminal gunnery tracking task, directional (rudder pedal) commands were usually negligible. For the air-to-ground Fixed Depressed Reticle tracking task in the presence of wind disturbances, rudder pedal deflection commands were found to be significant.
- DZ_{ϕ} , K_{ϕ} - These gain parameters, which relate the pilot's lateral stick forces due to the sensed differential bank angle between the target and attacker, are used to prevent excessive wing rocking.

4.4 Pilot Model Validation

This section presents representative tracking responses of the pilot model and of two Air Force pilots (Pilot A and Pilot B) for the weapon delivery tasks simulated in the manned simulation study. Both time history and frequency response curves are presented for the tracking errors and the aircraft commands. Although different aircraft configurations were used in developing and validating pilot models for weapon delivery as described in the Flight Control Requirements for Weapon Delivery Background Information Report, tracking responses are only shown in this section for the F-4E aircraft configured with the TWeaD flight control system and the gunline oriented along the body-X axis.

The pilot model parameter values used in obtaining the tracking responses are summarized in Figure 53. These values are for the same air-to-air and air-to-ground encounters in the manned simulation described in Section 3.2. This model was developed by correlating its dominant frequency characteristics in the elevation and traverse tracking error time histories with those of the two Air Force pilots. Its validity is shown by comparing its frequency response characteristics to those of the two pilots.

Time history curves are presented for the elevation and traverse tracking errors and for the longitudinal stick, lateral stick, and rudder pedal force commands. These curves, which are for the time interval from 10 to 20 seconds in both air-to-air and air-to-ground encounters, show how the pilot model tracking error responses are similar to those of the two USAF pilots.

The frequency responses corresponding to the tracking error and pilot aircraft commands for the time interval from 5 to 20 seconds are presented to show their similarity between the pilot model and human pilot closures. They were obtained with the computer programs described in Appendix VII. The program responses include:

- The longitudinal and lateral-directional gain and phase curves. They directly relate the elevation tracking error to the longitudinal stick commands and the traverse tracking error to the lateral stick commands. Associated with these curves are "1 σ " confidence bands.
- The multiple coherence functions, $\gamma_{F_{LON}}^2$ and $\gamma_{F_{LAT}}^2$ for the longitudinal (F_{LON}) and lateral (F_{LAT}) stick force commands. Since the elevation

Pilot Model Parameter Values						
	Longitudinal				Lateral Directional	
Sight	K_{PE}	K_R	K_L	ω_n	K_{AIL}	K_{RUD}
Director	6.3	1.0	2.5	1.0	0.36	0.0
LCOSS	9.3	1.0	2.5	1.0	0.6	0.0
FDR	5.4	1.0	2.0	1.0	1.8	6.2
CCIP	5.4	0.75	1.0	1.0	1.8	6.2
FIP	2.1	0.75	1.0	0.5	0.9	0.0
Parameters Not Changed	$\tau_\epsilon = 0, \zeta_n = 0.6, DZ_{\dot{\epsilon}_E} = 0.005 \text{ rad/sec}$				$\tau_T = 0, K_{RTR} = 1.0, K_\phi = 0, DZ_{\dot{\epsilon}_T} = 0.005 \text{ rad/sec}$	

GP75-0864-8

Figure 53. Summary of Pilot Model Parameter Values Used With F-4 TWeaD Aircraft Simulation

and traverse tracking errors are usually weakly correlated, $\gamma_{F_{LON}}^2$ is a close approximation to the fraction of the longitudinal stick force that is linearly related to the elevation tracking error. Likewise, $\gamma_{F_{LAT}}^2$ is a close approximation to the fraction of the lateral stick force that is linearly related to the traverse tracking error. As noted in Appendix VII, the confidence bands usually increase as the multiple coherence functions decrease.

- The stick force spectrum and remnant curves. These curves show the frequency content of the stick commands and that part of the stick commands not linearly related to the tracking errors. It may be noted that $(1 - \gamma_{F_{LON}}^2)$ times the longitudinal stick force spectrum is the longitudinal stick force remnant, and that the same relationship holds for the lateral stick force and rudder pedal remnants.
- The elevation and traverse tracking error spectra. They give the frequency content of the tracking error time histories.

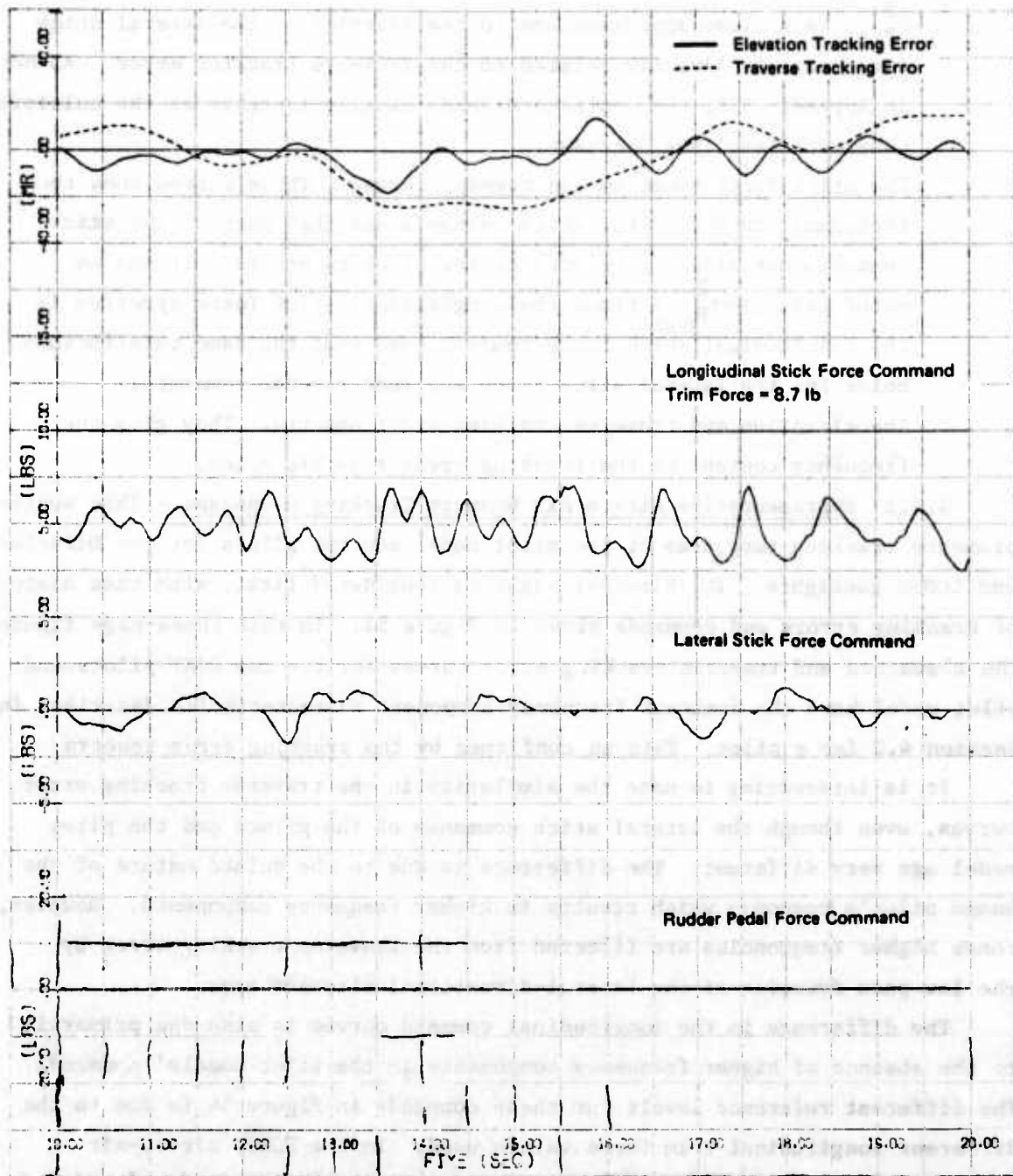
4.4.1 Representative Air-to-Air Gunnery Tracking Responses - This section presents tracking responses of the pilot model and two pilots for the Director and LCOSS gunsights. The Director sight is considered first, with time histories of tracking errors and commands given in Figure 54. In this three-page figure, the elevation and traverse tracking error curves for the two USAF pilots and pilot model have the dominant frequency component characteristics described in Section 4.2 for a pilot. This is confirmed by the tracking error spectra.

It is interesting to note the similarity in the traverse tracking error curves, even though the lateral stick commands of the pilots and the pilot model are very different. The difference is due to the pulsed nature of the human pilot's commands which results in higher frequency components. However, these higher frequencies are filtered from the traverse tracking error by the low-pass dynamics of the lateral-directional aircraft axes.

The difference on the longitudinal command curves is also due primarily to the absence of higher frequency components in the pilot models' commands. The different reference levels for these commands in Figure 54 is due to the different longitudinal trim force values used. In the FCRWD air-to-air simulation runs, the pilots were instructed to trim the longitudinal stick force at the start of the run to a value they desired. The trim value for the pilot model is a scaling factor for plotting in Figure 54.

● Aircraft Configuration 1
F-4 TWeaD

Pilot A

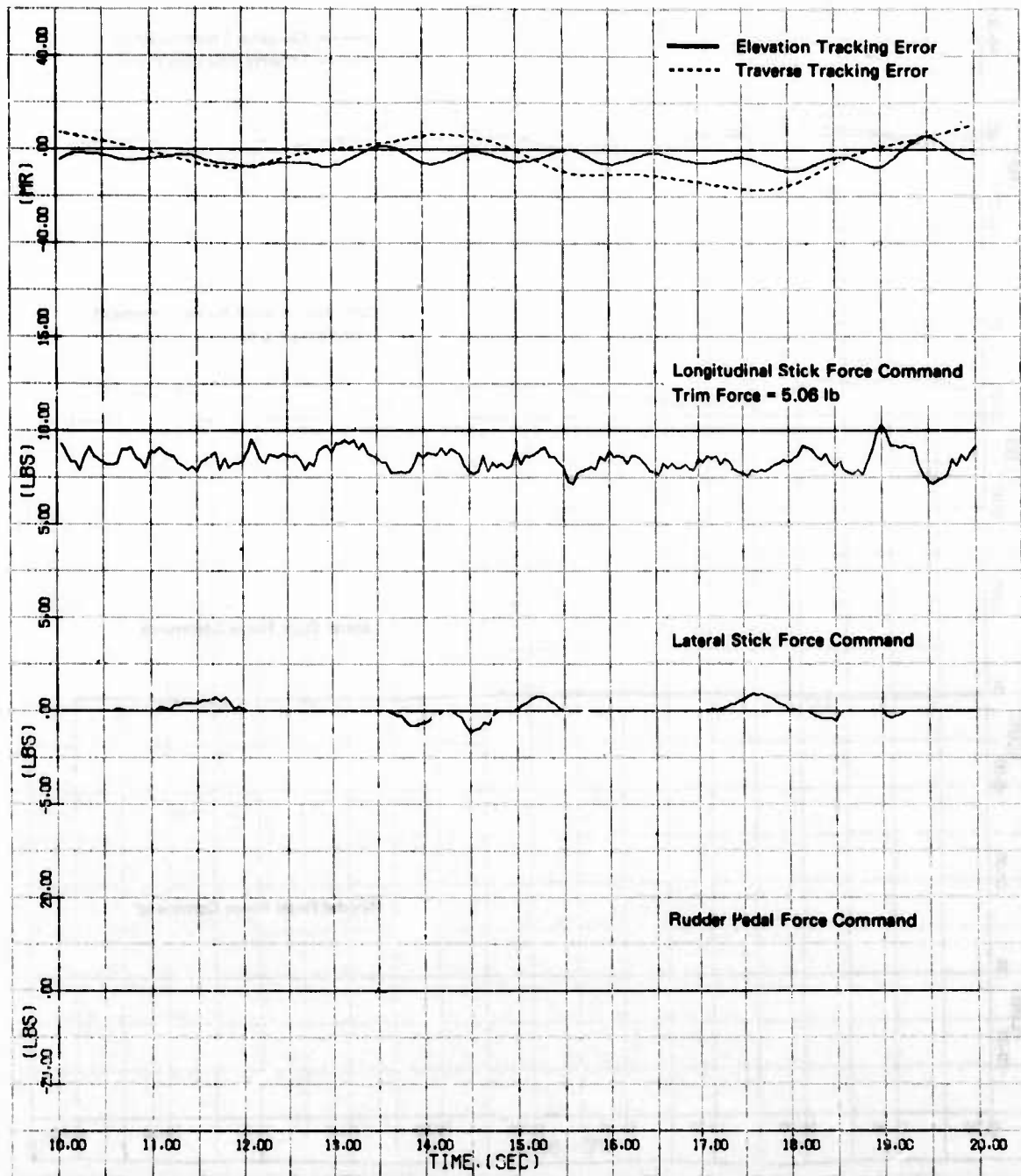


GP75-0864-9

Figure 54. Director Air-to-Air Gunnery Tracking Error and Aircraft Command Time Histories for F-4 TWeaD Aircraft Configuration (Mach 0.8 at 10,000 Ft Altitude, 4 G Target, 1500 Ft < Range < 1900 Ft)

● Aircraft Configuration 1
F-4 TWeeD

Pilot B

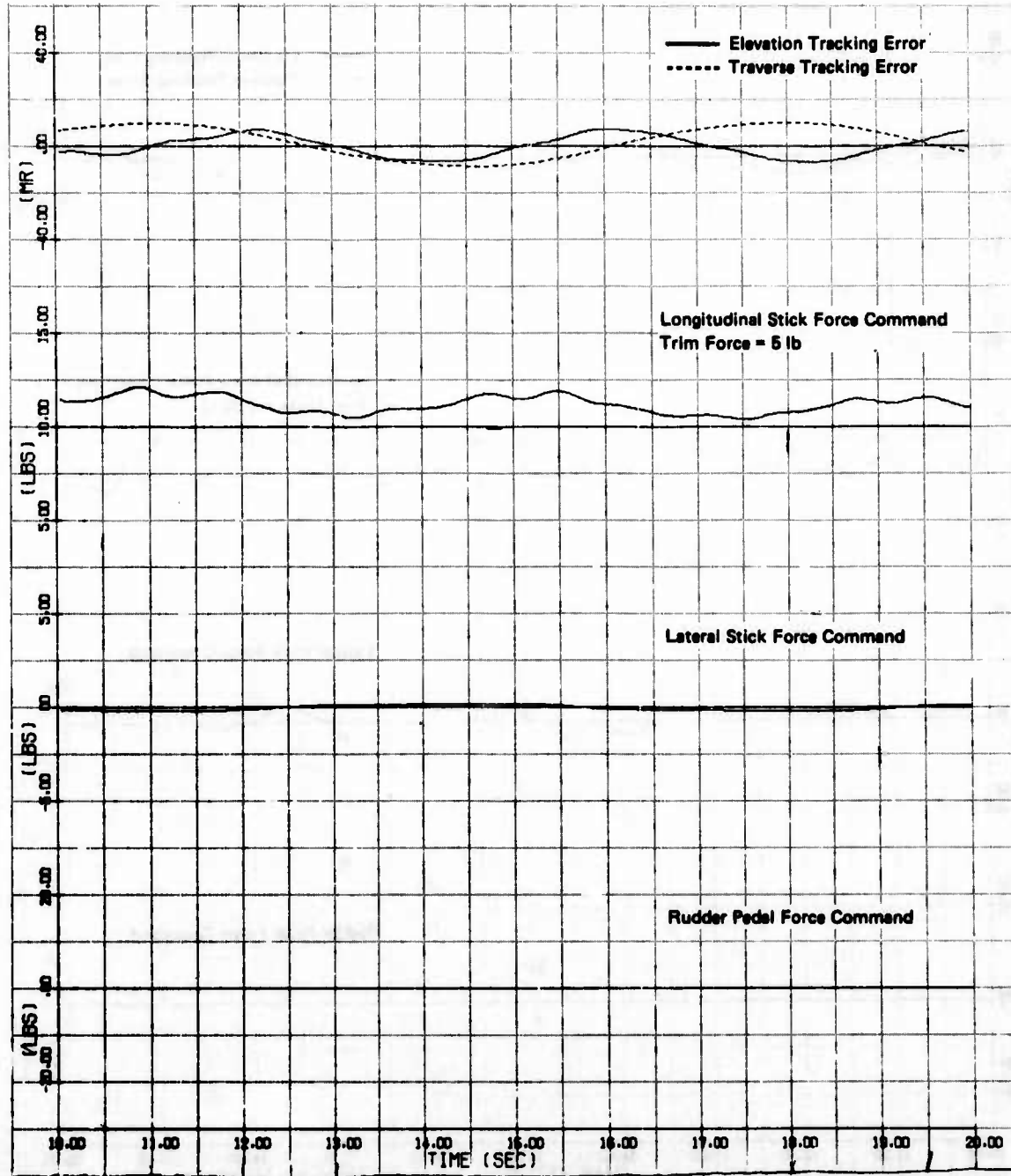


GP75-0004-10

Figure 54. Director Air-to-Air Gunnery Tracking Error and Aircraft Command Time Histories for F-4 TWeeD Aircraft Configuration (Continued)
(Mach 0.8 at 10,000 Ft Altitude, 4 G-Target, 1500 Ft < Range < 1900 Ft)

● Aircraft Configuration 1
F-4 TWeeD

Pilot Model



0979-0004-11

Figure 54. Director Air-to-Air Gunnery Tracking Error and Aircraft Command Time Histories for F-4 TWeeD Aircraft Configuration (Concluded)
(Mach 0.8 at 10,000 Ft Altitude, 4 G Target, 1500 Ft < Range < 1900 Ft)

Figure 55 shows longitudinal gain and phase curves which linearly relate the elevation tracking error to the longitudinal stick force command. Also shown is the multiple coherence curve for the longitudinal stick force. Corresponding spectral curves are given in Figure 56 for the elevation tracking error, and the longitudinal stick force and its remnant. These curves in Figures 55 and 56 are very similar for the two pilots and the pilot model. This close similarity resulted because the criterion used in developing the pilot model was to approximate the pilot's elevation tracking error frequency characteristics.

The lateral gain and phase curves and the multiple coherence curves are shown in Figure 57. Corresponding spectral curves are shown in Figure 58. These curves are very similar for the two pilots, indicating their control dynamics for this steady state 4g encounter with the Director sight and this particular aircraft were essentially the same. In addition, the traverse tracking error spectra for the pilots and the pilot model are also similar. At frequencies below approximately 5 rad/sec, the pilot and pilot model gain and phase curves are similar. Above this frequency, the difference is due to the presence of higher frequency components in the pilot's lateral stick force commands.

Time histories of tracking errors and commands for the two USAF pilots and pilot model using the LCOSS sight are given in Figure 59. The curves in this three-page figure are similar to those presented in Figure 54 for the Director sight, although the pilots had more difficulty in controlling the traverse tracking error. In addition, Pilot A made some use of the rudder in Figure 59. However, the pilots usually did not use the rudder during the time interval shown, which is for a steady state 4 g portion of the air-to-air gunnery encounter. Corresponding to Figure 59, Figure 60 shows longitudinal gain, phase, and multiple coherence curves while Figure 61 shows the spectral curves. Figures 62 and 63 contain lateral axis pilot frequency responses and spectral curves. In general the comments given above for comparing the pilots and pilot model tracking responses with the Director sight are also applicable to the LCOSS sight. For air-to-air gunnery the frequency response characteristics of the pilot model compare favorably with those of the human pilots within the frequency bandwidth of the tracking error.

The primary difference in the frequency responses in Figures 55 to 58 and Figures 60 to 63 for the Director and LCOSS sights is in the pilot phase

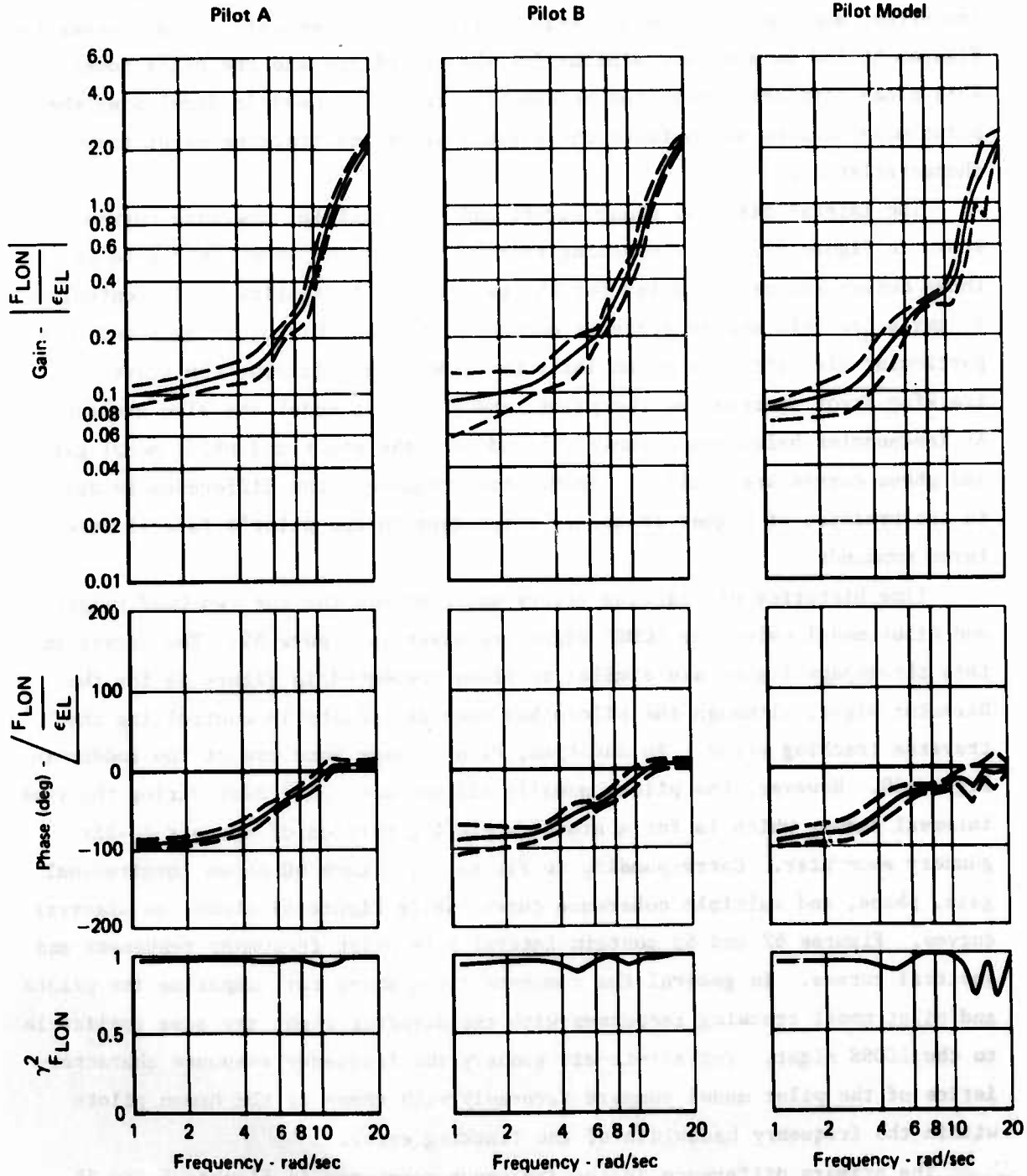
F_{LON} - Longitudinal Stick Force Command (lb)

ε_{EL} - Elevation Tracking Error (mr)

γ_{F_{LON}}² - Multiple Coherence of F_{LON}

--- - 1σ Confidence Band

● Aircraft Configuration 1
F-4 TWeaD

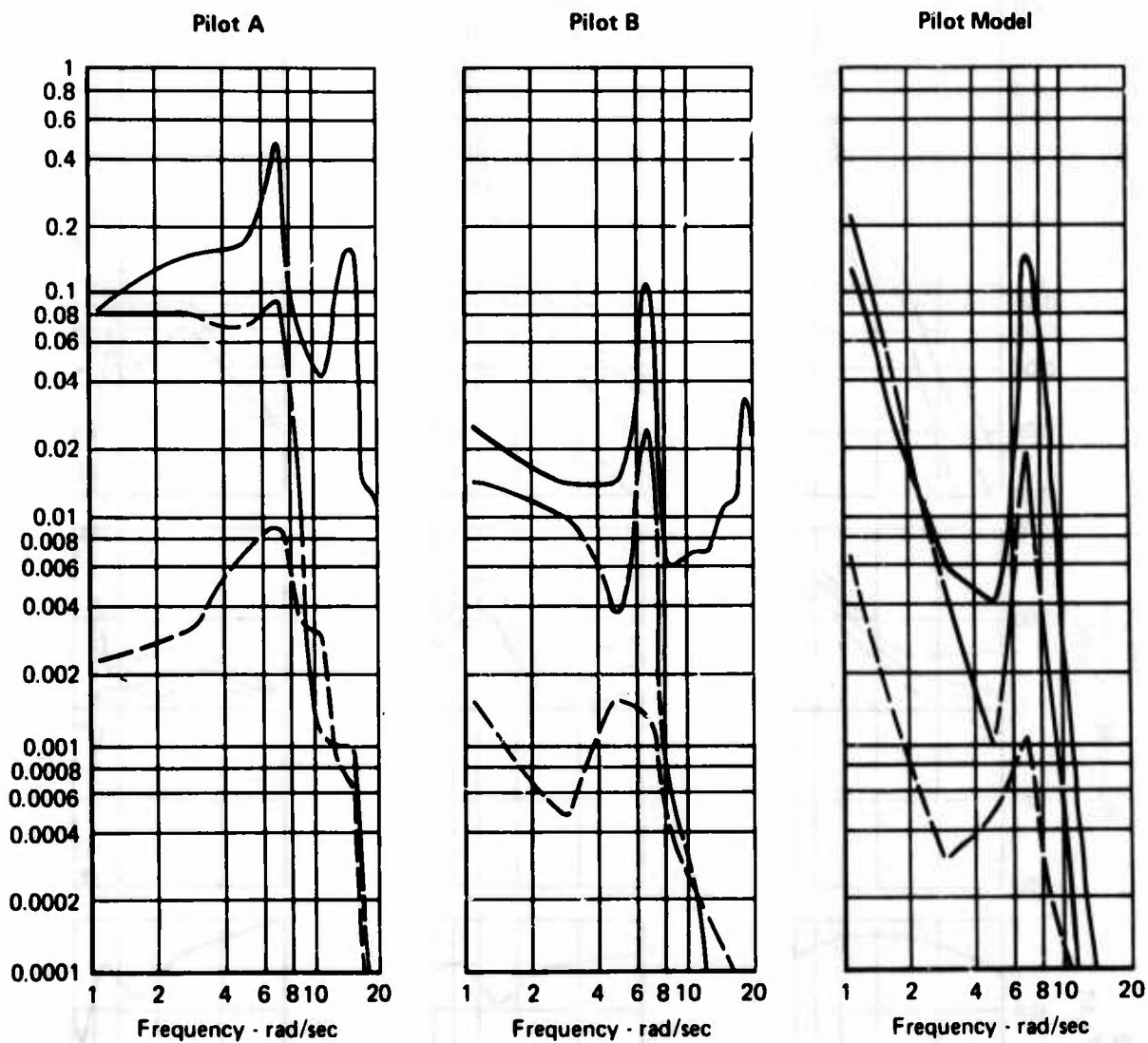


OP75-0064-429

Figure 55. Longitudinal Frequency Responses for Air-to-Air Gunnery Tasks with Director Sight and F-4 TWeaD Aircraft Configuration (Mach 0.8 at 10,000 Ft Altitude, 4 G Target, 1500 Ft < Range < 1900 Ft)

————— Longitudinal Stick Force Command Spectrum (lb²)
 - - - - - Longitudinal Stick Force Command Remnant (lb²)
 - - - - - Elevation Tracking Error Spectrum/100 (mr²)

● Aircraft Configuration 1
 F-4 TWeaD

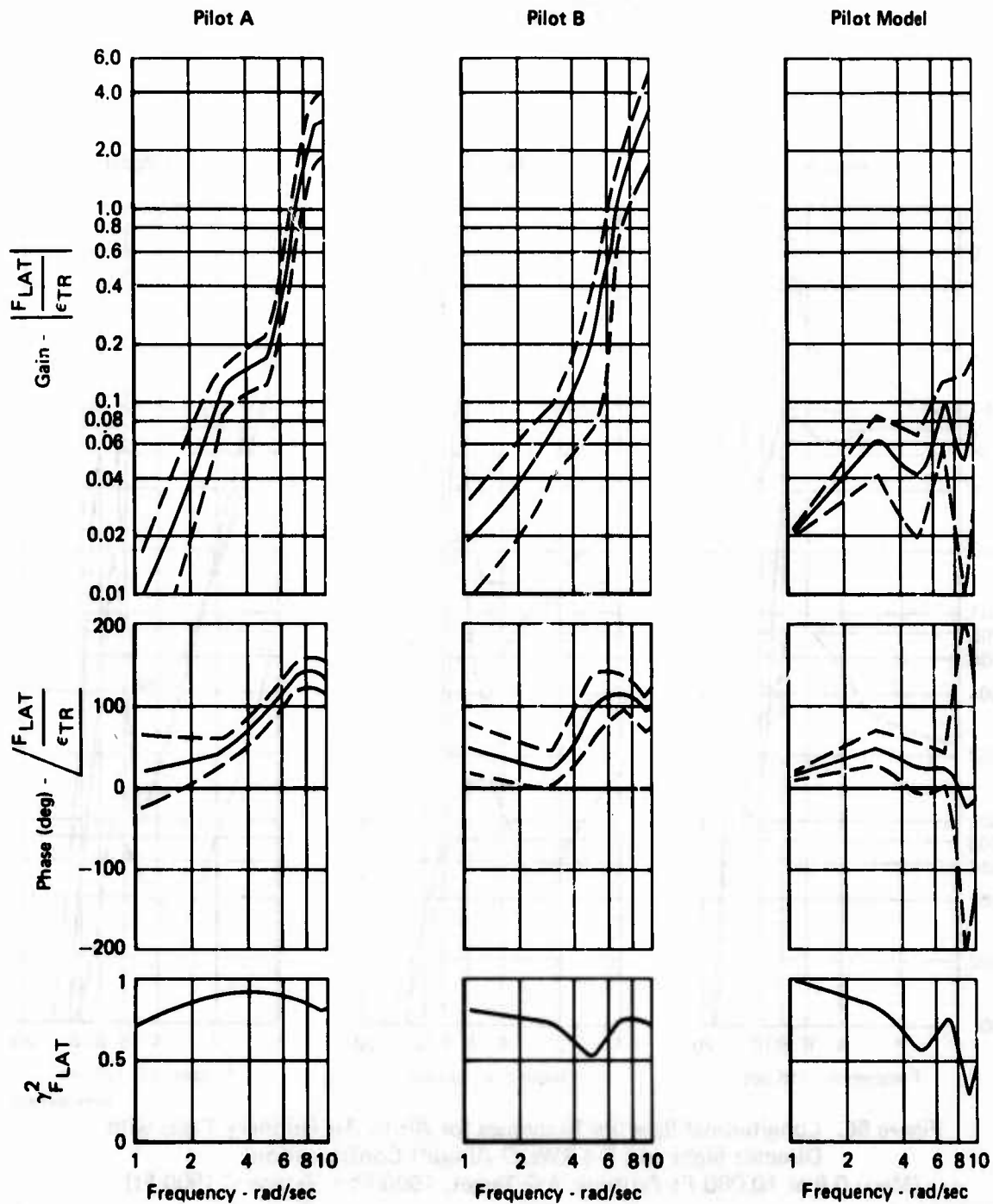


GP76-0884-430

Figure 56. Longitudinal Spectral Responses for Air-to-Air Gunnery Tasks with Director Sight and F-4 TWeaD Aircraft Configuration (Mach 0.8 at 10,000 Ft Altitude, 4 G Target, 1500 Ft < Range < 1900 Ft)

F_{LAT} - Lateral Stick Force Command (lb)
 ϵ_{TR} - Traverse Tracking Error (mr)
 γ_{FLAT}^2 - Multiple Coherence of F_{LAT}
 --- - 1 σ Confidence Band

● Aircraft Configuration 1
 F-4 TWeaD

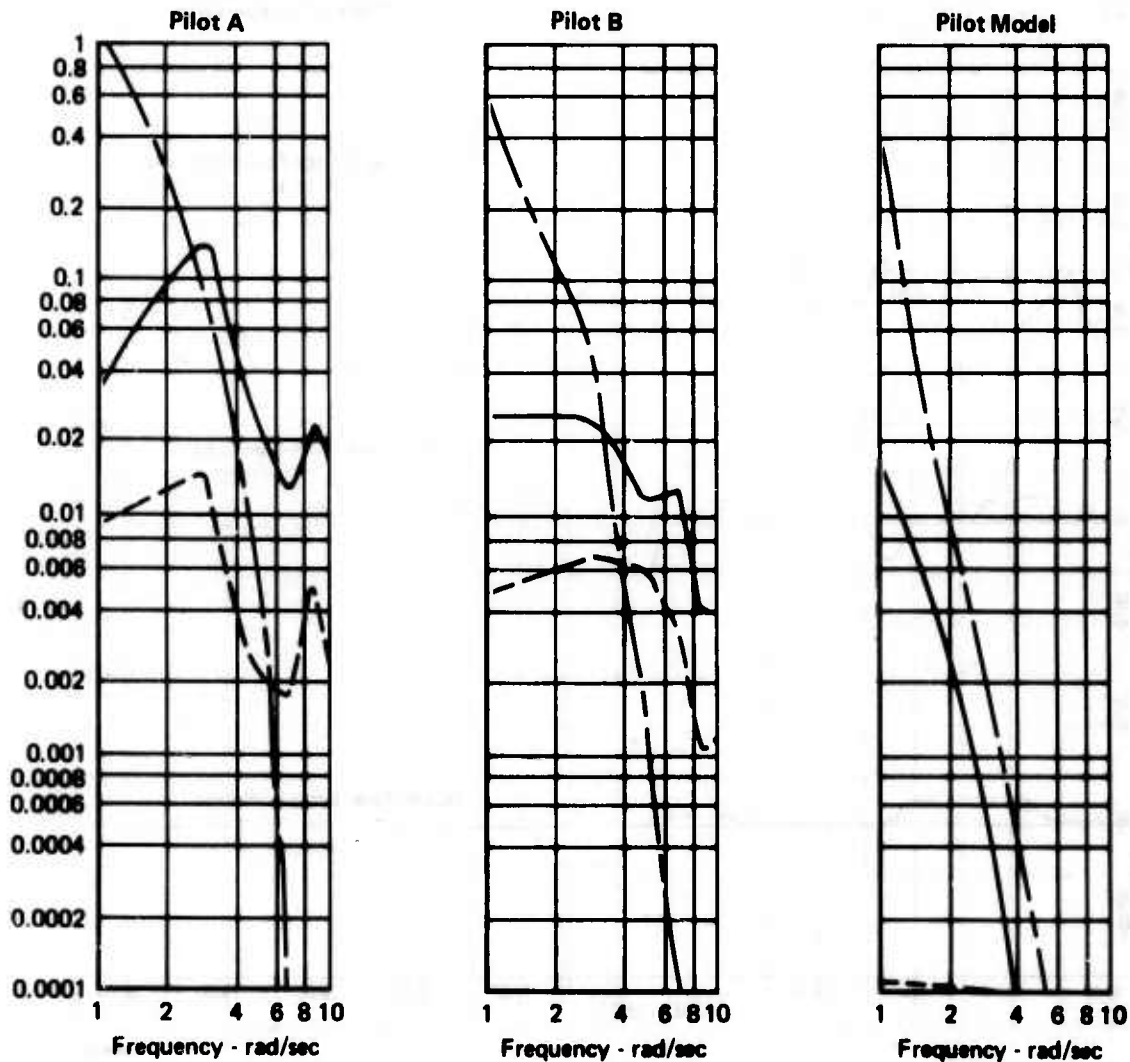


GP78-0864-431

Figure 57. Lateral Frequency Responses for Air-to-Air Gunnery Tasks with Director Sight and F-4 TWeaD Aircraft Configuration (Mach 0.8 at 10,000 Ft Altitude, 4 G Target, 1500 Ft < Range < 1900 Ft)

— Lateral Stick Force Command Spectrum (lb^2)
 - - - Lateral Stick Force Command Remnant (lb^2)
 — Traverse Tracking Error Spectrum/100 (mr^2)

● Aircraft Configuration 1
 F-4 TWeaD

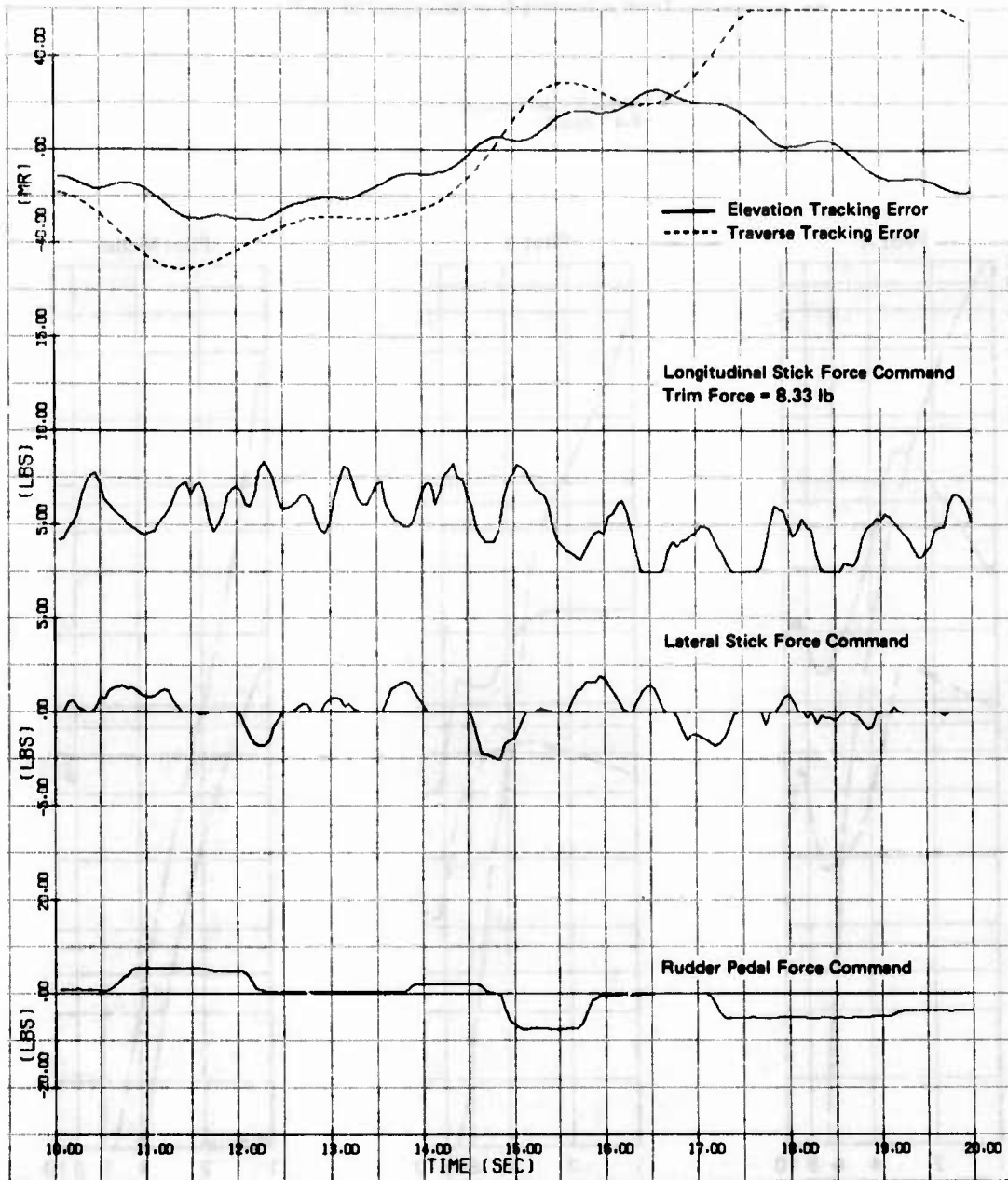


OP78-0064-432

Figure 58: Lateral Spectral Responses for Air-to-Air Gunnery Tasks with Director Sight and F-4 TWeaD Aircraft Configuration (Mach 0.8 at 10,000 Ft Altitude, 4 G Target, 1500 Ft < Range < 1900 Ft)

● Aircraft Configuration 1
F-4 TWeeD

Pilot A

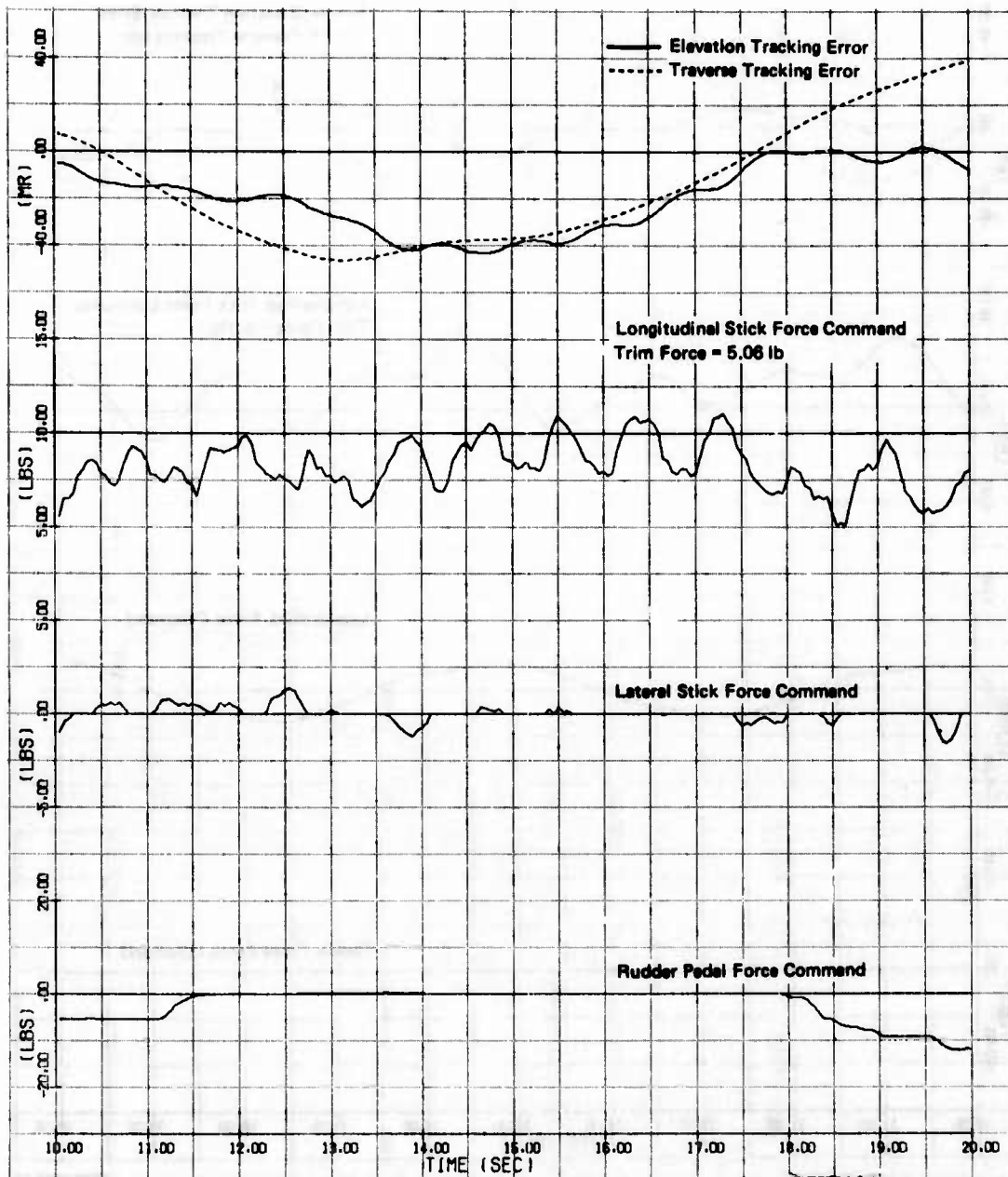


OP78-0884-10

Figure 59. LCOSS Air-to-Air Gunnery Tracking Error and Aircraft Command Time Histories for F-4 TWeeD Aircraft Configuration (Mach 0.8 at 10,000 Ft Altitude, 4 G Target, 1500 Ft < Range < 1900 Ft)

● Aircraft Configuration 1
F-4 TWeaD

Pilot B

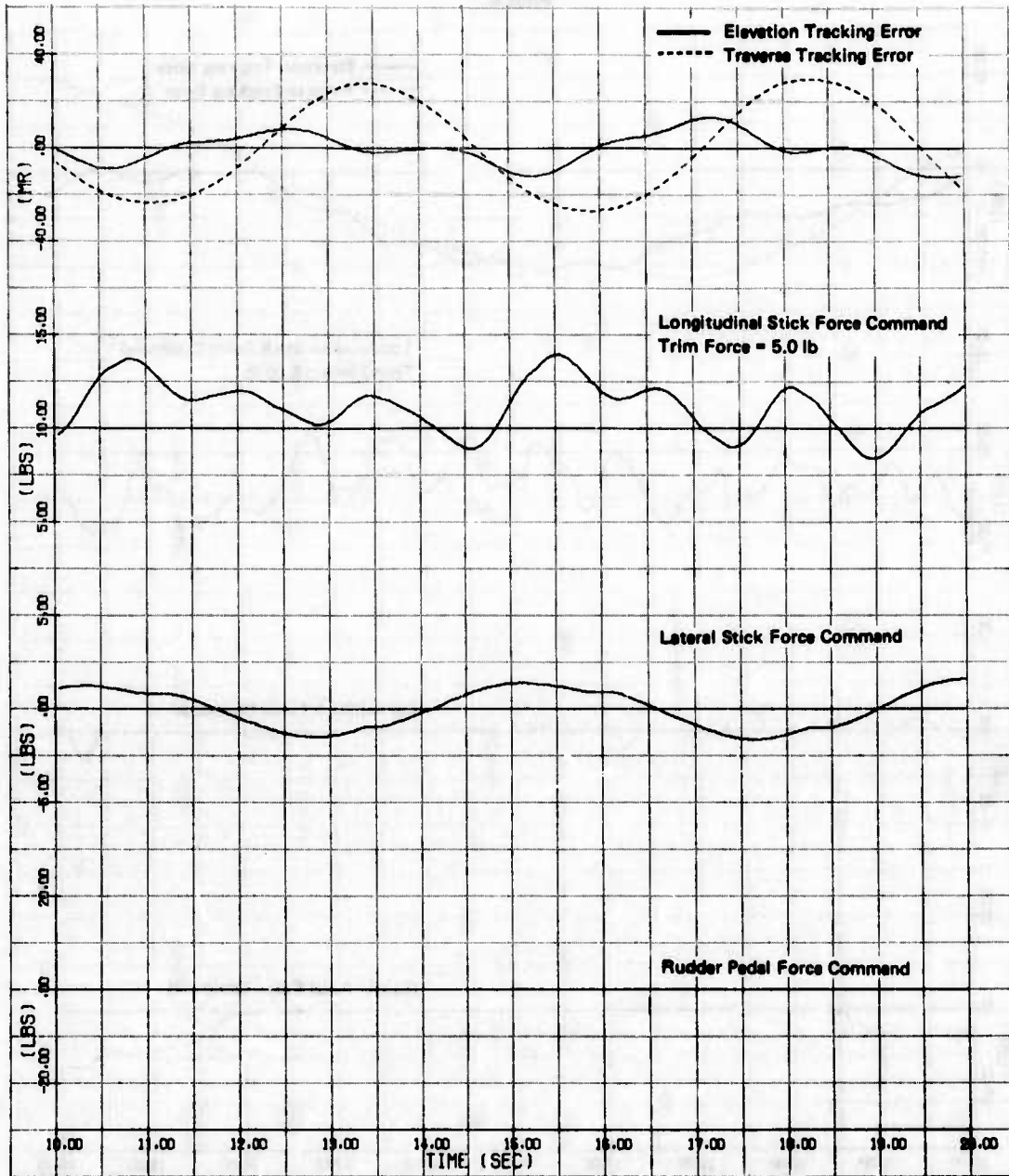


OP78-0004-17

Figure 59. LCOSS Air-to-Air Gunnery Tracking Error and Aircraft Command Time Histories for F-4 TWeaD Aircraft Configuration (Continued) (Mach 0.8 at 10,000 Ft Altitude, 4 G Target, 1500 Ft < Range < 1900 Ft)

● Aircraft Configuration 1
F-4 TWeaD

Pilot Model



OP75-0064-18

Figure 59. LCOSS Air-to-Air Gunnery Tracking Error and Aircraft Command Time Histories for F-4 TWeaD Aircraft Configuration (Concluded)
(Mach 0.8 at 10,000 Ft Altitude, 4 G Target, 1500 Ft < Range < 1900 Ft)

F_{LON} - Longitudinal Stick Force Command (lb)
 ϵ_{EL} - Elevation Tracking Error (mr)
 $\gamma_{F_{LON}}^2$ - Multiple Coherence of F_{LON}
 --- - 10 Confidence Band

● Aircraft Configuration 1
 F-4 TWeaD

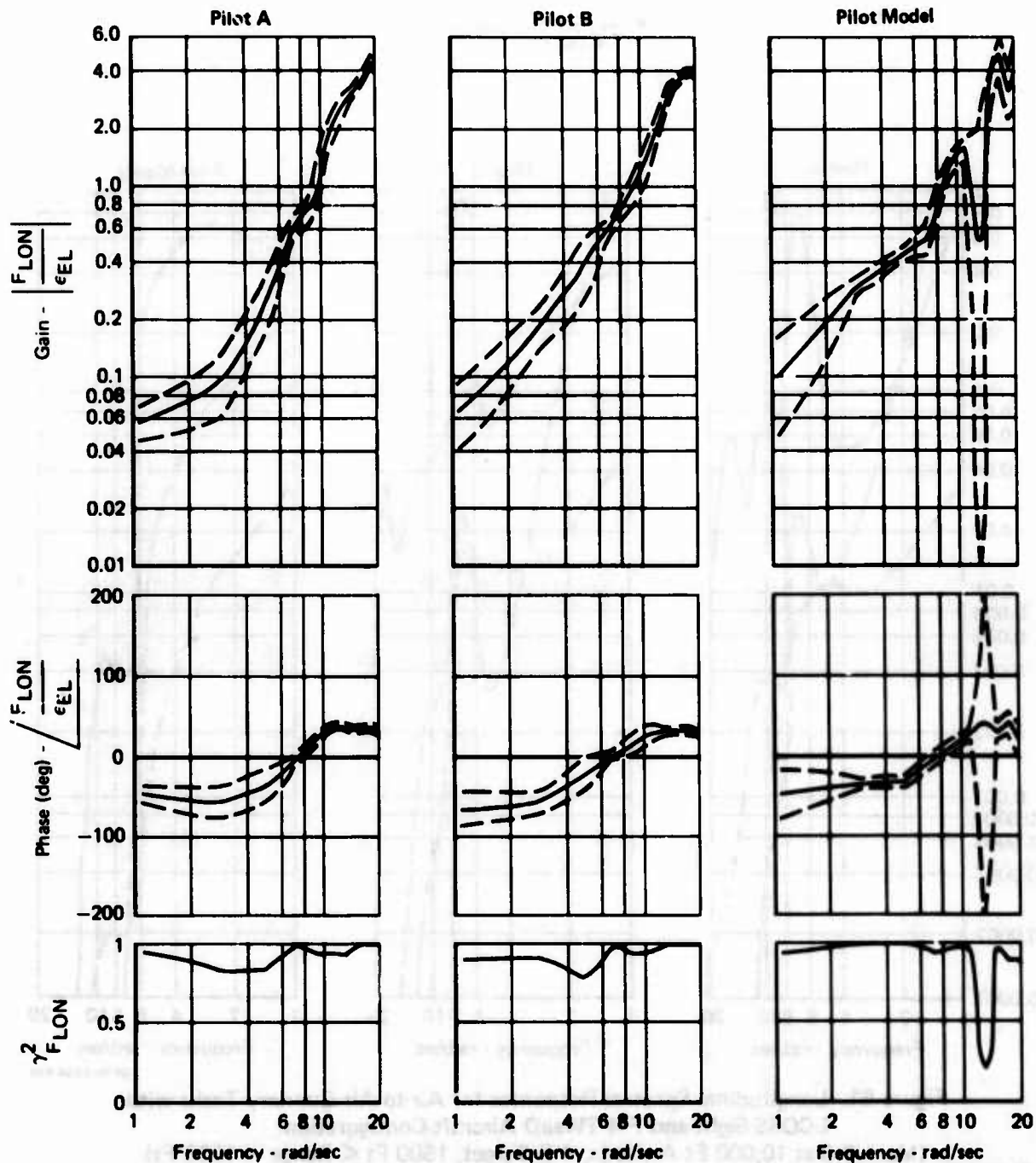
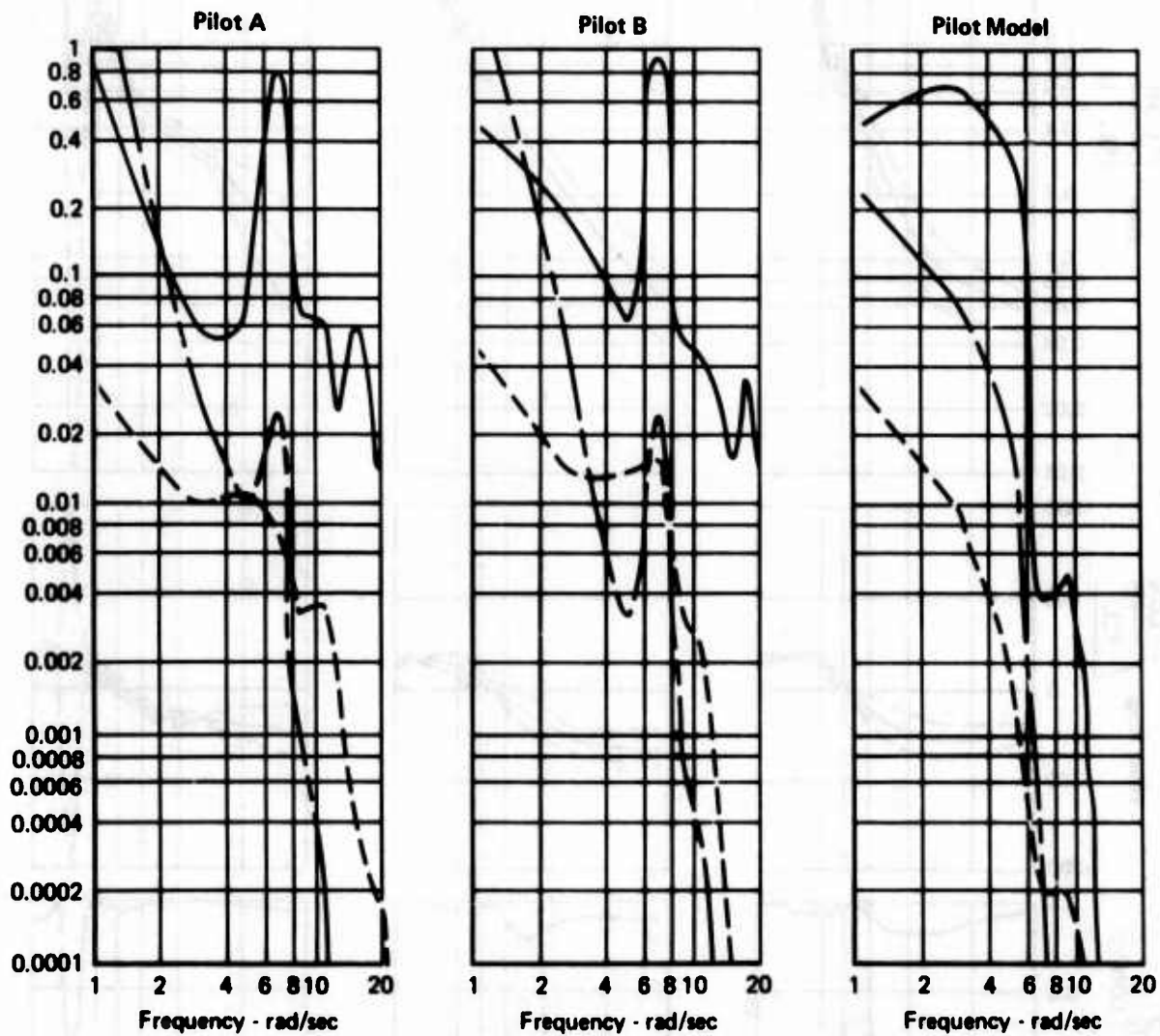


Figure 60. Longitudinal Frequency Responses for Air-to-Air Gunnery Tasks with
 LCOSS Sight and F-4 TWeaD Aircraft Configuration
 (Mach 0.8 at 10,000 Ft Altitude, 4 G Target, 1500 Ft < Range < 1900 Ft)

0975-0064-433

————— Longitudinal Stick Force Command Spectrum (lb^2)
 - - - - - Longitudinal Stick Force Command Remnant (lb^2)
 - - - - - Elevation Tracking Error Spectrum/100 (mr^2)

● Aircraft Configuration 1
 F-4 TWeaD



OP75-0884-434

**Figure 61. Longitudinal Spectral Responses for Air-to-Air Gunnery Tasks with
 LCOSS Sight and F-4 TWeaD Aircraft Configuration
 (Mach 0.8 at 10,000 Ft Altitude, 4 G Target, 1500 Ft < Range < 1900 Ft)**

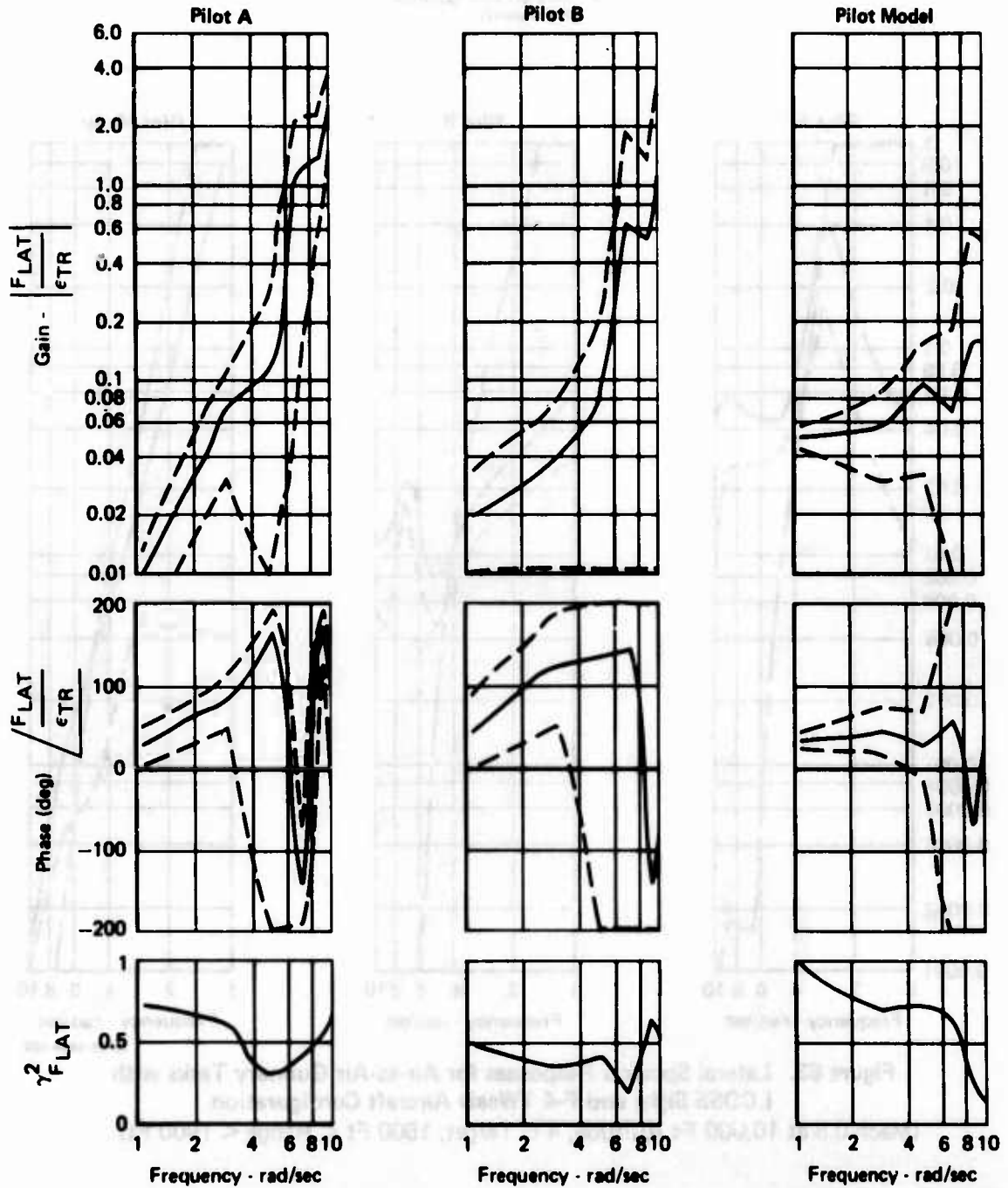
F_{LAT} - Lateral Stick Force Command (lb)

ϵ_{TR} - Traverse Tracking Error (mr)

$\gamma_{F_{LAT}}^2$ - Multiple Coherence of F_{LAT}

--- - 1 σ Confidence Band

● Aircraft Configuration 1
F-4 TWeaD

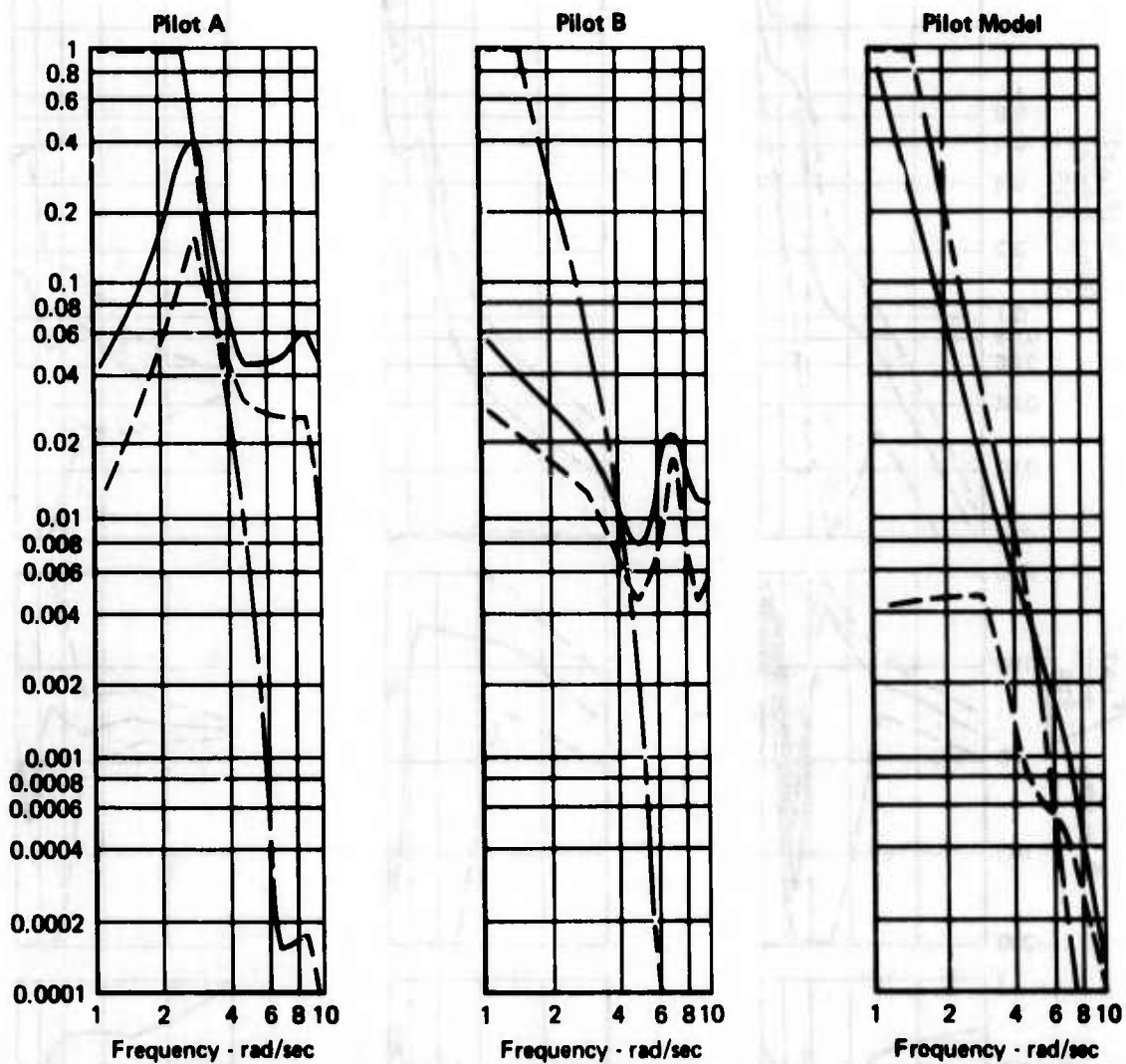


OP78-0864-436

Figure 62. Lateral Frequency Responses for Air-to-Air Gunnery Tasks with LCOSS Sight and F-4 TWeaD Aircraft Configuration (Mach 0.8 at 10,000 Ft Altitude, 4 G Target, 1500 Ft < Range < 1900 Ft)

_____ Lateral Stick Force Command Spectrum (lb^2)
 - - - - - Lateral Stick Force Command Remnant (lb^2)
 - - - - - Traverse Tracking Error Spectrum/100 (mr^2)

● Aircraft Configuration 1
 F-4 TWeaD



OP75-0064-436

**Figure 63. Lateral Spectral Responses for Air-to-Air Gunnery Tasks with
 LCOSS Sight and F-4 TWeaD Aircraft Configuration
 (Mach 0.8 at 10,000 Ft Altitude, 4 G Target, 1500 Ft < Range < 1900 Ft)**

angles. In the longitudinal axis, there is less phase lag with the LCOSS sight than there is for the Director sight. In the lateral axis, the phase curves are quite discontinuous for the LCOSS sight in comparison with the Director sight.

4.4.2 Representative Air-to-Ground Gunnery Tracking Responses - This section presents tracking responses with the air-to-ground CCIP gunsight first, and then the Fixed Depressed Reticule gunsight. These responses were obtained with Dryden continuous and discrete gust disturbances acting on the aircraft. Time history curves of the tracking errors and commands for the two USAF pilots and pilot model are given in Figure 64 for the CCIP sight. In this three-page figure, both pilots are allowing the pipper move up to the target instead of controlling the elevation tracking error about null during the time period before the firing range is reached. This is a characteristic way of using the CCIP sight.

The linear offset of the elevation tracking errors seen in Figure 64 is removed by detrending (as described in Appendix VII) before the frequency response curves are computed. To avoid the programming task required to make the longitudinal pilot model fly this type of tracking error profile like the actual pilots, the initial dive angle of the encounter was modified by a couple of degrees so that the elevation tracking error would vary approximately about zero.

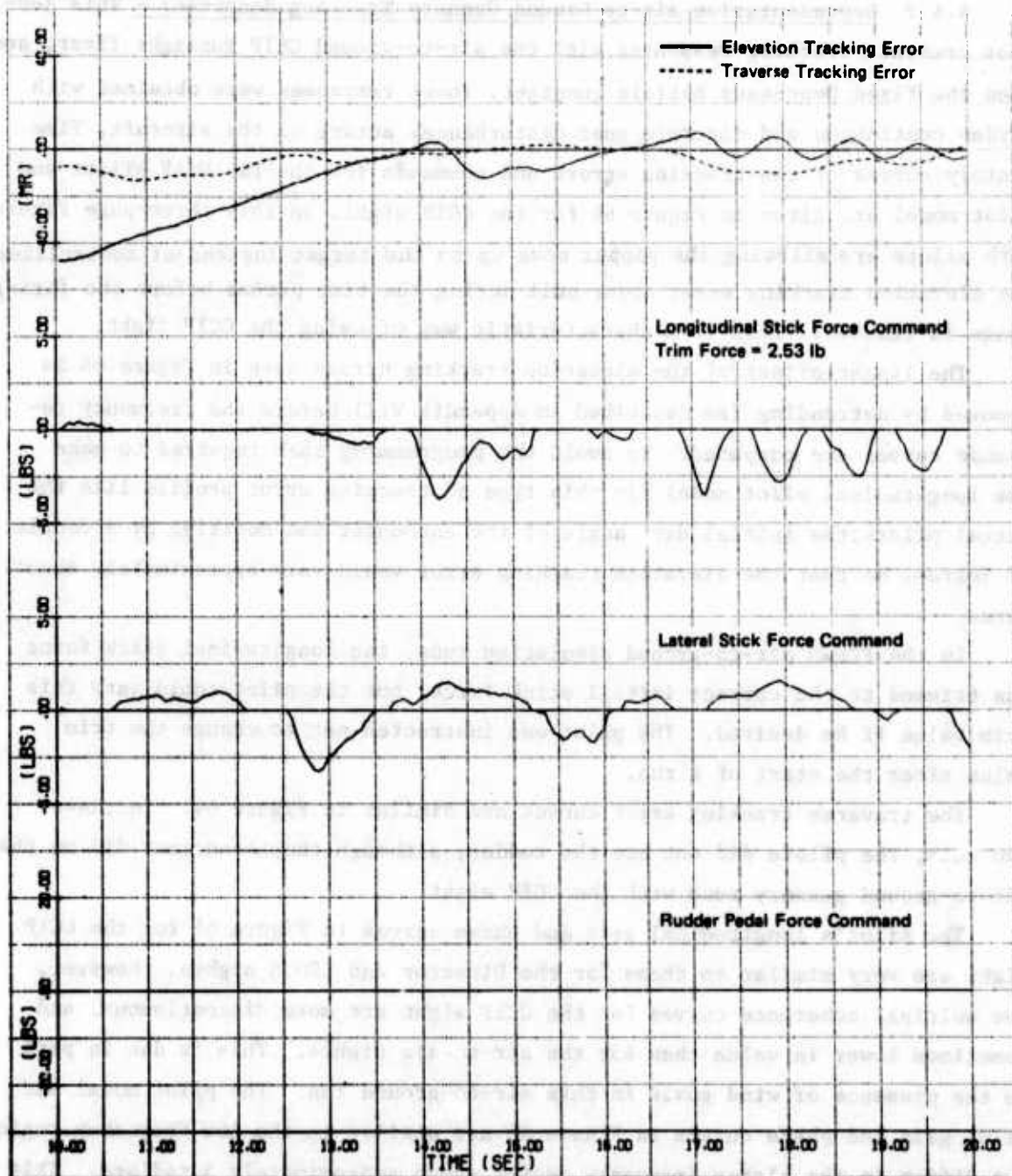
In the FCRWD air-to-ground simulation runs, the longitudinal stick force was trimmed to the correct initial stick force, but the pilot could vary this trim value if he desired. The pilot was instructed not to change the trim value after the start of a run.

The traverse tracking error curves are similar in Figure 64. In these two runs, the pilots did not use the rudder, although they sometimes did on the air-to-ground gunnery runs with the CCIP sight.

The pilot's longitudinal gain and phase curves in Figure 65 for the CCIP sight are very similar to those for the Director and LCOSS sights. However, the multiple coherence curves for the CCIP sight are more discontinuous, and sometimes lower in value than for the air-to-air sights. This is due in part to the presence of wind gusts in this air-to-ground run. The pilot model and pilot gain and phase curves in Figure 65 are similar in the low frequency region, but differ in the higher frequency region above approximately 5 rad/sec. This is due to the absence of higher frequency components in the pilot model commands, as shown by the spectral and remnant curves in Figure 66. For this air-to-

- Aircraft Configuration 1
F-4 TWeSD
- Dryden Continuous and
Discrete Gusts

Pilot A

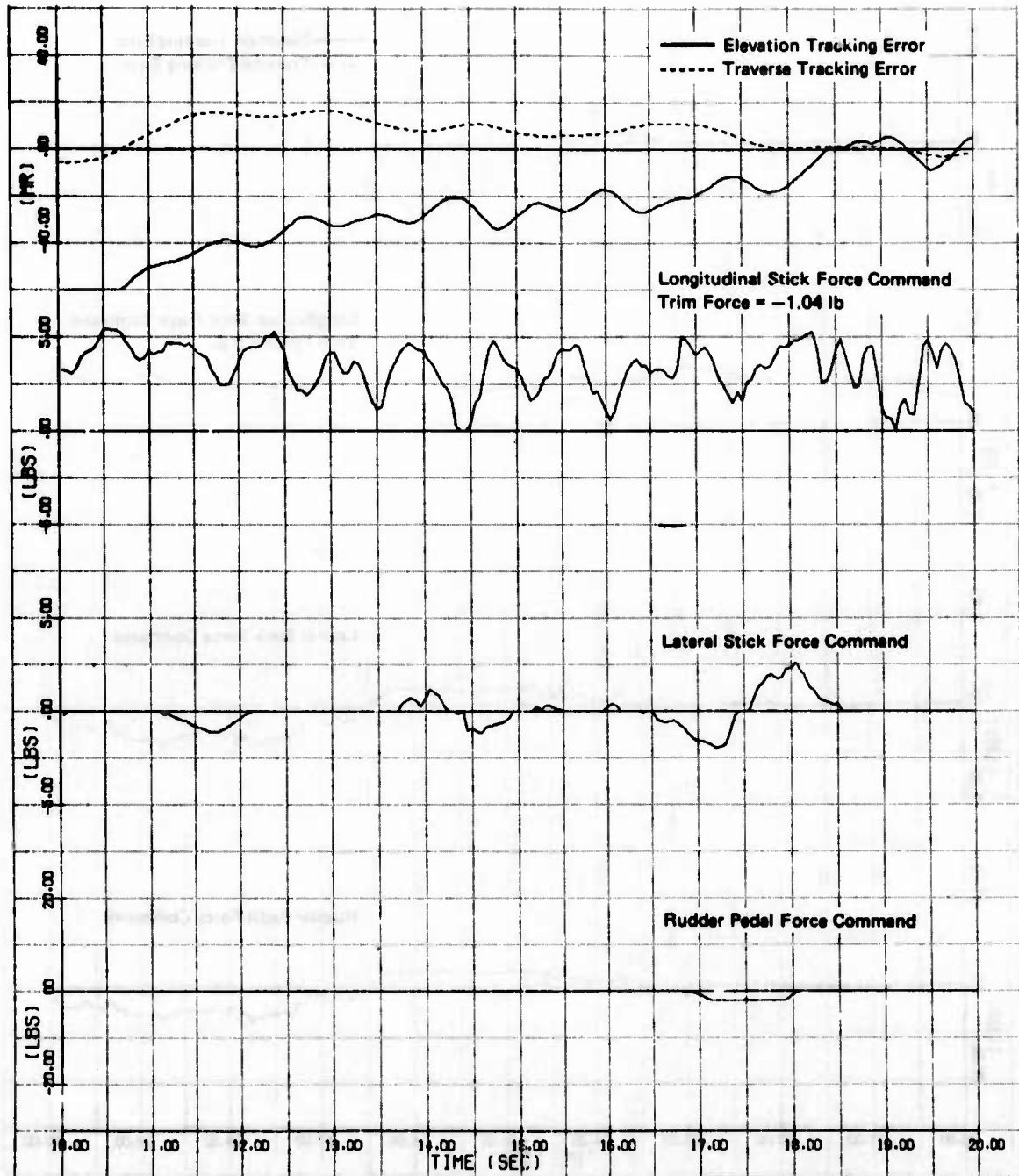


GP75-0064-23

Figure 64. CCIP Air-to-Ground Gunnery Tracking Error and Aircraft Command Time Histories for F-4 TWeSD Aircraft Configuration (450 Kt, 30° Dive)

- Aircraft Configuration 1
F-4 TWeeD
- Dryden Continuous and
Discrete Gusts

Pilot B

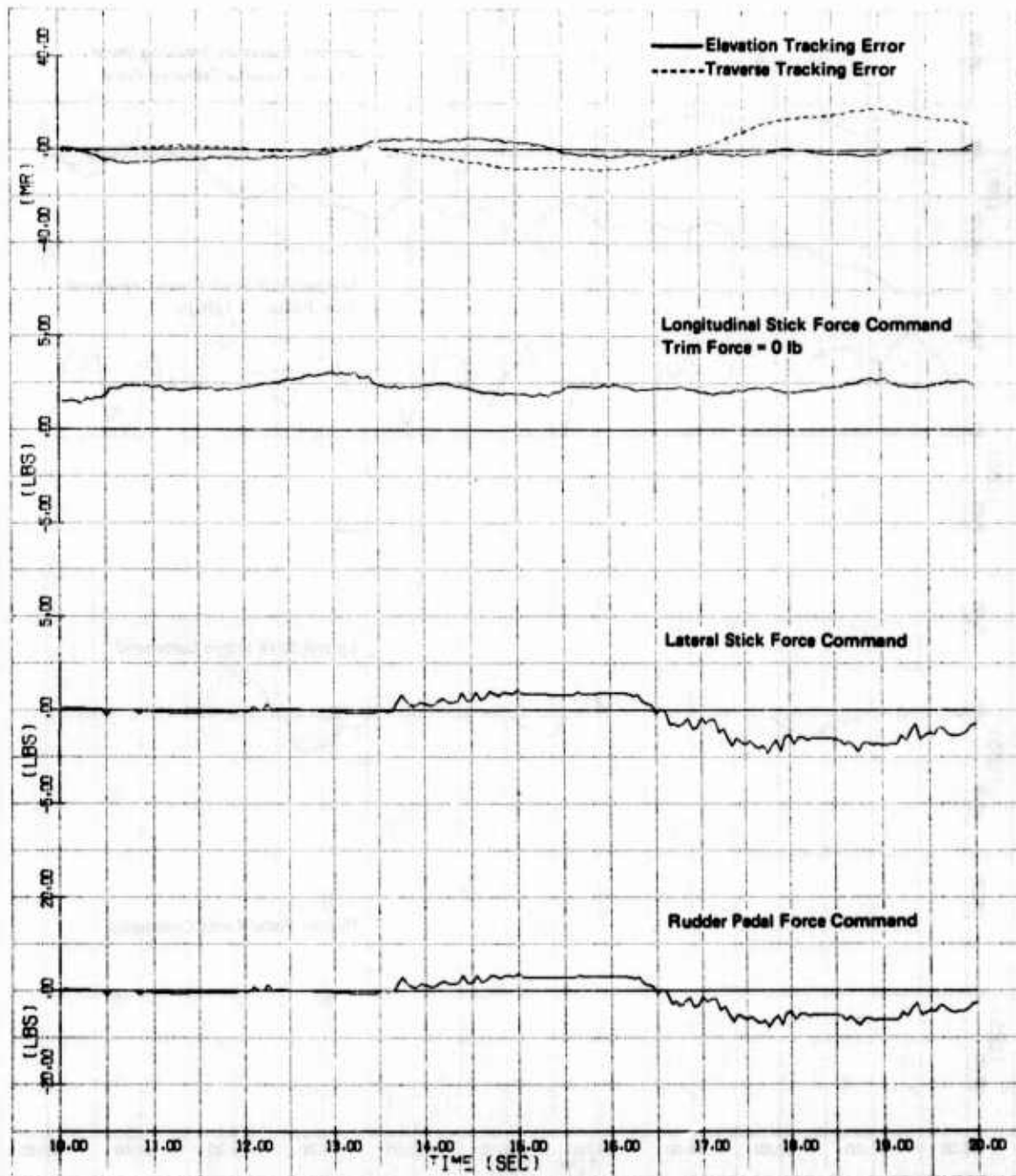


GP78-0664-24

Figure 64. CCIP Air-to-Ground Gunnery Tracking Error and Aircraft Command Time Histories for F-4 TWeeD Aircraft Configuration (Continued) (450 Kt, 30° Dive)

- Aircraft Configuration 1
F-4 TWeaD
- Dryden Continuous and
Discrete Gusts

Pilot Model



GP75-0864-25

Figure 64. CCIP Air-to-Ground Gunnery Tracking Error and Aircraft Command Time Histories for F-4 TWeaD Aircraft Configuration (Concluded) (450 Kt, 30° Dive)

F_{LON} - Longitudinal Stick Force Command (lb)
 ϵ_{EL} - Elevation Tracking Error (mr)
 $\gamma_{F_{LON}}^2$ - Multiple Coherence of F_{LON}
 - - - - 1σ Confidence Band

- Aircraft Configuration 1 F-4 TWeaD
- Dryden Continuous and Discrete Gusts

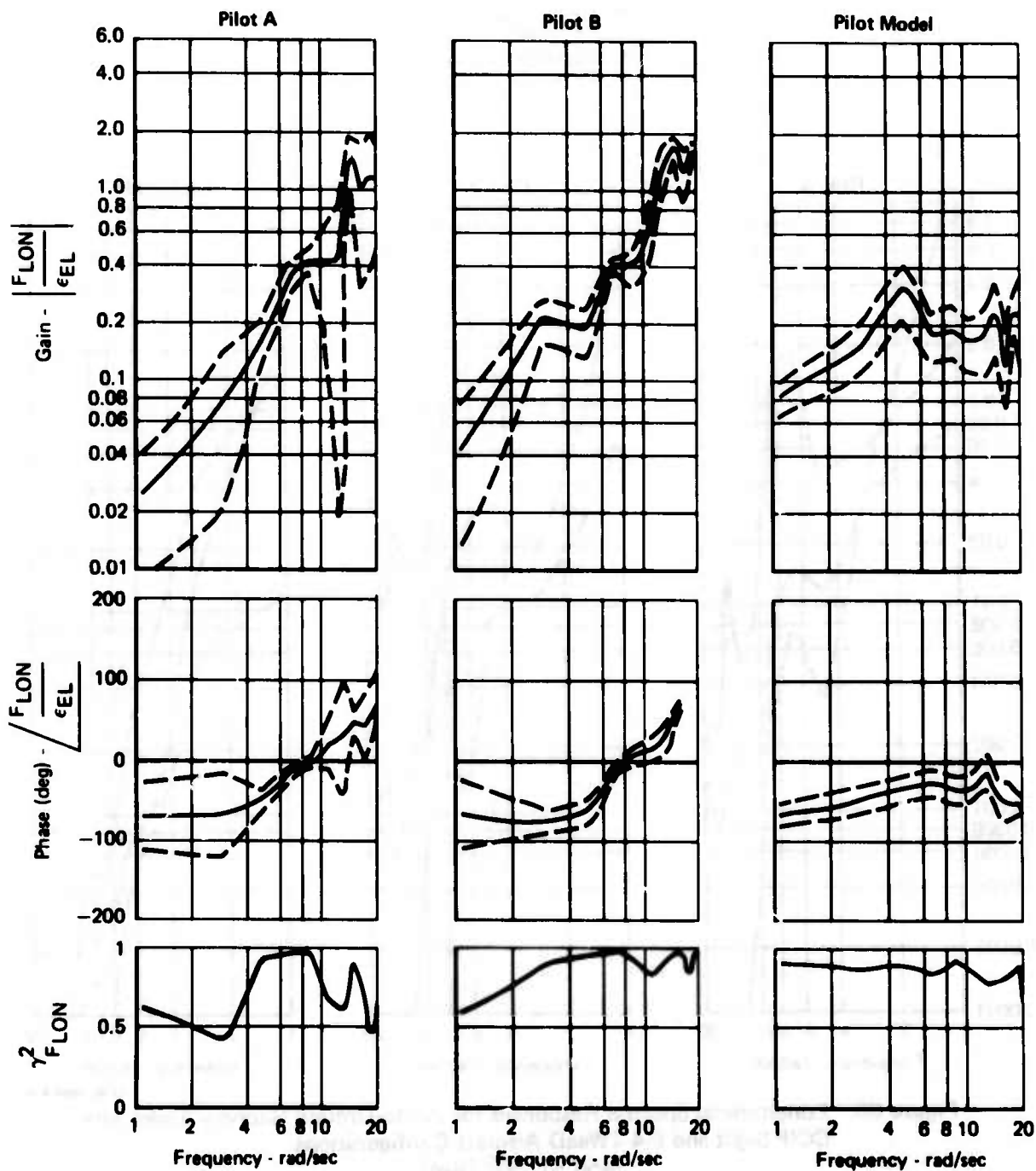
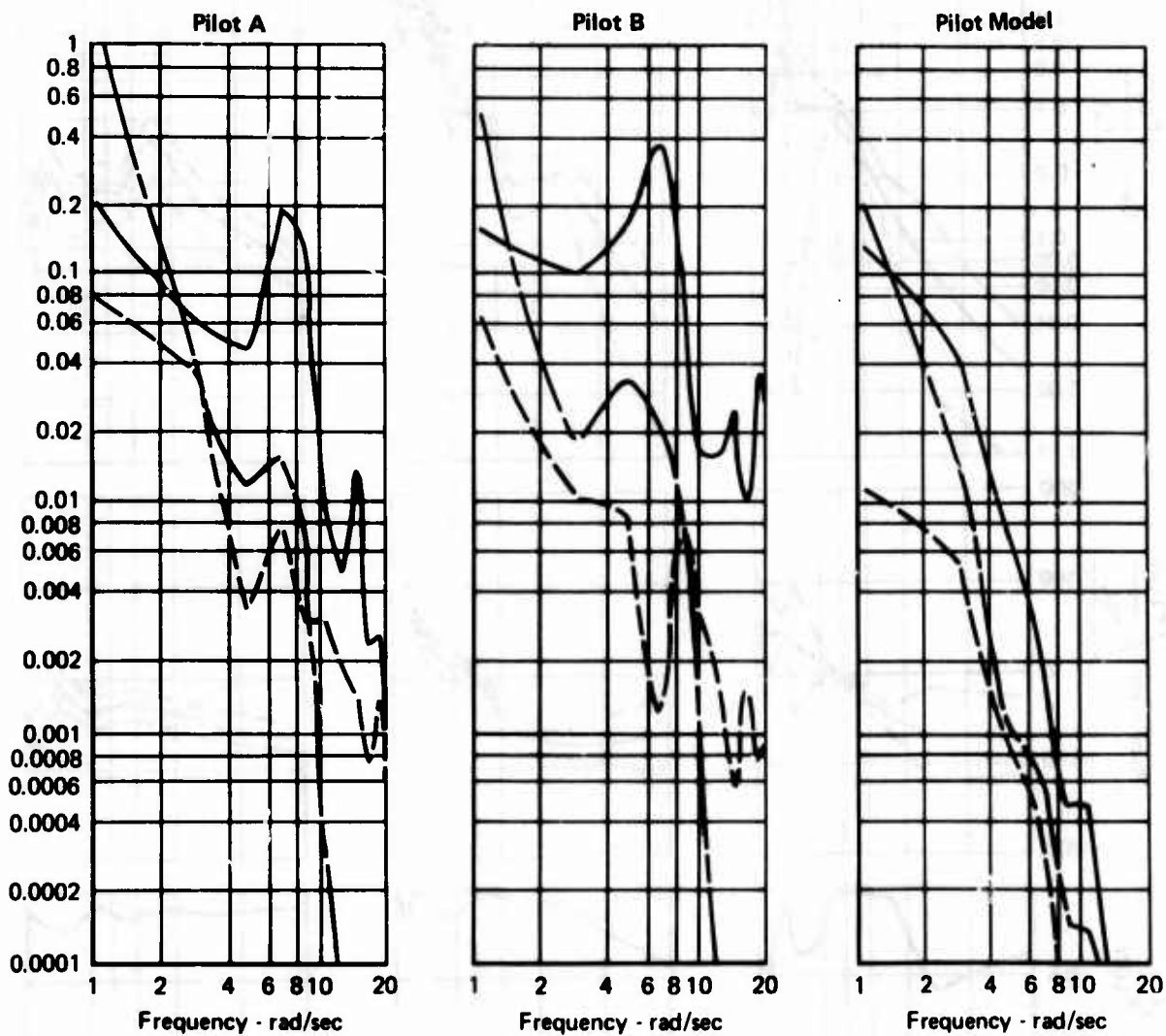


Figure 65. Longitudinal Frequency Responses for Air-to-Ground Gunnery Tasks with CCIP Sight and F-4 TWeaD Aircraft Configuration (450 Kt, 30° Dive)

GP78-0864-437

————— Longitudinal Stick Force Command Spectrum (lb^2)
 - - - - - Longitudinal Stick Force Command Remnant (lb^2)
 - - - - - Elevation Tracking Error Spectrum/100 (mr^2)

- Aircraft Configuration 32
F-4 TWeaD
- Dryden Continuous and
Discrete Gusts



GP76-0864-438

**Figure 66. Longitudinal Spectral Responses for Air-to-Ground Gunnery Tasks with
 CCIP Sight and F-4 TWeaD Aircraft Configurations
 (450 Kt, 30° Dive)**

ground weapon delivery task, the frequency response characteristics of the pilot model compare favorably with those of the human pilots within the frequency bandwidth of the tracking error.

For this series of runs with the CCIP sight, the lateral gain curves in Figure 67 are approximately the same for the pilots and pilot model, although the phase curves differ considerably, even for the two pilots. The three traverse tracking error spectra in Figure 68 are very similar, which should be expected since their time history curves in Figure 64 were also very similar. The lateral stick command spectra for the two pilots in Figure 67 are also very similar, and indicate that the pilot's lateral commands include significant amplitudes for frequencies up to 5 or 6 rad/sec.

Time history curves for the Fixed Depressed Reticle (FDR) sight are given in Figure 69 while corresponding longitudinal and lateral-directional frequency response curves are given in Figures 70 to 73. These curves, which were not available for Pilot B, are very similar to those for the CCIP sight. Since the pilot made significant use of rudder pedal commands, his directional gain and phase curves and corresponding spectra are included in Figures 72 and 73. The directional curves for the pilot model are not given, since they are proportional to the corresponding lateral curves. The comments given above for the pilots and pilot model tracking responses with the CCIP sight are also applicable in general to the Fixed Depressed Reticle sight.

4.4.3 Representative Air-to-Ground Bombing Tracking Responses - This section presents tracking responses for the FIP bombing task, whose tracking dynamics are similar to those associated with velocity vector tracking. Time history curves of tracking errors and commands for two USAF pilots and the pilot model are shown in Figure 74. These curves were obtained with Dryden continuous and discrete gusts acting on the aircraft. In this three-page figure, the high frequency component in the elevation tracking error is not as evident as it was for the gunnery sights. This is confirmed by the elevation tracking error spectra. The longitudinal gain, phase, and multiple coherence curves are shown in Figure 75 and the corresponding spectral and remnant curves are given in Figure 76. The elevation tracking error spectra in Figure 76 are very similar for both the pilots and the pilot model, even though the command spectrum for the pilot model does not have the high frequency components that the pilot's command spectra possess. Figure 77 shows the lateral gain, phase, and multiple

F_{LAT} - Lateral Stick Force Command (lb)
 ϵ_{TR} - Traverse Tracking Error (mr)
 $\gamma_{F_{LAT}}^2$ - Multiple Coherence of F_{LAT}
 --- - 1σ Confidence Band

● Aircraft Configuration 32
 F-4 TWeaD
 ● Dryden Continuous and
 Discrete Gusts

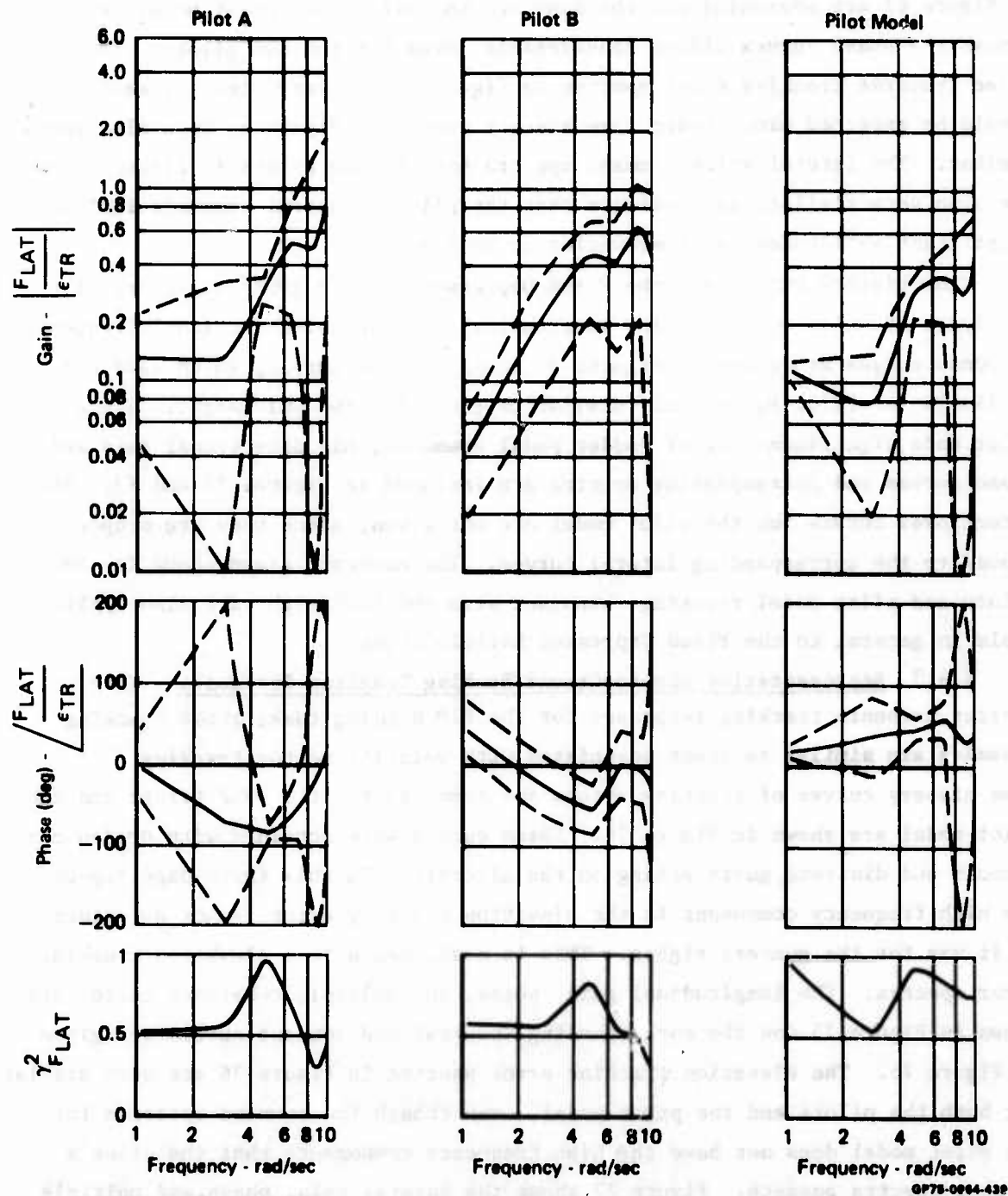


Figure 67. Lateral Frequency Responses for Air-to-Ground Gunnery Tasks with
 CCIP Sight and F-4 TWeaD Aircraft Configuration
 (450 Kt, 30° Dive)

——— Lateral Stick Force Command Spectrum (lb^2)
 - - - Lateral Stick Force Command Remnant (lb^2)
 - - - Traverse Tracking Error Spectrum/100 (mr^2)

- Aircraft Configuration 32
F-4 TWeaD
- Dryden Continuous and Discrete Gusts

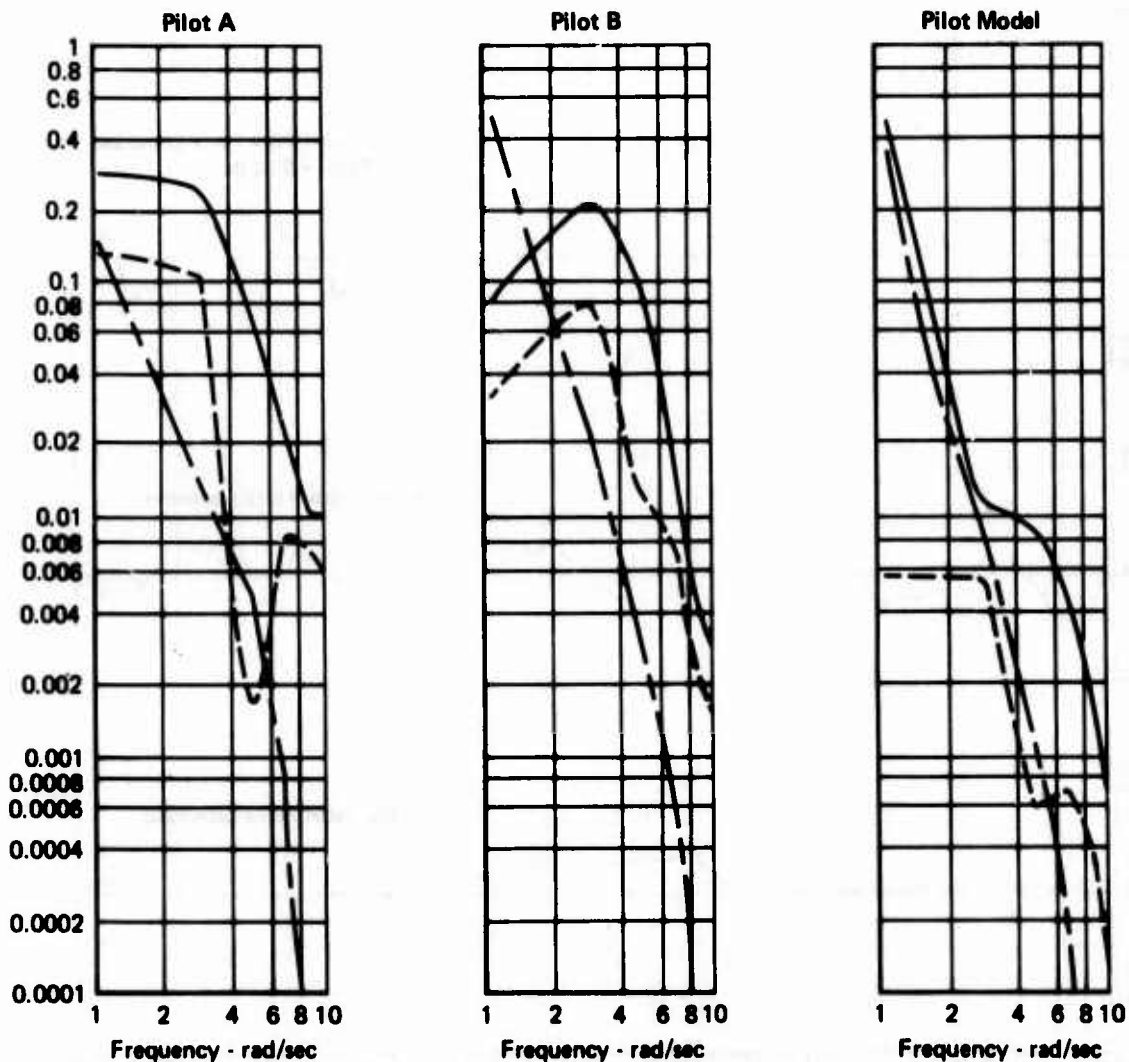
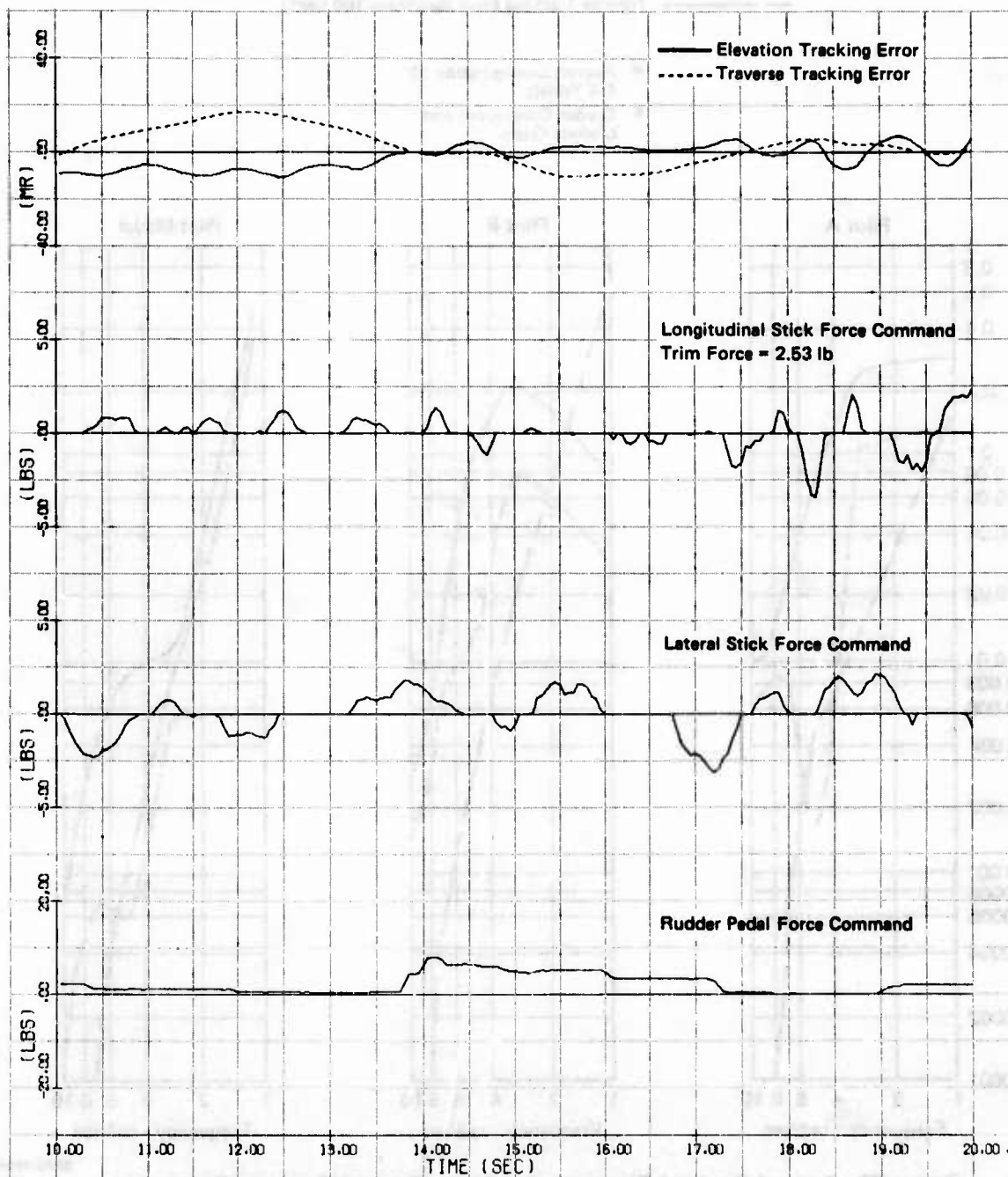


Figure 68. Lateral Spectral Responses for Air-to-Ground Gunnery Tasks with
 CCIP Sight and F-4 TWeaD Aircraft Configuration
 (450 Kt, 30° Dive)

GP75-0864-440

- Aircraft Configuration 1
F-4 TWaD
- Dryden Continuous and
Discrete Gusts

Pilot A

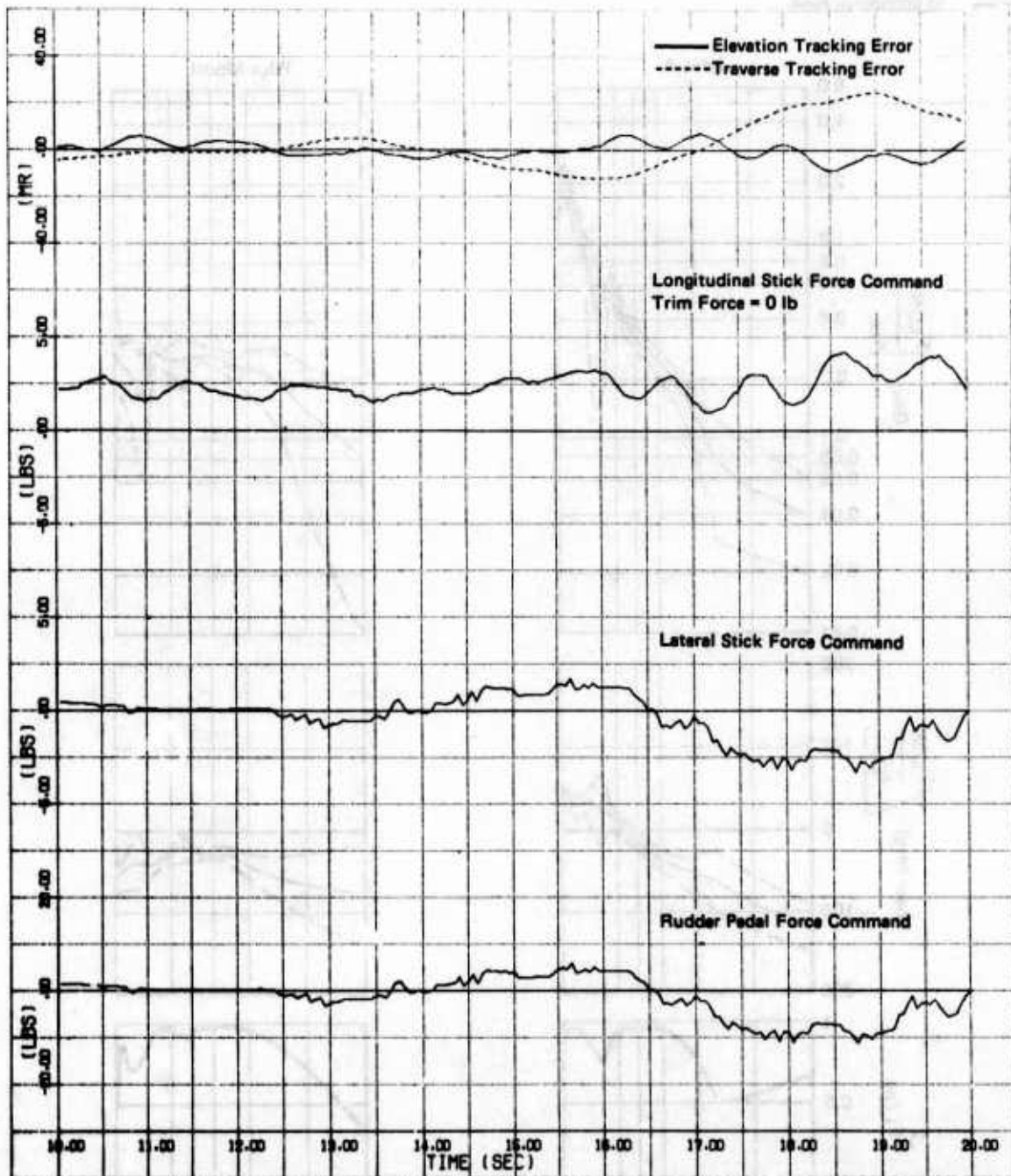


GP71-0884-30

Figure 69. FDR Air-to-Ground Gunnery Tracking Error and Aircraft Command Time Histories for F-4 TWaD Aircraft Configuration (450 Kt, 30° Dive)

- Aircraft Configuration 1
F-4 TWeaD
- Dryden Continuous and
Discrete Gusts

Pilot Model

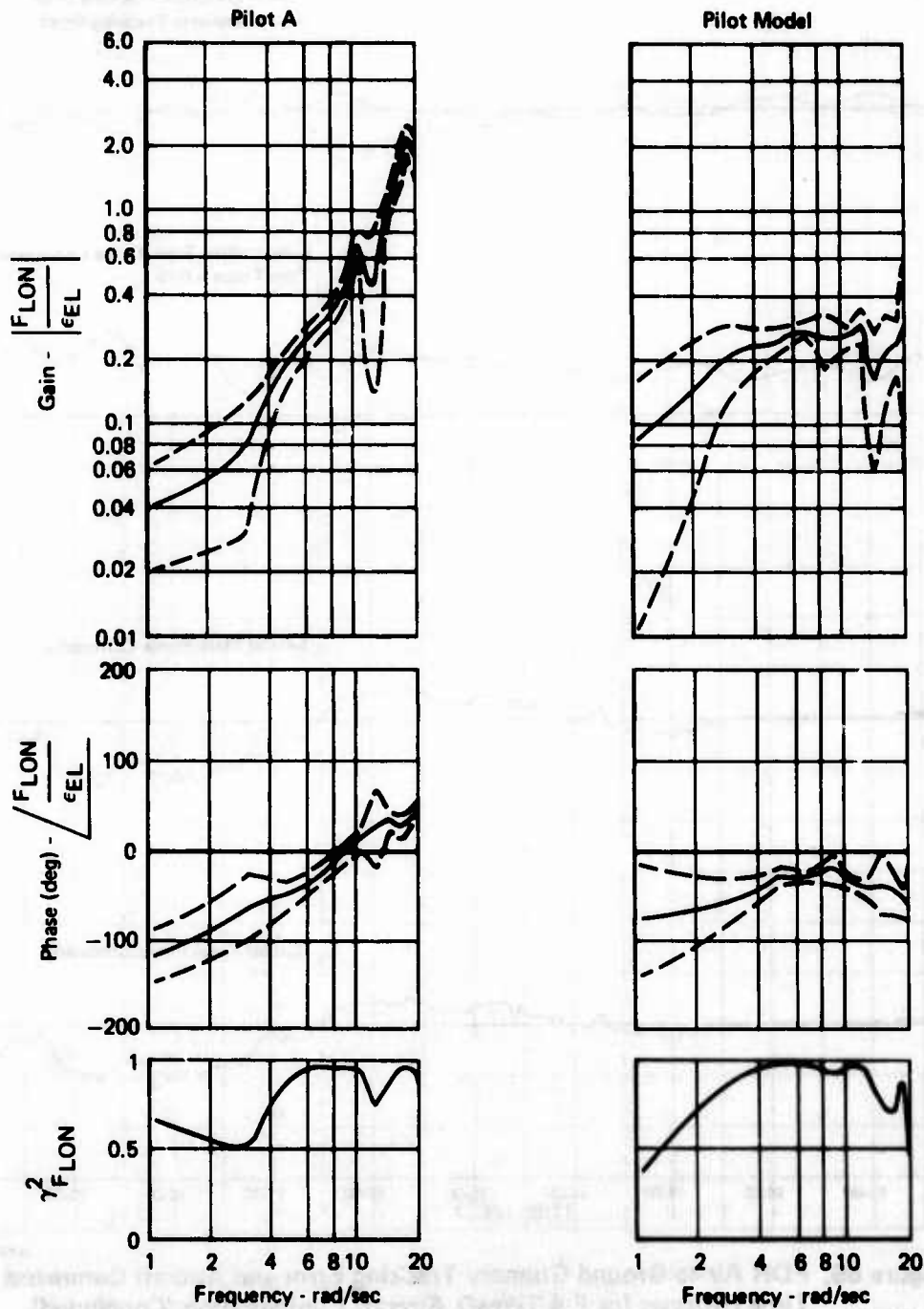


OP78-0084-31

Figure 89. FDR Air-to-Ground Gunnery Tracking Error and Aircraft Command Time Histories for F-4 TWeaD Aircraft Configuration (Concluded) (450 Kt, 30° Dive)

- F_{LON} - Longitudinal Stick Force Command (lb)
- ε_{EL} - Elevation Tracking Error (mr)
- γ_{F_{LON}}² - Multiple Coherence of F_{LON}
- — - 1σ Confidence Band

- Aircraft Configuration 1
F-4 TWeaD
- Dryden Continuous and
Discrete Gusts



GP75-0884-442

Figure 70. Longitudinal Frequency Responses for Air-to-Ground Gunnery Tasks with FDR Sight and F-4 TWeaD Aircraft Configuration (450 Kt, 30° Dive)

————— Longitudinal Stick Force Command Spectrum (lb^2)
 - - - - - Longitudinal Stick Force Command Remnant (lb^2)
 - - - - - Elevation Tracking Error Spectrum/100 (mr^2)

- Aircraft Configuration 1
F-4 TWeaD
- Dryden Continuous and
Discrete Gusts

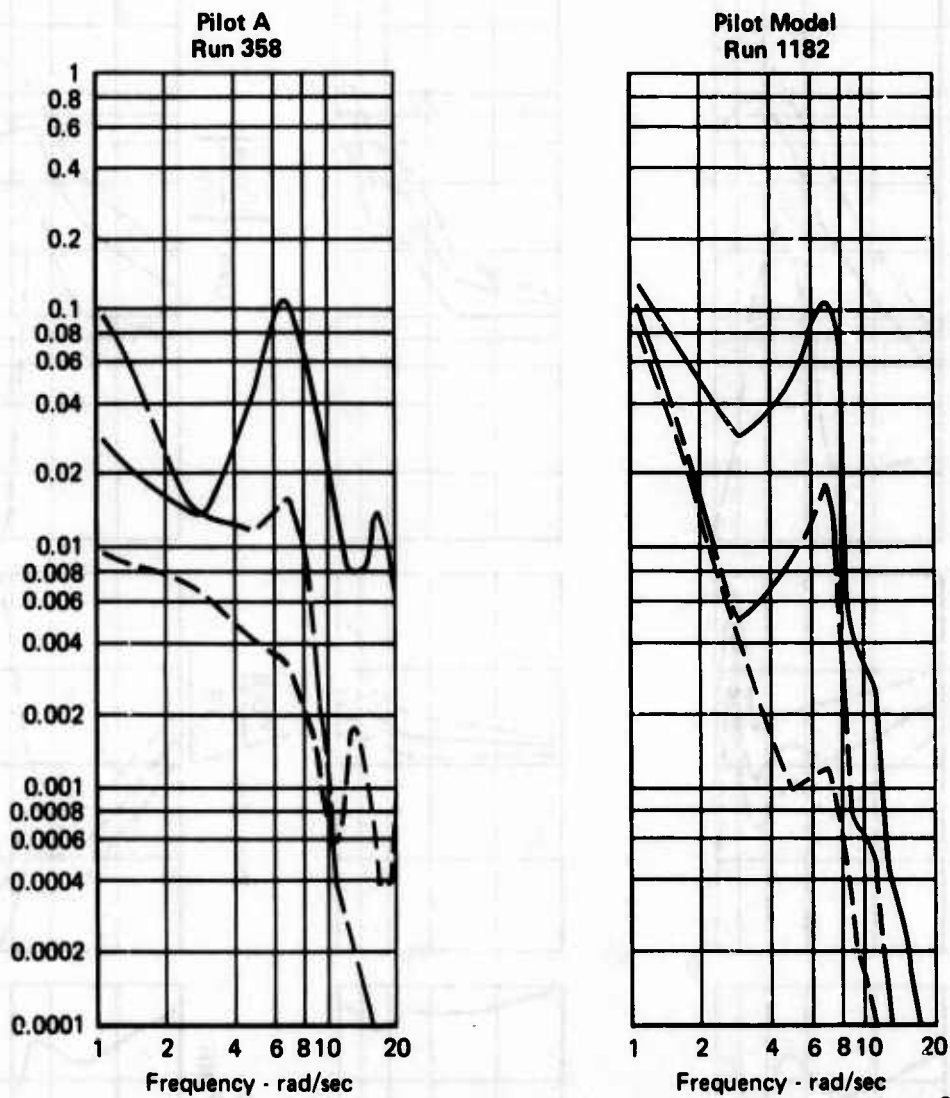
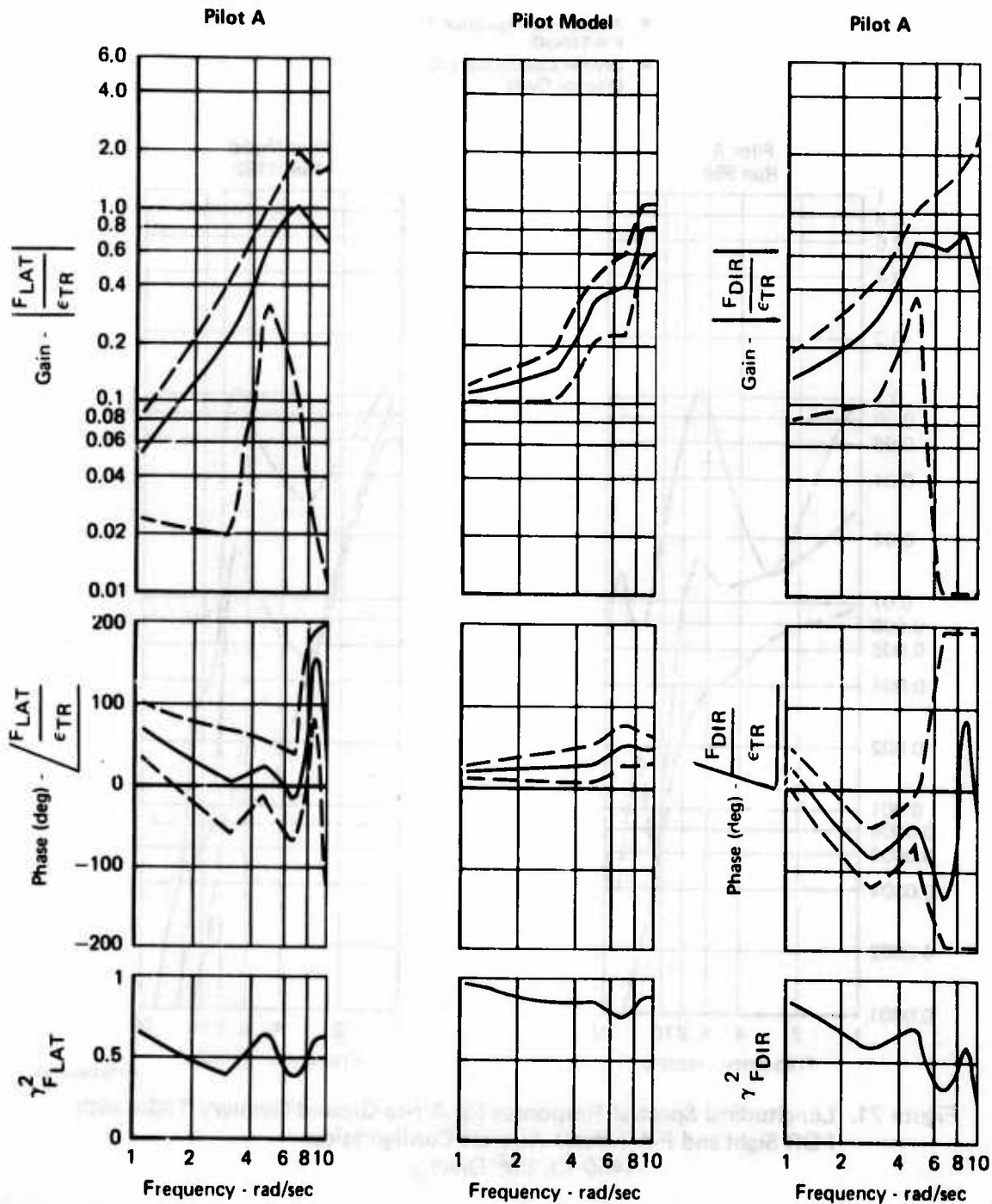


**Figure 71. Longitudinal Spectral Responses for Air-to-Ground Gunnery Tasks with
 FDR Sight and F-4 TWeaD Aircraft Configuration
 (450 Kt, 30° Dive)**

- F_{LAT} - Lateral Stick Force Command (lb)
- F_{DIR} - Rudder Pedal Force Command (lb)
- ϵ_{TR} - Traverse Tracking Error (mr)
- $\gamma_{F_{LAT}}^2$ - Multiple Coherence of F_{LAT}
- $\gamma_{F_{DIR}}^2$ - Multiple Coherence of F_{DIR}
- 1 σ Confidence Band

- Aircraft Configuration 1
F-4 TWeaD
- Dryden Continuous and
Discrete Gusts

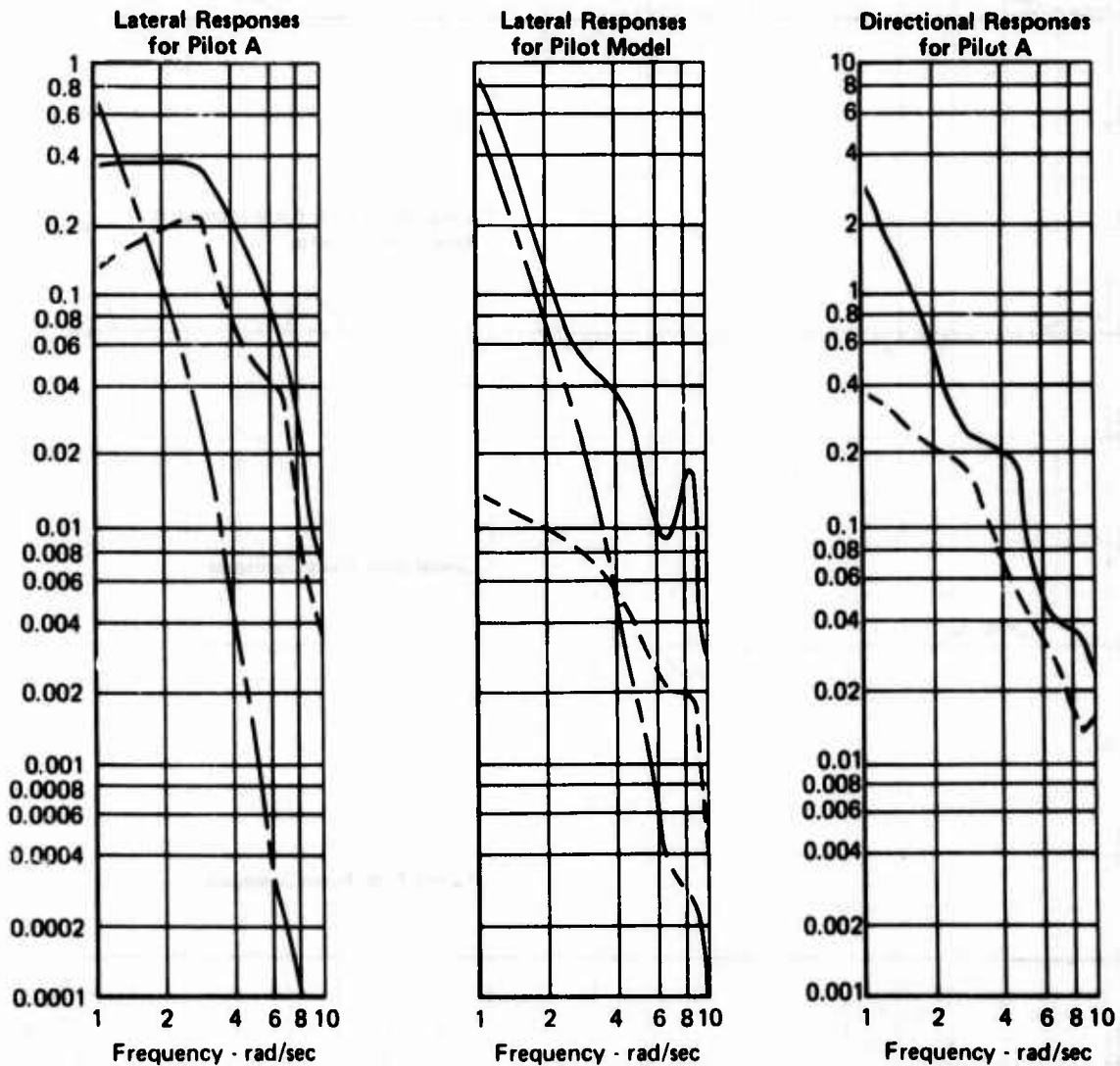


GP75-0884-441

Figure 72. Lateral and Directional Frequency Responses for Air-to-Ground Gunnery Tasks with FDR Sight and F-4 TWeaD Aircraft Configuration (450 Kt, 30° Dive)

- Lateral Stick or Rudder Pedal Force
- - - - - Command Spectrum (lb²)
- Lateral Stick or Rudder Pedal Force Command Remnant (lb²)
- - - - - Traverse Tracking Error Spectrum/100 (mr²)

- Aircraft Configuration 1 F-4 TWeaD
- Dryden Continuous and Discrete Gusts

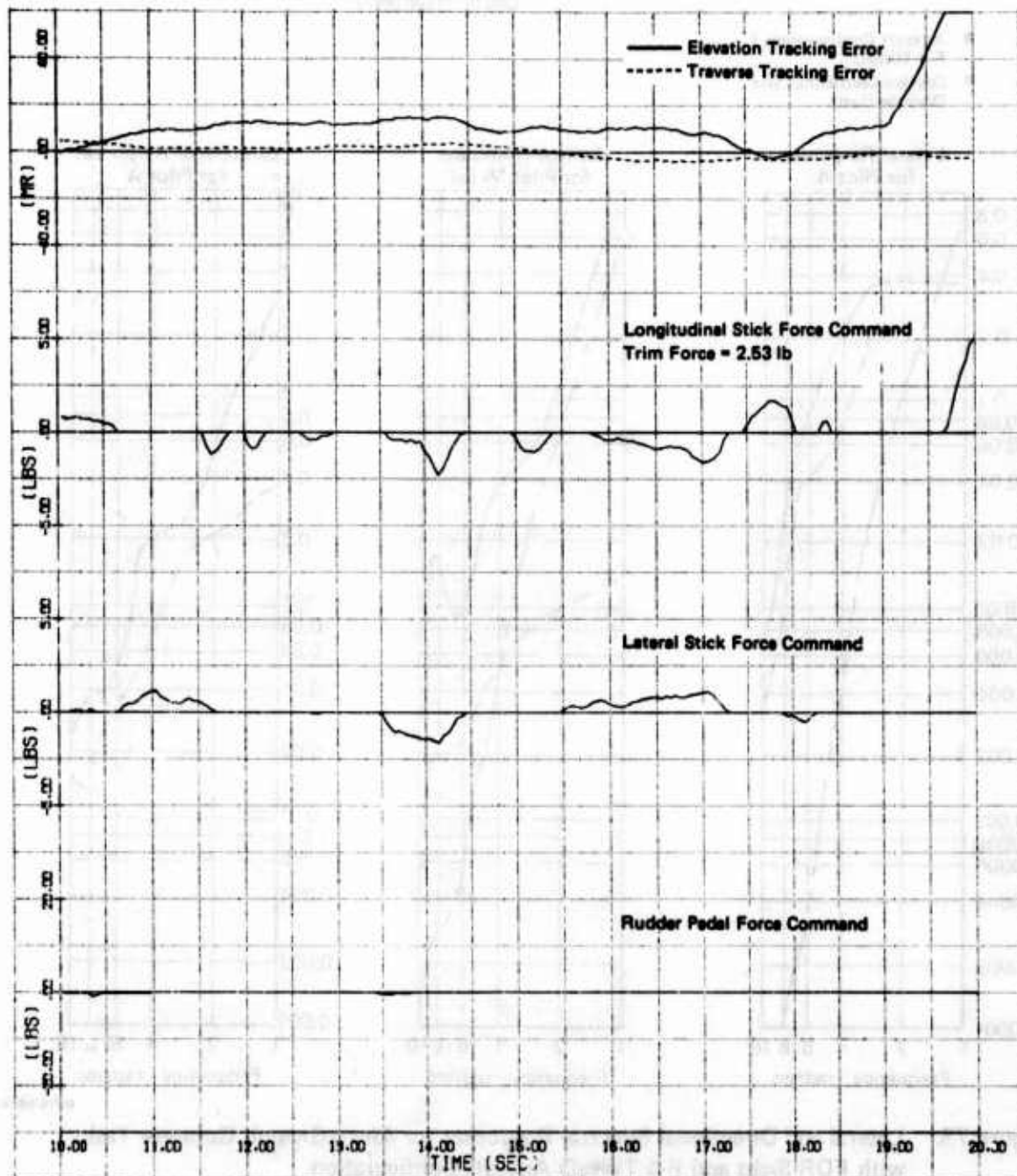


GP75-0864-444

Figure 73. Lateral and Directional Spectral Responses for Air-to-Ground Gunnery Tasks with FDR Sight and F-4 TWeaD Aircraft Configuration (450 Kt, 30° Dive)

- Aircraft Configuration 1
F-4 TWeeD
- Dryden Continuous and
Discrete Gusts

Pilot A

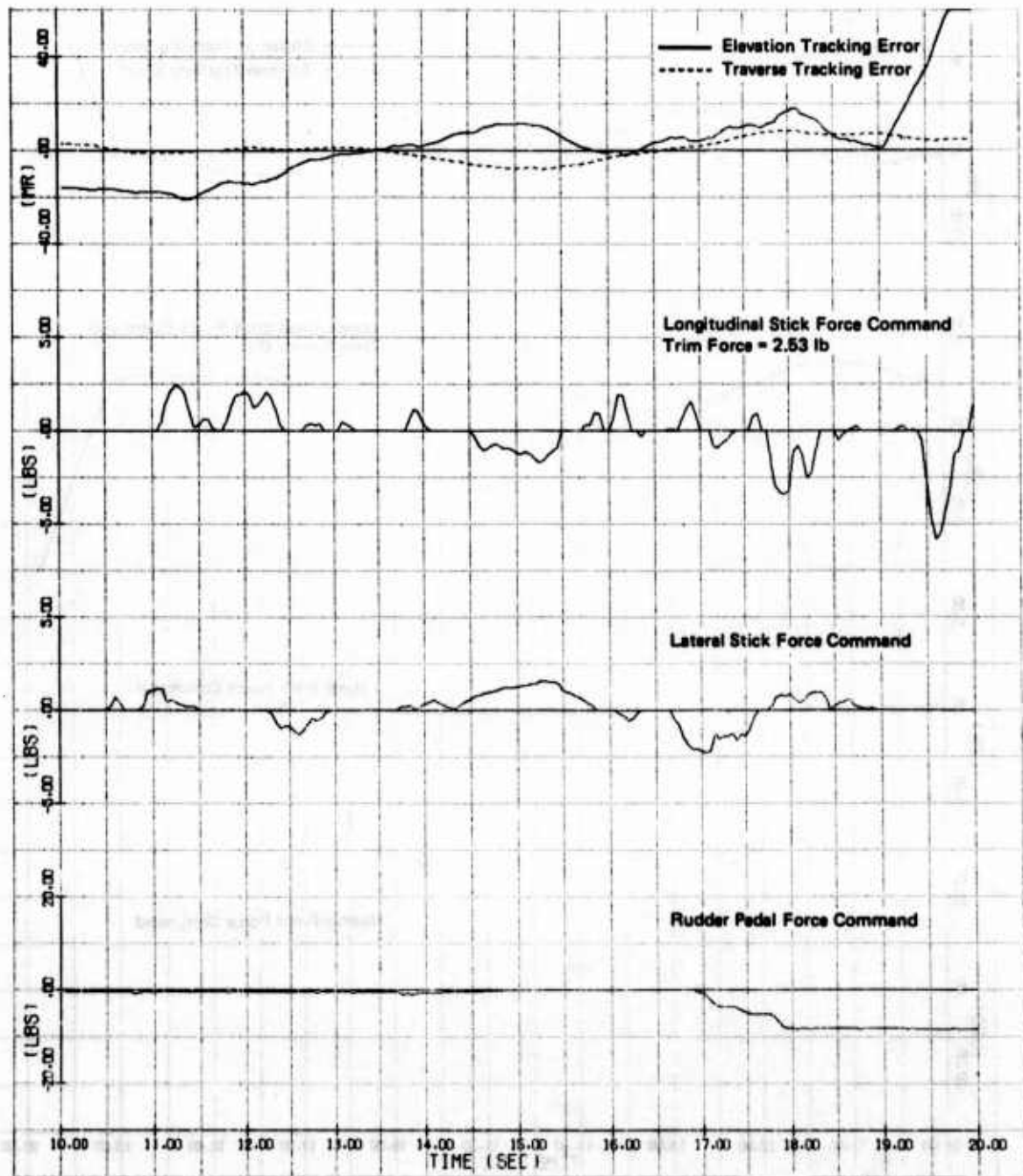


OP78-0004-30

Figure 74. FIP Air-to-Ground Bombing Tracking Error and Aircraft Command Time Histories for F-4 TWeeD Aircraft Configuration (450 Kt, 30° Dive)

- Aircraft Configuration 1
F-4 TWeeD
- Dryden Continuous and
Discrete Gusts

Pilot B

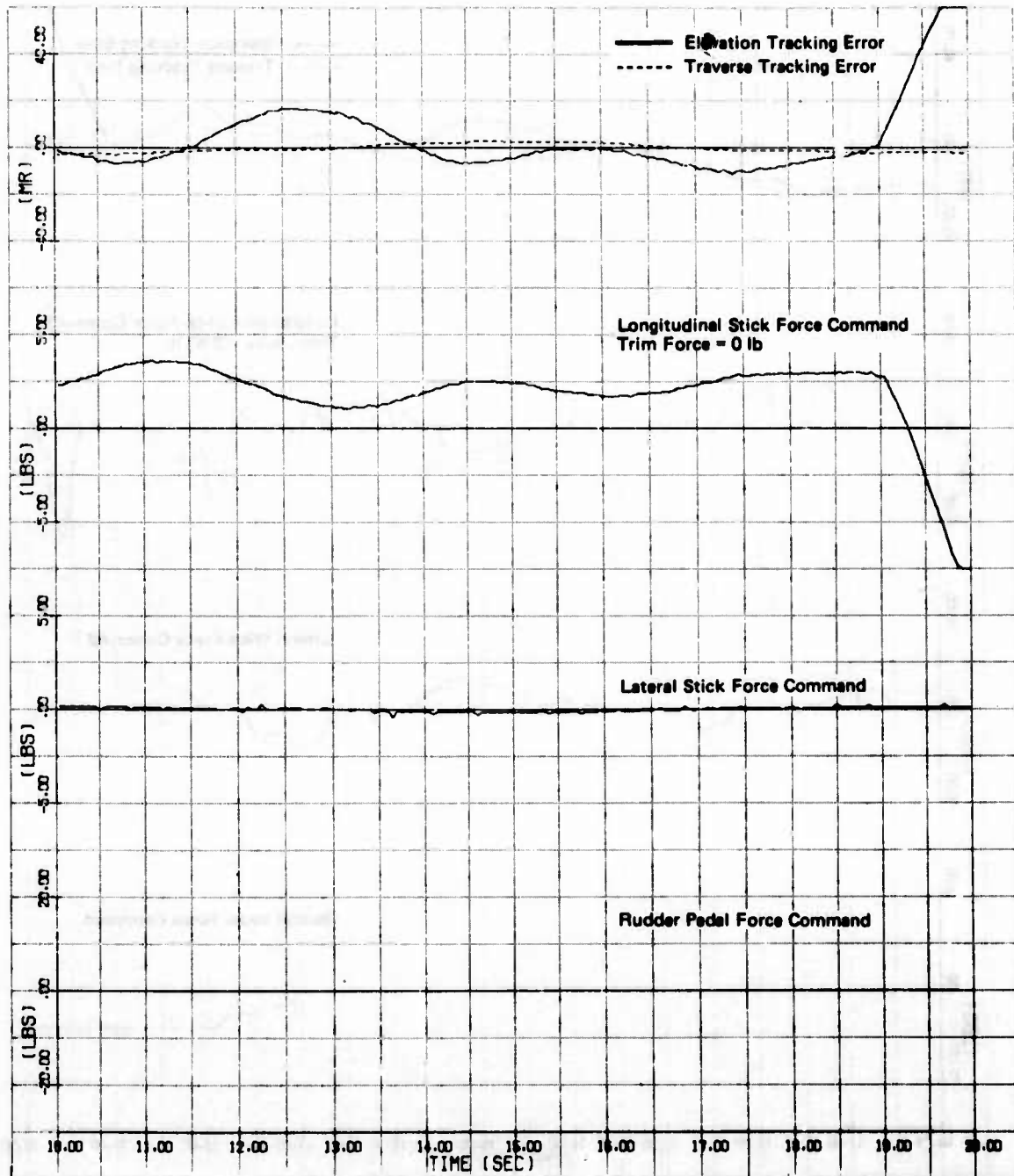


OP75-0864-37

Figure 74. FIP Air-to-Ground Bombing Tracking Error and Aircraft Command Time Histories for F-4 TWeeD Aircraft Configuration (Continued) (450 Kt, 30° Dive)

- Aircraft Configuration 1
F-4 TWeeD
- Dryden Continuous and
Discrete Gusts

Pilot Model



OP75-0004-3G

Figure 74. FIP Air-to-Ground Bombing Tracking Error and Aircraft Command Time Histories for F-4 TWeeD Aircraft Configuration (Concluded) (450 Kt, 30° Dive)

F_{LON} - Longitudinal Stick Force Command (lb)
 ϵ_{EL} - Elevation Tracking Error (mr)
 $\gamma_{F_{LON}}^2$ - Multiple Coherence of F_{LON}
 - - - - 10 Confidence Band

● Aircraft Configuration 1
 F-4 TWeaD
 ● Dryden Continuous and
 Discrete Gusts

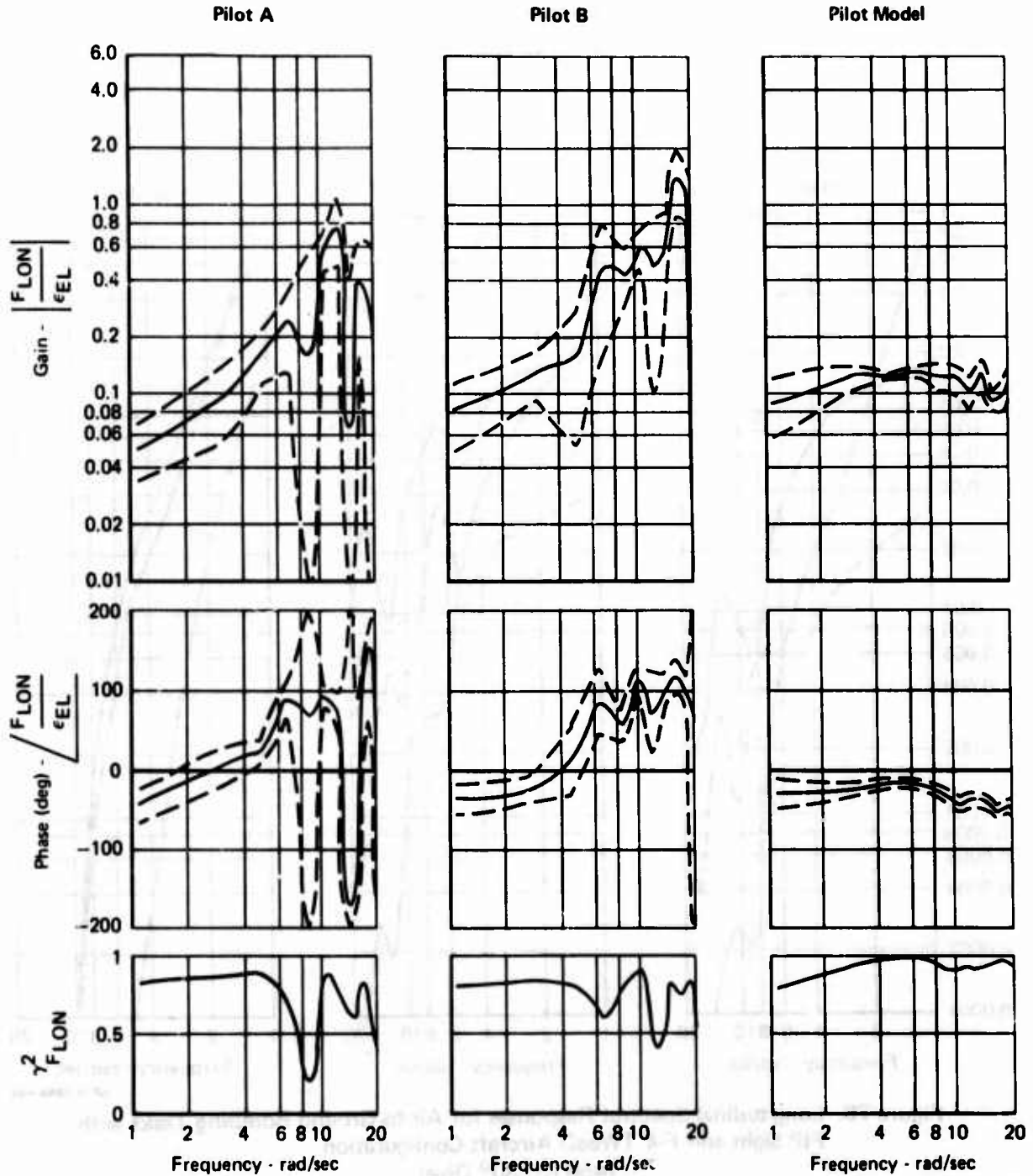
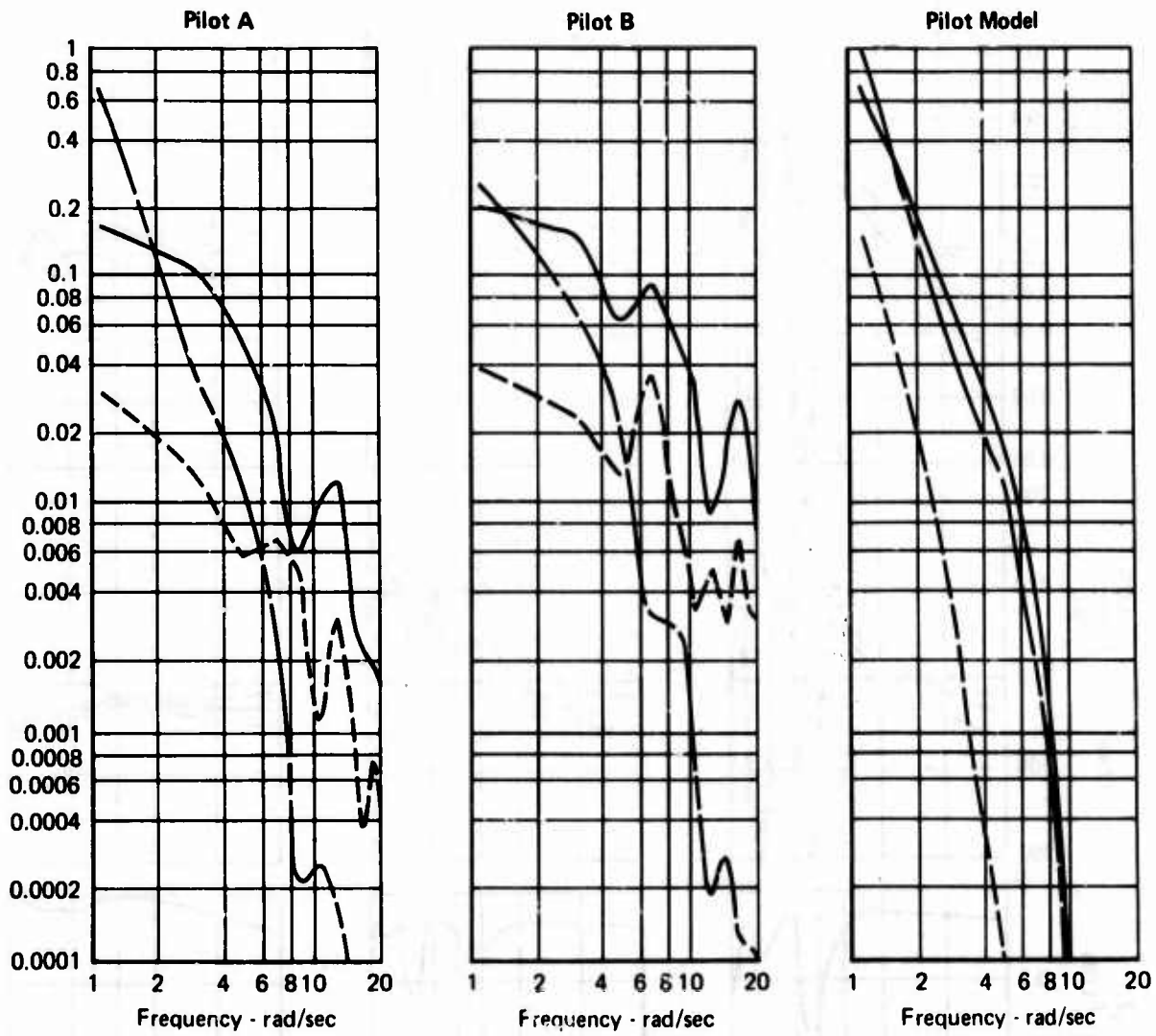


Figure 75. Longitudinal Frequency Responses for Air-to-Ground Bombing Tasks with
 FIP Sight and F-4 TWeaD Aircraft Configuration
 (450 Kt, 30° Dive)

GP75 2204-445

————— Longitudinal Stick Force Command Spectrum (lb^2)
 - - - - - Longitudinal Stick Force Command Remnant (lb^2)
 - - - - - Elevation Tracking Error Spectrum/100 (mr^2)

- Aircraft Configuration 1
F-4 TWeaD
- Dryden Continuous and
Discrete Gusts

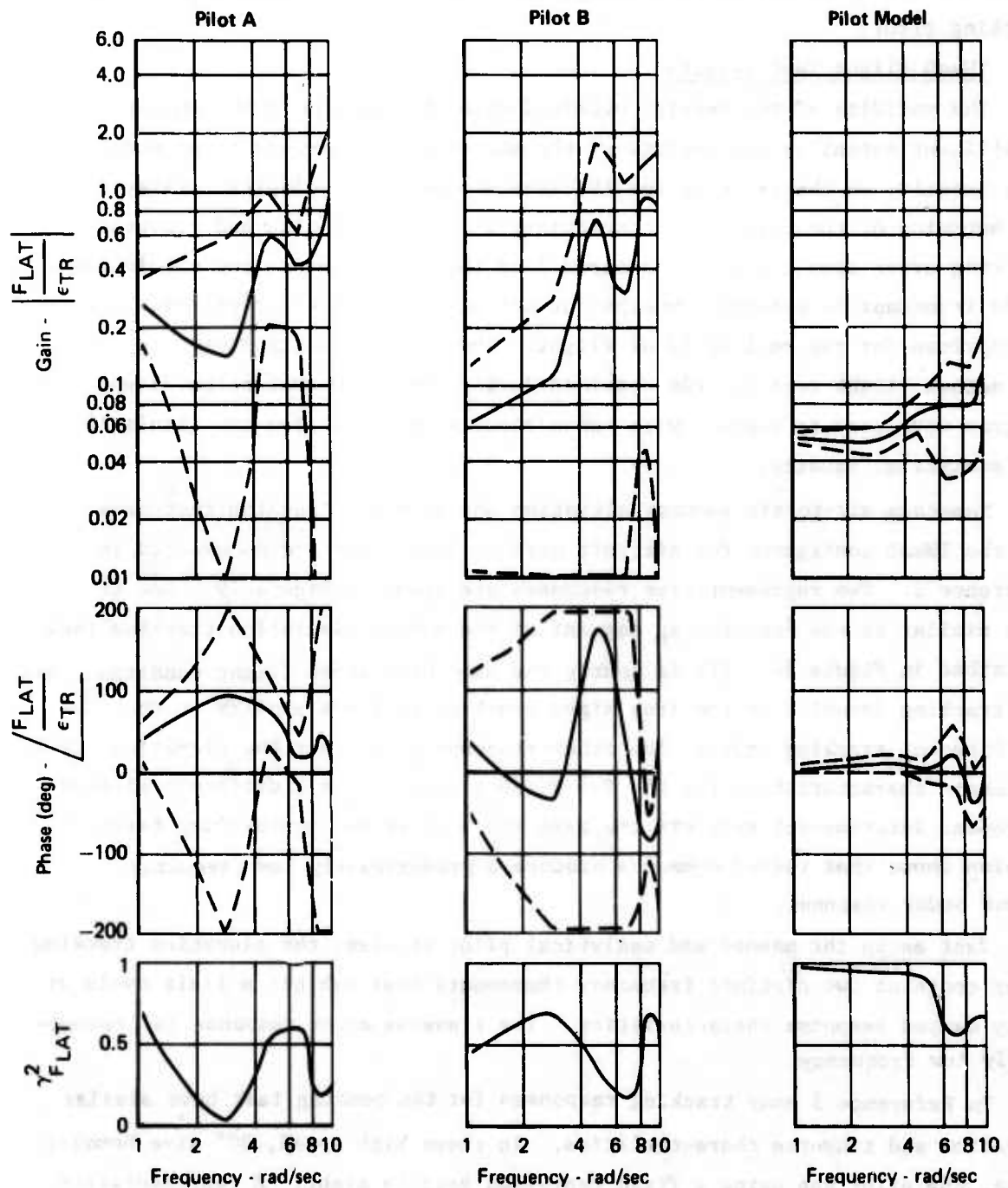


GP75-0864-446

**Figure 76. Longitudinal Spectral Responses for Air-to-Ground Bombing Tasks with
 FIP Sight and F-4 TWeaD Aircraft Configuration
 (450 Kt, 30° Dive)**

F_{LAT} - Lateral Stick Force Command (lb)
 ϵ_{TR} - Traverse Tracking Error (mr)
 $\gamma_{F_{LAT}}^2$ - Multiple Coherence of F_{LAT}
 --- - 1 σ Confidence Band

- Aircraft Configuration 1
F-4 TWeaD
- Dryden Continuous and
Discrete Gusts



GP75-0884-447

Figure 77. Lateral Frequency Responses for Air-to-Ground Bombing Tasks with FIP Sight and F-4 TWeaD Aircraft Configuration (450 Kt, 30° Dive)

coherence curves, with Figure 78 showing the corresponding spectral and remnant curves. The discontinuous nature generally observed for the pilots' lateral gain and phase curves when using the FIP sight is evident in Figure 78. For the bombing task the pilot model frequency response characteristics are comparable to those of the human pilots within the frequency bandwidth of the tracking error.

4.5 TWeaD Flight Test Results

The validity of the results obtained with the TAWDS programs depends to a significant extent on the quality of the analytical multi-axis pilot model and, consequently, on the criteria for its development. The principal criterion is the matching of the dominant characteristics in the elevation and traverse tracking error time histories measured from the pilot-in-the-loop simulations. It is important to establish whether or not the tracking error criteria are appropriate for the real world of flight. Therefore, results from the actual flight test records obtained during the TWeaD evaluation flight test program were used to compare with those results obtained from the simulation and analytical studies.

Numerous air-to-air gunnery elevation and traverse tracking responses for the TWeaD configured F-4 aircraft with an iron sight are documented in Reference 2. Two representative responses are shown in Figure 79. One is very similar to the constant 4g segment of the manned simulation tracking task described in Figure 34. (It is nearly the same high speed flight condition, and the tracking dynamics of the iron sight tracking task are similar to those of the Director tracking task.) The other response shows that the elevation tracking error characteristics for the F-4 TWeaD aircraft with a different aileron-to-rudder interconnect gain are the same for a different maneuvering target. It also shows that rudder commands produce a predominantly low frequency second order response.

Just as in the manned and analytical pilot studies, the elevation tracking error contains two distinct frequency components that exhibit a limit cycle or lowly damped response characteristics. The traverse error response is predominantly low frequency.

In Reference 5 many tracking responses for the bombing task have similar elevation and traverse characteristics. In these high speed, 30° dive bombing tasks, the pilot was using a Fixed Depressed Reticule sight. A representative air-to-ground bombing tracking error time history from Reference 5 is shown in Figure 80. The tracking error characteristics illustrated in Figure 80 are

— Lateral Stick Force Command Spectrum (lb^2)
 - - Lateral Stick Force Command Remnant (lb^2)
 - - - Traverse Tracking Error Spectrum/100 (mr^2)

- Aircraft Configuration 1
F-4 TWeaD
- Dryden Continuous and
Discrete Gusts

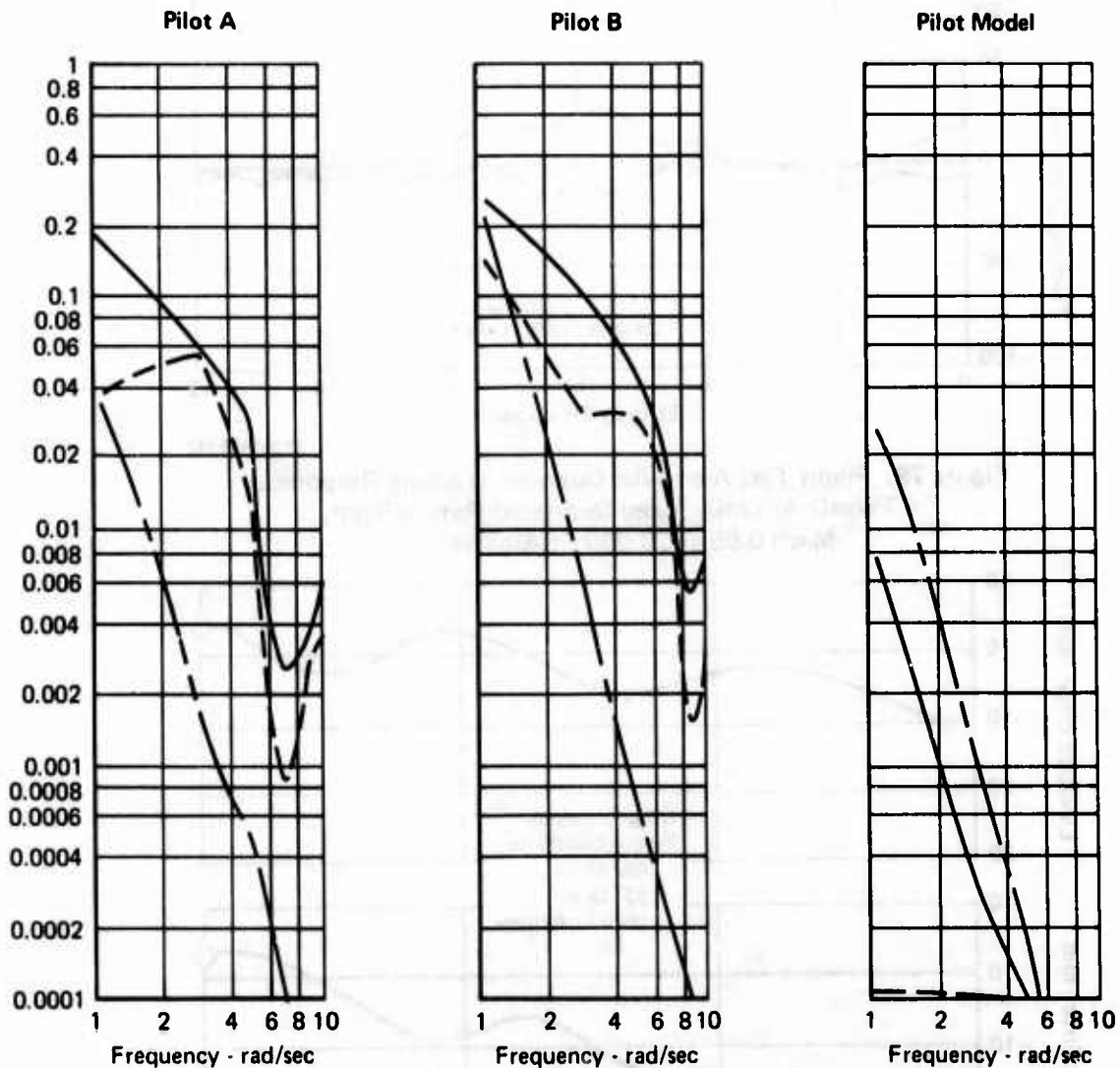
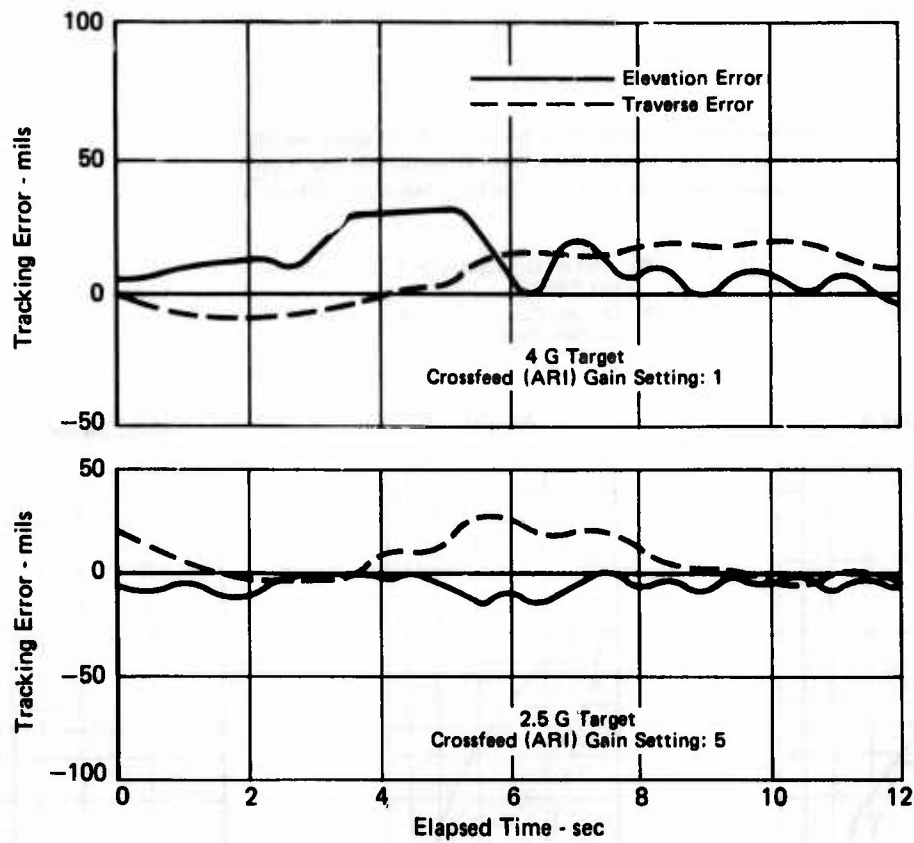


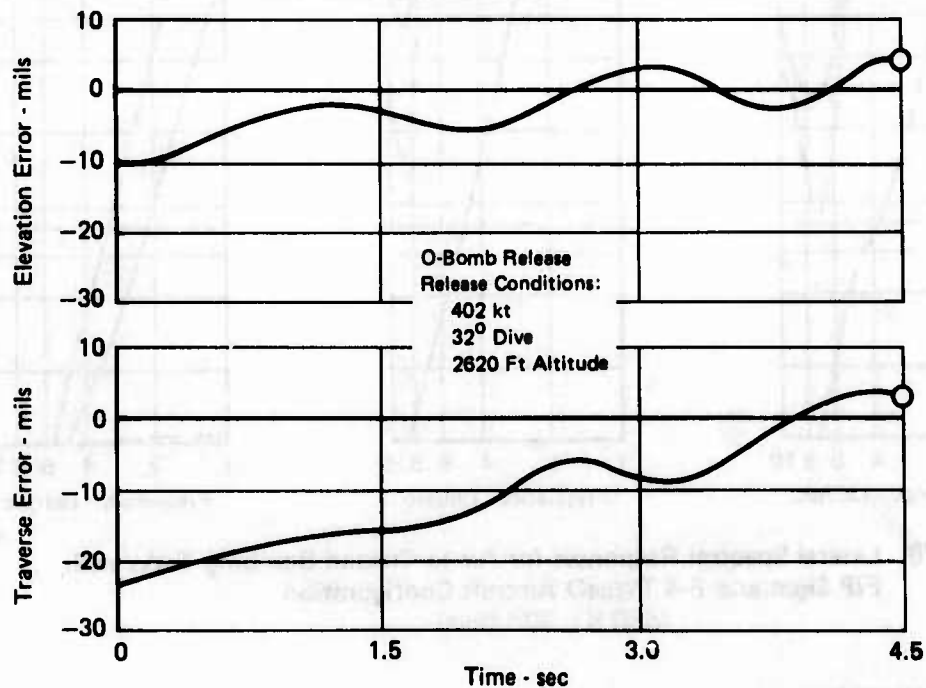
Figure 78. Lateral Spectral Responses for Air-to-Ground Bombing Tasks with
 FIP Sight and F-4 TWeaD Aircraft Configuration
 (450 Kt, 30° Dive)

GP75-0864-448



GP75-0864-427

Figure 79. Flight Test Air-to-Air Gunnery Tracking Responses
F-4 TWeaD Aircraft, Fixed Depressed Reticule Sight,
Mach 0.95 at 20,000 Ft Altitude



GP75-0864-428

Figure 80. Flight Test Air-to-Ground Bombing Tracking Response
F-4 TWeaD Aircraft, Fixed Depressed Reticule Sight

shown to be similar to those of the multi-axis analytical pilot, illustrated in Figure 74.

In this section, the developed multi-axis analytical pilot models have been shown to be appropriate and adequate for simulating the pilot performing weapon delivery. These pilot models were incorporated into the TAWDS programs, and were used to evaluate how aircraft flying qualities affect weapon delivery effectiveness. These flying qualities analyses are presented in the next section.

SECTION 5

TAWDS ANALYSES OF AIRCRAFT FLYING QUALITIES

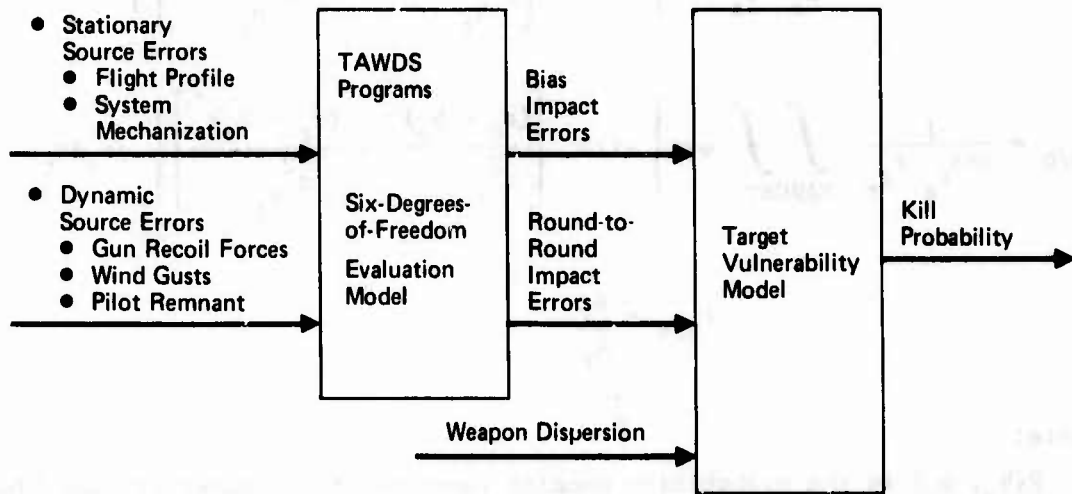
After establishing that the analytical pilot models were appropriate for simulating the pilot performing weapon delivery, these models were incorporated into the Terminal Aerial Weapon Delivery Simulation (TAWDS) programs. The TAWDS programs were used to evaluate weapon delivery accuracy for manually coupled aircraft weapon systems performing air-to-air gunnery, air-to-ground gunnery, and air-to-ground bombing weapon delivery tasks. For a specific number of aircraft weapon system configurations, corresponding to those flown by the two USAF pilots in the manned simulation studies, this weapon effectiveness analysis was performed to (1) determine the best range of flying qualities for aircraft to attain maximized weapon delivery effectiveness, (2) demonstrate the methodology formulated in the TAWDS computer programs, and (3) provide guidelines for the best set of aircraft flying qualities needed to attain maximum kill probability for air-to-air and air-to-ground weapon delivery. In this section, the TAWDS air-to-air and air-to-ground flying qualities evaluation studies and results are presented. The use of the TAWDS set of flying qualities in formulating guidelines for flight control system requirements are discussed in Section 6.

5.1 Description of TAWDS Flying Qualities Evaluation Studies

These analytical weapon delivery effectiveness studies took into account the interacting dynamic characteristics of the integrated airframe/flight control/pilot/sight/geometry/weapon system for the various aircraft studied. In this study, the measure used for weapon delivery effectiveness is relative kill probability, which is the ratio of the kill probability for various aircraft configurations with a given weapon sight system to the kill probability corresponding to the baseline F-4 TWeAD configuration with the same sight system. As diagrammed in Figure 81, the bias and round-to-round impact errors generated by the TAWDS programs are transformed into kill probabilities assuming realistic values for target areas and conditional probabilities for weapon lethality.

The probability of achieving a kill per burst or pass, written in terms of ensemble burst or pass statistics is summarized by:

$$P_{K/BURST} = \int_{-\infty}^{\infty} \int_{-\infty}^{\infty} (1 - (1 - P_{H/b} P_{K/H})^n) P(b_e, b_t) db_e db_t \quad (15)$$



GP75-0684-375

Figure 81. Functional Block Diagram of Weapon Delivery Effectiveness Model

$$P(b_e, b_t) = \frac{1}{2\pi\sigma_{b_e}\sigma_{b_t}} \exp \left\{ -1/2 \left[\frac{(b_e - \bar{b}_e)^2}{\sigma_{b_e}^2} + \frac{(b_t - \bar{b}_t)^2}{\sigma_{b_t}^2} \right] \right\} \quad (16)$$

$$P_{H/b} = \frac{1}{2\pi\sigma_{r_e}\sigma_{r_t}} \int \int_{\text{TARGET}} \exp \left\{ -1/2 \left[\frac{(r_e - b_e)^2}{\sigma_{r_e}^2} + \frac{(r_t - b_t)^2}{\sigma_{r_t}^2} \right] \right\} dr_e dr_t \quad (17)$$

$$P_{K/H} = \frac{A_V}{A_P} \quad (18)$$

where:

$P(b_e, b_t)$ is the probability density function of the burst or pass bias impact (b_e, b_t) .

$P_{H/b}$ is the probability that an individual round within the burst or pass impacts within the presented area of the target.

$P_{K/H}$ is the single round probability of target kill given a hit on its presented area, as approximated by the ratio A_V/A_P .

A_P is the target presented area from the line-of-sight approach aspect

A_V is the target vulnerable area corresponding to A_P .

n is the number of rounds in the burst.

For the air-to-ground bombing task, the number of rounds in the burst becomes just one.

The TAWDS programs simulated the terminal tracking and gunfiring or bomb release segments of the weapon delivery tasks. These segments of the attack geometry for each weapon delivery task are similar to those flown in the manned simulation tests. For all air-to-ground weapon delivery tasks where the attack aircraft is in a 30° dive at a speed of 450 kt, a two second precision tracking task prior to bomb release or gunfiring is simulated. The gunfiring phase occurs continuously for one second prior to initiating a 4g pull up maneuver to clear the ground at an altitude of 500 ft.

For the air-to-air encounter occurring at Mach 0.8, 10,000 ft altitude where the attack aircraft is tracking a 4g target at a 2000 ft range, a six second precision tracking task is simulated. During this terminal weapon

delivery task, the pilot fires the gun as dictated by firing logic which is a function of the digital pilot's estimated gun fire solution.

The flying qualities of the various aircraft analyzed by the TAWDS programs are similar to those considered in the manned simulation studies. For both the air-to-ground Mach 0.7 and air-to-air Mach 0.8 flight conditions, the longitudinal and lateral-directional aircraft configurations are tabulated in Figures 82 and 83. The generic longitudinal and lateral-directional TWeaD flight control systems are illustrated in Figures 84 and 85 respectively. The longitudinal time history responses due to longitudinal stick step inputs are presented in Figures 86 and 87 for the longitudinal TWeaD aircraft configurations tabulated in Figure 82. For these longitudinal responses, the short-period mode characteristics are the resultant eigenvalue characteristics of the augmented basic airframe short-period mode. Consequently, the resultant time history responses are not second order as the short-period nomenclature implies. The lateral-directional time history responses due to lateral stick step inputs are shown in Figures 88 and 89 for the lateral-directional aircraft configurations depicted in Figure 83. In addition to the aircraft flying qualities configurations for the air-to-ground Mach 0.7 flight condition, several configurations for the air-to-ground Mach 0.5 flight condition were analyzed to demonstrate the interaction of attack geometry kinematics with aircraft flying qualities.

The TAWDS air-to-ground weapon delivery results reported here are for the FDR and CCIP air-to-ground gunnery, and FIP bombing modes. In these analyses, the stationary source errors considered are those associated with the sight systems for the air-to-ground weapon delivery tasks. The along-track and cross-track stationary source error standard deviations for these tasks are defined in Figures 90 through 92. The dynamic source errors modeled are gust disturbances, weapon release forces and pilot remnant. These error sources are described in Figure 93.

For the air-to-air gunnery task, the aircraft was configured with a Director or LCOSS sight. The along-track and cross-track error sources associated with these sights are presented in Figures 94 and 95. The dynamic source errors for the air-to-air gunnery tasks are gust disturbances and gun recoil forces. The values for these disturbance sources are the same as those for the air-to-ground weapon delivery tasks.

Air-to-Ground Weapon Delivery Tasks - Mach 0.7, 5,000 Ft Altitude Flight Condition

Case	Flying Qualities Variations	Aircraft Characteristics			Flight Control System Parameters							
		F _s /G	ζ _{sp}	ω _{sp}	K _θ	K _{nz}	K _E	K _I	K _M	K _R L	G _C (s)	
1	Short-Period Frequency Variations	4 lb/G	0.7	3.6	0.16	0.0	0.134	0.0	0.259	0.75	1.0	
2	↓	↓	↓	4.5	0.5	2.0	0.8	1.0	0.58	2.2	G _F (s)	
3			0.7	6.4	1.0	4.0	1.6	4.0	↓	2.2	G _F (s)	
4			Short-Period Frequency Variations	0.5	3.25	0.55	0.0	0.12	0.0	0.223	0.75	1.0
5			↓	↓	3.9	0.25	1.0	0.4	1.0	0.58	2.2	G _F (s)
6					5.1	0.5	4.5	1.42	4.0	↓	↓	↓
7*					4 lb/G	5.4	0.5	2.0	0.8	↓	↓	↓
8			Stick Force per G Variations	2 lb/G	↓	5.4	0.5	↓	1.6	↓	↓	↓
9	4 lb/G	↓	↓	↓		0.8	↓	↓	↓	↓		
10	6 lb/G	0.5	5.4	0.5		2.0	0.533	4.0	0.58	2.2	G _F (s)	

Air-to-Air Weapon Delivery Tasks - Mach 0.8, 10,000 Ft Altitude Flight Condition

Case	Flying Qualities Variations	Aircraft Characteristics			Flight Control System Parameters								
		F _s /G	ζ _{sp}	ω _{sp}	K _θ	K _{nz}	K _E	K _I	K _M	K _R L	G _C (s)		
21	Short-Period Damping Variations	4 lb/G	0.33	4.5	0.25	1.0	0.384	4.0	0.58	2.2	G _F (s)		
22	↓	↓	0.6	4.5	0.5	3.0	1.018	1.0	↓	↓	↓		
23			0.88	4.5	0.7	6.3	1.95	1.0	↓	↓	↓		
24			Short-Period Frequency Variations	4 lb/G	0.6	4.5	0.5	3.0	1.018	1.0	↓	↓	↓
25	↓	↓	0.6	6.0	0.7	4.2	1.425	4.0	↓	↓	↓		
26			Stick Force per G Variations	2 lb/G	0.5	5.5	0.5	2.0	1.637	4.0	↓	↓	↓
27*			4 lb/G	↓	↓	↓	↓	0.818	↓	↓	↓	↓	
28	6 lb/G	0.5	5.5	0.5	2.0	0.545	4.0	0.58	2.2	G _F (s)			

Forward Loop Compensation: $G_F(s) = \frac{(0.25s + 1)(0.1s + 1)}{(s + 1)(0.05s + 1)}$

GP75-0864-415

*Baseline F-4 TWeaD Longitudinal Configuration

Figure 82. Longitudinal Flight Control System Configurations for Aircraft Weapon Delivery Tasks

Air-to-Ground Weapon Delivery Tasks - Mach 0.7, 5,000 Ft Altitude Flight Conditions

Case	Flying Qualities Variations	Aircraft Characteristics				Flight Control System Parameters					
		τ_R	ζ_D	ω_D	$\beta_2/FLAT$	K_{mc}	K_{me}	K_{ARI}	K_{ny}	K_{rr}	T_R
11	Dutch Roll Mode Damping Variations	0.33	0.2	3.5	0.15	2.87	1.0	1.0	30.0	2.1	0.33
12	↓	↓	0.4	3.4	↓	↓	↓	↓	↓	4.0	↓
13*	↓	↓	0.6	3.3	↓	↓	↓	↓	↓	5.7	↓
14	↓	↓	0.8	3.0	0.15	↓	↓	↓	↓	7.2	↓
15	Proverse/Adverse Yaw Variations	↓	0.6	3.3	0.4	↓	↓	-10.0	↓	5.7	↓
16	↓	↓	↓	↓	0.15	↓	↓	1.0	↓	↓	↓
17	↓	0.33	↓	↓	-0.4	2.87	1.0	20.0	↓	↓	0.33
18	Roll Rate Sensitivity Variations	0.25	↓	↓	0.15	0.1	3.33	1.0	↓	↓	0.25
19	↓	0.33	↓	↓	0.15	0.1	3.33	1.0	↓	↓	0.33
20	↓	0.5	0.6	3.3	0.15	0.1	3.33	1.0	30.0	5.7	0.5

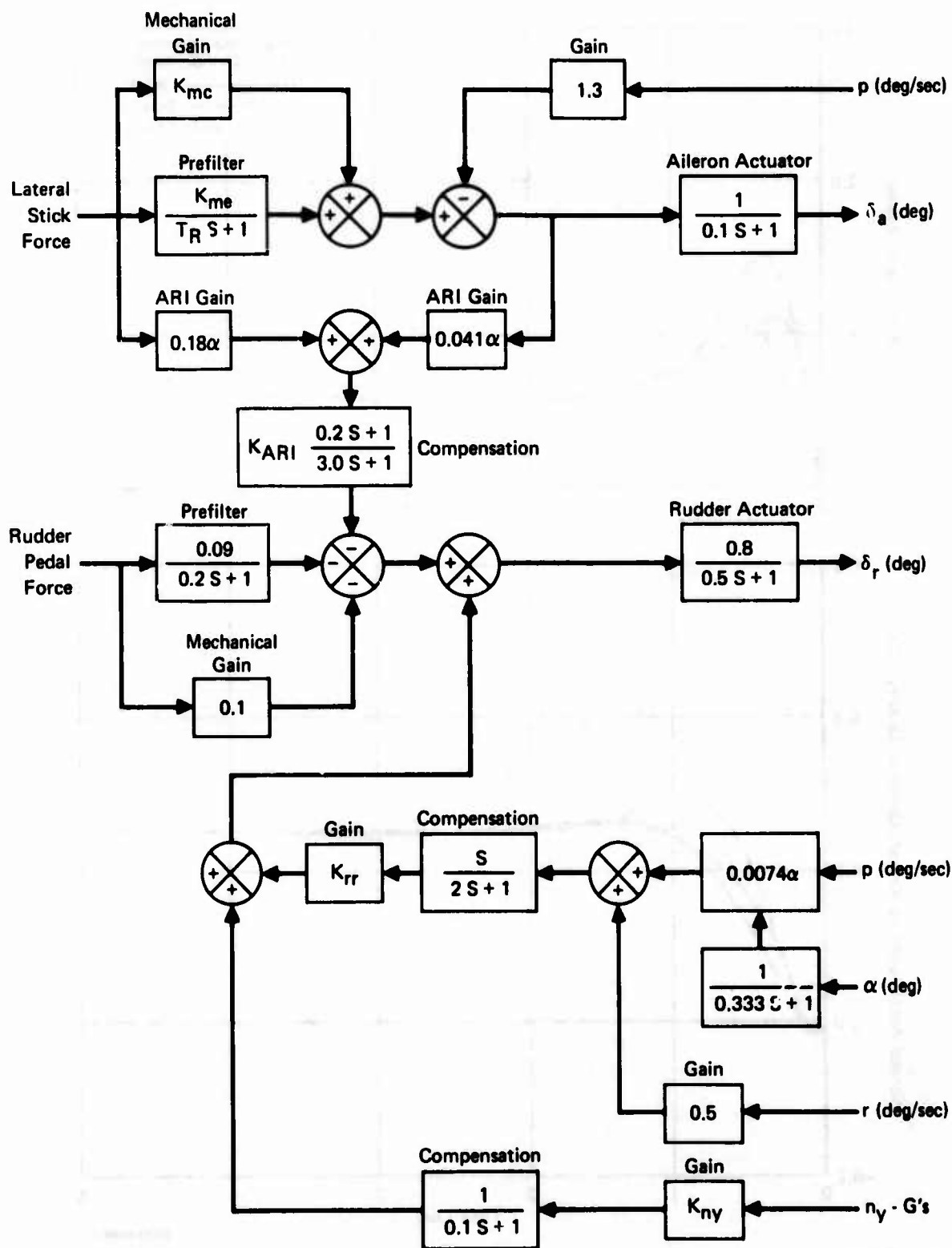
Air-to-Air Weapon Delivery Tasks - Mach 0.8, 10,000 Ft Altitude Flight Condition

Case	Flying Qualities Variations	Aircraft Characteristics				Flight Control System Parameters					
		τ_R	ζ_D	ω_D	$\beta_2/FLAT$	K_{mc}	K_{me}	K_{ARI}	K_{ny}	K_{rr}	T_R
29	Dutch Roll Mode Damping Variations	0.33	0.2	3.7	0.12	2.87	1.0	1.0	30.0	2.4	0.33
30	↓	↓	0.4	↓	↓	↓	↓	↓	↓	4.0	↓
31*	↓	↓	0.6	↓	↓	↓	↓	↓	↓	5.7	↓
32	↓	↓	0.8	0.12	↓	↓	↓	1.0	↓	7.4	↓
33	Proverse/Adverse Yaw Variations	↓	0.6	↓	0.3	↓	↓	-10.0	↓	5.7	↓
34	↓	↓	↓	↓	0.12	↓	↓	1.0	↓	↓	↓
35	↓	↓	↓	-0.3	↓	↓	20.0	↓	↓	↓	↓
36	Roll Rate Sensitivity Variations	0.33	↓	↓	0.12	2.87	1.0	1.0	↓	↓	0.33
37	↓	0.5	↓	↓	0.12	0.1	3.33	3.33	↓	↓	0.5
38	↓	1.0	0.6	3.7	0.12	0.1	3.33	3.33	30.0	5.7	1.0

* Baseline F-4 TWaD Lateral-Directional Configuration

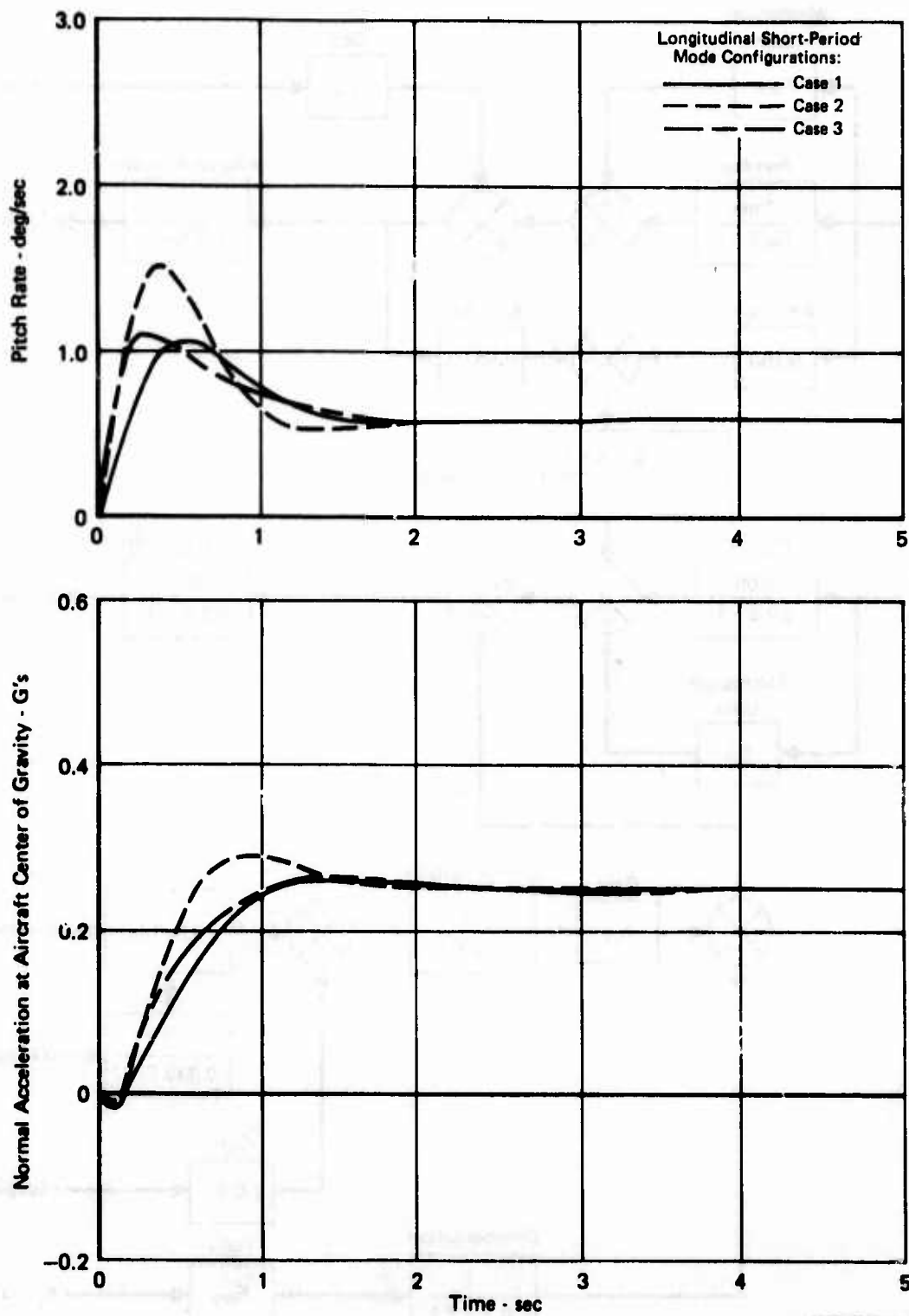
GP75-0864-418

Figure 83. Lateral-Directional Flight Control System Configurations for Aircraft Weapon Delivery Tasks



OP78-0864-104

Figure 85. Generic Lateral-Directional TWeaD Flight Control System



GP75-0864-411

Figure 86. Longitudinal Responses Due to Unit Step Longitudinal Stick Command for Various Longitudinal Aircraft Configurations (Mach 0.7 at 5,000 Ft Altitude Flight Condition)

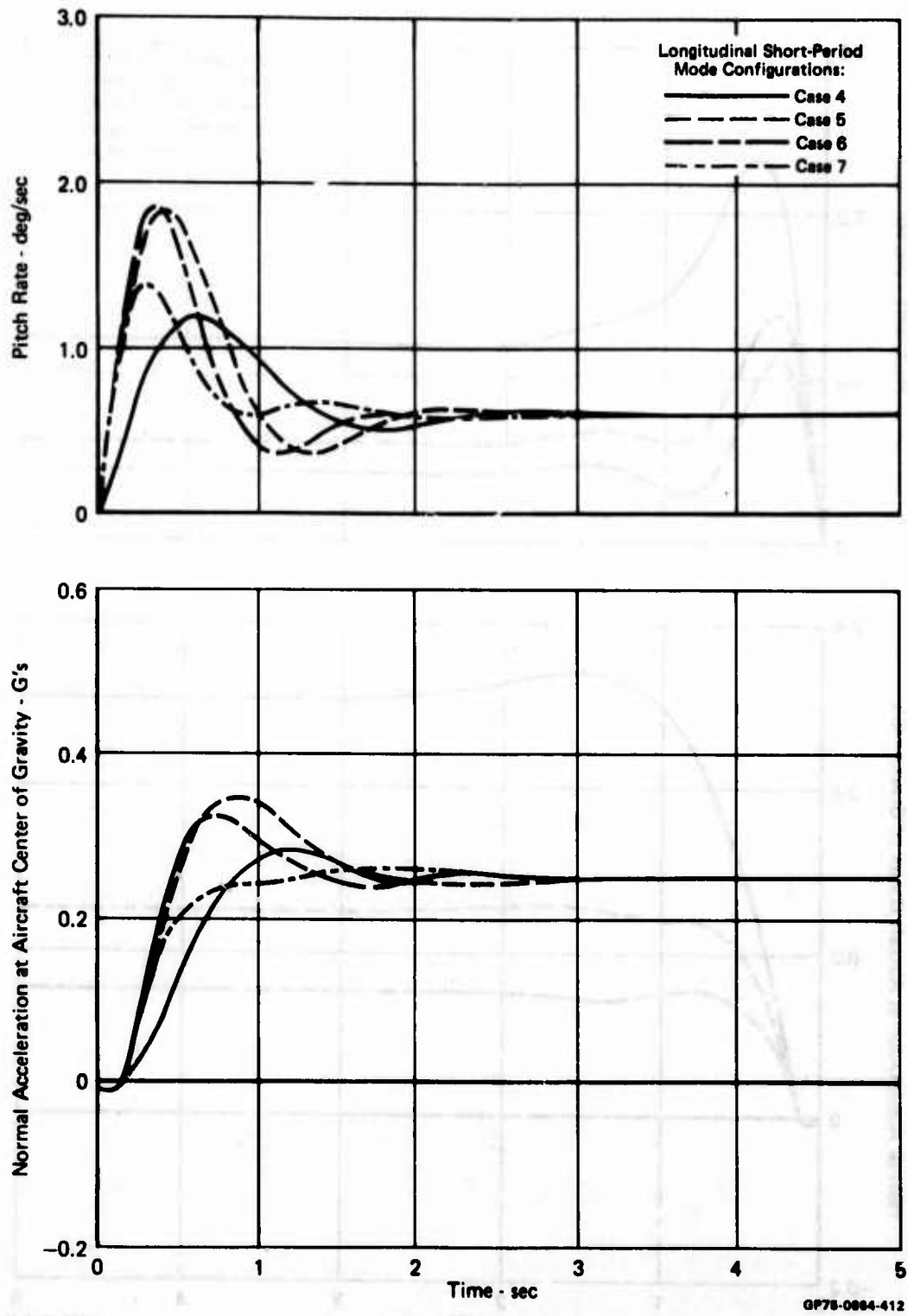


Figure 86. Longitudinal Responses Due to Unit Step Longitudinal Stick Command for Various Longitudinal Aircraft Configurations (Continued) (Mach 0.7 at 5000 Ft Altitude Flight Condition)

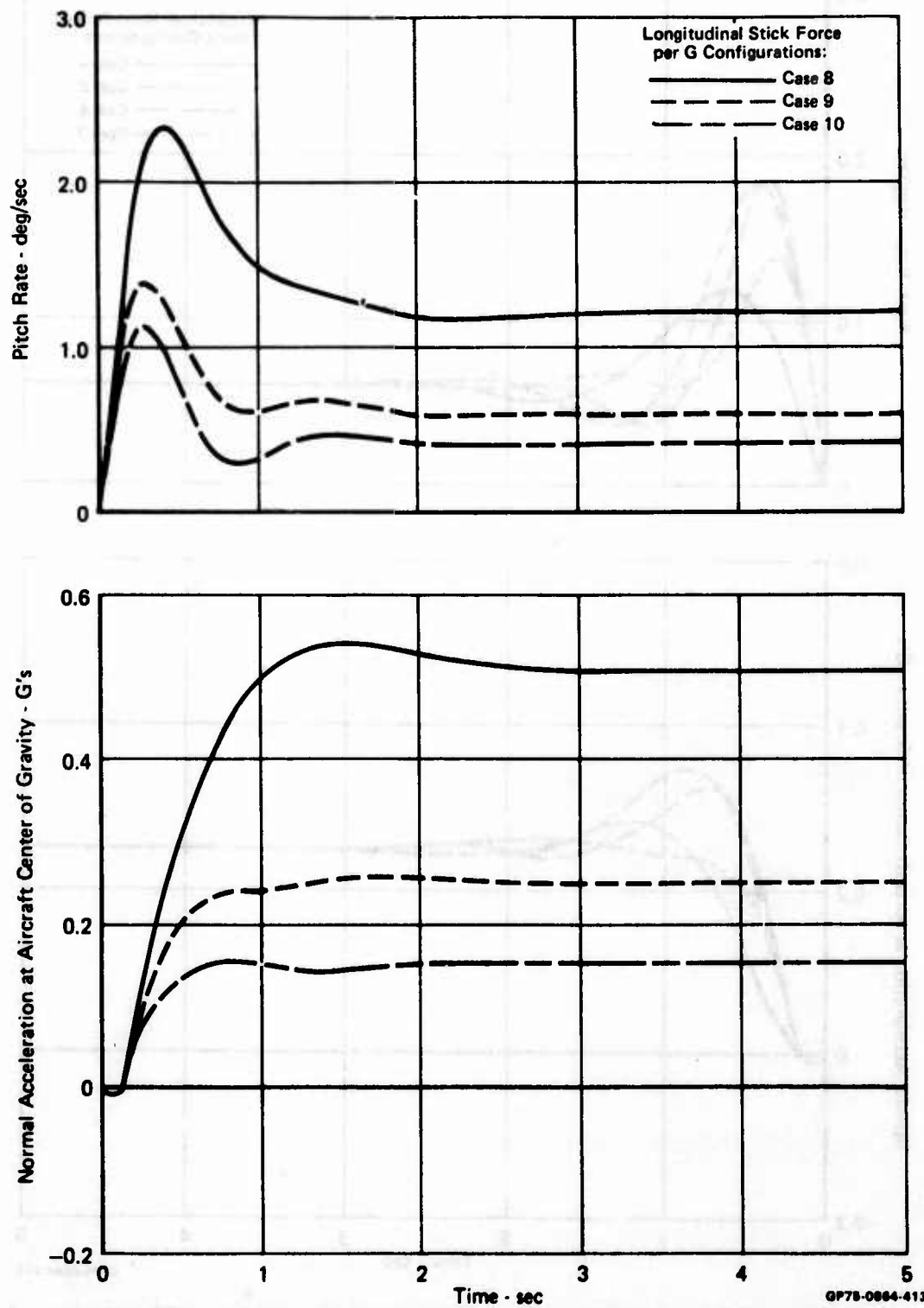


Figure 86. Longitudinal Responses Due to Unit Step Longitudinal Stick Command for Various Longitudinal Aircraft Configurations (Concluded) (Mach 0.7 at 5,000 Ft Altitude Flight Condition)

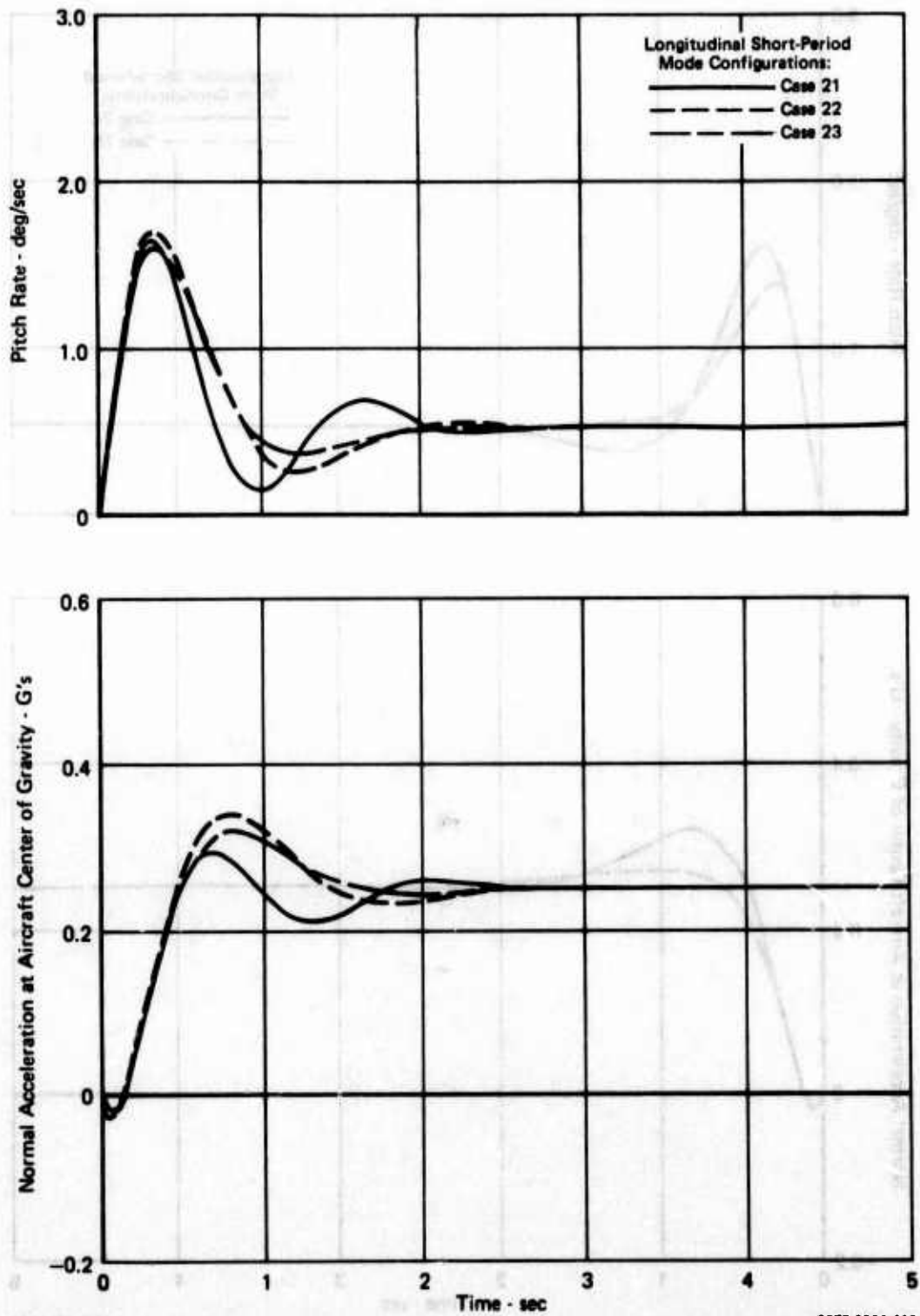
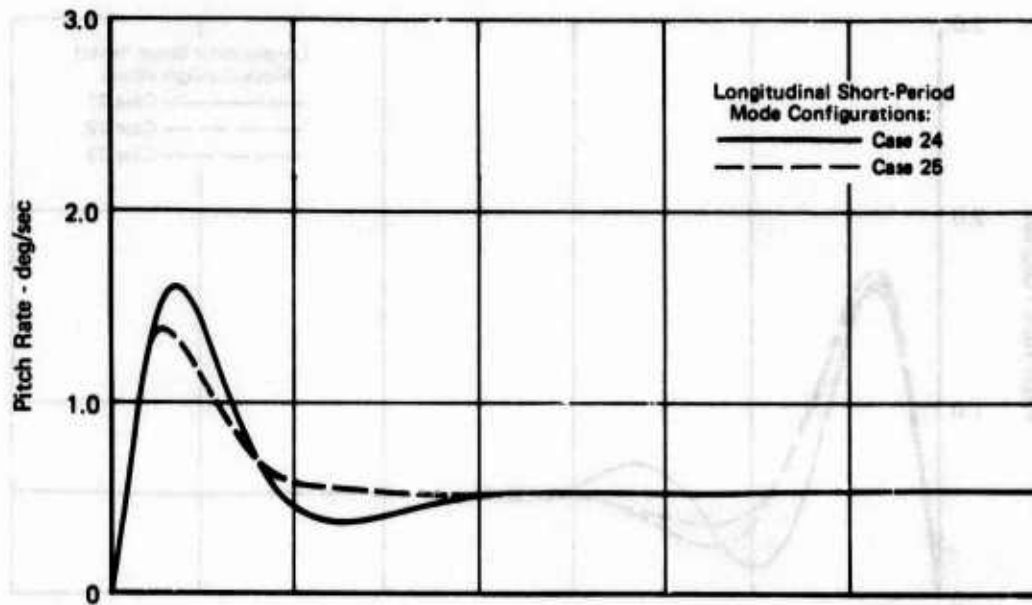


Figure 87. Longitudinal Responses Due to Unit Step Longitudinal Stick Command for Various Longitudinal Aircraft Configurations (Mach 0.8 at 10,000 Ft Altitude Flight Condition)



GP78-0864-414

Figure 87. Longitudinal Responses Due to Unit Step Longitudinal Stick Command for Various Longitudinal Aircraft Configurations (Continued) (Mach 0.8 at 10,000 Ft Altitude Flight Condition)

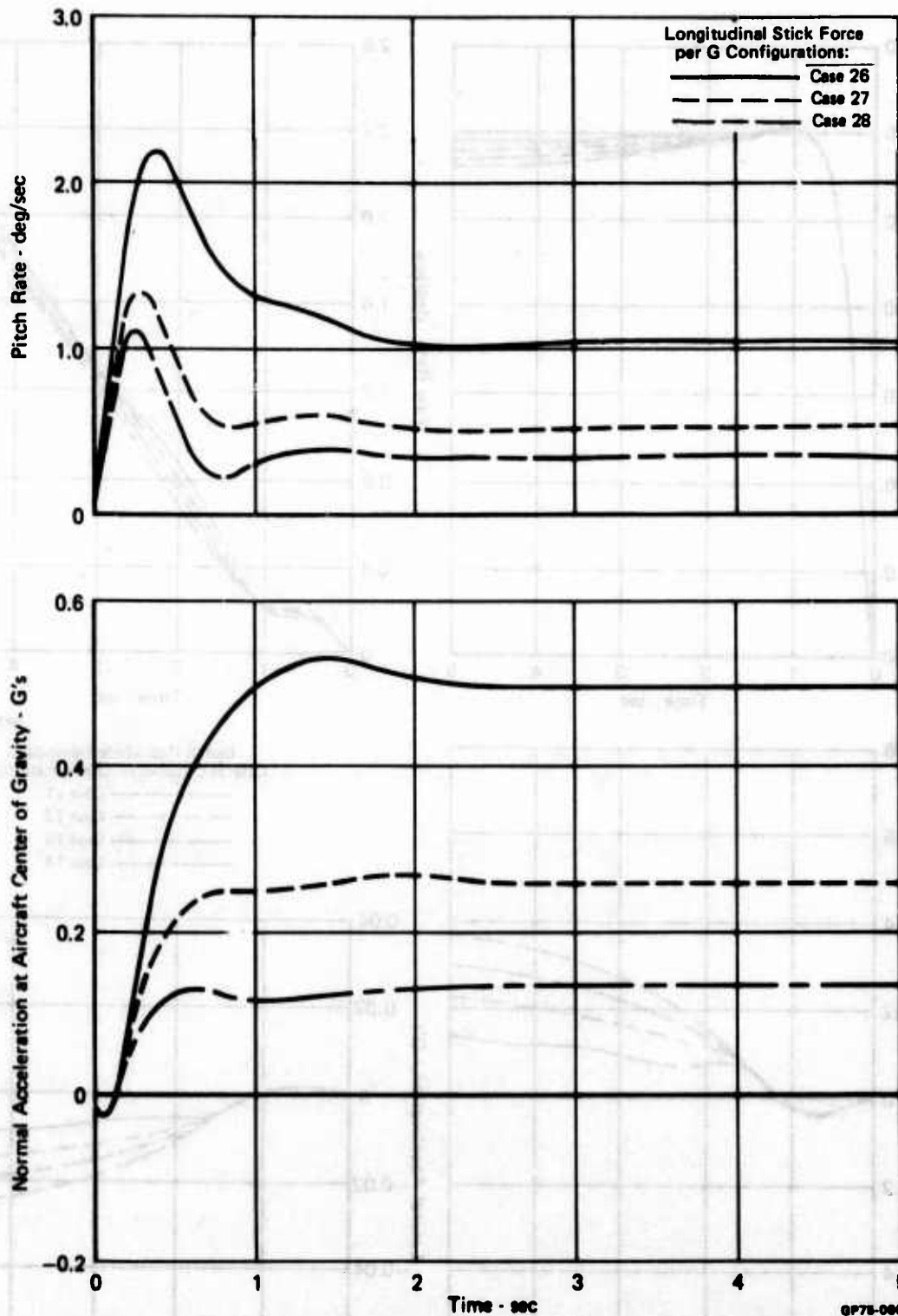


Figure 87. Longitudinal Responses Due to Unit Step Longitudinal Stick Command for Various Longitudinal Aircraft Configurations (Concluded)
(Mach 0.8 at 10,000 Ft Altitude Flight Condition)

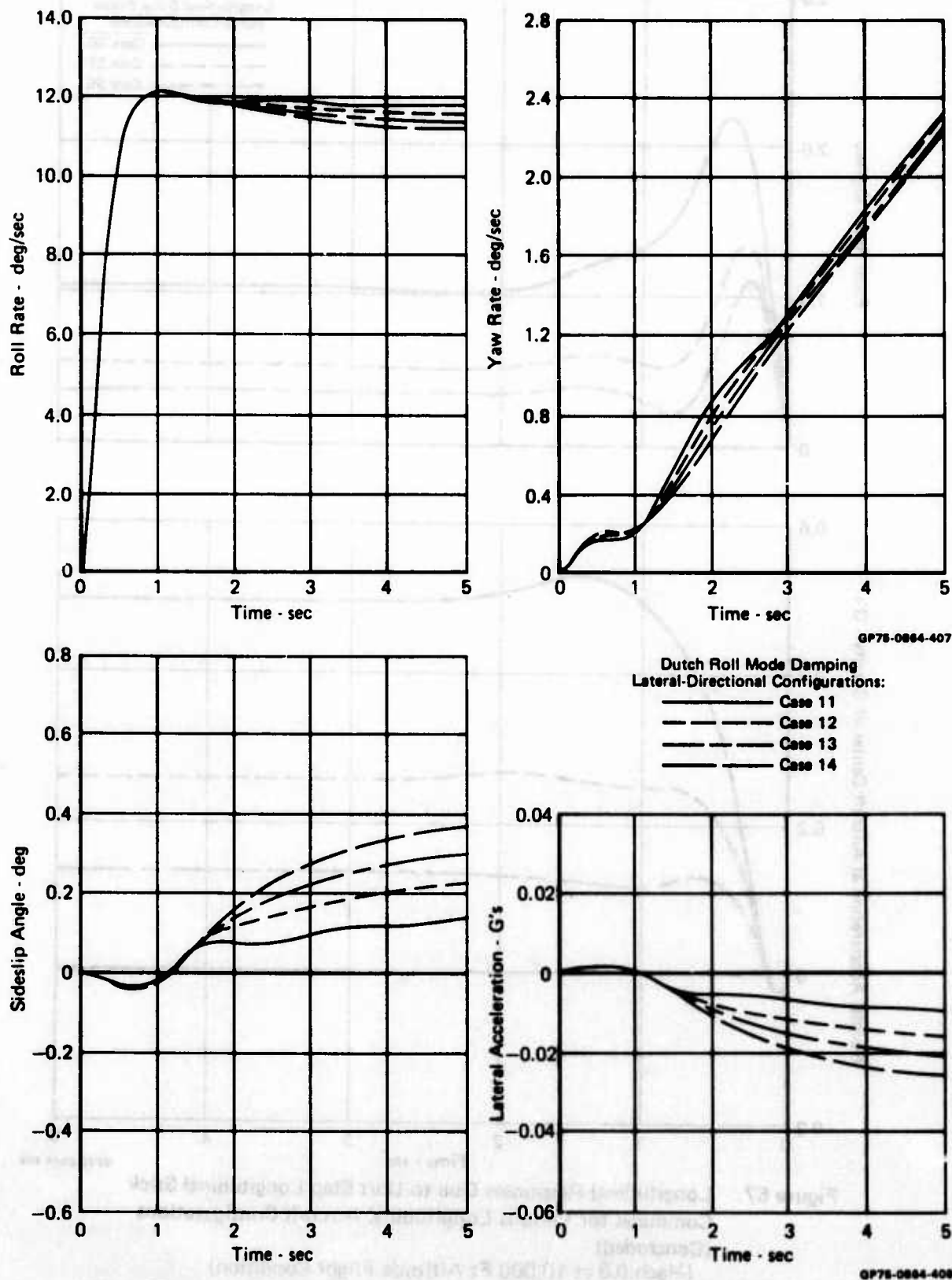


Figure 88. Lateral-Directional Responses Due to Unit Step Lateral Stick Command for Various Lateral-Directional Aircraft Configurations (Mach 0.7 at 5,000 Ft Altitude Flight Condition)

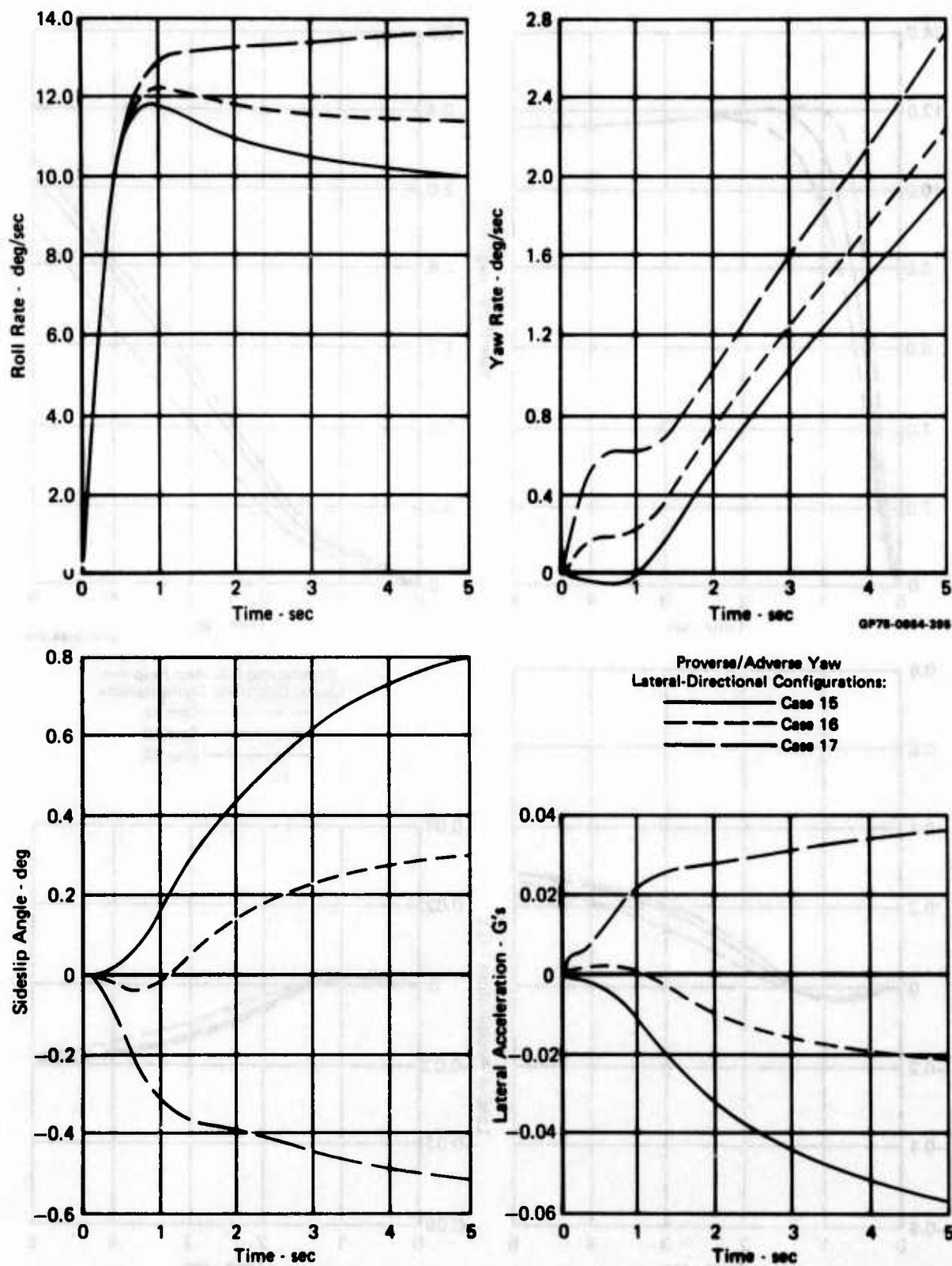
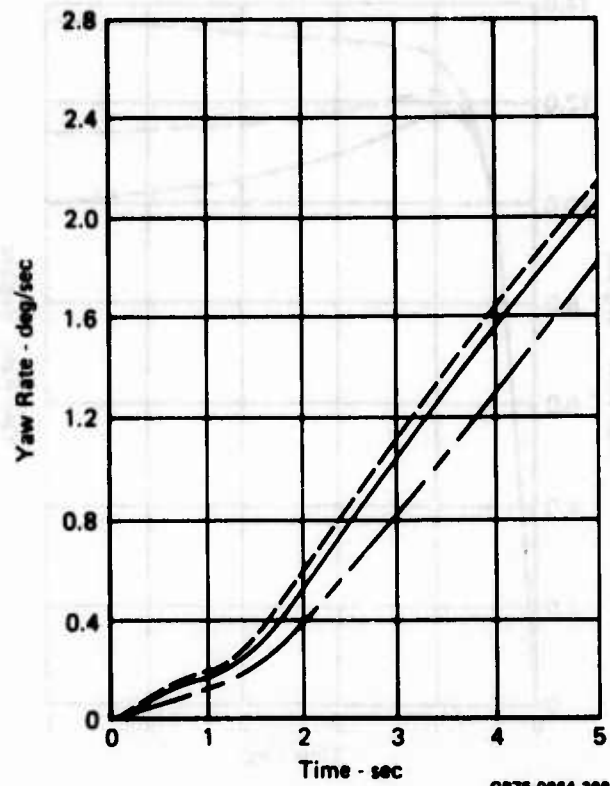
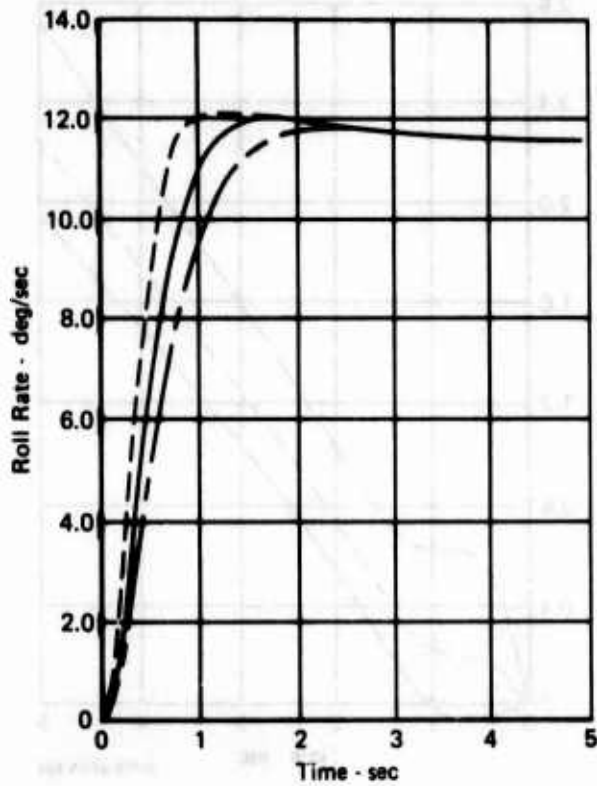
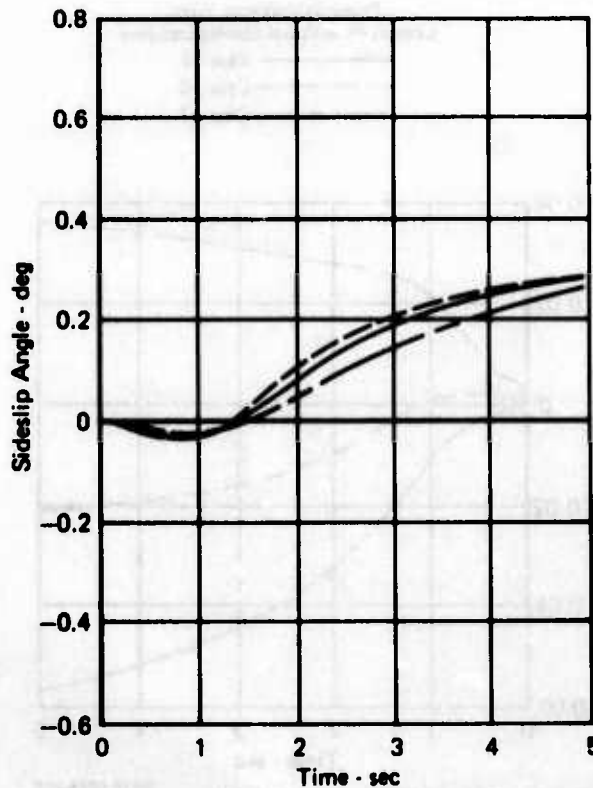


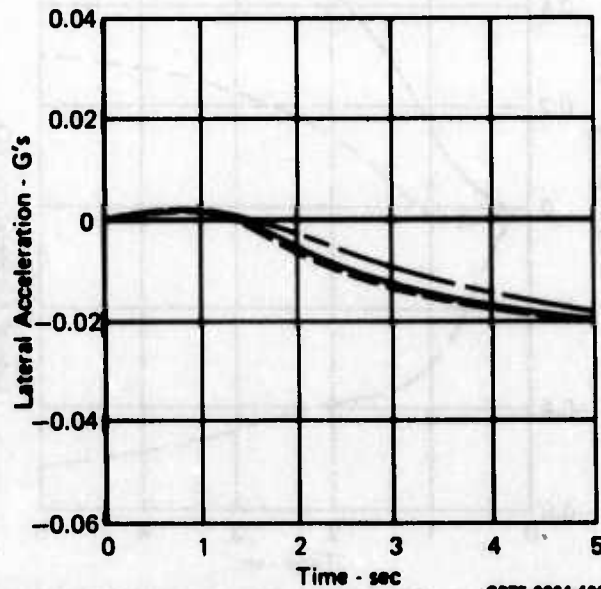
Figure 88. Lateral-Directional Responses Due to Unit Step Lateral Stick Command for Various Lateral-Directional Aircraft Configurations (Continued)
 (Mach 0.7 at 5,000 Ft Altitude Flight Condition)



GP75-0084-399

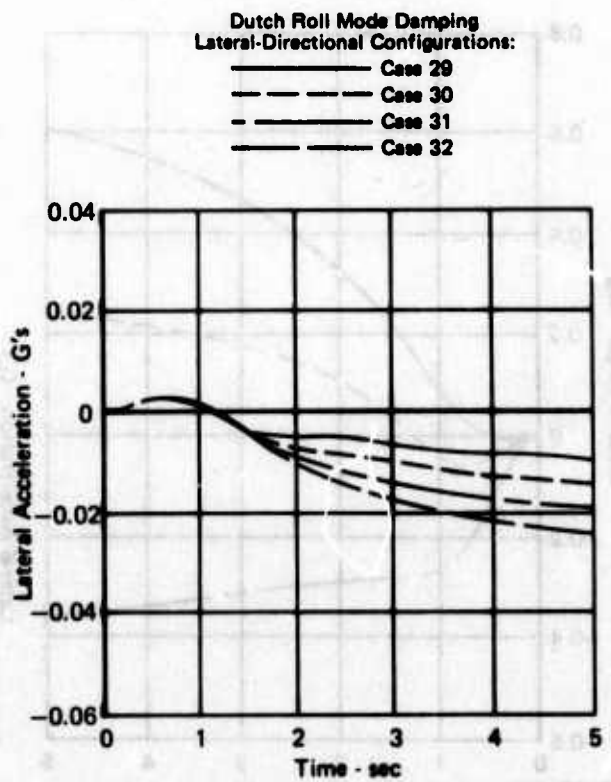
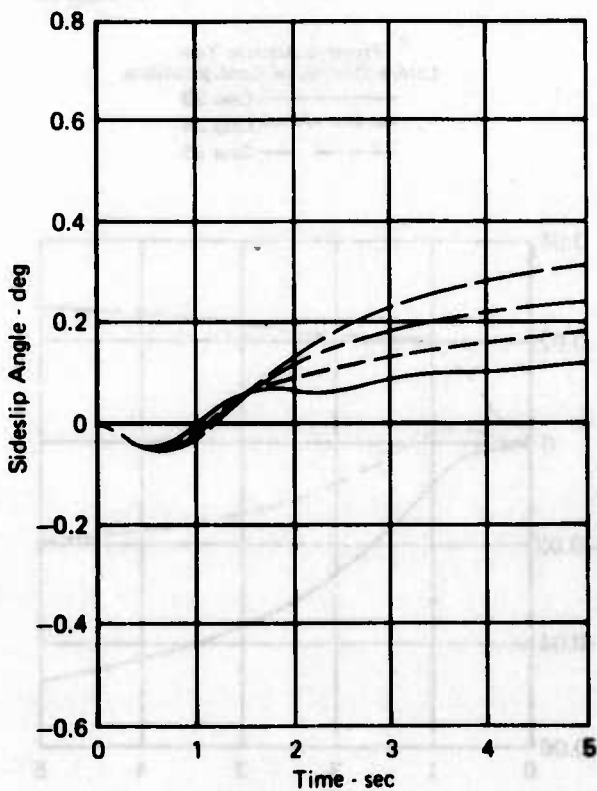
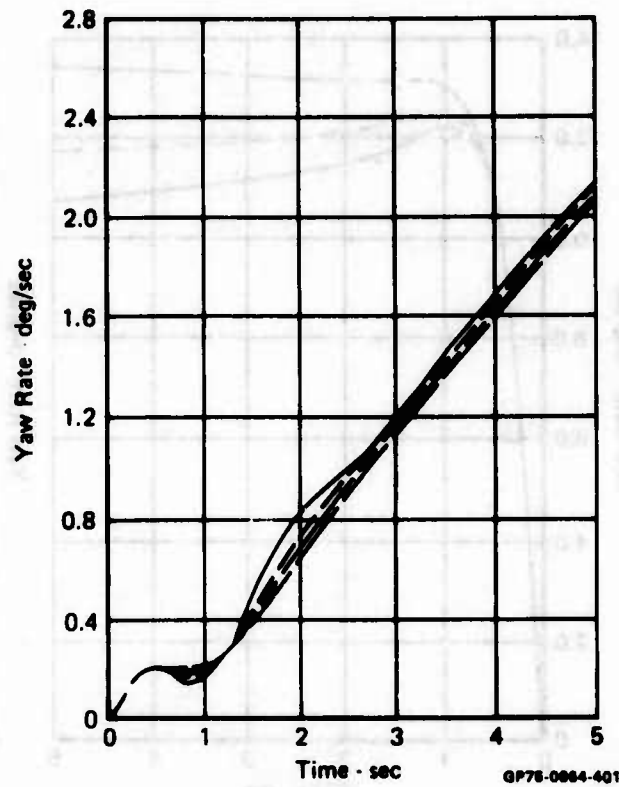
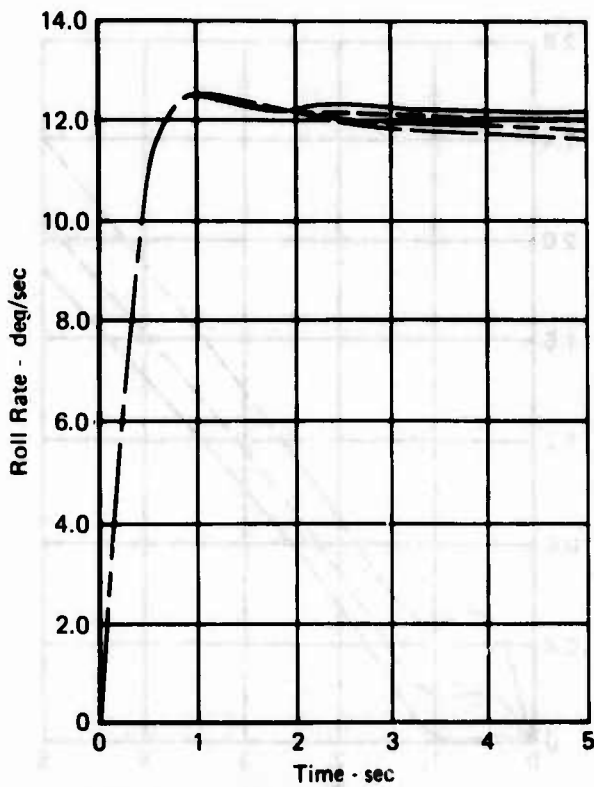


Commanded Roll Rate Response
Lateral-Directional Configurations:
- - - Case 18
— Case 19
- · - Case 20



GP75-0084-400

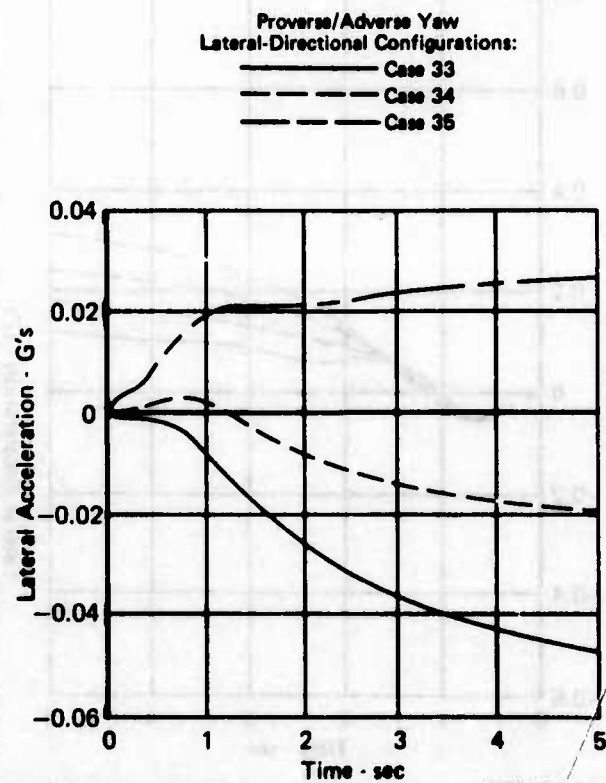
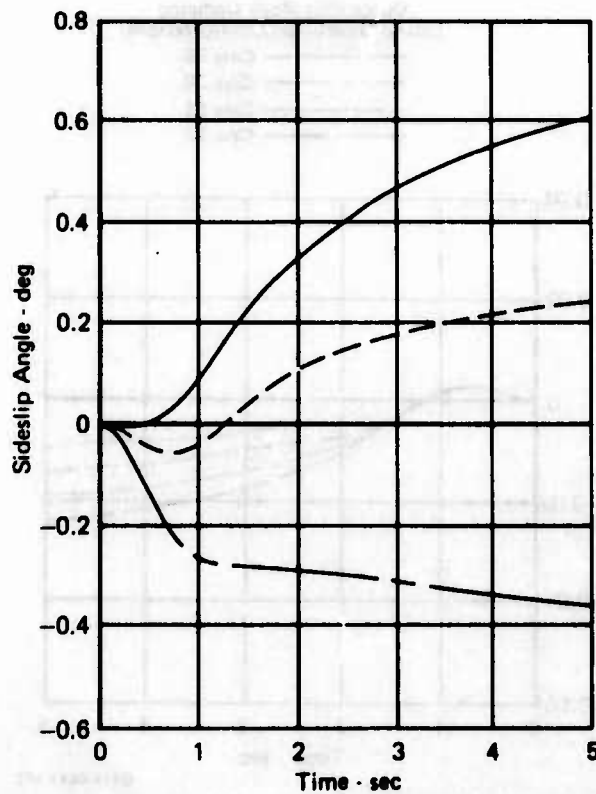
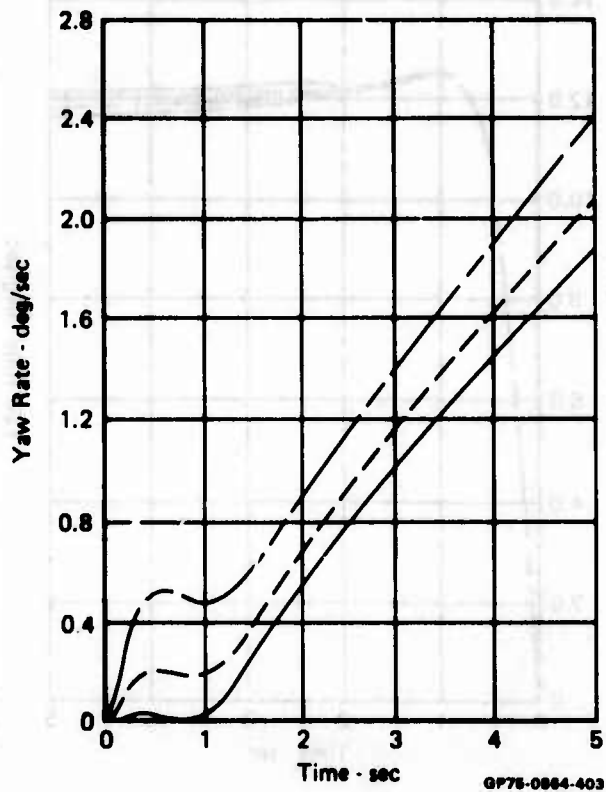
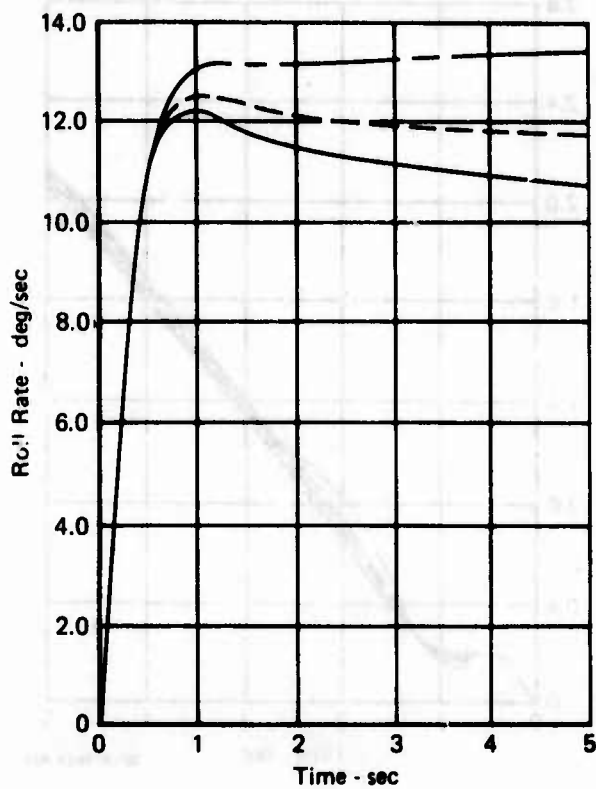
Figure 88. Lateral-Directional Responses Due to Unit Step Lateral Stick Command for Various Lateral-Directional Aircraft Configuration: (Concluded) (Mach 0.7 at 5,000 Ft Altitude Flight Condition)



Dutch Roll Mode Damping
Lateral-Directional Configurations:

- Case 29
- - - Case 30
- · - Case 31
- - - Case 32

Figure 89. Lateral-Directional Responses Due to Unit Step Lateral Stick Command for Various Lateral-Directional Aircraft Configurations (Mach 0.8 at 10,000 Ft Altitude Flight Conditions)



Proverse/Adverse Yaw
Lateral-Directional Configurations:
 Case 33
 Case 34
 Case 35

Figure 89. Lateral-Directional Responses Due to Unit Step Lateral Stick Command for Various Lateral-Directional Aircraft Configurations (Continued) (Mach 0.8 at 10,000 Ft Altitude Flight Condition)

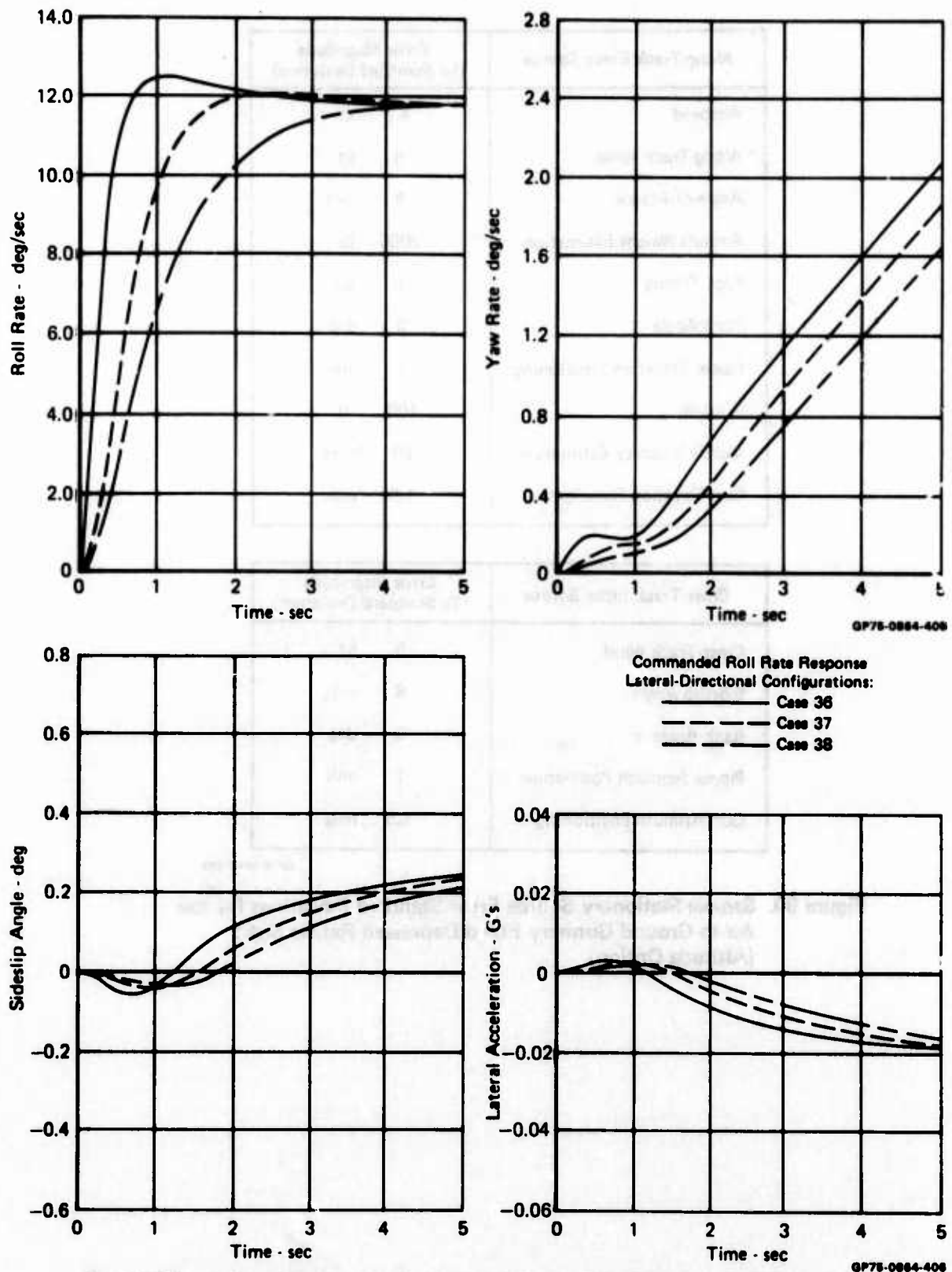


Figure 89. Lateral-Directional Responses Due to Unit Step Lateral Stick Command for Various Lateral-Directional Aircraft Configurations (Concluded)
 (Mach 0.8 at 10,000 Ft Altitude Flight Condition)

Along-Track Error Source	Error Magnitude (1 σ Standard Deviation)
Airspeed	4.7 kt
Along-Track Wind	5 kt
Angle-of-Attack	6 mils
Aircraft Weight Estimation	2000 lb
Pilot Timing	1 sec
Pitch Angle	2 deg
Pipper Elevation Positioning	1 mils
Altitude	100 ft
Muzzle Velocity Estimation	50 ft/sec
Gun Elevation Boresight	1.5 mils

Cross-Track Error Source	Error Magnitude (1 σ Standard Deviation)
Cross-Track Wind	5 kt
Sideslip Angle	8 mils
Bank Angle	3 deg
Pipper Azimuth Positioning	1 mils
Gun Azimuth Positioning	1.5 mils

GP75-0864-388

Figure 90. Sample Stationary Source Error Standard Deviations for the Air-to-Ground Gunnery Fixed Depressed Reticle Sight (Altitude Option)

Along-Track Error Source	Error Magnitude (1 σ Standard Deviation)	
Along-Track Inertial Velocity	4	ft/sec
Vertical Inertial Velocity	3	ft/sec
Airspeed	3	kt
Pitch Angle	2.24	mils
Pipper Elevation Positioning	1.41	mils
Radar Range Measurement	1.5	%
Radar Elevation Positioning	1.73	mils
Muzzle Velocity	50	ft/sec
Gun Elevation Boresight	1.5	mils

Cross-Track Error Source	Error Magnitude (1 σ Standard Deviation)	
Cross-Track Inertial Velocity	4	ft/sec
Heading Angle	2.24	mils
Sideslip Angle	3	mils
Pipper Azimuth Positioning	1.41	mils
Gun Azimuth Boresight	1.5	mils

G-78-0864-387

Figure 91. Sample Stationary Source Error Standard Deviations for the Air-to-Ground Gunnery Continuously Computed Impact Point Sight

Along-Track Error Source	Error Magnitude (1 σ Standard Deviation)	
Along-Track Inertial Velocity	2	ft/sec
Vertical Inertial Velocity	2	ft/sec
Airspeed	0	ft/sec
Pitch Angle	2	mils
Pipper Elevation Positioning	2	mils
Radar Range Measurement	1	%
Radar Elevation Positioning	2	mils
Bomb Ejection Velocity	1.5	ft/sec
Rack Release Time Delay	0.1	tenths of a sec
Along-Track Bomb Dispersion	3	mils

Cross-Track Error Source	Error Magnitude 1 σ Standard Deviation	
Cross-Track Inertial Velocity	2	ft/sec
Heading Angle	3	mils
Sideslip Angle	3	mils
Pipper Azimuth Positioning	2	mils
Cross-Track Bomb Dispersion	3	mils

GP78-0884-388

Figure 92. Sample Stationary Source Error Standard Deviations for the Air-to-Ground Bombing Future Impact Point Sight

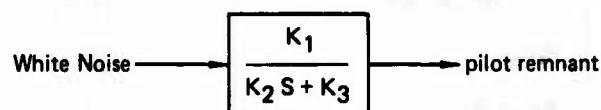
I. Dryden Wind Gust Model

$$\Phi(\omega) = \left| W_G \right|^2 \frac{L}{u} \left(\frac{1 + \frac{3L^2}{u^2} \omega^2}{\left(1 + \frac{L^2}{u^2} \omega^2 \right)^2} \right)$$

where $|W_G|$ is the root mean square value of the wind gust velocity (ft/sec)
 u is the airspeed of the aircraft (ft/sec)
 ω is frequency (rad/sec)
 L is 1000 ft if altitude \geq 1000 ft above sea level
altitude (ft) if altitude $<$ 1000 ft above sea level

In TAWDS Sample Runs, $|W_G| = 6$ ft/sec

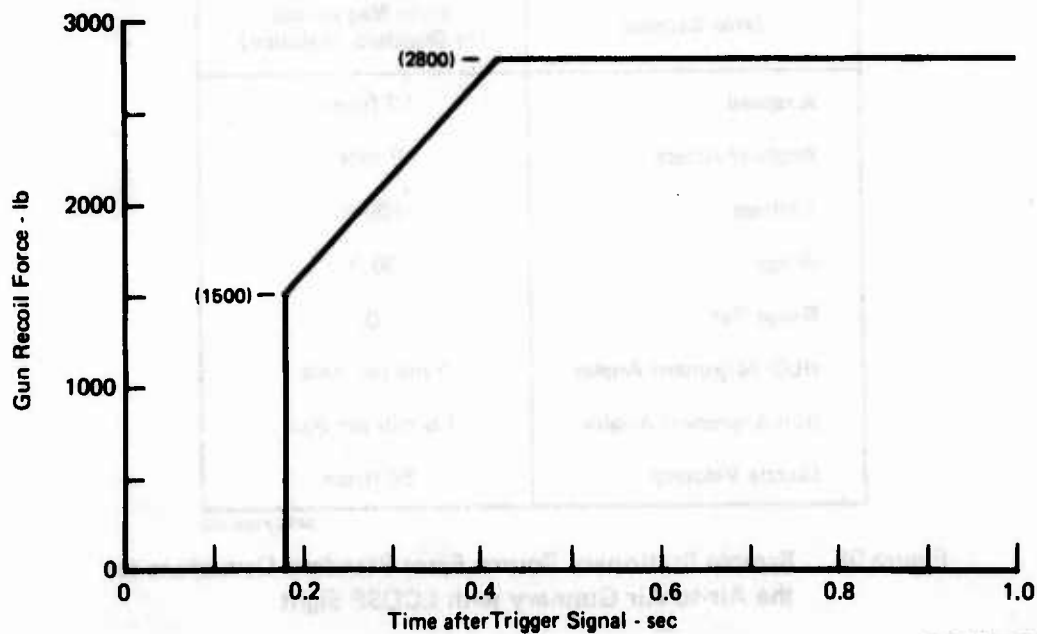
II. Pilot Remnant



Weapon	Sight	Channel	K ₁	K ₂	K ₃
Gun	Fixed Depressed Reticle	Longitudinal	0.00643	1	1.542
		Lateral	0.02140	1	3.544
		Directional	0.02737	1	1.080
	Continuously Computed Impact Point	Longitudinal	0.01107	1	2.060
Lateral		0.03019	1	5.000	
Directional		0.02164	1	1.110	
Bomb	Future Impact Point	Longitudinal	0.01510	1	3.020
		Lateral	0.01632	1	2.880
		Directional	Not Used	Not Used	Not Used

III. Gun Recoil Force

GP75-0864-391



GP75-0864-208

Figure 93. Sample Dynamic Source Errors

Error Sources	Error Magnitude (1 σ Standard Deviation)
Airspeed	4.7 ft/sec
Angle-of-Attack	3 mils
Altitude	100 ft
Line-of-Sight Rates	10 mils/sec per Axis at 1500 ft Range
Second Order Correlation	
Damping	0.5
Bandwidth	0.5 Hz
Range	30 ft
Range Rate	0.
HUD Alignment Angles	1 Mil per Axis
Gun Alignment Angles	1.5 mils per Axis
Muzzle Velocity	50 ft/sec

GP78-0884-423

Figure 94. Sample Stationary Source Error Standard Deviations for the Air-to-Air Gunnery with Director Sight

Error Sources	Error Magnitudes (1 σ Standard Deviation)
Airspeed	4.7 ft/sec
Angle-of-Attack	3 mils
Altitude	100 ft
Range	30 ft
Range Rate	0.
HUD Alignment Angles	1 mil per Axis
Gun Alignment Angles	1.5 mils per Axis
Muzzle Velocity	50 ft/sec

GP78-0884-422

Figure 95. Sample Stationary Source Error Standard Deviations for the Air-to-Air Gunnery with LCOSS Sight

The multi-axis pilot models discussed in Section 4 provided the same tracking error response characteristics as those obtained from the manned simulation study. Consequently, these pilot models were incorporated into the air-to-air and air-to-ground TAWDS programs. Mathematical representations of the multi-axis pilot models used in these analyses are presented in Figures 96 through 99. The Flight Control Requirements for Weapon Delivery Background Information Report describes the development of the criteria for selecting values for the multi-axis pilot model parameters. The pilot remnant Power Spectral Density functions for the air-to-ground weapon delivery tasks were measured from manned simulation data. These remnant functions, which augment the pilot's stick and rudder pedal force outputs of the linearized describing functions for the nonlinear multi-axis pilot models, were incorporated into the air-to-ground TAWDS(AG) program.

5.2 TAWDS Flying Qualities Analyses

In the air-to-ground TAWDS analyses the air-to-ground weapon delivery tasks studied were FDR gunnery, CCIP gunnery, and FIP bombing. The air-to-air gunnery tasks evaluated were Director and LCOSS gunnery. For each weapon delivery task the weapon delivery effectiveness measure is relative kill probability which is the ratio of probability of kill for a given aircraft configuration to the aircraft configured with the baseline TWeAD flight control system. Although the relative kill probability for a given aircraft flying quality configuration cannot be compared with respect to different sight systems, the weapon delivery accuracy measures such as ensemble mean point of impact, standard deviation of burst or pass means, and standard deviation of burst or pass rounds can be compared with respect to sight systems. For air-to-ground gunnery the CCIP sight/aircraft configurations were more nearly accurate than the FDR sight/aircraft configurations. For the air-to-air gunnery tasks, more gunfiring opportunities occurred for the Director gunsight than for the LCOSS sight system. The gunfire opportunities for the Director and LCOSS gunsights resulted in relatively the same impact error accuracies.

For all the aircraft configurations investigated, the baseline F-4 TWeAD lateral-directional flight control system was used when the longitudinal flying qualities characteristics were varied, and the baseline F-4 TWeAD longitudinal flight control system was employed when the lateral-directional flying qualities characteristics were changed.

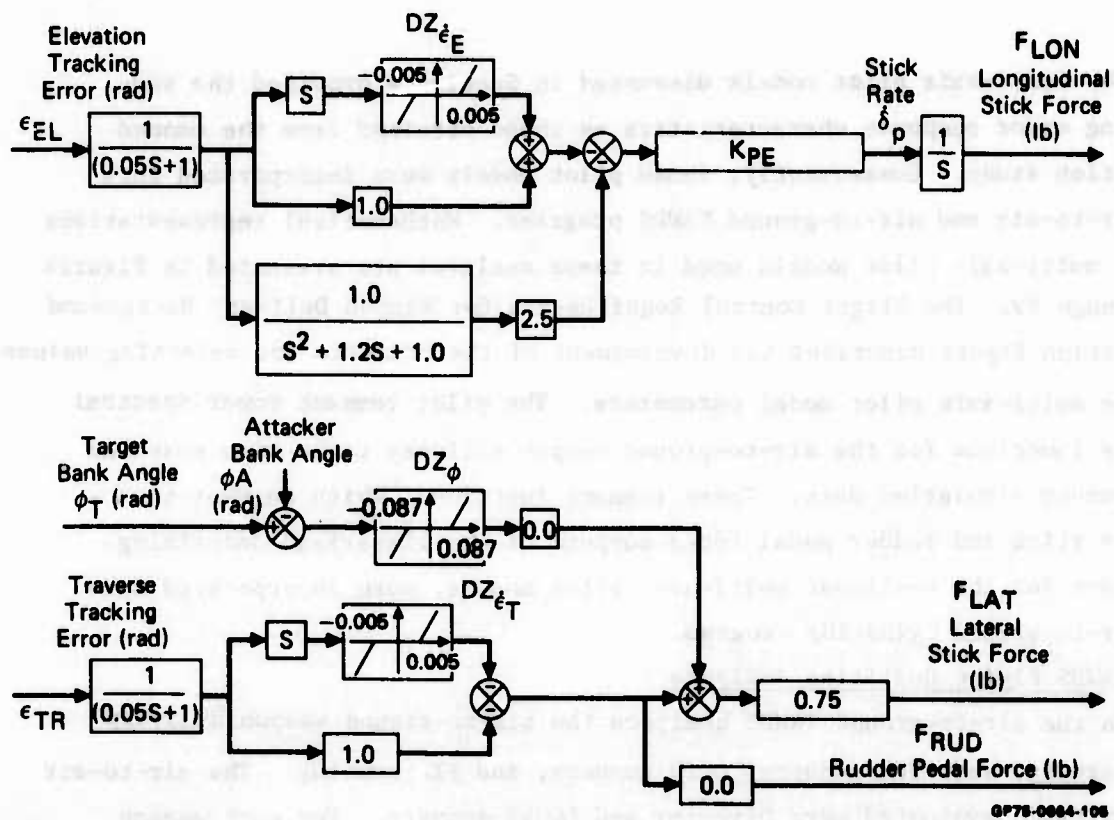


Figure 96. Multiaxis Pilot Model Structure for Air-to-Air Gunnery Task

Case	Longitudinal Flying Qualities Variations	Aircraft Characteristics			Pilot Model Parameter	
		F_g/G	ζ_{sp}	ω_{sp}	KPE	
					Director	LCOSS
21	Short-Period Damping Variation	4 lb/G	0.33	4.5	1.4	3.2
22	↓	↓	0.6	4.5	1.8	4.2
23	↓	↓	0.88	4.5	1.7	3.6
24	Short-Period Frequency Variations	4 lb/G	0.6	4.5	1.8	4.2
25	↓	↓	0.6	6.0	3.0	7.2
26	Stick Force per G Variations	2 lb/G	0.5	5.5	1.45	5.6
27	↓	4 lb/G	↓	↓	2.5	6.0
28	↓	6 lb/G	0.5	5.5	3.0	7.8

GP75-0084-117

Figure 97. Longitudinal Pilot Gain Variations for Air-to-Air Gunnery Tasks (Mach 0.8 at 10,000 Ft Altitude Flight Conditions)

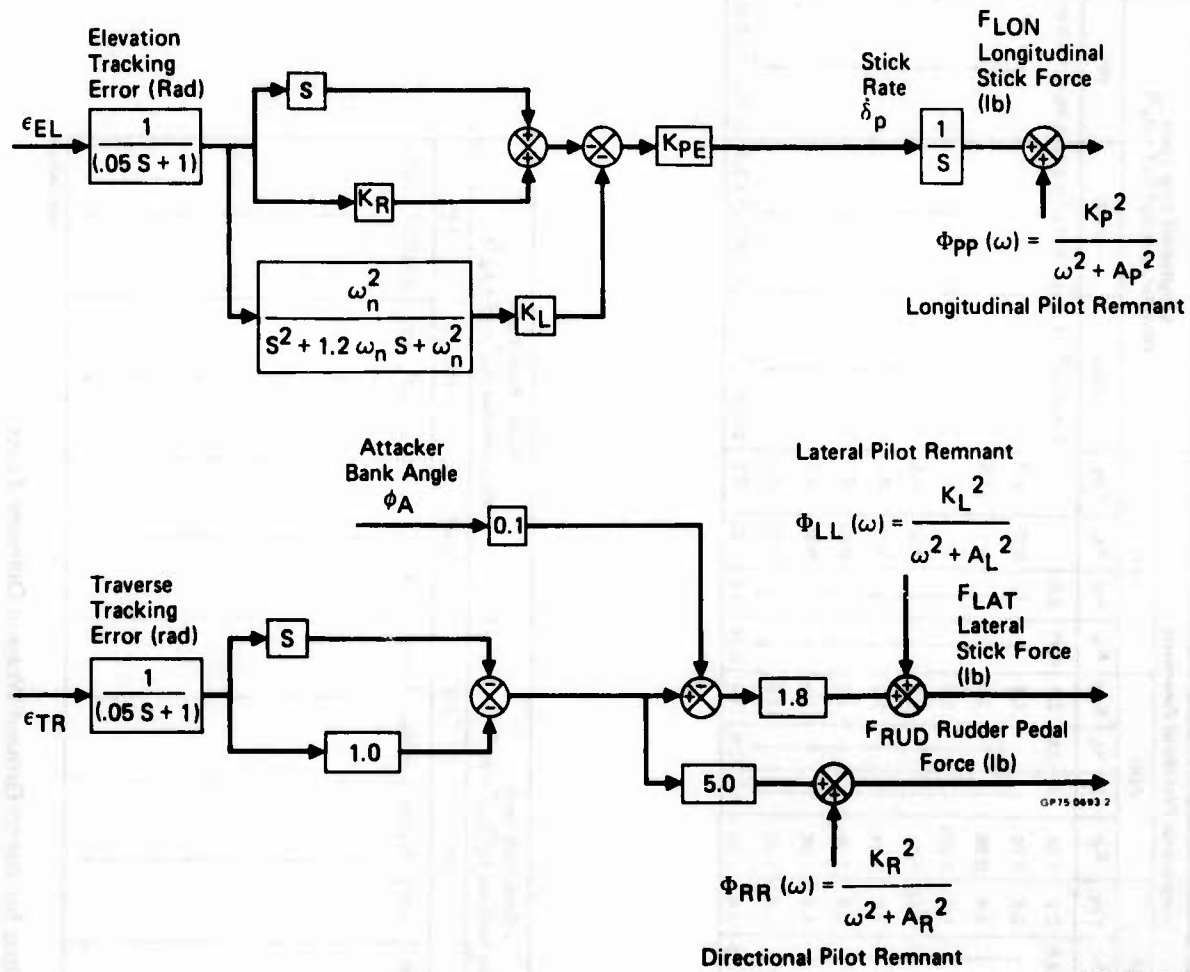


Figure 98. Linear Multi-Axis Pilot Model Structure for Air-to-Ground Weapon Delivery Tasks

Case	Longitudinal Flying Qualities Variations	Longitudinal Aircraft Characteristics			Longitudinal Pilot Model Parameters													
		F _z /G	ζ _{sp}	ω _{3p}	CCIP			FDR			FIP			Longitudinal Stick Force Pilot Remnant $K_R^2/(\omega^2 + A_p^2)$				
					K _R	ω _n	K _L	K _P E	K _R	ω _n	K _L	K _P E	K _R	ω _n	K _L	K _P E	CCIP	FDR
1*	Short-Period Frequency Variations	4 lb/G	0.7	3.6	0.99	1.0	2.5	2.2	1.24	1.0	2.5	2.0	0.75	0.5	-	0.402/(ω ² + 4.2)	0.135/(ω ² + 2.4)	0.75/(ω ² + 9.0)
2	↓	↑	↑	↑	0.90	4.5	1.15	2.4	1.15	2.5	2.5	2.5	2.5	0.60	-2.0	↑	↑	↑
3	↑	↓	↓	↓	0.71	6.4	0.96	3.8	0.96	3.5	3.5	3.5	3.5	1.1	-1.9	↑	↑	↑
4*	Short-Period Frequency Variations	4 lb/G	0.5	3.25	1.05	1.4	1.275	1.4	1.275	1.4	1.4	1.5	1.5	-	-	0.402/(ω ² + 4.2)	0.135/(ω ² + 2.4)	0.75/(ω ² + 9.0)
5	↓	↑	↑	↑	0.96	3.9	1.21	1.45	1.21	1.5	1.5	1.5	1.5	0.50	-1.5	↑	↑	↑
6	↑	↓	↓	↓	0.86	5.1	1.11	1.6	1.11	1.5	1.5	1.5	1.5	0.75	-2.1	↑	↑	↑
7	↑	↓	↓	↓	0.81	5.4	1.06	2.6	1.06	2.5	2.5	2.5	2.5	0.85	-3.2	↑	↑	↑
8	Stick Force per G Variations	2 lb/G	0.5	5.4	0.81	1.4	1.06	1.4	1.06	1.5	1.5	1.5	1.5	0.85	-5.2	↑	↑	↑
9	↓	↑	↑	↑	0.81	4 lb/G	↑	2.5	1.06	2.5	2.5	2.5	2.5	0.85	-3.2	↑	↑	↑
10	↑	↓	↓	↓	0.81	6 lb/G	0.5	5.4	0.81	1.0	2.5	3.0	1.06	1.0	1.0	0.402/(ω ² + 4.2)	0.135/(ω ² + 2.4)	0.75/(ω ² + 9.0)

* These longitudinal configurations were not evaluated for bombing tasks

Case	Lateral-Directional Flying Qualities Variations	Lateral Stick Force Pilot Remnant $K_L^2/(\omega^2 + A_L^2)$			Rudder Pedal Force Pilot Remnant $K_R^2/(\omega^2 + A_R^2)$		
		CCIP	FDR	FIP	CCIP	FDR	FIP
11	Dutch Roll Mode Damping Variations	3.0/(ω ² + 24.98)	1.49/(ω ² + 12.3)	0.86/(ω ² + 8.3)	1.54/(ω ² + 1.23)	2.3/(ω ² + 1.2)	0.64/(ω ² + 0.82)
12	↓	↑	↑	↑	↑	↑	↑
13	↑	↓	↓	↓	↓	↓	↓
14	↑	↓	↓	↓	↓	↓	↓
15	Proverse/Adverse Yaw Variations	↑	↓	↓	↓	↓	↓
16	↓	↑	↑	↑	↑	↑	↑
17	↑	↓	↓	↓	↓	↓	↓
18	Roll Rate Sensitivity Variations	↑	↓	↓	↓	↓	↓
19	↓	↑	↑	↑	↑	↑	↑
20	↑	↓	↓	↓	↓	↓	↓

0775-0004-110

Figure 99. Pilot Gain Variations for Air-to-Ground Weapon Delivery Tasks (Mach 0.7 at 5,000 Ft Altitude Flight Conditions)

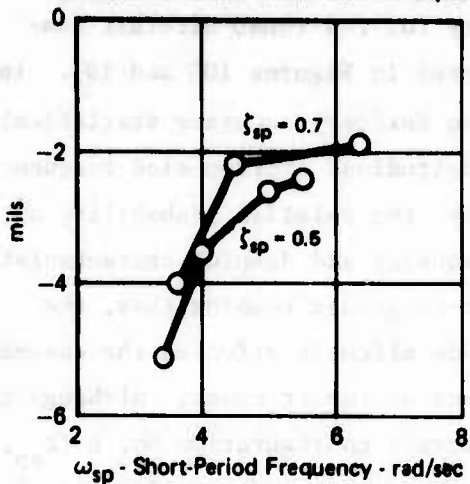
5.2.1 TAWDS Analyses of Longitudinal Flying Qualities for Air-to-Ground Weapon Delivery Tasks - The effects of longitudinal short-period frequency and damping variations on air-to-ground gunnery for F-4 TWeaD aircraft configured with FDR and CCIP gunsights are presented in Figures 100 and 101. In both these figures, the magnitude of all weapon delivery accuracy statistical error measures decreased as the aircraft's longitudinal short-period frequency and damping parameters increased. Consequently, the relative probability of kill increased as the longitudinal short-period frequency and damping characteristics increased. As shown in Figure 102 for the air-to-ground bombing task, the variations in the longitudinal short-period mode slightly affected the ensemble mean point of impact and the standard deviations of impact means. Although the relative kill probability is maximized for aircraft configuration No. 6 (ζ_{sp} , $\omega_{sp} = .5, 5.1$ rad/sec) the weapon delivery of the other configurations is almost as effective.

For the Mach 0.7 flight condition the effects of varying the F-4 TWeaD aircraft's longitudinal stick force per g parameter on the air-to-ground weapon delivery impact errors and weapon system effectiveness are shown in Figures 103 through 105. For the air-to-ground gunnery FDR and CCIP configurations, the relative kill probability was maximized for the 4 lb/g configuration. For these variations the importance of using one scalar measure such as probability of kill is demonstrated because all the weapon delivery accuracy measures do not continually decrease or increase in unison as stick force per g is increased. For the air-to-ground bombing task the relative probability of kill and weapon delivery accuracy were significantly improved as the stick force per g was increased to 6 lb/g.

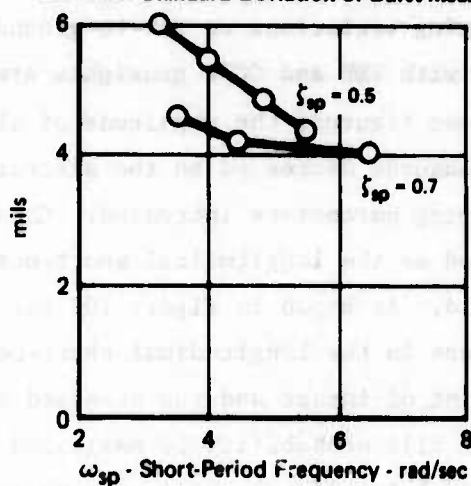
For both the FDR gunnery and FIP bombing weapon delivery modes the TWeaD aircraft's longitudinal stick force per g parameter was varied for a Mach 0.5 flight condition to demonstrate the effect of aircraft speed or range rate on weapon delivery accuracy and effectiveness. These TAWDS results show that the sensitivity of weapon delivery accuracy and effectiveness to flying qualities varies with respect to attack geometry encounters.

5.2.2 TAWDS Analyses of Lateral-Directional Flying Qualities for Air-to-Ground Weapon Delivery - The effects of the Dutch roll mode damping variations on weapon delivery accuracy and effectiveness for the F-4 TWeaD aircraft

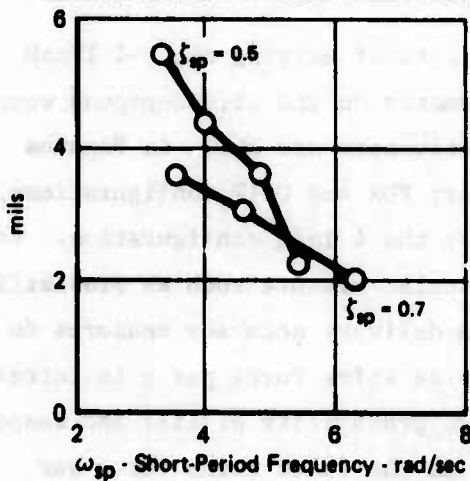
Elevation Ensemble Mean Point of Impact



Elevation Standard Deviation of Burst Means

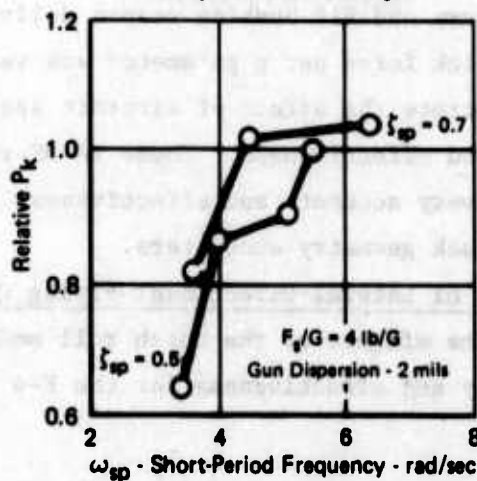


Elevation Standard Deviation of Burst Rounds



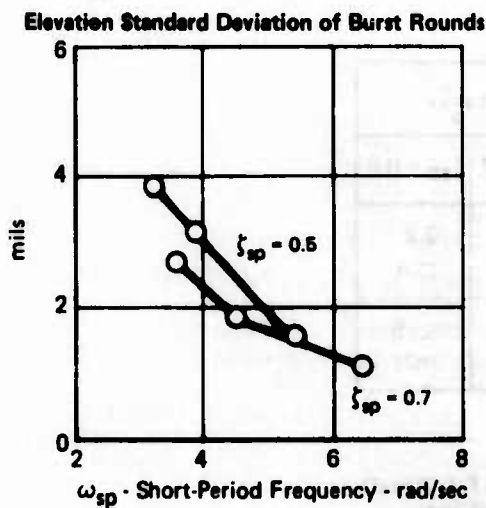
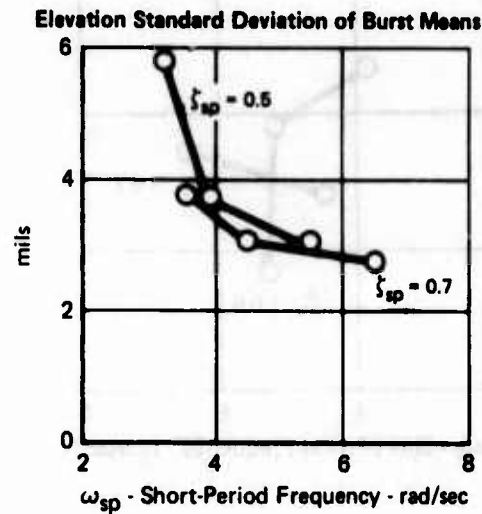
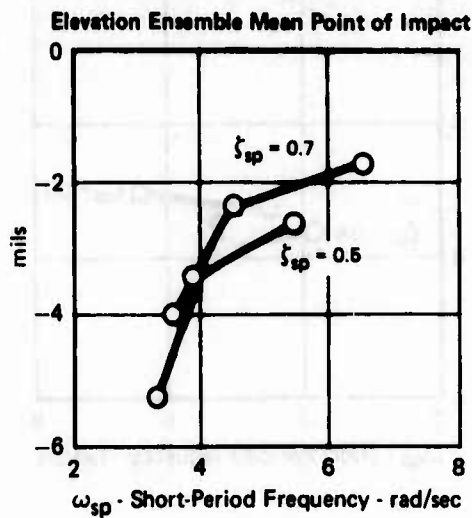
Transverse Impact Error Statistics		
	$\zeta_{sp} = 0.7$	$\zeta_{sp} = 0.5$
Ensemble Mean Point of Impact	2.08 mils	2.08 mils
Standard Deviation of Burst Means	7.70 mils	7.70 mils
Standard Deviation of Burst Rounds	3.67 mils	3.67 mils

Kill Probability Relative to F-4 TWaD Configured with FDR Sight

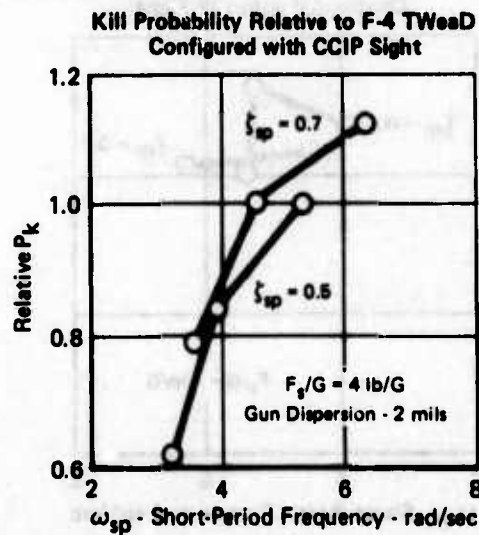


OP78-0004-248

Figure 100. Effects of Longitudinal Short-Period Frequency and Damping Variations on Air-to-Ground Gunnery Task for F-4 TWaD Aircraft Configured with FDR Sight (Mach 0.7, 30° Dive, 4800 Ft Firing Range)

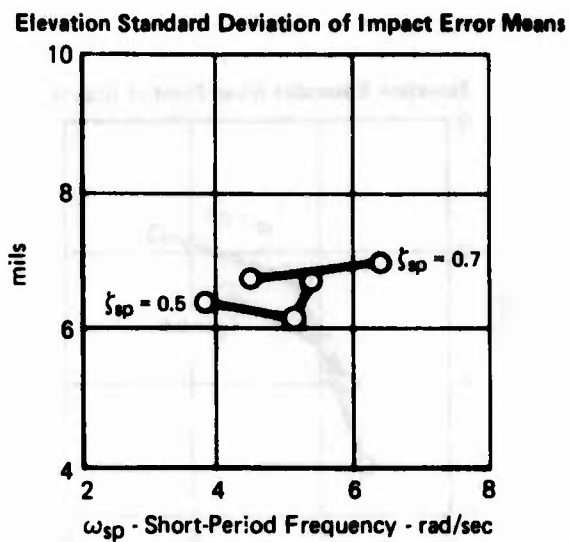
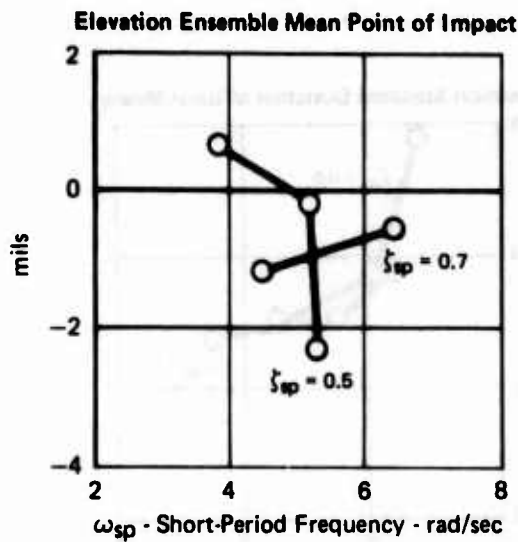


Traverse Impact Error Statistics		
	$\zeta_{sp} = 0.7$	$\zeta_{sp} = 0.5$
Ensemble Mean Point of Impact	2.21 mils	2.21 mils
Standard Deviation of Burst Means	6.14 mils	6.14 mils
Standard Deviation of Burst Rounds	3.19 mils	3.19 mils

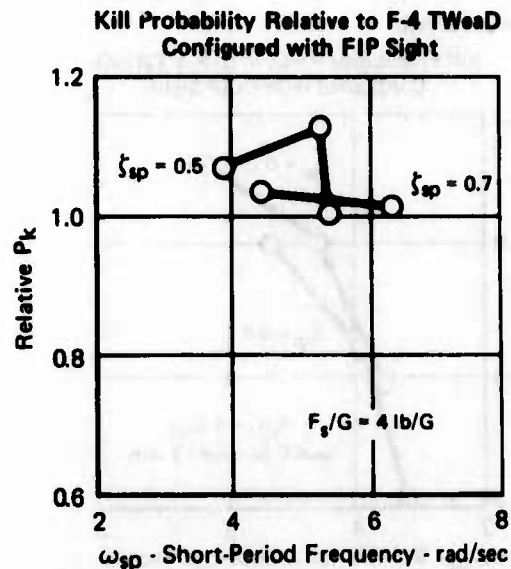


OP78-0004-240

Figure 101. Effects of Longitudinal Short-Period Frequency and Damping Variations on Air-to-Ground Gunnery Task for F-4 TWeaD Aircraft Configured with CCIP Sight (Mach 0.7, 30° Dive, 4800 Ft Firing Range)



Traverse Impact Error Statistics		
	$\zeta_{sp} = 0.7$	$\zeta_{sp} = 0.5$
Ensemble Mean Point of Impact	2.27 mils	2.27 mils
Standard Deviation of Impact Error Means	5.15 mils	5.15 mils



OP75-0864-248

Figure 102. Effects of Longitudinal Short-Period Frequency and Damping Variations on Air-to-Ground Bombing Task for F-4 TWaD Aircraft Configured with FIP Sight (Mach 0.7, 30° Dive, 5340 Ft Bomb Range)

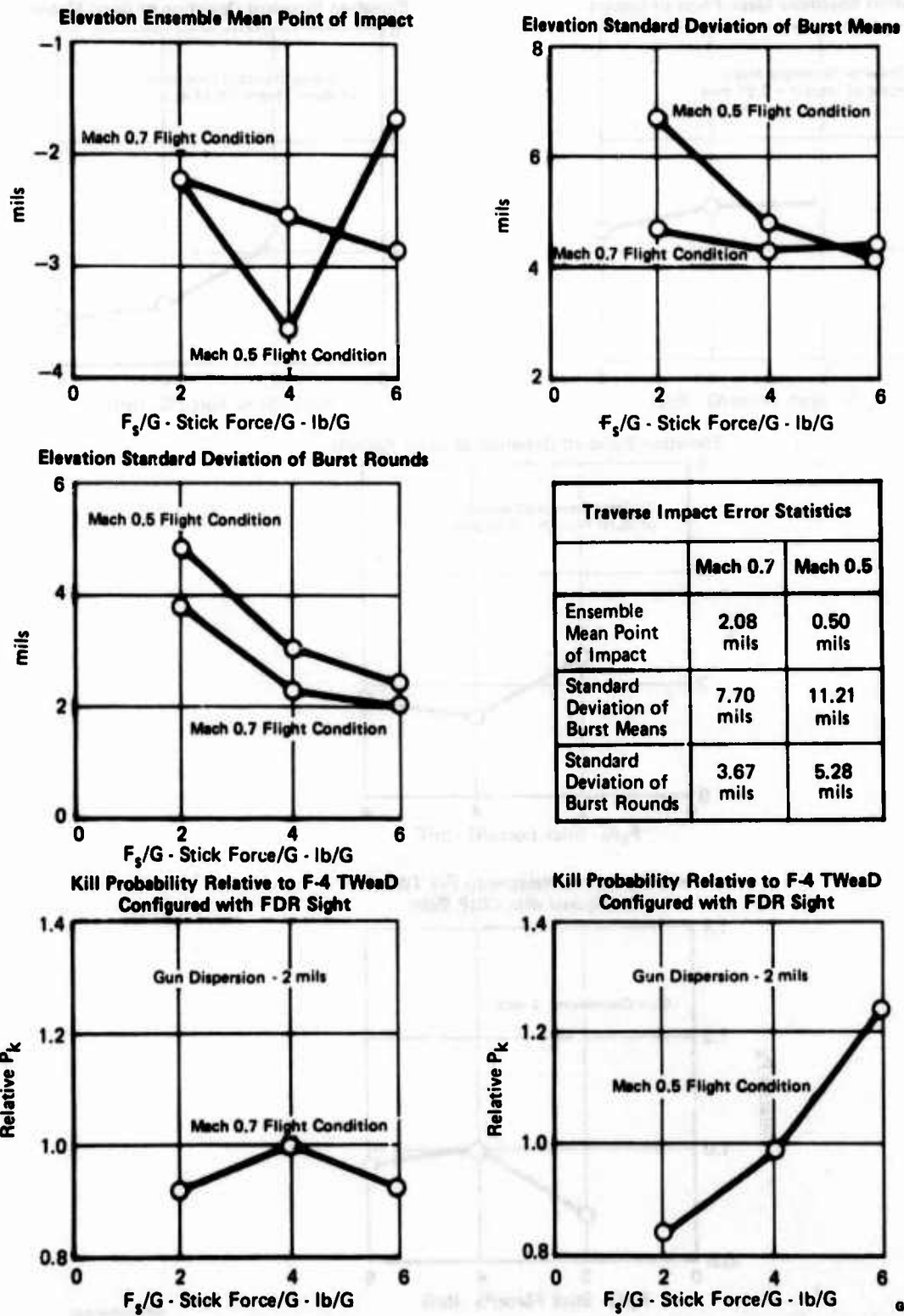


Figure 103. Effects of Longitudinal Stick Force Per G Variations on Air-to-Ground Gunnery Task for F-4 TWeaD Aircraft Configured with FDR Sight (30° Dive, 4800 Ft Firing Range)

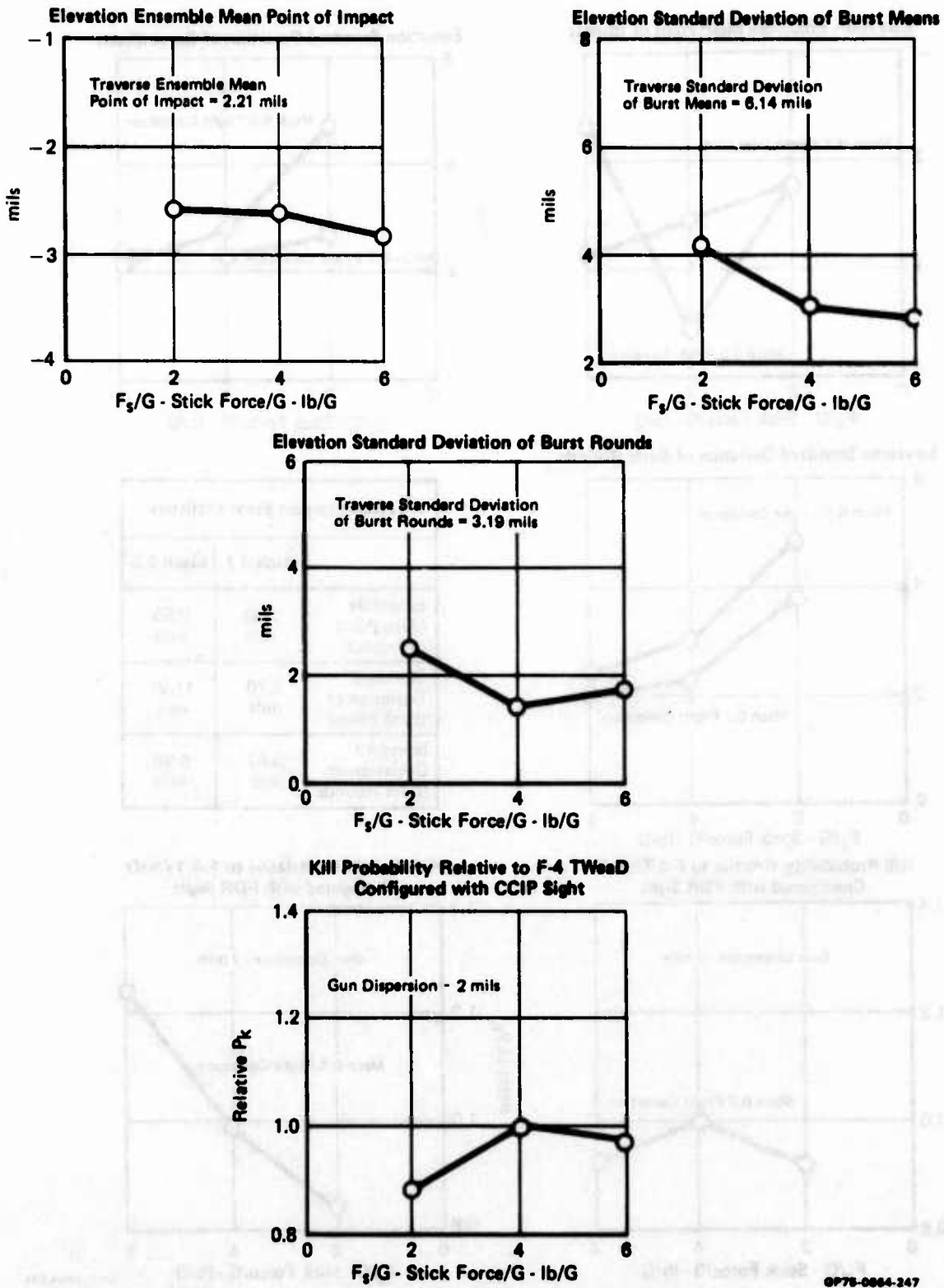
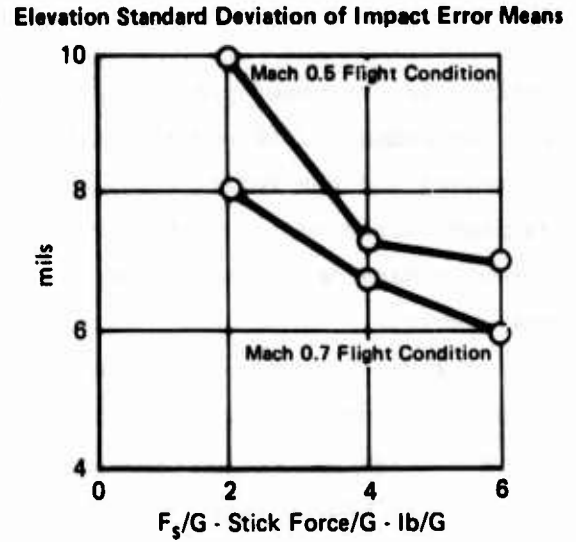
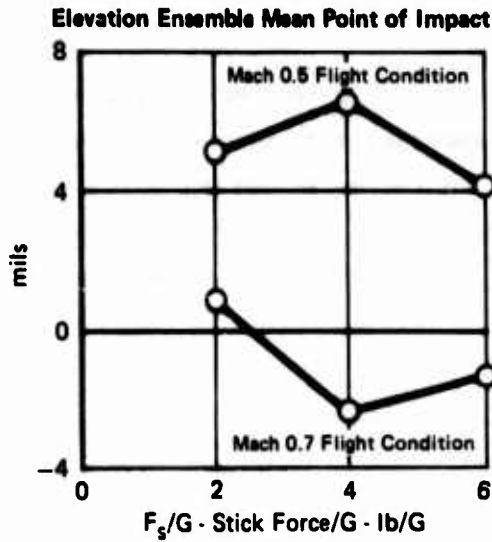
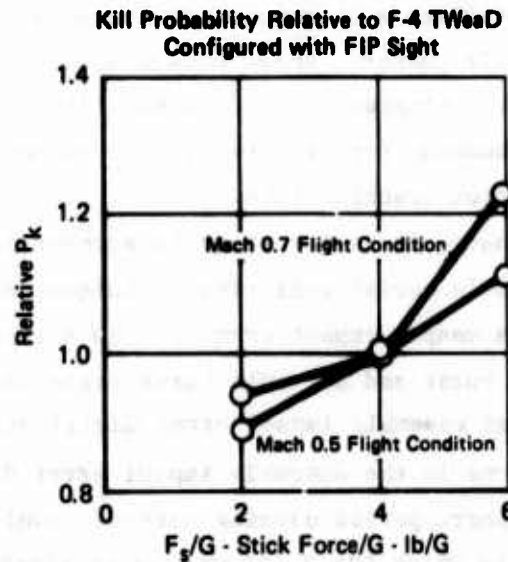


Figure 104. Effects of Longitudinal Stick Force Per G Variations on Air-to-Ground Gunnery Task for F-4 TWeaD Aircraft Configured with CCIP Sight (Mach 0.7, 30° Dive, 4800 Ft Firing Range)



Traverse Impact Error Statistics		
	Mach 0.7	Mach 0.5
Ensemble Mean Point of Impact	2.27 mils	1.6 mils
Standard Deviation of Impact Error Means	5.15 mils	5.75 mils



GP75-0884-250

Figure 105. Effects of Longitudinal Stick Force Per G Variations on Air-to-Ground Bombing Task for F-4 TWeaD Aircraft Configured with FIP Sight (30° Dive, 5340 Ft Bomb Range)

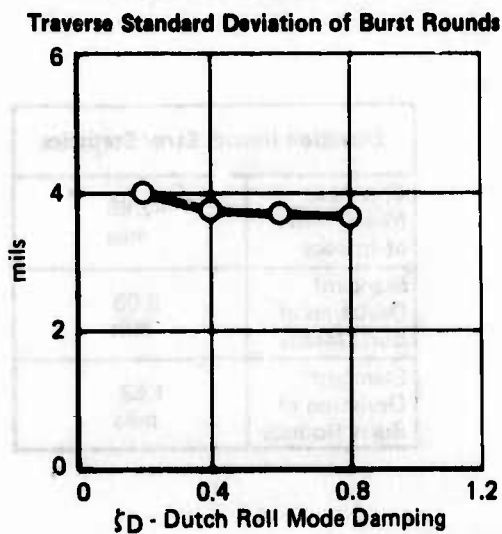
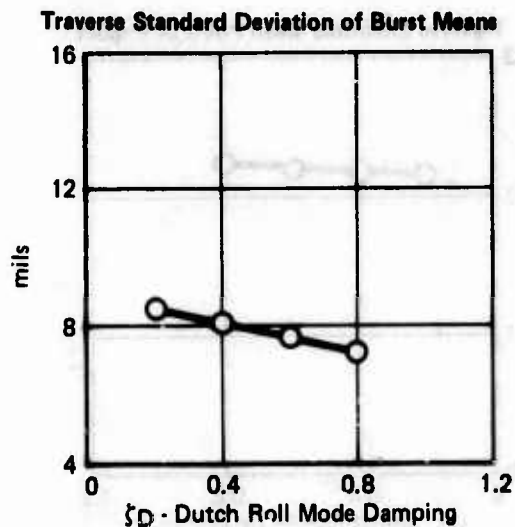
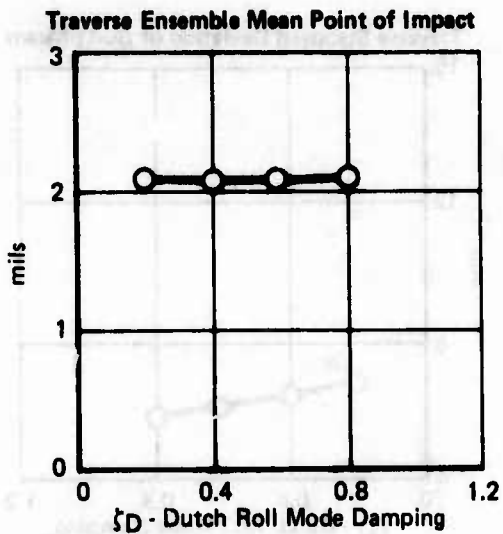
during air-to-ground gunnery and bombing are shown in Figures 106 through 108. For the gunnery CCIP and FDR sights, the weapon delivery accuracy measures decreased and the relative kill probability increased as the Dutch roll mode damping increased. For the FIP bombing mode the weapon delivery accuracy and effectiveness measures remained constant as the Dutch roll mode damping ratio was changed.

Figures 109 through 111 show the weapon delivery accuracy and effectiveness variations with respect to proverse/adverse yaw characteristics. For the air-to-ground FDR and CCIP gunnery modes, weapon delivery accuracy increased and weapon effectiveness improved as the aircraft's yaw characteristics due to lateral stick commands became more proverse. For air-to-ground FIP bombing, the effect of changes in proverse/adverse yaw on weapon delivery accuracy and effectiveness was insignificant.

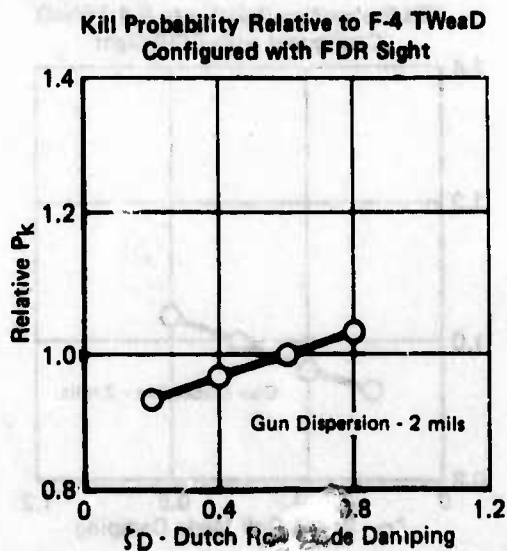
The effects of commanded roll rate sensitivity on FDR and CCIP gunnery modes and the FIP bombing mode are illustrated in Figures 112 through 114. The TAWDS analyses show that the kill probability measure decreased as the aircraft roll sluggishness increased for the air-to-ground gunnery modes. The air-to-ground bombing effectiveness was insensitive to the commanded roll rate time constant variations.

5.2.3 Multiple Burst Criteria for Air-to-Air Gunnery Tasks - In air-to-ground gunnery the pilot fires a long burst at close range prior to initiating "pull-ups". In air-to-air gunnery, short bursts with different lengths are fired whenever the pilot estimates a gun fire solution. Figure 115 illustrates this multiple burst phenomenon for five repetitive manned simulations of an air-to-air gunnery Director tracking task.

For air-to-air gunnery, it is important to account for multiple burst because this is the pilot's aerial gunfiring technique and this multiple burst firing technique affects weapon impact errors. The difference in weapon delivery accuracy between single burst and multiple burst criteria is demonstrated by comparing their resultant ensemble impact error distributions. Figure 116 illustrates the variations in the ensemble impact error distributions for different longitudinal short-period damping aircraft configurations performing an LCOSS gunnery task, in which the pilot was constrained to fire a single one-second burst. Figure 117 also illustrates variations in ensemble impact error distributions for the same piloted aircraft configurations performing the same LCOSS gunnery tasks, in which the pilot was firing multiple burst, based upon his

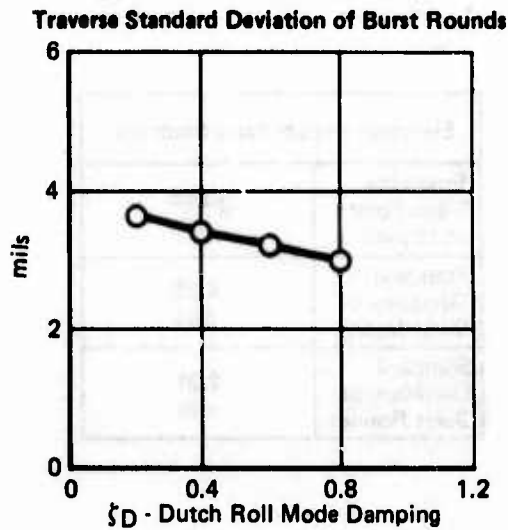
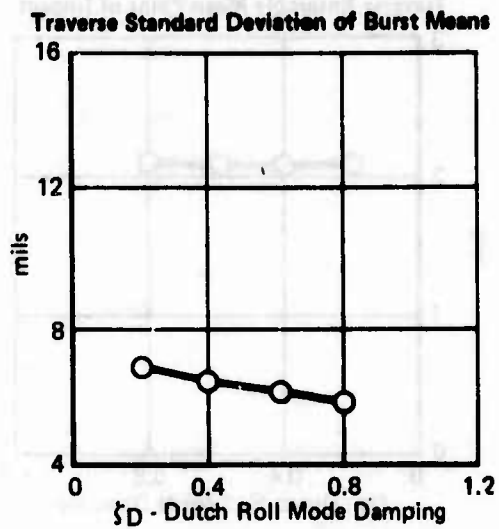
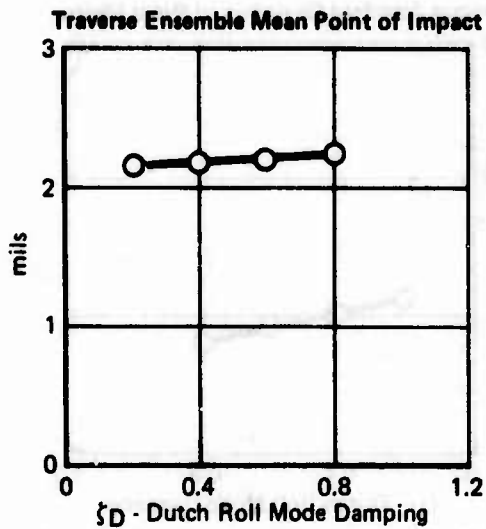


Elevation Impact Error Statistics	
Ensemble Mean Point of Impact	-2.56 mils
Standard Deviation of Burst Means	4.25 mils
Standard Deviation of Burst Rounds	2.21 mils

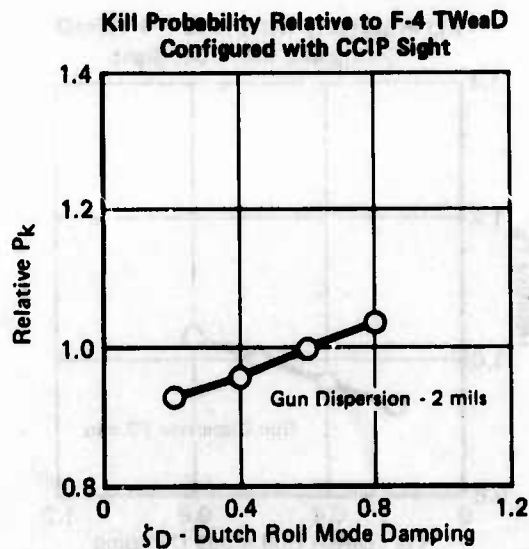


GP75-0864-239

Figure 106. Effects of Dutch Roll Mode Damping Variations on Air-to-Ground Gunnery Task for F-4 TWeaD Aircraft Configured with FDR Sight (Mach 0.7, 30° Dive, 4800 Ft Firing Range)

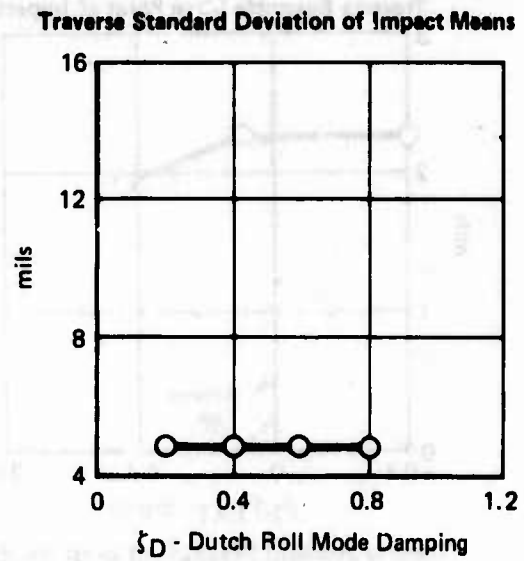
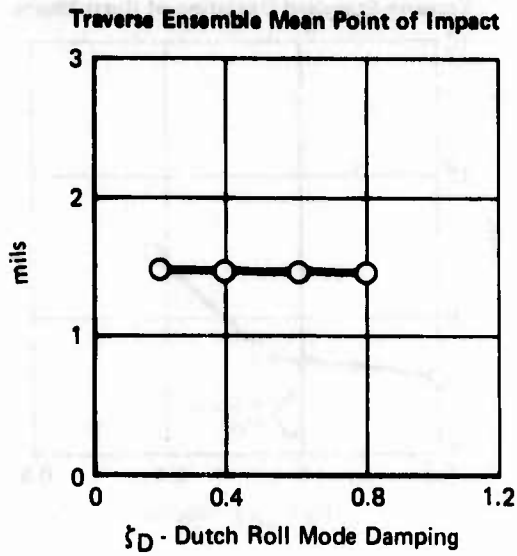


Elevation Impact Error Statistics	
Ensemble Mean Point of Impact	-2.85 mils
Standard Deviation of Burst Means	3.03 mils
Standard Deviation of Burst Rounds	1.58 mils

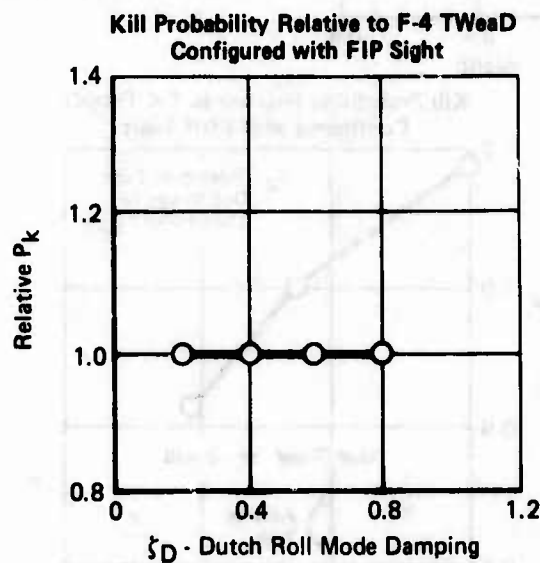


GP78-0884-243

Figure 107. Effects of Dutch Roll Mode Damping Variations on Air-to-Ground Gunnery Task for F-4 TWeaD Aircraft Configured with CCIP Sight (Mach 0.7, 30° Dive, 4800 Ft Firing Range)

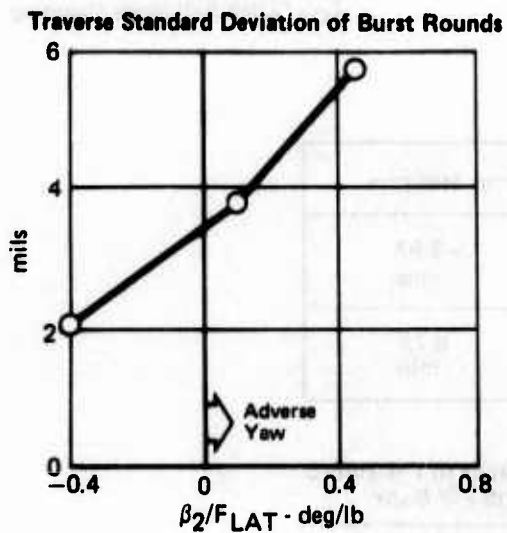
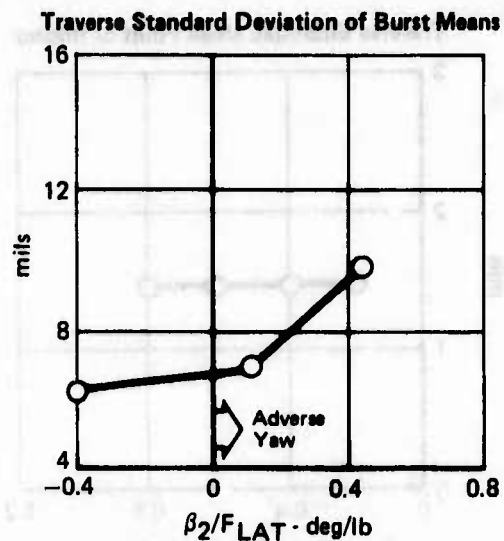
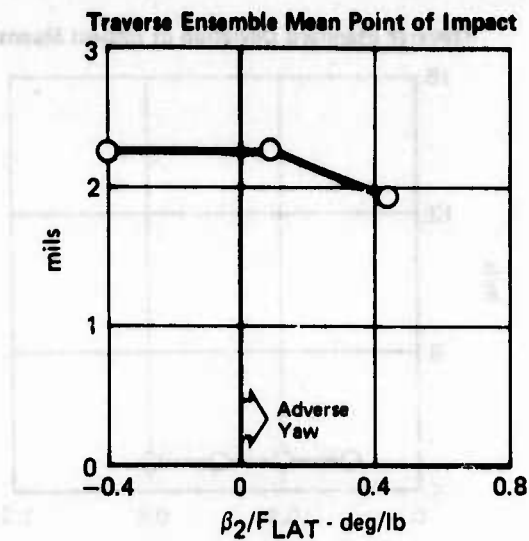


Elevation Impact Error Statistics	
Ensemble Mean Point of Impact	-2.97 mils
Standard Deviation of Impact Error Means	6.73 mils

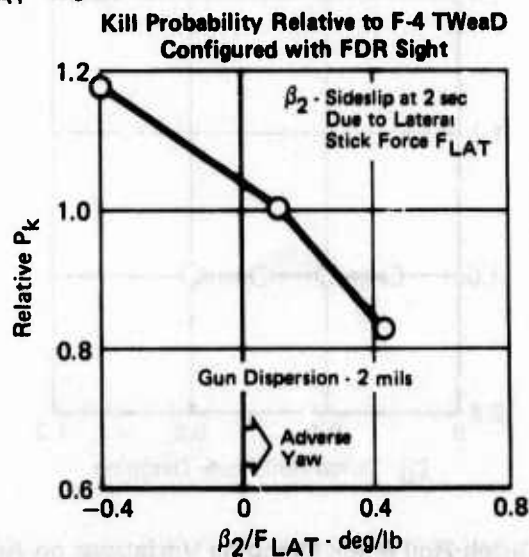


075-0864-236

Figure 108. Effects of Dutch Roll Mode Damping Variations on Air-to-Ground Bombing Task for F-4 TWaD Aircraft Configured with FIP Sight (Mach 0.7, 30° Dive, 5340 Ft Bomb Range)



Elevation Impact Error Statistics	
Ensemble Mean Point of Impact	-2.56 mils
Standard Deviation of Burst Means	4.25 mils
Standard Deviation of Burst Rounds	2.21 mils



GP78-0864-240

Figure 109. Effects of Proverse/Adverse Yaw Variations on Air-to-Ground Gunnery Task for F-4 TWaD Aircraft Configured with FDR Sight (Mach 0.7, 30° Dive, 4800 Ft Firing Range)

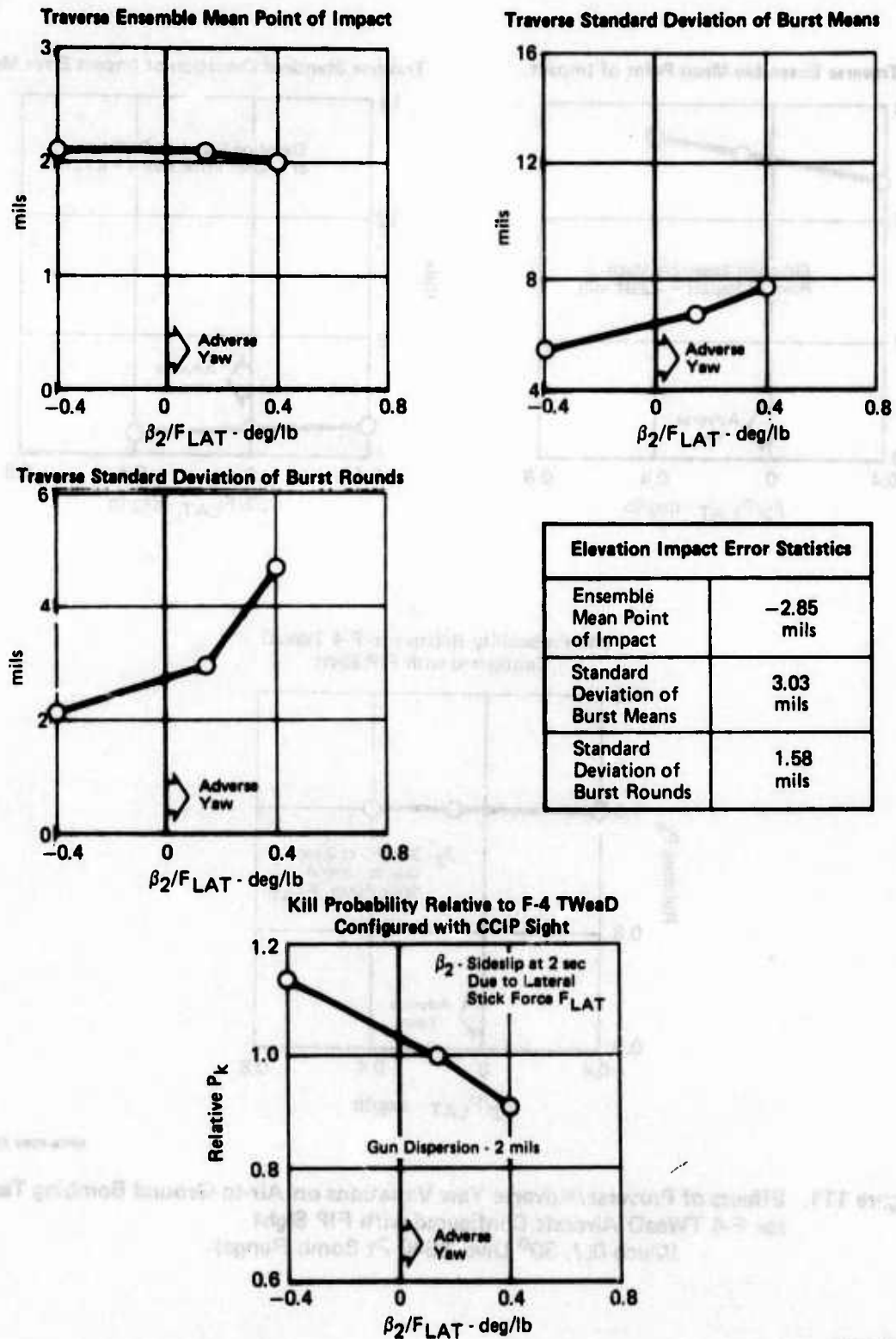
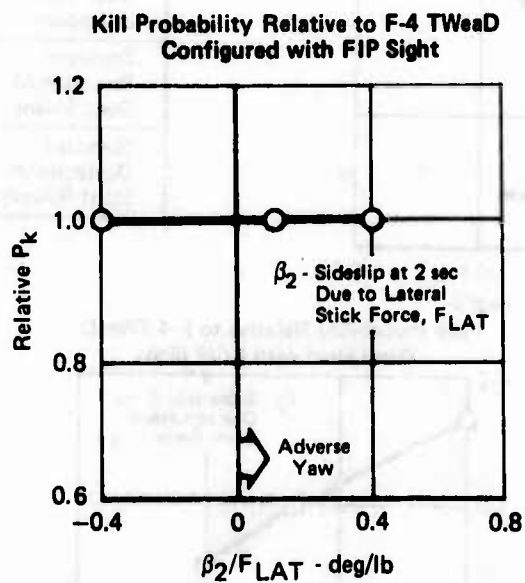
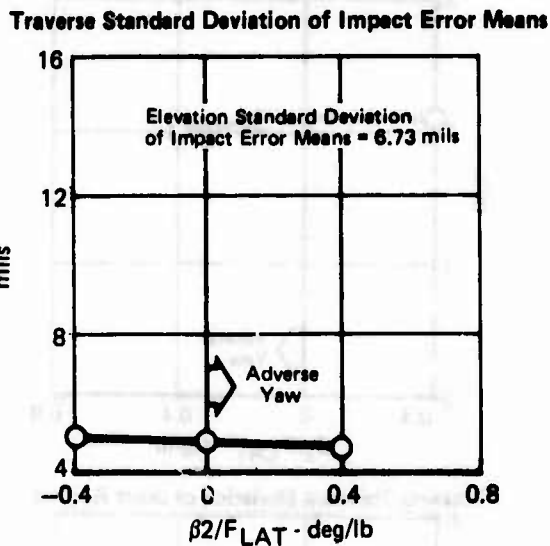
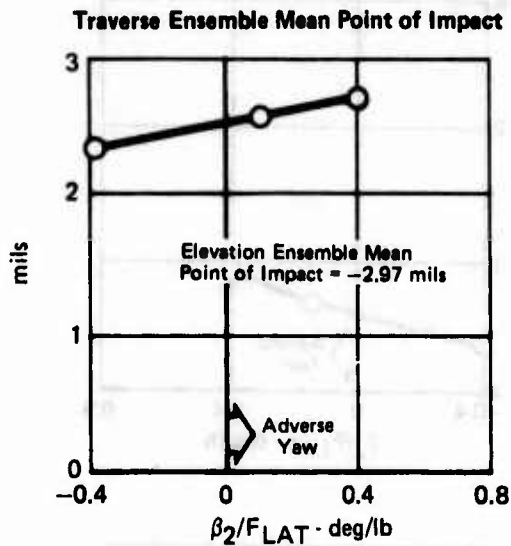
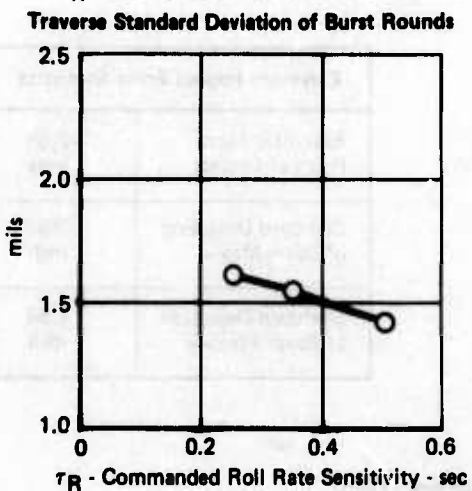
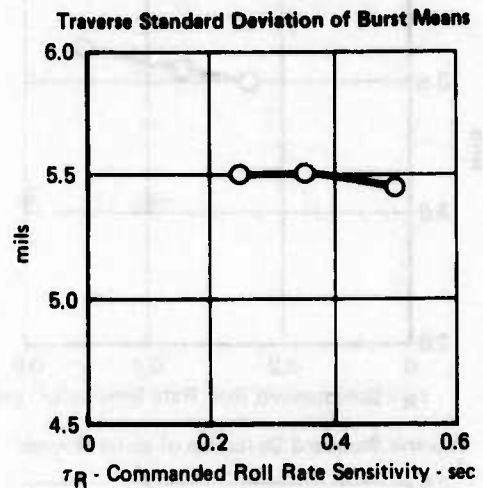
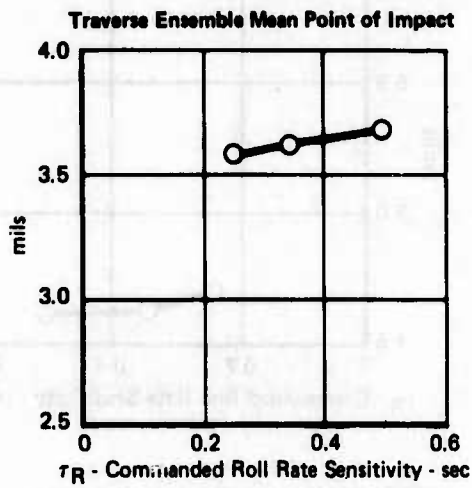


Figure 110. Effects of Proverse/Adverse Yaw Variations on Air-to-Ground Gunnery Task for F-4 TWeaD Aircraft Configured With CCIP Sight (Mach 0.7, 30° Dive, 4800 Ft Firing Range)

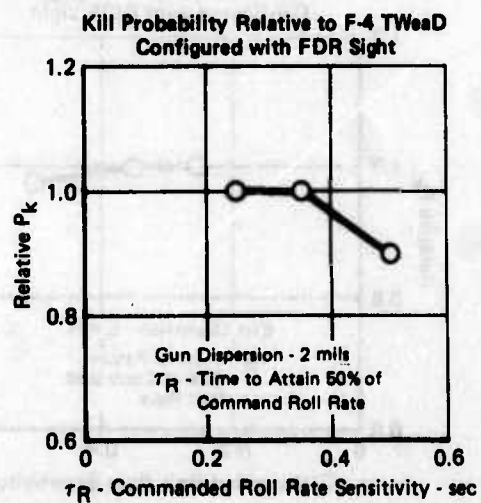


GP76-0864-237

Figure 111. Effects of Proverse/Adverse Yaw Variations on Air-to-Ground Bombing Task for F-4 TWeaD Aircraft Configured with FIP Sight (Mach 0.7, 30° Dive, 5340 Ft Bomb Range)

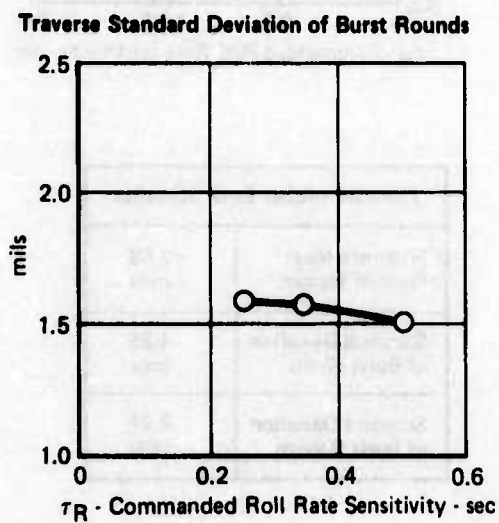
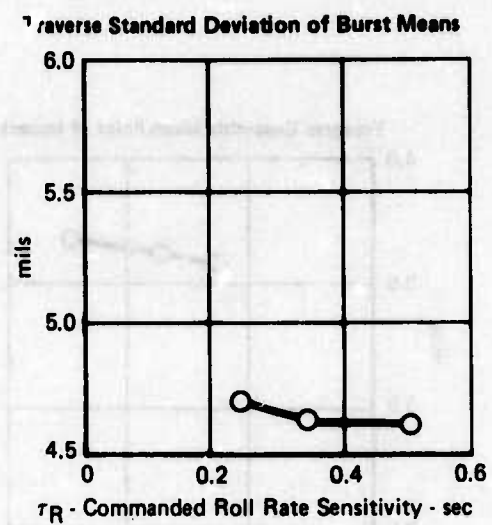
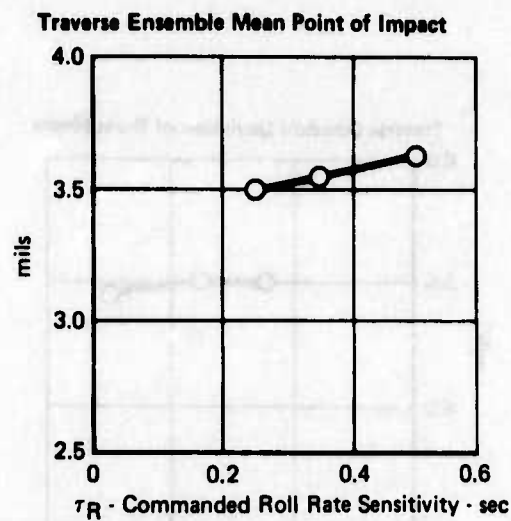


Elevation Impact Error Statistics	
Ensemble Mean Point of Impact	-2.56 mils
Standard Deviation of Burst Means	4.25 mils
Standard Deviation of Burst Rounds	2.21 mils

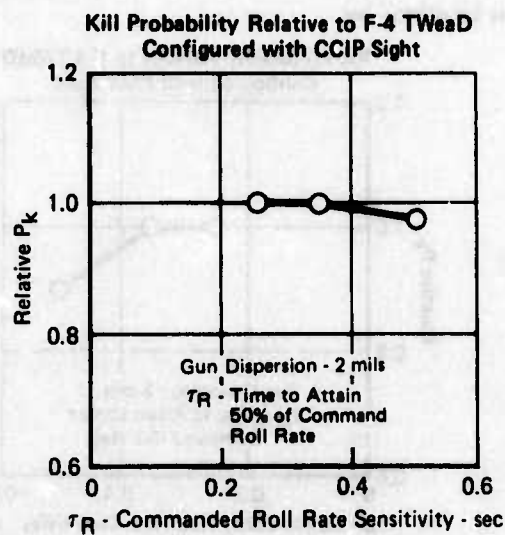


GP76-0864-241

Figure 112. Effects of Commanded Roll Rate Sensitivity Variations on Air-to-Ground Gunnery Task for F-4 TWeaD Aircraft Configured with FDR Sight (Mach 0.7, 30° Dive, 4800 Ft Firing Range)

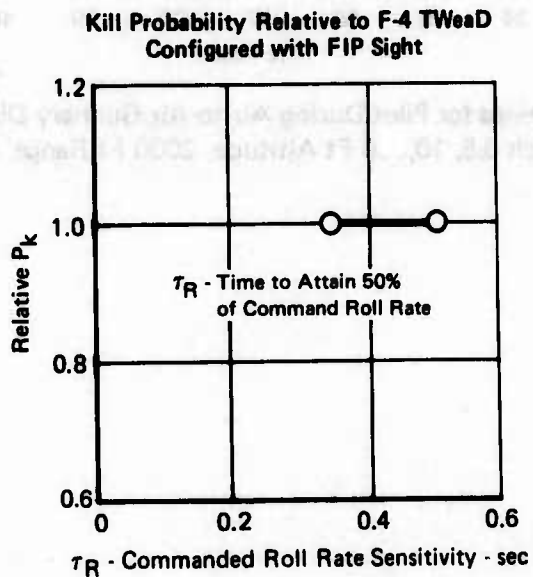
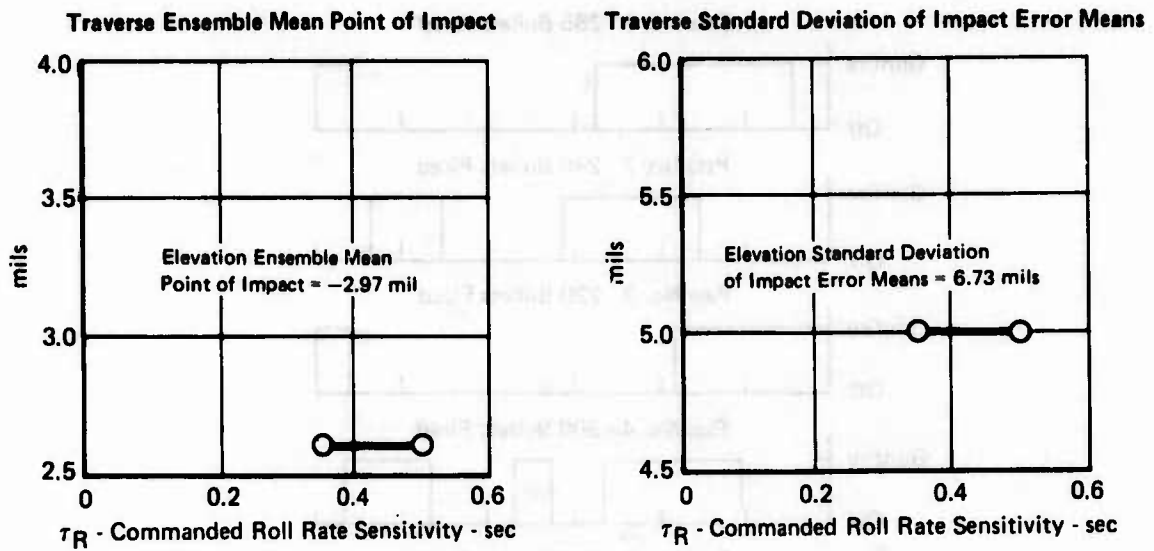


Elevation Impact Error Statistics	
Ensemble Mean Point of Impact	-2.85 mils
Standard Deviation of Burst Means	3.03 mils
Standard Deviation of Burst Rounds	1.58 mils



GP78-0864-244

Figure 113. Effects of Commanded Roll Rate Sensitivity Variations on Air-to-Ground Gunnery Task for F-4 TWeaD Aircraft Configured with CCIP Sight (Mach 0.7, 30° Dive, 4800 Ft Firing Range)



GP76-0864-238

Figure 114. Effects of Commanded Roll Rate Sensitivity Variations on Air-to-Ground Bombing Task for F-4 TWaD Aircraft Configured with FIP Sight (Mach 0.7, 30° Dive, 5340 Ft Bombing Range)

Human Pilot - Manned Simulation

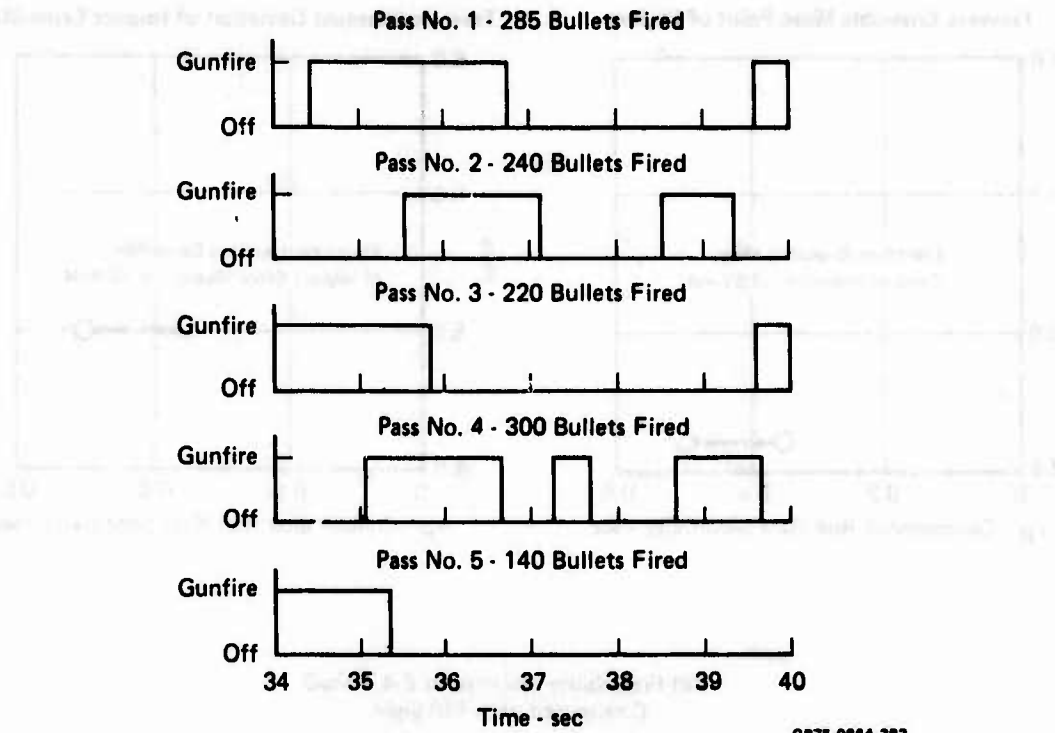
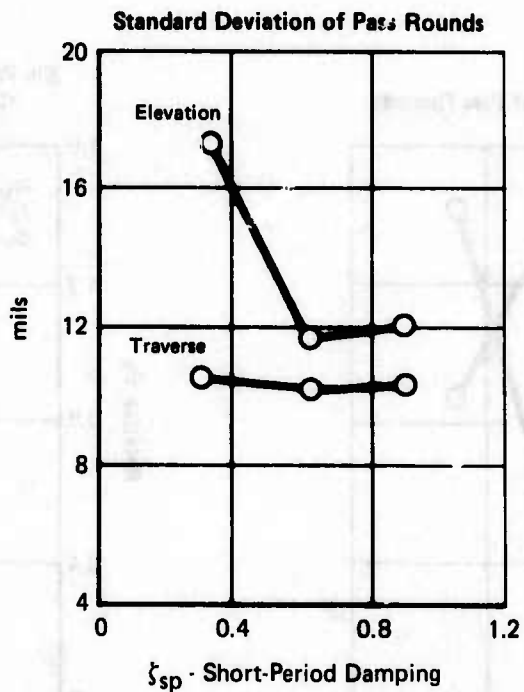
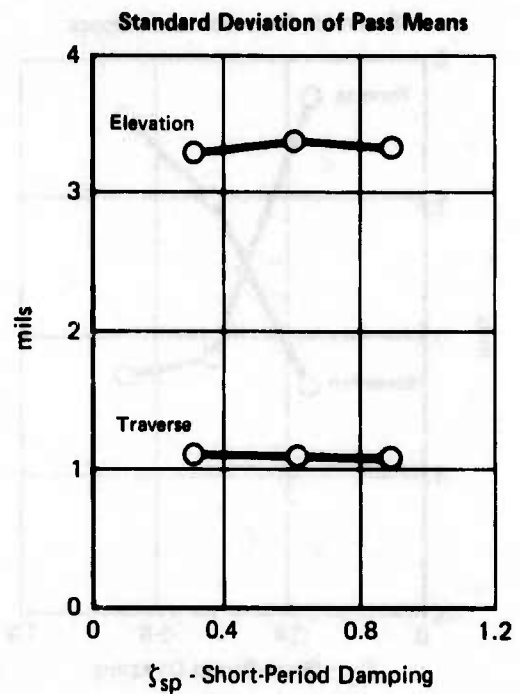
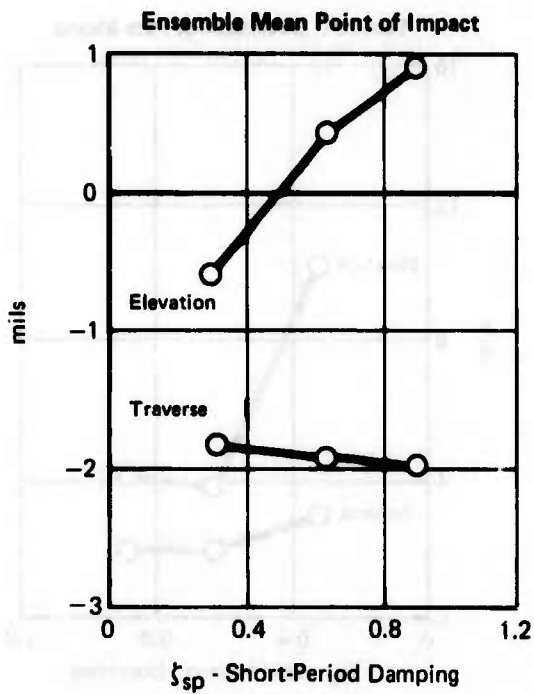
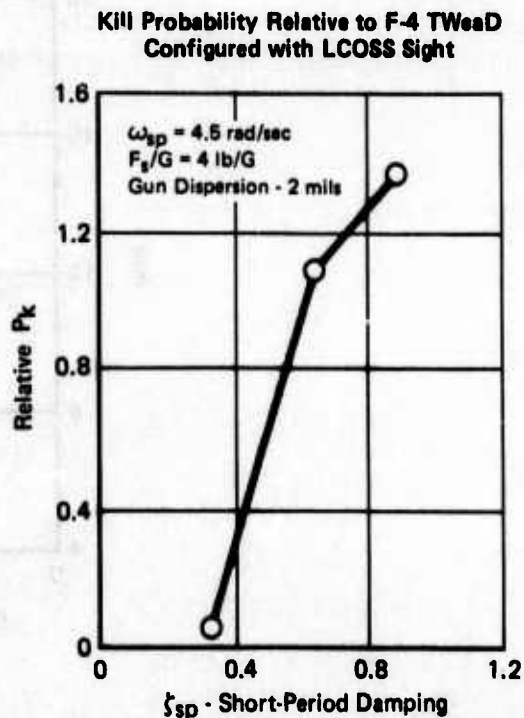
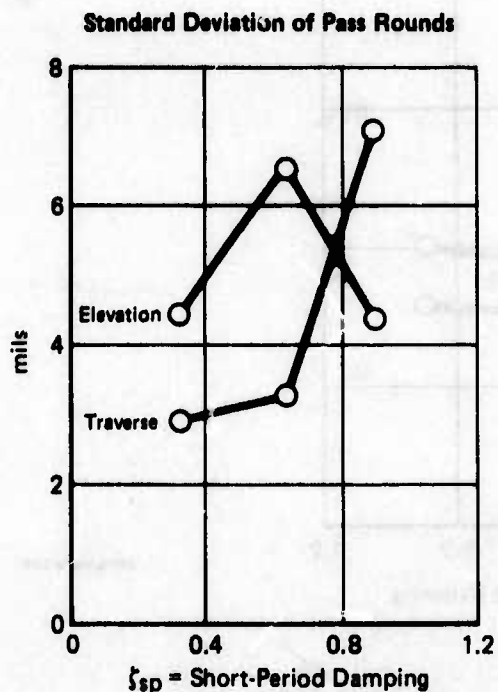
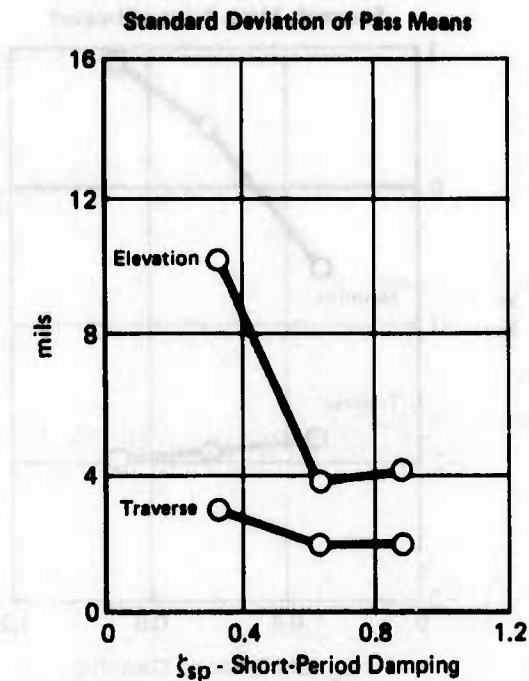
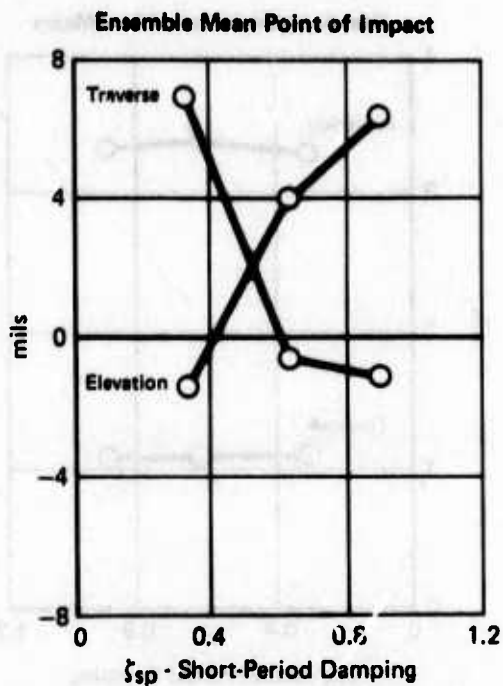


Figure 115. Gunfire Durations for Pilot During Air-to-Air Gunnery Director Tracking Task (F-4 Aircraft, Mach 0.8, 10,000 Ft Altitude, 2000 Ft Range, 4 G Target)



GP75-0884-264

Figure 116. Weapon Delivery Accuracy Statistics
 Longitudinal Short-Period Damping Variations, Short-Period Frequency = 4.5 Rad/Sec
 F-4 Aircraft, Mach 0.8 at 10,000 Ft Altitude, 2,000 Ft Range, LCOSS Sight
 4 G Target, Fixed Firing Interval Specified



OP78-0884-254

Figure 117. Effects of Longitudinal Short-Period Damping Variations on Air-to-Air Gunnery Task for F-4 TWeaD Aircraft Configured with LCOSS Sight (Mach 0.8 at 10,000 Ft Altitude, 4 G Target, 2000 Ft Range)

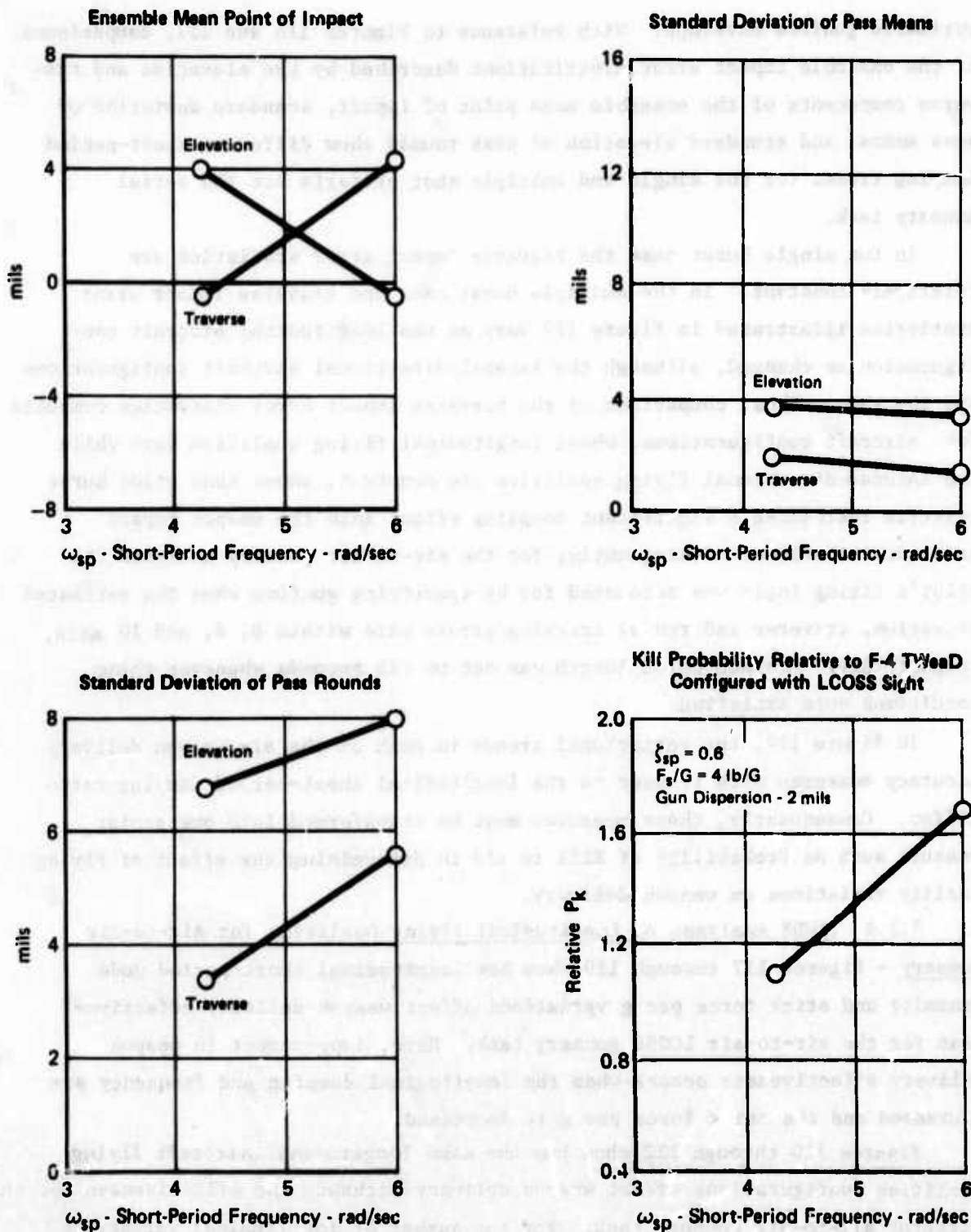
estimated gunfire envelope. With reference to Figures 116 and 117, comparisons of the ensemble impact error distributions described by the elevation and traverse components of the ensemble mean point of impact, standard deviation of pass means, and standard elevation of pass rounds show different short-period damping trends for the single and multiple shot criteria for the aerial gunnery task.

In the single burst case the traverse impact error statistics are relatively constant. In the multiple burst case the traverse impact error statistics illustrated in Figure 117 vary as the longitudinal aircraft configuration is changed, although the lateral-directional aircraft configurations are the same. Thus, comparison of the traverse impact error statistics computed for aircraft configurations, whose longitudinal flying qualities vary while the lateral-directional flying qualities are constant, shows that pilot burst criteria introduces a significant coupling effect into the weapon impact error distributions. Consequently, for the air-to-air gunnery analyses the pilot's firing logic was accounted for by specifying gunfire when the estimated elevation, traverse and radial tracking errors were within 8, 6, and 10 mils, respectively. Minimum burst length was set to .25 seconds whenever these conditions were satisfied.

In Figure 117, the variational trends in each of the six weapon delivery accuracy measures with respect to the longitudinal short-period damping ratio differ. Consequently, these measures must be transformed into one scalar measure such as Probability of Kill to aid in determining the effect of flying quality variations on weapon delivery.

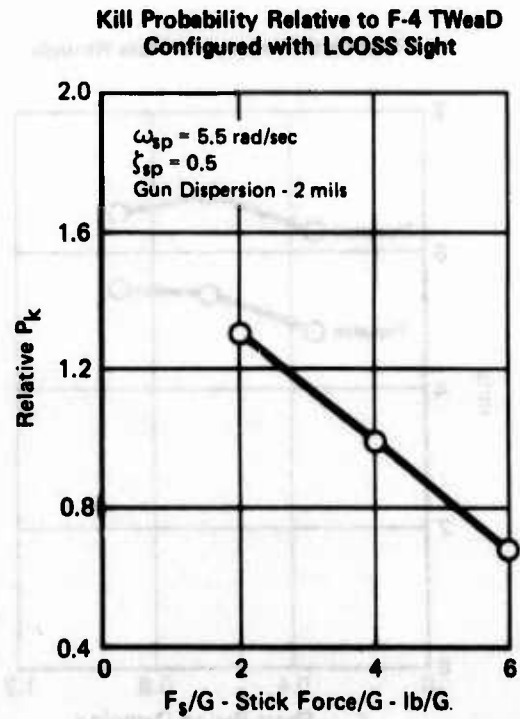
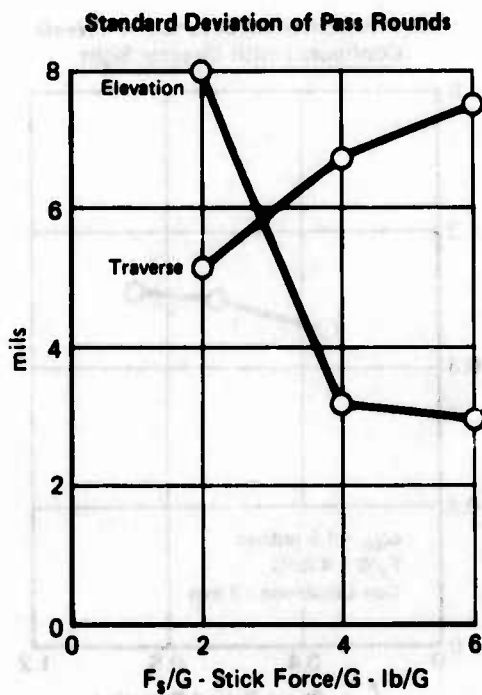
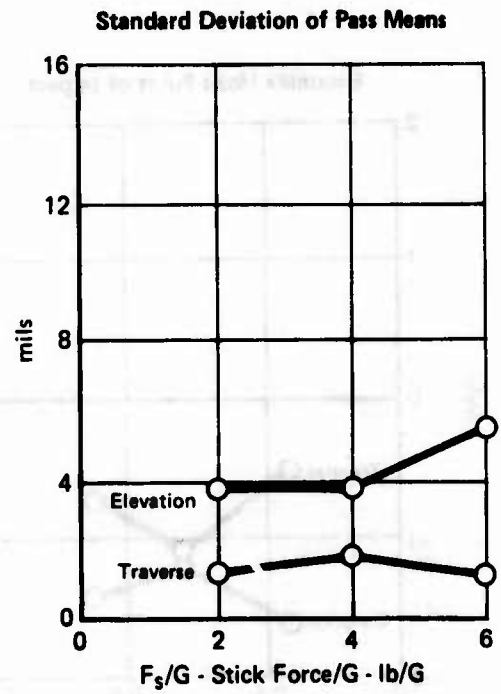
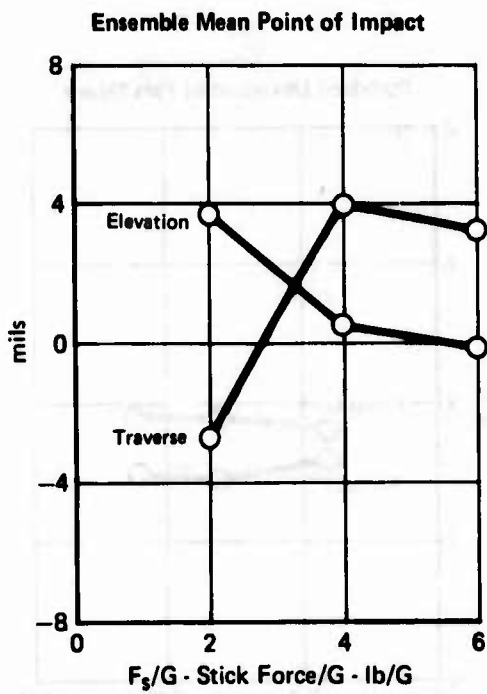
5.2.4 TAWDS Analyses of Longitudinal Flying Qualities for Air-to-Air Gunnery - Figures 117 through 119 show how longitudinal short-period mode dynamics and stick force per g variations affect weapon delivery effectiveness for the air-to-air LCOSS gunnery task. Here, improvement in weapon delivery effectiveness occurs when the longitudinal damping and frequency are increased and the stick force per g is decreased.

Figures 120 through 122 show how the same longitudinal aircraft flying qualities configurations affect weapon delivery accuracy and effectiveness for the Director air-to-air gunnery task. For the number of longitudinal variations considered, improved weapon delivery effectiveness results when short-period damping is increased and the stick force per g is 4 lb/g. Weapon delivery effectiveness slightly decreased as the longitudinal short-period frequency was increased.



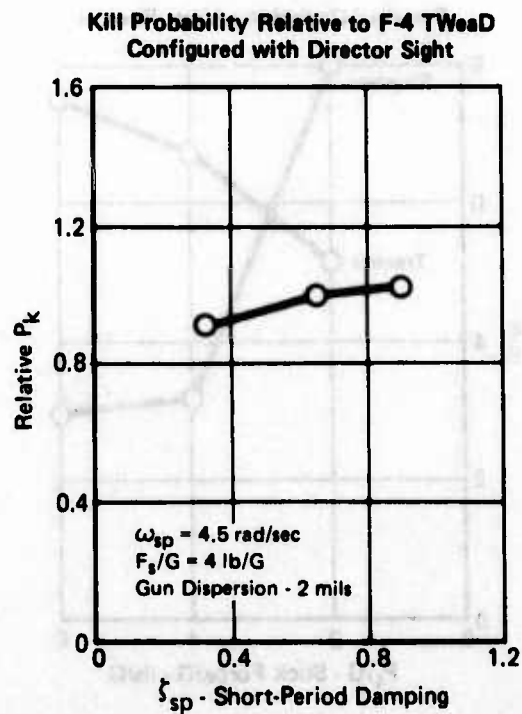
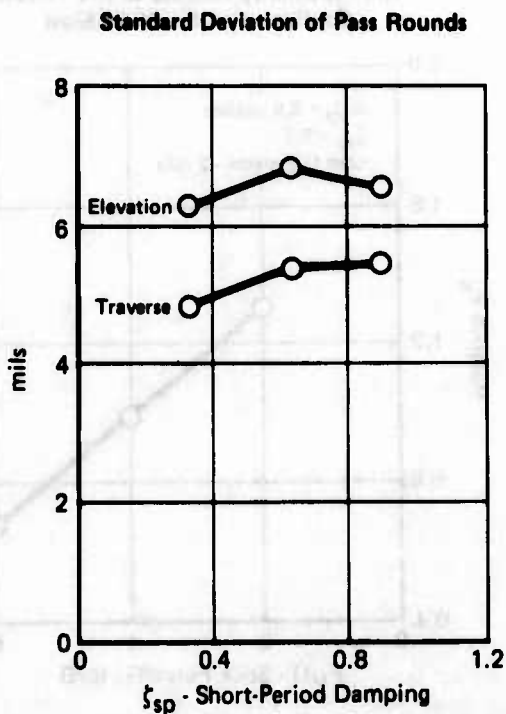
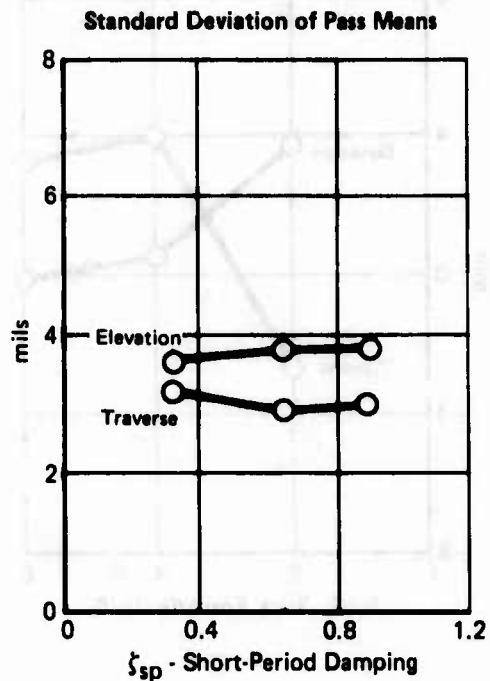
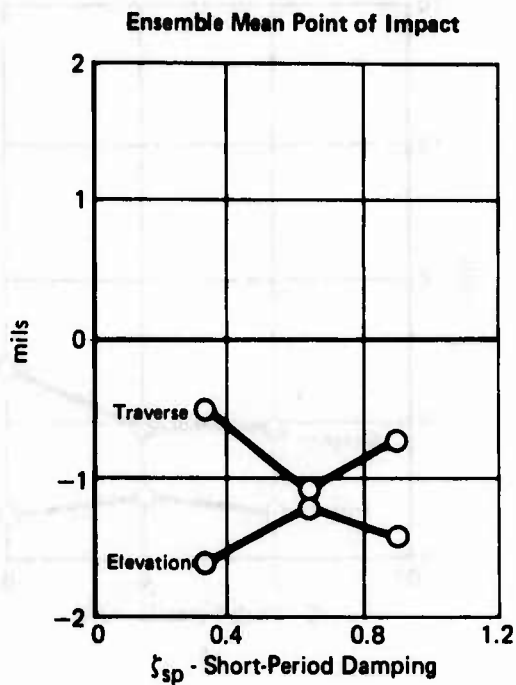
GP78-0884-253

Figure 118. Effects of Longitudinal Short-Period Frequency Variations on Air-to-Air Gunnery Task for F-4 TWeaD Aircraft Configured with LCOSS Sight (Mach 0.8 at 10,000 Ft Altitude, 4 G Target, 2000 Ft Range)



OP75-0004-262

Figure 119. Effects of Longitudinal Stick Force per G Variations on Air-to-Air Gunnery Task for F-4 TWeaD Aircraft Configured with LCOSS Sight (Mach 0.8 at 10,000 Ft Altitude, 4 G Target, 2000 Ft Range)



GP75-0004-265

Figure 120. Effects of Longitudinal Short-Period Damping Variations on Air-to-Air Gunnery Task for F-4 TWeaD Aircraft Configured with Director Sight (Mach 0.8 at 10,000 Ft Altitude, 4 G Target, 2000 Ft Range)

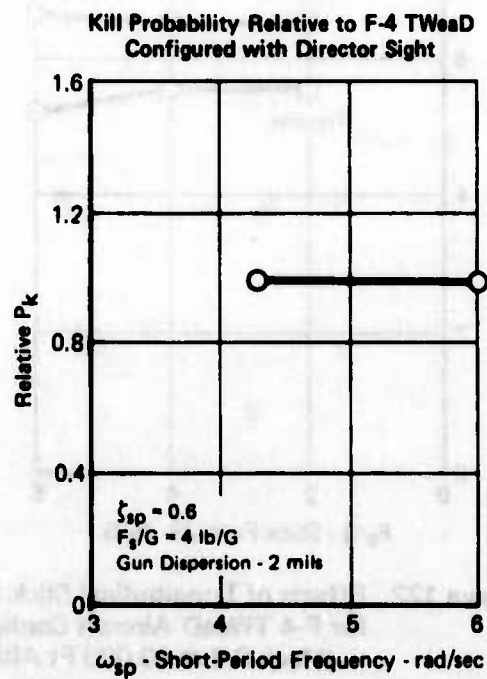
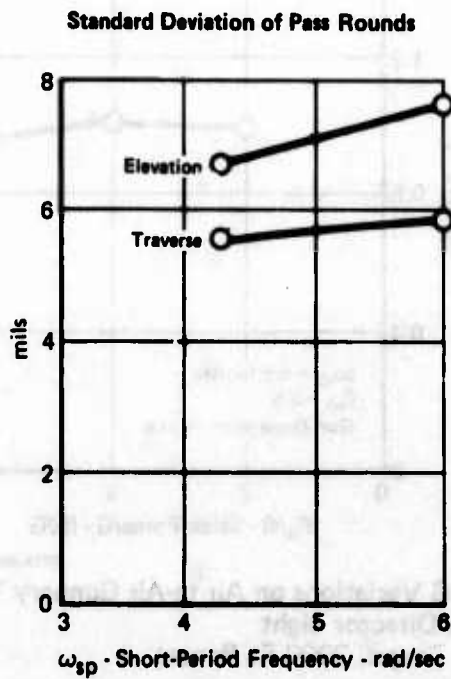
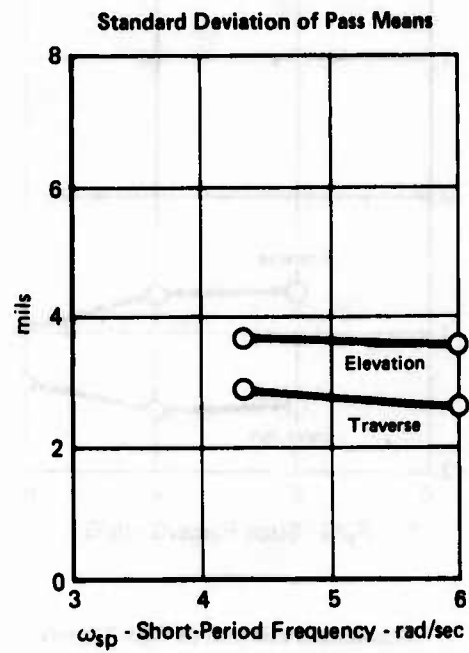
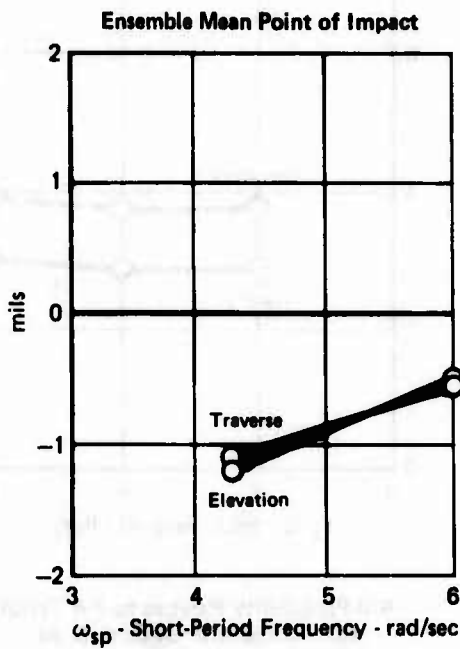
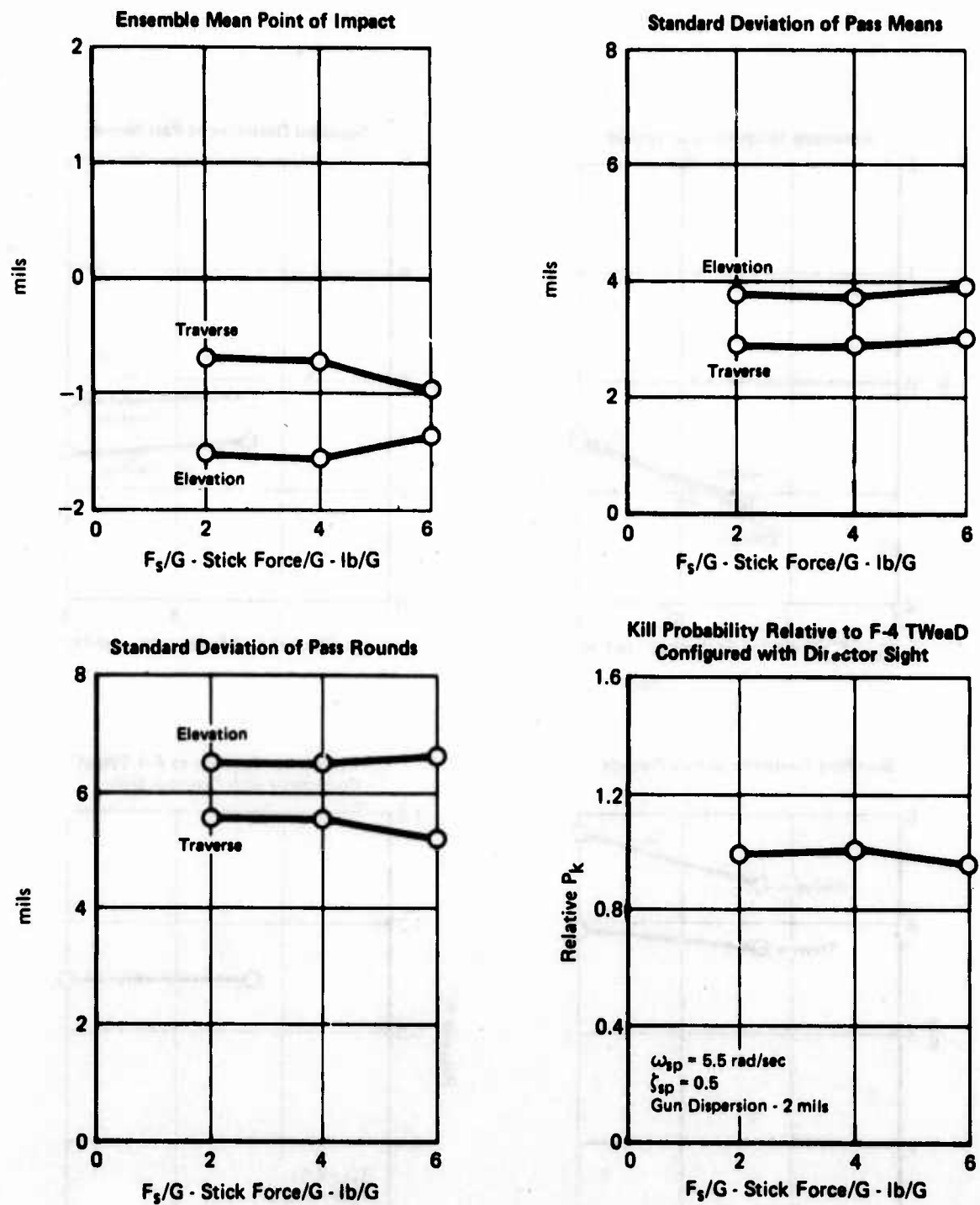


Figure 121. Effects of Longitudinal Short-Period Frequency Variations on Air-to-Air Gunnery Task for F-4 TWeaD Aircraft Configured with Director Sight (Mach 0.8 at 10,000 Ft Altitude, 4 G Target, 2000 Ft Range)

GP78-0884-256



OP78-0864-287

Figure 122. Effects of Longitudinal Stick Force per G Variations on Air-to-Air Gunnery Task for F-4 TWeaD Aircraft Configured with Director Sight (Mach 0.8 at 10,000 Ft Altitude, 4 G Target, 2000 Ft Range)

5.2.5 TAWDS Analyses of Lateral-Directional Flying Qualities for Air-to-Air Gunnery - The effects of Dutch roll mode damping on air-to-air gunnery effectiveness for an aircraft tracking a 4g target at Mach 0.8 and 10,000 ft. altitude are shown in Figures 123 and 124. With the Director, weapon delivery effectiveness improved as the Dutch roll mode damping is increased from 0.2 to 0.8. With the LCOSS, it decreased as the Dutch roll mode damping is increased from 0.2 to 0.8.

For the Director and LCOSS gunnery modes, the effects of proverse/adverse yaw variations on air-to-air gunnery effectiveness are given in Figures 125 and 126. For the range of yaw characteristics studied, the weapon delivery effectiveness for both gunsights increased as the yaw due to lateral stick command became more proverse.

For the Director and LCOSS gunnery modes the effects of commanded roll rate sensitivity on air-to-air gunnery effectiveness are given in Figures 127 and 128. For the Director sight, gunnery effectiveness significantly decreased as the aircraft's roll rate time constant increased from .33 to 1 second. For the LCOSS sight it was maximum for the aircraft roll rate time constant of .5 seconds and then it rapidly decreased as the aircraft's roll rate time constant increased to 1 second.

In this section it was demonstrated how the TAWDS programs can be used to determine the effects of flying qualities on weapon delivery accuracy for aircraft performing air-to-air or air-to-ground weapon delivery. The best set of flying qualities, determined by the TAWDS analyses to maximize weapon delivery effectiveness was used to formulate guidelines for flight control system requirements for weapon delivery. This topic is discussed in the next section.

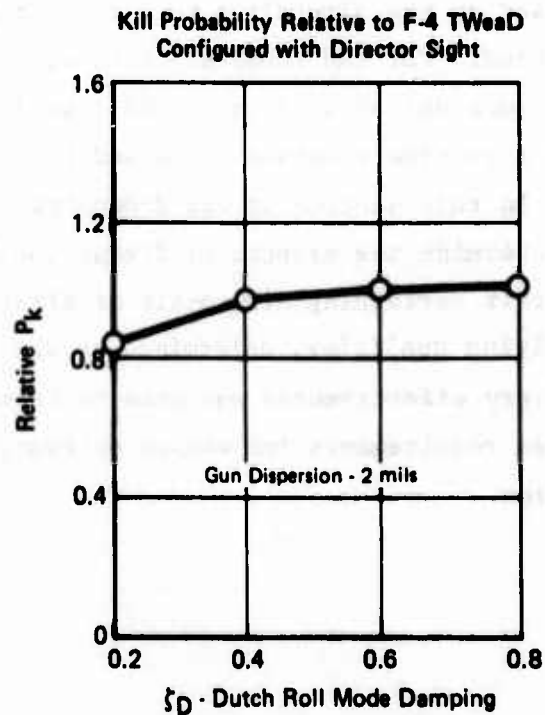
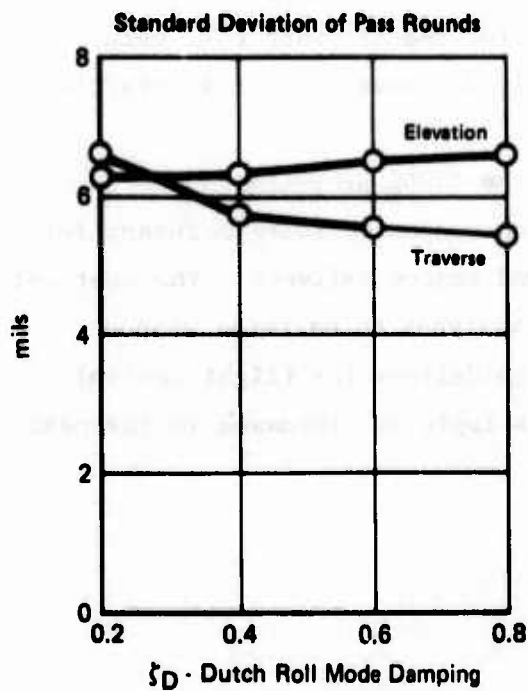
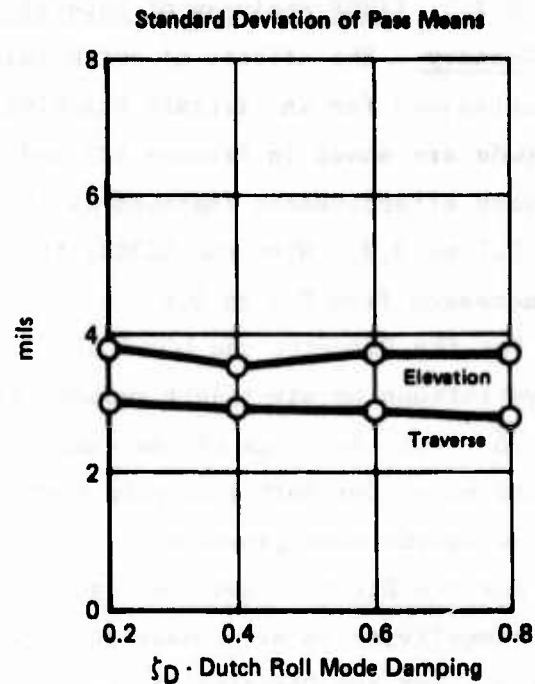
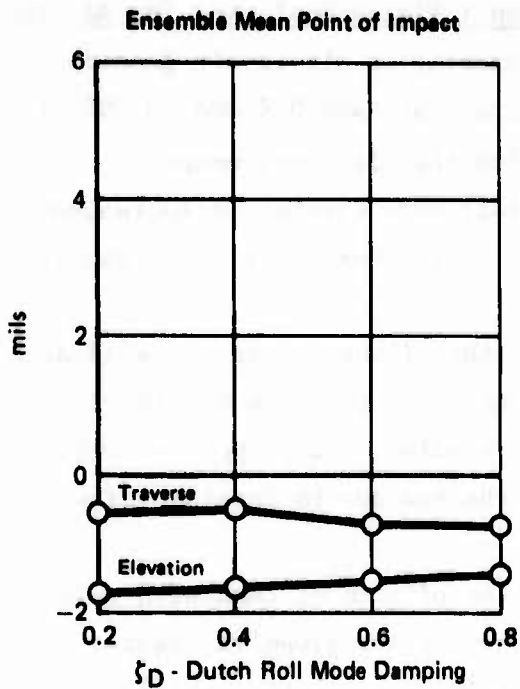


Figure 123. Effects of Dutch Roll Mode Damping Variations on Air-to-Air Gunnery Task for F-4 TWeaD Aircraft Configured with Director Sight (Mach 0.8 at 10,000 Ft Altitude, 4 G Target, 2000 Ft Range)

OP75-0884-283

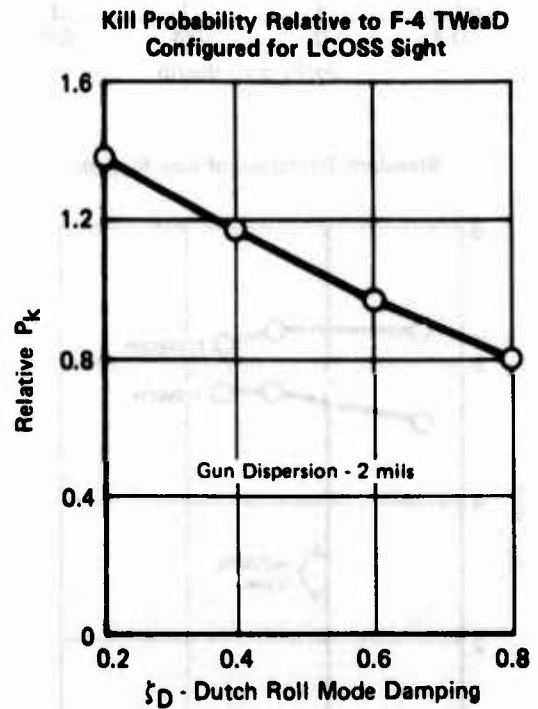
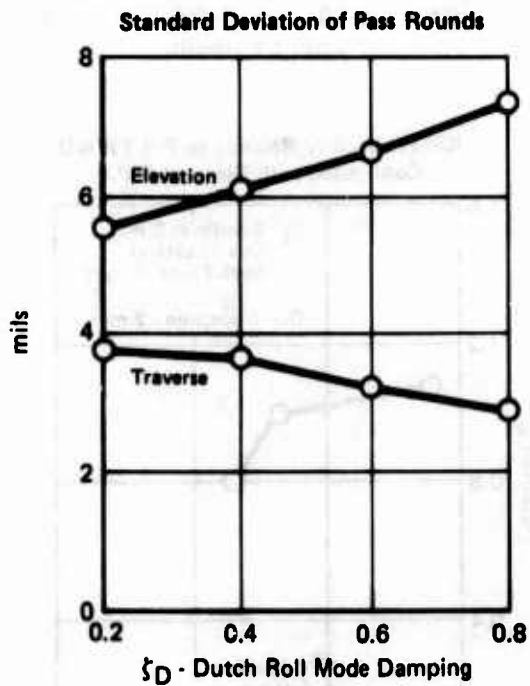
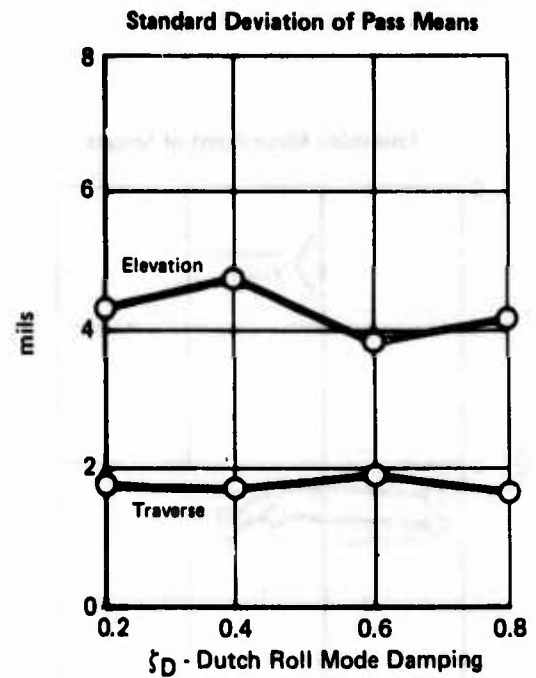
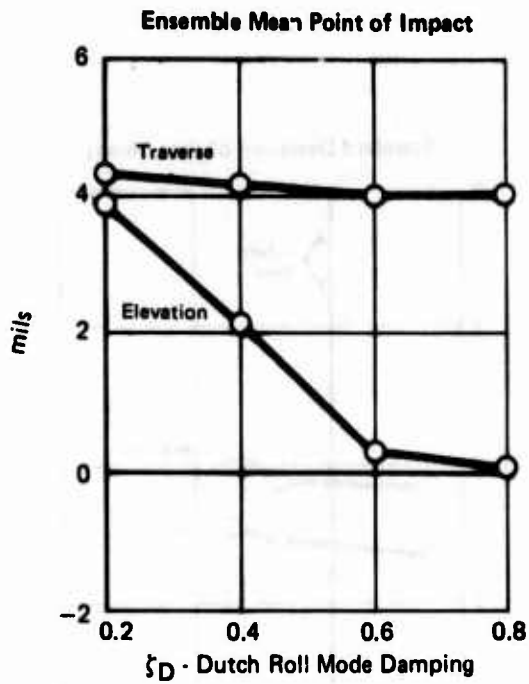


Figure 124. Effects of Dutch Roll Mode Damping Variations on Air-to-Air Gunnery Task for F-4 TWeaD Aircraft Configured with LCOSS Sight (Mach 0.8 at 10,000 Ft Altitude, 4 G Target, 2000 Ft Range)

GP75-0064-260

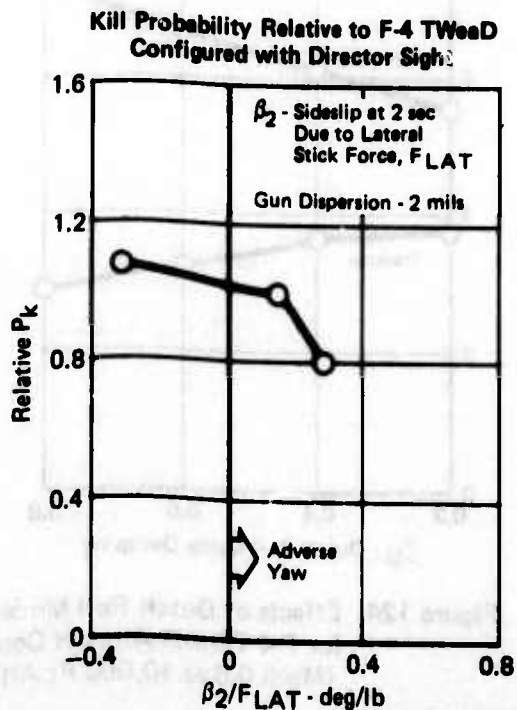
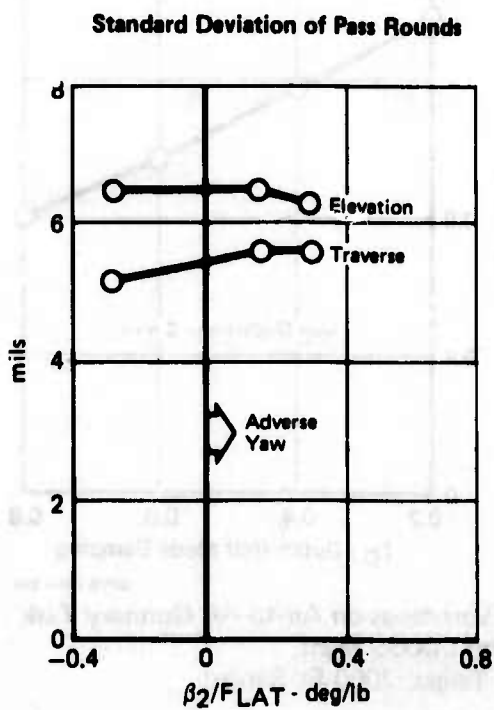
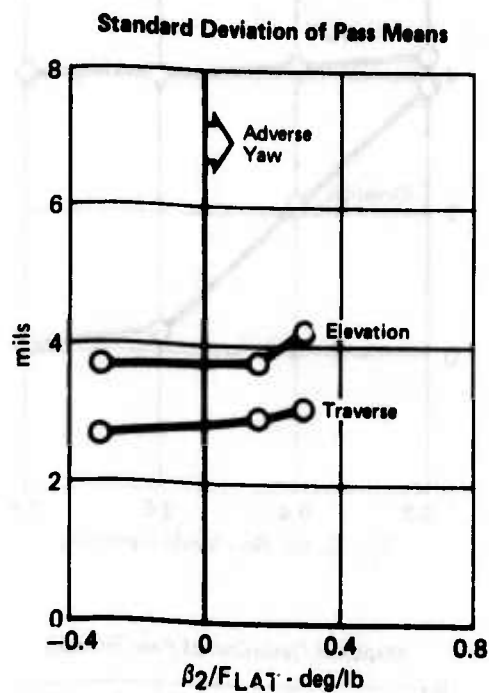
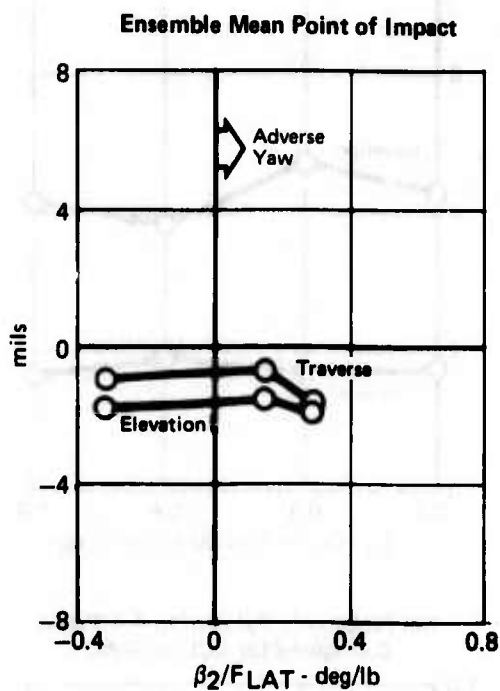


Figure 125. Effects of Proverse/Adverse Yaw Variations on Air-to-Air Gunnery Task for F-4 TWeaD Aircraft Configured with Director Sight (Mach 0.8 at 10,000 Ft Altitude, 4 G Target, 2000 Ft Range)

OP75-0864-262

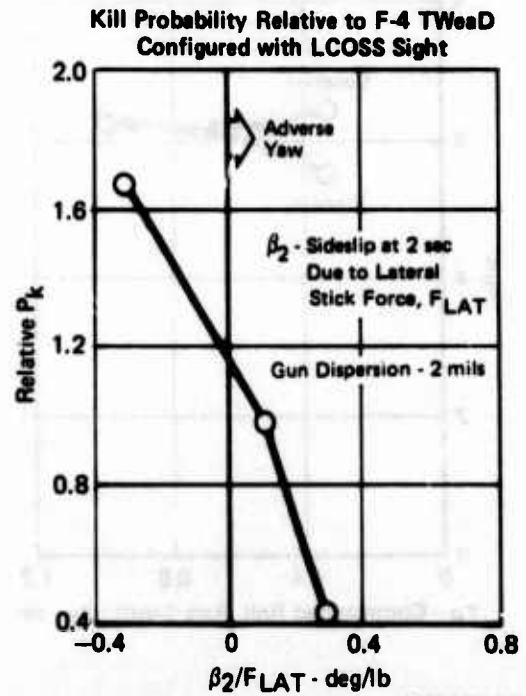
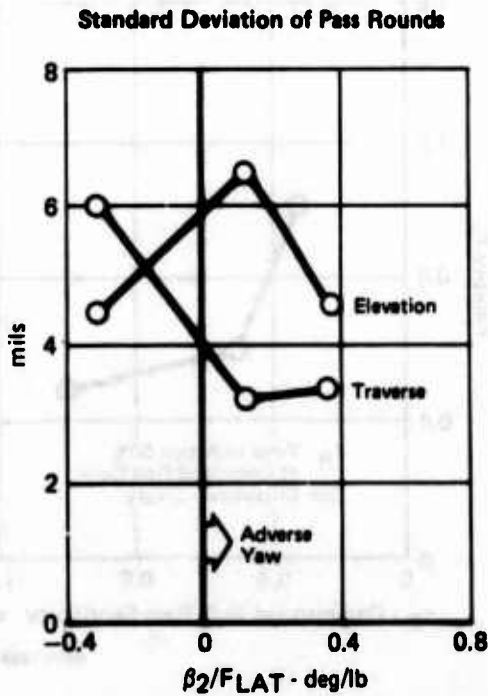
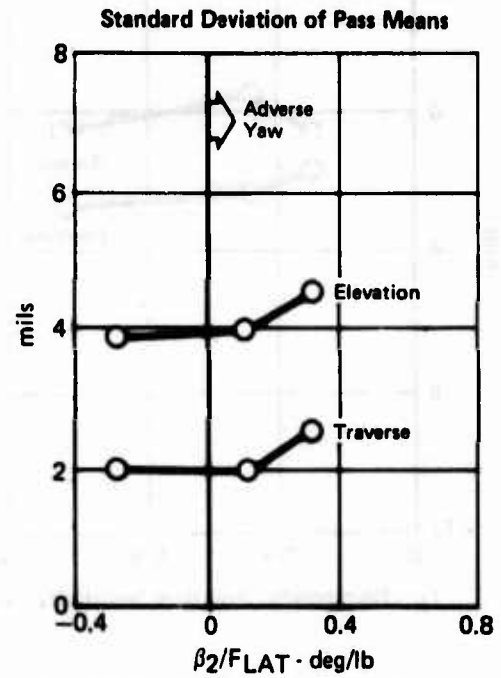
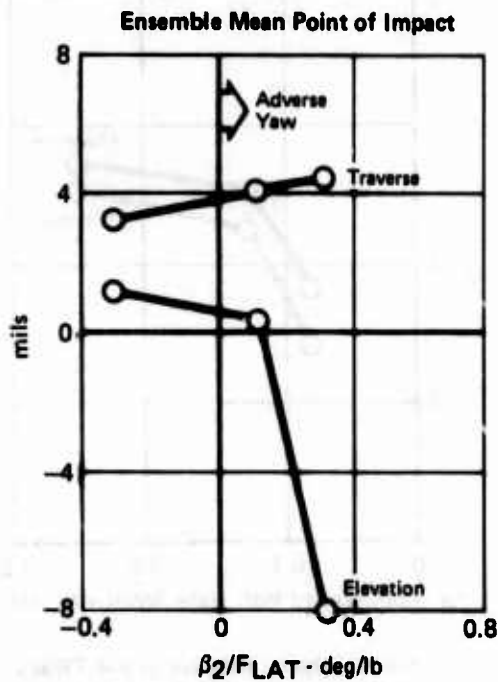
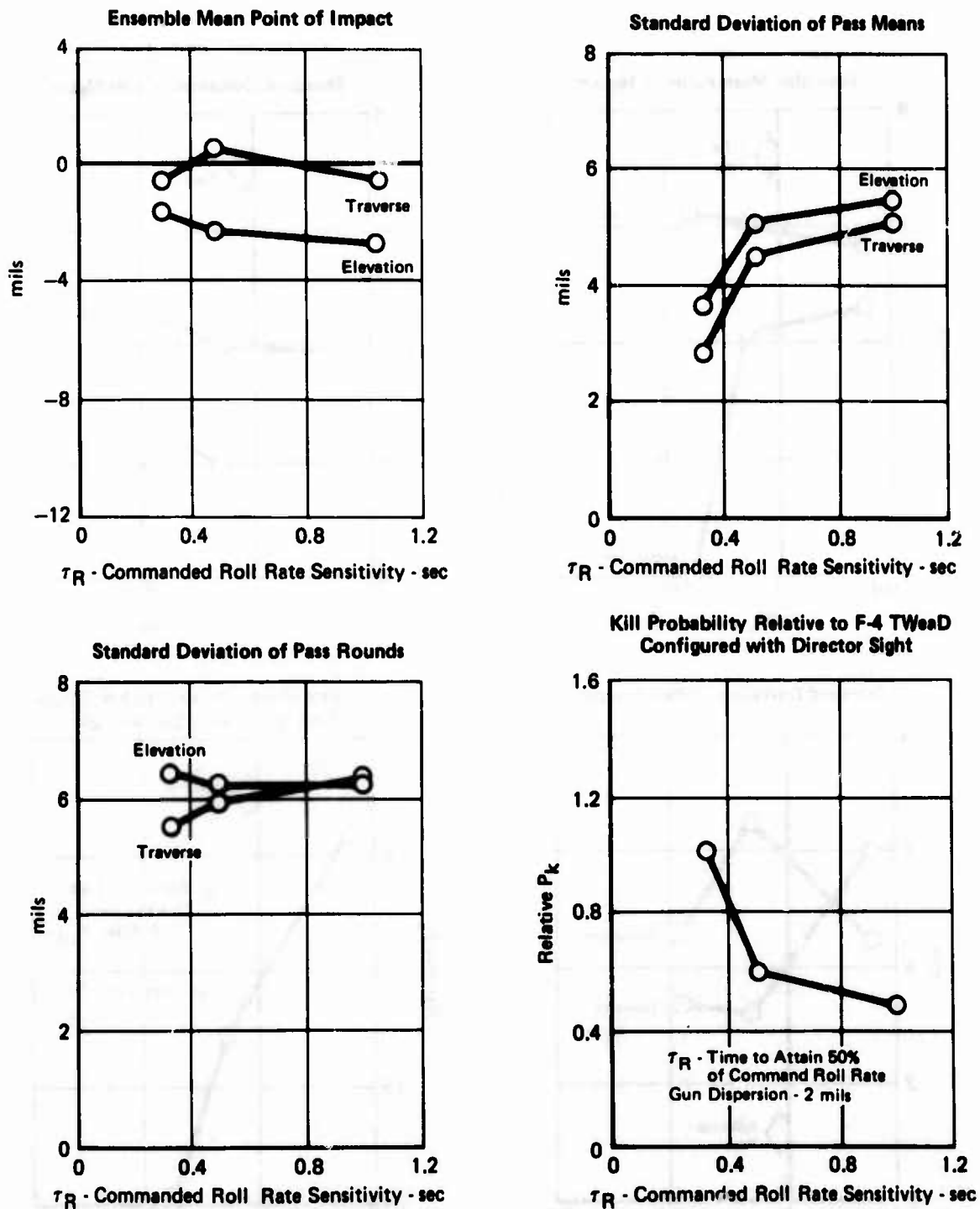


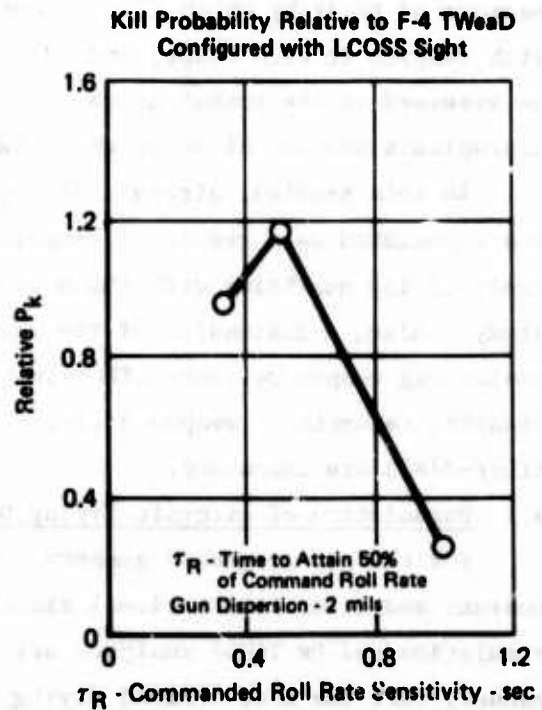
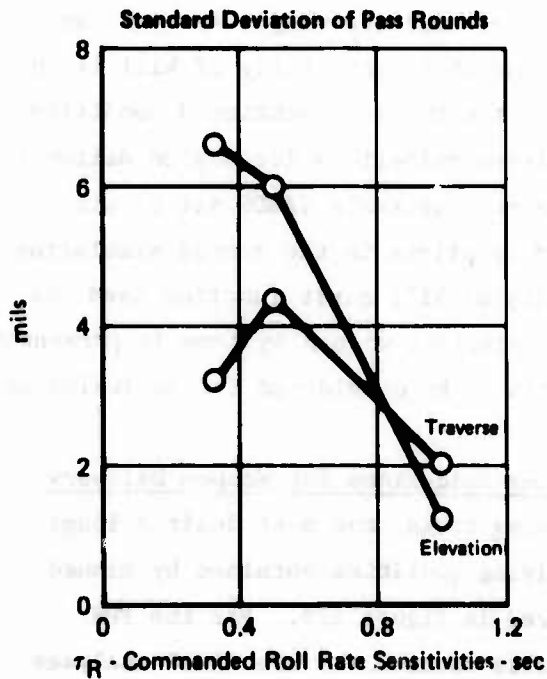
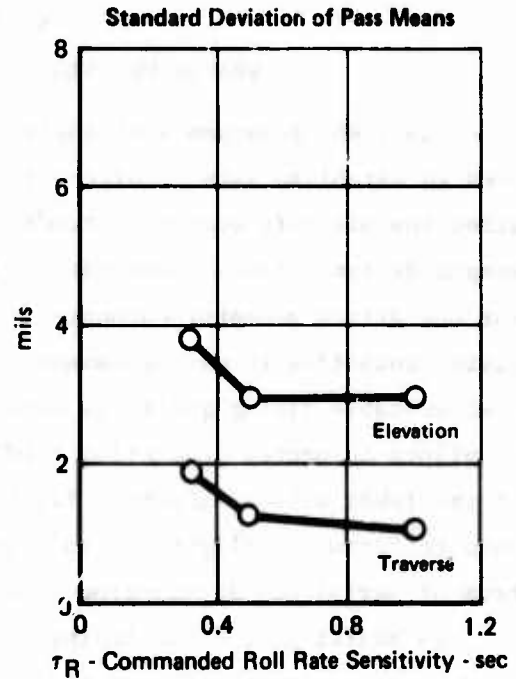
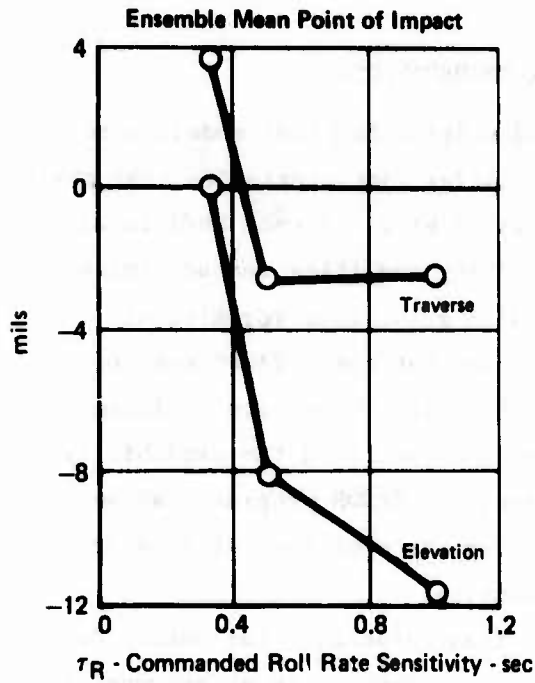
Figure 126. Effects of Proverse/Adverse Yaw Variations on Air-to-Air Gunnery Task for F-4 TWeaD Aircraft Configured with LCOSS Sight (Mach 0.8 at 10,000 Ft Altitude, 4 G Target, 2000 Ft Range)

GP76-0004-258



GP75-0864-261

Figure 127. Effects of Commanded Roll Rate Sensitivity Variations on Air-to-Air Gunnery Task for F-4 TWeaD Aircraft Configured with Director Sight (Mach 0.8 at 10,000 Ft Altitude, 2000 Ft Range)



GP75-0864-259

Figure 128. Effects of Commanded Roll Rate Sensitivity Variations on Air-to-Air Gunnery Task for F-4 TWaaD Aircraft Configured with LCOSS Sight (Mach 0.8 at 10,000 Ft Altitude, 4 G Target, 2000 Ft Range)

SECTION 6

WEAPON DELIVERY CRITERIA CONSIDERATIONS

The TAWDS programs with their analytical multi-axis pilot models were used to establish sets of aircraft flying qualities characteristics that maximized the aircraft weapon system's probability of kill for each individual weapon delivery task. Each set of aircraft flying qualities was determined for one attack geometry encounter. To establish guidelines for aircraft flying qualities it was necessary to demonstrate that these TAWDS sets of most suitable flying qualities compare favorably with those sets evaluated by pilots in manned simulation studies. Having established the credibility of the TAWDS sets of aircraft flying qualities, the TAWDS programs can be used to formulate flight control system requirements over the entire spectrum of aerial and air-to-ground attack encounters.

In addition to establishing flying qualities guidelines for weapon delivery, another important area of investigation was determining an appropriate measure of merit by which (1) various aircraft weapon systems can be evaluated with respect to each other, and (2) the cost of aircraft weapon systems can be assessed in the combat arena. It was found that probability of kill is an appropriate measure of merit which satisfies the two aforementioned conditions.

In this section, aircraft flying qualities guidelines for weapon delivery are formulated as a result of comparing the most suitable TAWDS set of aircraft flying qualities with those evaluated by pilots in the manned simulation study. Also, a discussion of the probability of kill merit function used for evaluating weapon delivery effectiveness of aircraft weapon systems is presented. Finally, recommended weapon delivery criteria to be considered for inclusion in MIL-F-8785B are discussed.

6.1 Formulation of Aircraft Flying Qualities Guidelines for Weapon Delivery

For the air-to-ground gunnery and bombing tasks, the most desired longitudinal and lateral-directional aircraft flying qualities obtained by manned simulation and by TAWDS analyses are compared in Figure 129. For the FDR gunnery task the most desired flying qualities obtained by the TAWDS analyses and pilot evaluation are in close agreement. The flying qualities characteristic that resulted in the greatest difference was the Dutch roll mode damping.

Flying Qualities Characteristic	Air-to-Ground FDR Gunnery		Air-to-Ground CCIP Gunnery		Air-to-Ground FIP Bombing	
	Pilot Opinion	TAWDS Analyses	Pilot Opinion	TAWDS Analyses	Pilot Opinion	TAWDS Analyses
Longitudinal Stick Force per G (lb/G)	6.0	6.0	4.0	4.0	4.0	6.0
Longitudinal Short-Period Damping	0.8	0.7	0.8	0.7	0.8	0.5
Longitudinal Short-Period Frequency (rad/sec)	6.5	6.0	6.5	6.5	4.0 - 6.5	4.5
Dutch Roll Mode Damping	0.6	0.8	0.6	0.8	0.4	0.2 - 0.8
Proverse/Adverse Yaw β_2/FLAT , deg/lb	-0.4 (Proverse)	-0.4 (Proverse)	0.15 (Adverse)	-0.4 (Proverse)	0.15 (Adverse)	-0.4 - 0.4
Commanded Roll Rate Sensitivity (sec)	0.25	0.33	0.25	0.33	0.25	0.25 - 0.5

GP75-0864-425

Figure 129. Comparison of Most Desired Sets of Aircraft Flying Qualities Obtained by Manned Simulation Evaluation and TAWDS Analyses for Air-to-Ground Weapon Delivery Tasks
Mach 0.7 Flight Condition, 30° Dive

Comparison of the time history response characteristics for the 0.6 and 0.8 Dutch roll mode damping configurations in Figure 88 shows that the lateral-directional aircraft responses obtained for these two configurations are similar.

The longitudinal flying qualities determined most suitable for CCIP air-to-ground gunnery by both pilot opinion and probability of kill analyses are very similar. For the lateral-directional flying quality variations considered for CCIP gunnery task, the optimum proverse/adverse yaw values determined by the two different evaluation methods are different. This difference is attributed to (1) the different criteria used in evaluating aircraft flying qualities by manned simulations and TAWDS analyses, and (2) the restrictiveness of the analytical pilot model when compared to the pilot's adaptive control technique for performing weapon delivery tasks.

There are significant differences in the flying qualities characteristics found suitable for the air-to-ground bombing task in manned simulation and probability of kill analyses. These differences are due to (1) the insensitivity of kill probability for the bombing task with respect to changes in flying qualities characteristics, and (2) the pilot opinion criterion associated

with evaluating aircraft flying qualities is different than the probability of kill criterion used in the TAWDS analyses.

For the air-to-air gunnery tasks, comparisons of the most desired longitudinal and lateral-directional flying qualities obtained by manned simulations and TAWDS analyses are shown in Figure 130. For the Director gunnery task, the selected flying qualities characteristics agree except for the proverse and adverse yaw characteristics. For the LCOSS gunnery task, only the optimum longitudinal short-period frequency and damping values agree. Again, it must be emphasized that the values of the most desirable flying qualities characteristics do not agree mainly because of the different criteria associated with evaluating aircraft flying qualities by manned simulation and TAWDS analyses, and because the analytical pilot model is limited when compared to the pilot's adaptive method for reducing tracking errors.

Figures 129 and 130 represent a suitable set of guidelines for designing aircraft with the flying qualities tailored for these particular air-to-air and air-to-ground weapon delivery tasks. These figures show that there is a small difference in specifying guidelines in terms of pilot opinion and weapon

Flying Qualities Characteristic	Air-to-Air Director Gunnery		Air-to-Air LCOSS Gunnery	
	Pilot Opinion	TAWDS Analyses	Pilot Opinion	TAWDS Analyses
Longitudinal Stick Force per G (lb/G)	4.0	4.0	4.0	2.0
Longitudinal Short-Period Damping	0.8	0.8	0.8	0.8
Longitudinal Short-Period Frequency (rad/sec)	6.0	4.5 - 6.0	6.7	6.0
Dutch Roll Mode Damping	0.8	0.8	0.4	0.2
Proverse/Adverse Yaw ($\beta_2/FLAT$, deg/lb)	0.15 (Adverse)	-0.4 (Proverse)	0.15 (Adverse)	-0.4 (Proverse)
Commanded Roll Rate Sensitivity (sec)	0.25	0.33	0.25	0.5

GP73-0884-426

Figure 130. Comparison of Most Desired Sets of Aircraft Flying Qualities Obtained by Manned Simulation Evaluation and TAWDS Analyses for Air-to-Air Gunnery Tasks
Mach 0.8 at 10,000 Ft Altitude Flight Condition, 4 G Target, 2,000 Ft Range

delivery accuracy or probability of kill analyses. Consequently, it is concluded that use of the TAWDS analysis procedure will provide suitable sets of aircraft flying qualities for integrated flight control/fire control weapon systems performing weapon delivery over a variety of attack encounters.

6.2 Merit Functions for Weapon Delivery

Cost is a major design factor in the development, production and survivability of any aircraft weapon system. The TAWDS programs can assess numerous combinations of integrated fighter aircraft/weapon systems in terms of weapon delivery accuracy. With the TAWDS programs, the complexity and quality of integrated aircraft weapon systems required to meet design specifications can be established. After defining such systems in terms of their components, the designer will be able to formulate the cost or merit function for developing and producing integrated aircraft weapon systems.

Another, even more important, cost factor is the ability to predict how well the integrated aircraft weapon system can accomplish its mission and yet survive. Under the assumption that enough sorties are flown against defending targets until the target is destroyed, it was determined that probability of kill is a good measure of mission survivability because it is inversely proportional to the number of sorties required to accomplish the mission.

Probability of kill is determined by transforming a set of ensemble impact error distributions through target vulnerability models. This program effort was addressed towards developing a procedure for relating the dynamic characteristics of the entire integrated aircraft weapon system to weapon impact errors. In the following narration, the effect of dynamic characteristics of these impact error distributions on probability of kill are discussed.

6.2.1 Use of Ensemble Burst Statistics - It has been shown in Reference 15 that the use of ensemble burst or pass statistics permits the separation of impact variance into two uncorrelated components, that which appears as a bias for the burst, σ_s^2 , and that which appears as dispersion within a burst, σ_d^2 . In the terminology of Reference 15, the probability distribution of impact points which results from a time-varying impact error process can, for a set of passes made with the same nominal delivery conditions, be replaced by two separate, statistically independent, bivariate Gaussian distributions.

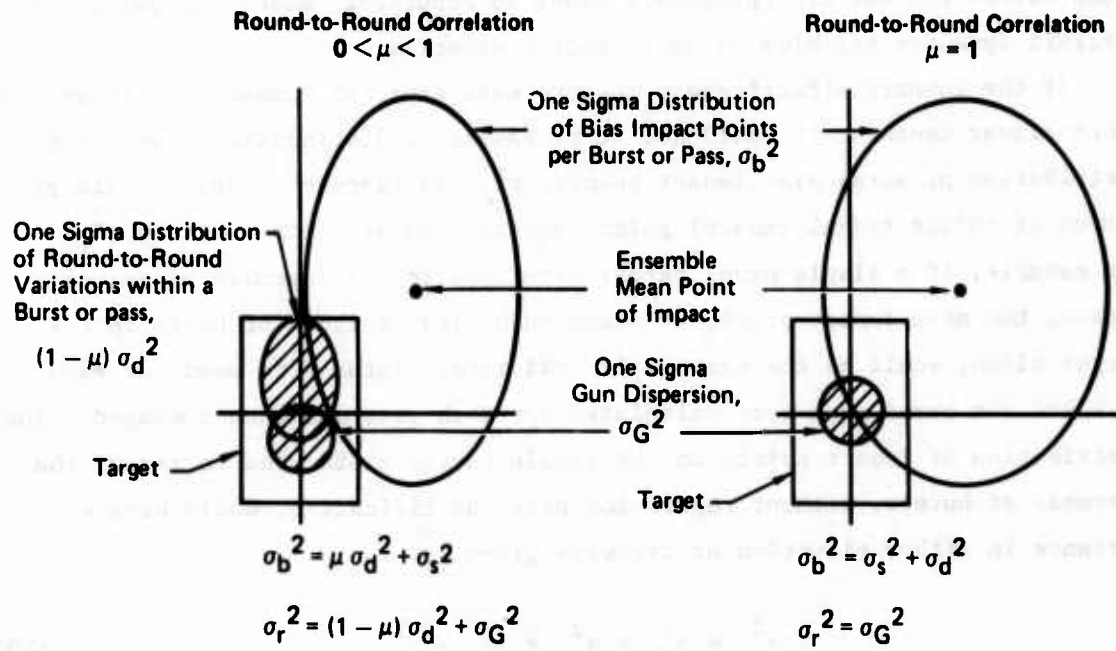
These describe the distribution of bias impact points, σ_b^2 , and the distribution of individual rounds (impact points) with respect to particular bias impact points, σ_r^2 . When the round-to-round correlation is nearly unity, only one bivariate distribution is needed to represent the impact error distribution. The relationships of the impact error distributions as functions of round-to-round correlation, bias for a burst due to stationary source errors, and burst dispersion due to dynamic source errors are shown in Figure 131.

Error sources are classified as being "stationary" if their correlation time constant is long compared to the duration of the firing burst, while "nonstationary" or "dynamic" error sources are those having correlation times which are short relative to the duration of the burst or pass. In other words, the effect of stationary source errors is to yield a bias impact error over the burst, while the effect of dynamic source errors is to yield a time-varying impact error (aim wander) over the burst. The parameter " μ " is defined in Figure 131 by the equation

$$\mu = \frac{1}{n^2} \sum_{i=1}^n \sum_{j=1}^n \rho(|i-j|) \quad (19)$$

where n is the number of rounds fired during the burst or pass and $\rho(|i-j|)$ is the autocorrelation coefficient relating the impact errors of the i^{th} and j^{th} rounds. Thus, the aim errors due to dynamic source errors are prorated by the constants μ and $(1 - \mu)$ between that portion, $\mu\sigma_d^2$, which can be considered to affect all rounds in the same way, just as the stationary errors do, and that portion, $(1 - \mu)\sigma_d^2$, which can be considered to affect each round separately, just as ballistic dispersion does. Consequently, the accuracy of a firing burst can be represented by an equivalent salvo with one probability distribution for bias impact points and a separate, statistically independent, probability distribution for individual round impact points about particular bias impact points. If ballistic dispersion were also considered, its variance in each component (elevation and traverse) would be added to the corresponding component of σ_r^2 .

The above discussion, which parallels that of Reference 15, implicitly assumes that: (1) either σ_d^2 is constant or an average value of σ_d^2 is used, and (2) the time-varying aim wander is a first-order Gauss-Markov process.



GP75-0864-382

Figure 131. Impact Error Dispersion Patterns

In addition, the simple proration of σ_d^2 between σ_b^2 and σ_r^2 on the basis of μ and $(1 - \mu)$ is appropriate only when the bias impact point distribution has a zero mean, that is, when the ensemble mean impact error is zero (the EMPI coincides with the point target). The TAWDS program employs more general expressions for σ_b^2 and σ_r^2 which permit removal of the above limiting assumptions. In addition, the time-varying impact error process is modeled as a Gauss-Markov process of appropriate order to accurately model the pilot and aircraft dynamics tracking response characteristics.

If the gunnery effectiveness measure were expected number of hits or some other linear measure, it would not be necessary to distinguish between the distribution of burst bias impact points, with variance σ_b^2 , and the distribution of impact (ideal impact) points within a burst, with variance σ_r^2 . For example, if a single panel target were used for an ensemble of gunnery passes, the mean impact point, as measured by the centroid of holes in the target cloth, would be the same as if individual cloths were used for each pass and the burst mean were calculated for each pass and then averaged. The distribution of impact points on the single target cloth used to record the ensemble of bursts, without regard for pass identification, would have a variance in either elevation or traverse given by

$$\sigma_a^2 = \sigma_b^2 + \sigma_r^2 = \sigma_s^2 + \sigma_d^2 \quad (20)$$

using the above notation. The expected number of hits on a target could be obtained by a simple numerical integration of the single bivariate Gaussian distribution over the target, as shown in Figure 132 for a circular target. The calculation is referred to as the expected hits on an offset circular target, and tables are available for the special case when $\sigma_{a_e}^2 = \sigma_{a_t}^2$, that is, when the distribution of impact points is circular normal. When the target is square or rectangular, as depicted in Figure 133, and when the elevation and traverse components of the impact point variance are statistically independent, the calculation can be made by a simple use of a standard normal distribution table. Finding the probability that an impact point lies within the target limits in elevation and traverse separately and then multiplying the two probabilities to get the single-shot hit probability, P_H , the expected number of hits for a burst of n rounds is given by

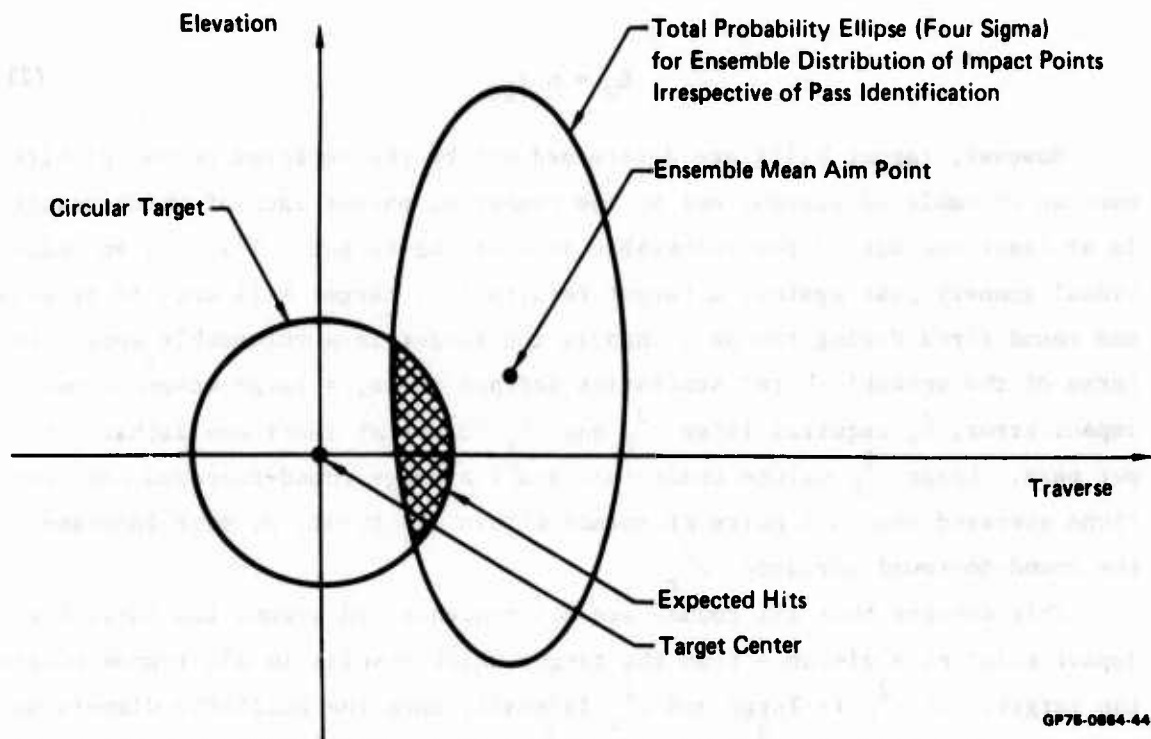


Figure 132. Ensemble Expected Hits on an Offset Circular Target

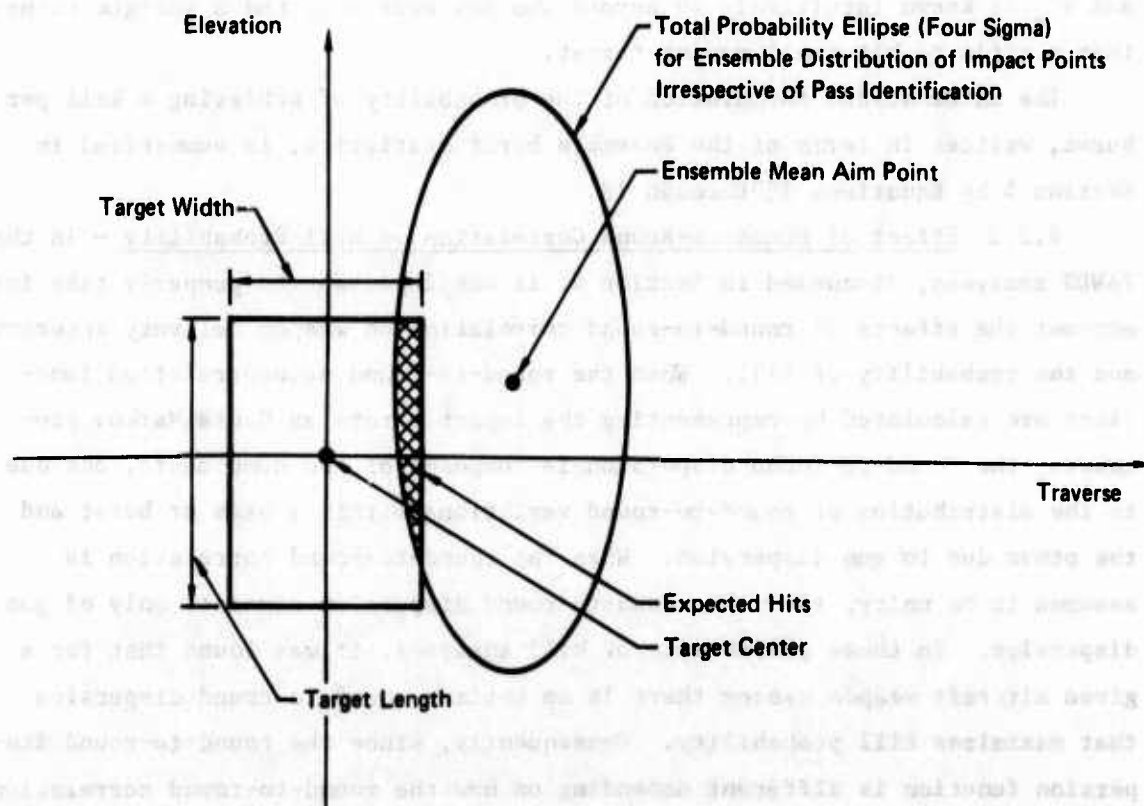


Figure 133. Ensemble Expected Hits on an Offset Rectangular Target

$$E_H = n P_H. \quad (21)$$

However, target kills are determined not by the expected number of hits over an ensemble of passes, but by the number of passes each of which result in at least one hit on the vulnerable area of the target. That is, an individual gunnery pass against a target results in a target kill only if at least one round fired during the pass impacts the target in a vulnerable spot. In terms of the ensemble burst statistics defined above, a large ensemble mean impact error, \bar{b} , requires large σ_b^2 and σ_r^2 to get at least one lethal hit per pass. Large σ_b^2 values means that small average round-to-round correlations averaged over all pairs of rounds within the burst, μ , must increase the round-to-round variance, σ_r^2 .

This ensures that all rounds are not concentrated around the burst bias impact point at a distance from the target which results in all rounds missing the target. If σ_b^2 is large and σ_r^2 is small, then the ballistic dispersion variance, which adds to σ_r^2 must be increased to increase the probability of at least one lethal hit per pass. The procedure for trading off between σ_b^2 and σ_r^2 is known intuitively by anyone who has ever selected a shotgun rather than a rifle to hit small moving target.

The mathematical formulation of the probability of achieving a kill per burst, written in terms of the ensemble burst statistics, is summarized in Section 5 by Equations 15 through 18.

6.2.2 Effect of Round-to-Round Correlation on Kill Probability - In the TAWDS analyses, discussed in Section 5, it was important to properly take into account the effects of round-to-round correlation on weapon delivery accuracy and the probability of kill. When the round-to-round autocorrelation functions are calculated by representing the impact errors as Gauss Markov processes, the round-to-round dispersion is composed of two components, one due to the distribution of round-to-round variations within a pass or burst and the other due to gun dispersion. When the round-to-round correlation is assumed to be unity, then the round-to-round dispersion consists only of gun dispersion. In these probability of kill analyses, it was found that for a given aircraft weapon system there is an optimum round-to-round dispersion that maximizes kill probability. Consequently, since the round-to-round dispersion function is different depending on how the round-to-round correlation

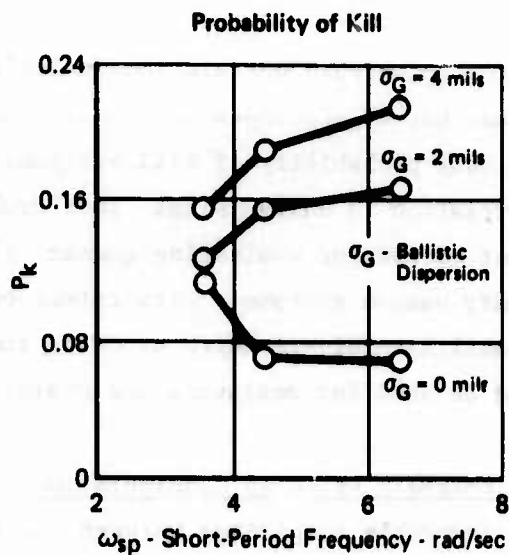
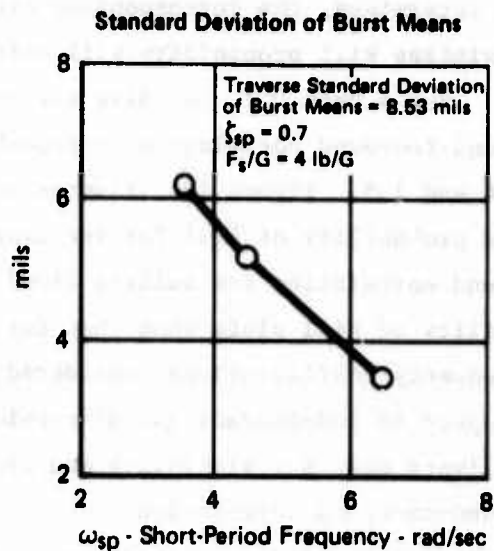
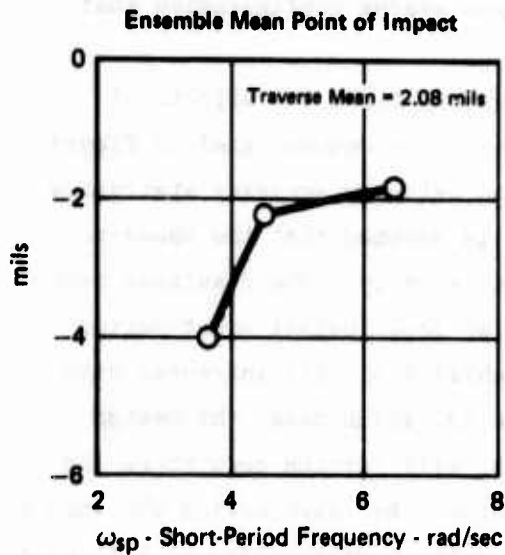
is determined, the corresponding aircraft weapon system configuration that maximizes kill probability will differ also.

For a Mach 0.7, 30° dive air-to-ground gunnery task, the effects of round-to-round correlation on probability of kill are demonstrated in Figures 134 and 135. Figure 134 illustrates the weapon delivery accuracy statistics and probability of kill for the case where it is assumed that the round-to-round correlation for bullets fired in a burst is unity. The resultant probability of kill plots show that for the range of longitudinal short-period frequency configurations considered, the probability of kill increases with respect to independent gun dispersion. Figure 135 illustrates the weapon delivery accuracy statistics and probability of kill for the case where the round-to-round correlation functions are calculated by representing the impact errors as Gauss Markov processes. Here the resultant probability of kill plots show that for the range of longitudinal short-period frequency configurations considered, the probability of kill decreases as the independent gun dispersion increases.

In Section 2, the round-to-round correlations calculated by representing the impact errors as Gauss Markov processes were validated. Consequently, this validation implies that probability of kill analyses using the assumption that round-to-round correlation is unity (single shot probability of kill analysis) is an incorrect method for evaluating gunnery effectiveness of entire integrated aircraft weapon systems. With reference to Figures 134 and 135, multiple shot probability analysis which properly accounts for round-to-round correlation should be used for designing and evaluating integrated aircraft weapon systems.

6.3 Recommended Weapon Delivery Criteria Consideration

As a result of the favorable comparison between the TAWDS most suitable set of aircraft flying qualities and those obtained from pilot evaluation of weapon delivery tracking task from a manned simulation study, it is recommended that the TAWDS set of flying qualities for aircraft performing weapon delivery as shown in Figures 129 and 130 be considered for inclusion into MIL-F-8785B as a guideline for designing fighter aircraft flying qualities characteristics to assure high probability of kill for aircraft performing weapon delivery. It is also recommended that the TAWDS methodology for relating the weapon system dynamic characteristics to weapon delivery accuracy and to probability of kill



OP75-0884-303

Figure 134. Weapon Delivery Accuracy Statistics for Unity Round-to-Round Correlation (Air-to-Ground Gunnery, Mach 0.7, 30° Dive, 4800 Ft Firing Range, Fixed Depressed Reticule Sight)

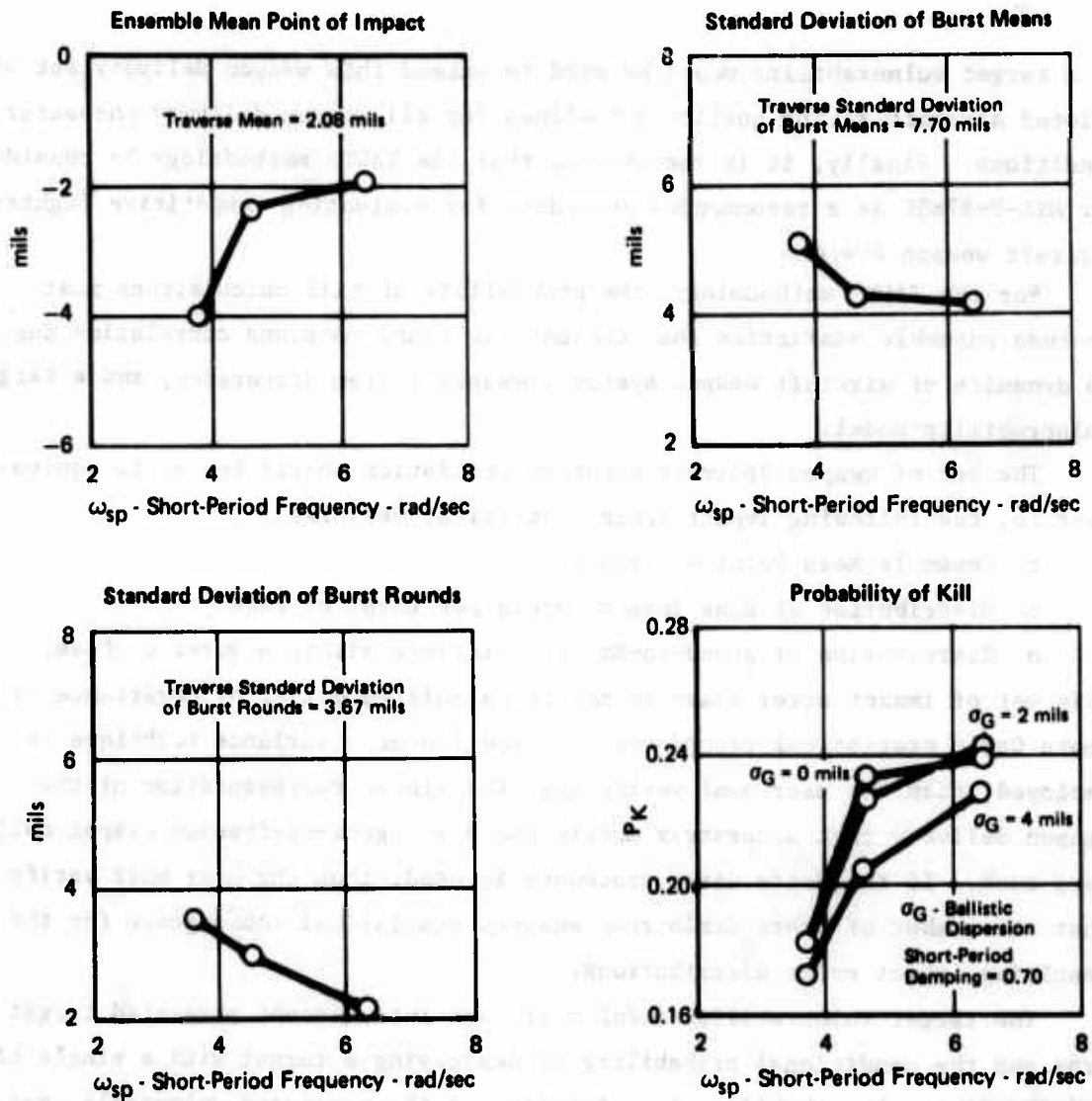


Figure 135. Weapon Delivery Accuracy Statistics for Gauss Markov Round-to-Round Correlation (Air-to-Ground Gunnery, F-4 Aircraft, Mach 0.7, 30° Dive, 4800 Ft Firing Range, Fixed Depressed Reticule Sight)

by a target vulnerability model be used to extend this weapon delivery set of piloted aircraft flying quality guidelines for all weapon delivery encounter conditions. Finally, it is recommended that the TAWDS methodology be considered for MIL-F-8785B as a recommended procedure for evaluating competitive fighter aircraft weapon systems.

For the TAWDS methodology, the probability of kill calculations must include ensemble statistics that account for round-to-round correlation due to dynamics of aircraft weapon systems, weapon system dispersion, and a target vulnerability model.

The set of weapon delivery accuracy statistics should be, or be equivalent to, the following impact error statistical measures:

- o Ensemble Mean Point of Impact
- o Distribution of Bias Impact Points per Burst of Pass
- o Distribution of Round-to-Round Variations within a Burst or Pass.

This set of impact error measures may be calculated either by covariance or Monte Carlo statistical procedures. If the linear covariance technique is employed, then the user must verify that the linear representation of the weapon delivery task accurately models the six-degree-of-freedom weapon delivery task. If the Monte Carlo procedure is used, then the user must verify that the number of Monte Carlo runs ensures statistical convergence for the resulting impact error distributions.

The target vulnerability model must take into account presented target area and the conditional probability of destroying a target with a single hit. This conditional probability is a function of the presented vulnerable area of the target.

In this study, it has been shown that the TAWDS methodology is a useful tool for evaluating aircraft weapon system effectiveness. In considering the TAWDS methodology for MIL-F-8785B, realistic ranges of values for the target area, the conditional probability of destroying a target with a single hit, and the appropriate multi-axis pilot models must be agreed upon. In addition to choosing an appropriate multi-axis pilot model (of which the pilot model developed in this study program may be a candidate), it is also necessary to develop algorithms for selecting values for the pilot model parameters. Derivation of appropriate algorithms requires a suitable criterion. The rationale

and backup data which support the pilot model development, performed in this study, as discussed in Section 4, are presented in the Volume II, Flight Control Requirements for Weapon Delivery Background Information Report.

In this program, the TAWDS methodology, which enables one to evaluate aircraft weapon system effectiveness using multiple shot probability procedures, was developed for application to manually coupled aircraft weapon systems. This same methodology also can be extended to include automatically coupled aircraft weapon systems, aircraft with direct force capability, and aircraft with moveable gun or fuselage aiming capability.

SECTION 7

CONCLUSIONS AND RECOMMENDATIONS

The most significant accomplishment of this study is the development of the Terminal Aerial Weapon Delivery Simulation (TAWDS) digital computer programs. The TAWDS programs, by enabling all-digital simulations to be performed for various closed loop weapon delivery systems under manual control, can be used to predict and evaluate weapon delivery accuracy. The programs determine ensemble impact error statistics which account for the entire integrated aircraft weapon system, including appropriate modeling for the pilot's weapon delivery steering task. For a given weapon delivery task, these programs can be used to evaluate weapon delivery accuracy for many combinations of flight control systems, sight systems, and fire control computers. Use of the TAWDS programs provide (1) effective aircraft weapon delivery system design guidelines which can be further refined in manned simulation studies, and (2) a statistically significant weapon-effectiveness measure which can be compared with established weapon delivery effectiveness criteria or specifications.

To develop the TAWDS programs, it was necessary to develop multi-axis pilot models which relate weapon delivery tracking errors to steering commands.

This development effort has demonstrated that:

- o The use of the analytical nonlinear multi-axis pilot models with constant gain parameters produces elevation and traverse tracking error characteristics which are similar to those obtained from the Manned Air Combat Simulator and from the TWeaD flight test evaluation programs.
- o The frequency (magnitude and phase) responses, computed for the multi-axis pilot model and for the human pilot, exhibit similar characteristics within the aircraft's longitudinal and lateral-directional primary control bandwidth.
- o The use of multi-axis pilot models provides weapon delivery accuracy results comparable to those obtained by pilots flying weapon delivery tasks in the manned simulator.

Further pilot model development is required to match the pilot's sequential on-off control techniques. It is hypothesized that these characteristics can be modeled by adaptively scheduling certain pilot model gains as a function of tracking error kinematics.

A manned simulation program evaluated longitudinal and lateral-directional flying qualities variations for air-to-air and air-to-ground weapon

delivery. As a result of this portion of the study program, the following observations about the pilots' subjective evaluation of flying qualities characteristics are made:

- o The pilots' opinion of the most desired flying qualities characteristics varied with the weapon delivery task.
- o The pilots accepted a wider range of aircraft flying qualities variations for FIP air-to-ground bombing than for gunnery.
- o The pilots' flying qualities evaluations indicate that the F-4 TWeaD lateral-directional flying qualities are the most desired for all the weapon delivery tasks. The F-4 TWeaD longitudinal flying qualities are acceptable for each weapon delivery task, but they can be improved by more selective active feedback flight control system gain settings.

The TAWDS analyses demonstrated how the TAWDS computer programs are used to evaluate longitudinal and lateral-directional flying qualities characteristics for air-to-ground and air-to-air weapon delivery. For the aircraft sight system configurations studied, the following conclusions can be made:

- o Multiple shot analysis which accounts for round-to-round correlation must be used to properly assess target kill probability.
- o Weapon delivery accuracy statistical distributions need to be transformed into a scalar probability of kill measure of merit to assess the impact of various aircraft weapon systems on weapon delivery accuracy.
- o Flying qualities characteristics required to optimize probability of kill for the same weapon delivery task vary with respect to sight systems and attack geometries.
- o Without considering flow interference effects on bombs before they attain their ballistic trajectory, variations in longitudinal and lateral-directional flying qualities have less impact on weapon delivery effectiveness for air-to-ground bombing than for the air-to-ground gunnery. The reasons for the relative insensitivity of bomb delivery effectiveness to flying qualities variations are: (1) the destructive force of bombs is a more predominant factor than improvement of impact accuracy, and (2) the round-to-round impact error distribution, which allows the aircraft dynamics to act as a controlled dispersion factor for gunnery burst, doesn't pertain to dive bombing.

Good comparisons were obtained between (1) TAWDS weapon delivery accuracy results and those measured from the manned simulation, and (2) most desired aircraft flying qualities characteristics obtained by TAWDS analyses and those obtained from pilot evaluation in the manned simulation studies. These comparisons verify that the TAWDS programs yield results representative of manned simulation and flight test obtained data. Therefore, it is recommended that the most suitable set of TAWDS flying qualities be considered for inclusion into MIL-F-8785B as guidelines for design of fighter aircraft flying qualities characteristics to assure high probability of kill for these aircraft performing weapon delivery. It is also recommended that probability of kill, which is a function of weapon impact error statistics and target vulnerability, be considered for MIL-F-8785B as a procedure for evaluating competitive fighter aircraft weapon delivery systems.

In this program, the TAWDS programs and their pilot models were validated by comparing the TAWDS ensemble impact error statistics and the TAWDS tracking responses with those measured from a relatively small sample of pilot-in-the-loop manned simulation runs. To more completely validate the TAWDS programs, two additional areas of investigation are recommended for future study:

- (1) Determine the statistical distributions of impact errors from an extensive Monte Carlo manned simulation study and ascertain if these distributions converge to those determined by the TAWDS program.
- (2) Validate the analytical multi-axis pilot models by comparing their tracking performance with those of fighter aircraft configurations other than the F-4 aircraft. The F-15 aircraft is recommended as a desirable candidate for this additional system effort. For such a study, it would be preferable to use more flight test tracking data than was available for this study. This would provide more validation for the proposed analytical pilot models.

REFERENCES

1. Carleton, D.L., et al., "Development and Evaluation of the TWeaD II Flight Control Augmentation System," FTC-TD-72-1, November 1970.
2. Carleton, D.L. and Powell, C.W., "Limited Air-to-Air Tracking and Qualitative Flying Qualities Evaluation of Selected Flight Control System Configurations in the F-4C/E Aircraft," FTC-TD-71-4, August 1971.
3. Rubertus, D.P., "TWeaD Control Augmentation System," National Aerospace Electronics Conference, Dayton, Ohio, 15-17 May 1972.
4. Richard, R.R., et al., "Stability and Control Evaluation of an F-4C Aircraft with a High Gain Adaptive Control Augmentation System," FTC-SD-71-17, June 1971.
5. Orwat, J.C., et al., "Weapon Delivery Evaluation of an F-4C Aircraft with a High Gain Adaptive Control Augmentation System," FTC-TR-71-35, August 1971.
6. Kisslinger, R.L. and Wendl, M.J., "Survivable Flight Control System, Interim Report No. 1 - Studies, Analyses and Approach, Supplement 1 - Supplement for Control Criteria Studies," Technical Report AFFDL-TR-71-20, May 1971.
7. Hooker, D.S., Kisslinger, R.L., et al., "Survivable Flight Control System Final Report," Technical Report AFFDL-TR-73-105, December 1973.
8. Etinger, R.C., Majoros, R.L., and Powell, C.W., "Air Force Evaluation of the Fly-By-Wire Portion of the Survivable Flight Control System Advanced Development Program," FTC-TR-73-32.
9. Quinlivan, R.P., "Multimode Flight Control Definition Study for Precision Weapon Delivery," Technical Report AFFDL-TR-71-39, June 1971.
10. Quinlivan, R.P., "Multimode Flight Control Definition Study," Technical Report AFFDL-TR-72-55, June 1972.
11. Berger, J.B., et al., "Flight Control Requirements for Weapon Delivery, Interim Report for Period June 1973 - May 1974," Technical Report AFFDL-TR-74-119.
12. Williams, A.H., Landy, R.J., and Murphy, W.J., "Aerial Gunnery Methodology, Volume II - Air-to-Ground Gunnery," AFATL-TR-72-218, Volume II, November 1972.
13. Berg, R.L., and Sears, M.M., "Air-to-Air Fire Control Exposition, Phase III (EXPO III)," AFAL-TR-73-287, September 1973.
14. "Air-to-Air Fire Control Exposition, Phase IV (EXPO IV)," AFAL-TR-74-XXX.

REFERENCES (Continued)

15. "Institute for Air Weapon Research, Gun and Rocket Armaments for Fighter to-Fighter Combat" (IAWR) Study G(A) 9 August 1953, CONFIDENTIAL (formerly SECRET).

*Older than 20
28 yrs old?*

APPENDIX I

NONLINEAR AIRCRAFT EQUATIONS FOR THE TAWDS(AA) PROGRAM

The TAWDS(AA) program uses nonlinear six-degree-of-freedom airframe equations and a set of linear differential equations with state constraints for the flight control system to simulate the dynamic motion of fighter aircraft.

I.1 Airframe Equations of Motion

The TAWDS(AA) program models attacker's forward acceleration (\dot{v}), the wind angle rates ($\dot{\alpha}$ and $\dot{\beta}$), the body axis angular accelerations (\dot{P} , \dot{Q} , \dot{R}), and the Euler angle rates ($\dot{\phi}$, $\dot{\theta}$, $\dot{\psi}$). To account for body angular rates measured off the center of gravity, the aircraft's accelerometer equations have also been mechanized.

The coordinate transformations used in the TAWDS(AA) program are shown in Figure I-1.

The six degree-of-freedom airframe equations of motion that are digitally simulated are:

$$\dot{v} = \cos \beta [T \cos (\alpha + \delta_e) - \bar{q} S C_{D}] / m + \bar{q} S \sin \beta C_{Y} / m - g \sin \gamma + F_{G_Y} / (m \cos \alpha) \quad (\text{I-1})$$

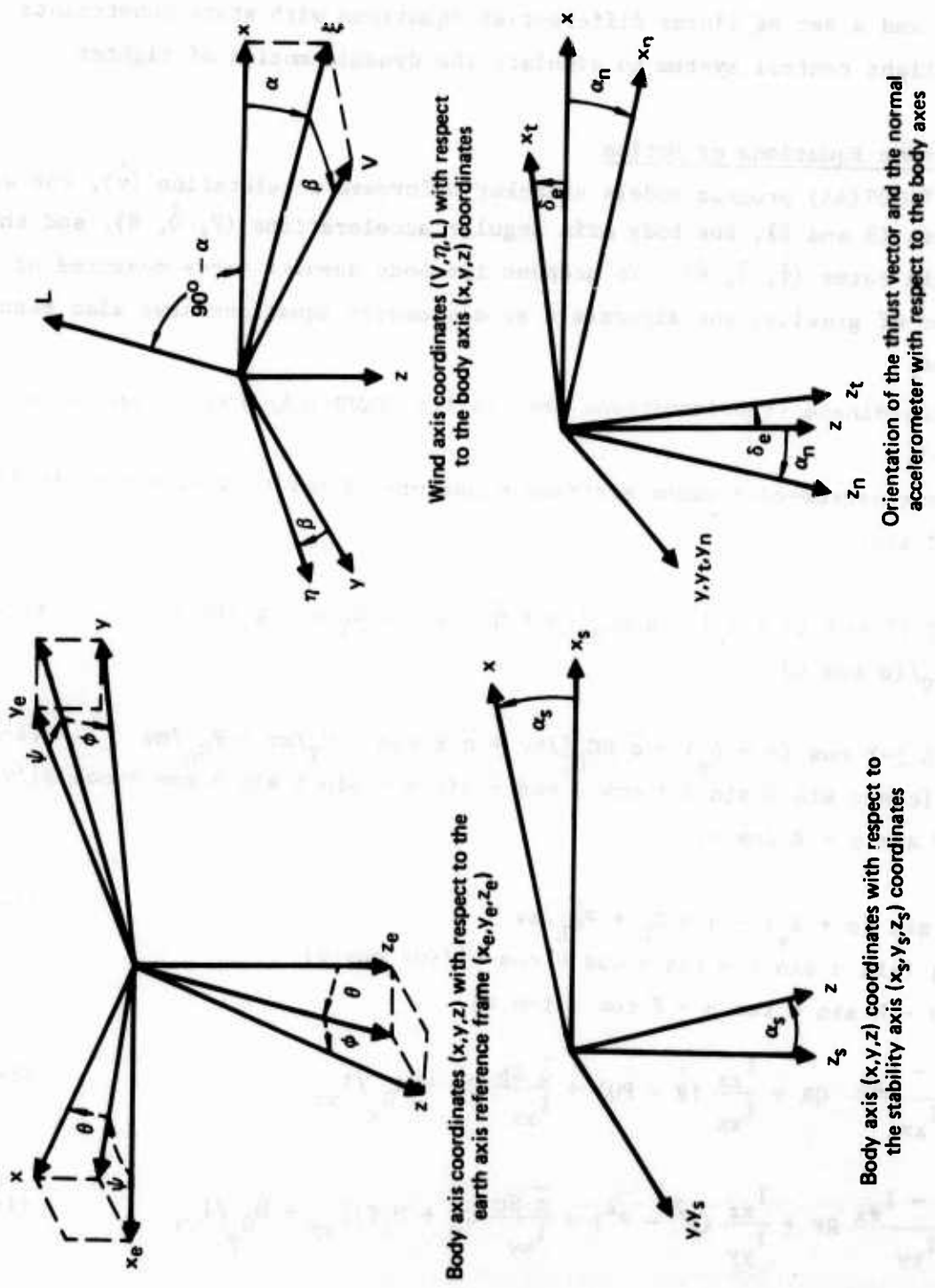
$$\dot{\beta} = \sin \beta [-T \cos (\alpha + \delta_e) + \bar{q} S C_{D}] / m v + \bar{q} S \cos \beta C_{Y} / m v + F_{G_n} / m v + g [\cos \alpha \sin \beta \sin \theta + \cos \beta \cos \theta \sin \phi - \sin \alpha \sin \beta \cos \theta \cos \phi] / v + (P \sin \alpha - R \cos \alpha) \quad (\text{I-2})$$

$$\dot{\alpha} = [-T \sin (\alpha + \delta_e) - \bar{q} S C_L + F_{G_L} / m v + mg (\sin \alpha \sin \theta + \cos \alpha \cos \theta \cos \phi)] / (m v \cos \beta) + [Q - R \sin \alpha \tan \beta - P \cos \alpha \tan \beta] \quad (\text{I-3})$$

$$\dot{P} = \frac{I_{yy} - I_{zz}}{I_{xx}} QR + \frac{I_{xz}}{I_{xx}} (\dot{R} + PQ) + \frac{\bar{q} S b}{I_{xx}} C_{\ell} + M_{G_x} / I_{xx} \quad (\text{I-4})$$

$$\dot{Q} = \frac{I_{zz} - I_{xx}}{I_{yy}} RP + \frac{I_{xz}}{I_{yy}} (R^2 - P^2) + \frac{\bar{q} S c}{I_{yy}} C_m + M_t T / I_{yy} + M_{G_y} / I_{yy} \quad (\text{I-5})$$

$$\dot{R} = \frac{I_{xx} - I_{yy}}{I_{zz}} PQ + \frac{I_{xz}}{I_{zz}} [\dot{P} - QR] + \frac{\bar{q} S b}{I_{zz}} C_n + M_{G_z} / I_{zz} \quad (\text{I-6})$$



Wind axis coordinates (V, η, L) with respect to the body axis (x, y, z) coordinates

Body axis (x, y, z) coordinates with respect to the stability axis (x_s, y_s, z_s) coordinates

Orientation of the thrust vector and the normal accelerometer with respect to the body axes

OP75-0064-420

Figure I-1. The Geometry of the Airframe Simulation

$$\dot{\theta} = Q \cos \phi - R \sin \phi \quad (\text{I-7})$$

$$\dot{\phi} = P + \dot{\Psi} \sin \theta \quad (\text{I-8})$$

$$\dot{\Psi} = (R \cos \phi + Q \sin \phi) / \cos \theta \quad (\text{I-9})$$

$$\sin \gamma = -\sin \phi \cos \theta \sin \beta - \cos \beta \sin \alpha \cos \theta \cos \phi + \cos \alpha \cos \beta \sin \theta \quad (\text{I-10})$$

$$\bar{q} = \rho v^2 / 2 \quad (\text{I-11})$$

$$h = \int_{t_0}^t v \sin \gamma dt + h(t_0) \quad (\text{I-12})$$

Equations I-1, -2, and -3 describe the resultant component forces acting upon the aircraft in terms of the forward acceleration and wind angle rates. These force equations are written in the wind axis (V, η , L) coordinate system. Equations I-4, -5, and -6 describe the angular accelerations defined in the body axis coordinate system by the wind angles α and β as shown in Figure I-1. Equations I-7, -8, and -9 are the kinematic relationships between the airframe body rates and the Euler angular rates. Equations I-10, -11, and -12 define the sine of the flight path angle, γ , the dynamic pressure, \bar{q} , and the altitude, h.

The equations of motion include gun recoil forces and moments. In Equations I-1, -2, and -3, the force components, F_{G_V} , F_{G_η} , and F_{G_L} are determined by transforming the gun recoil force from gun to wind axis coordinates. In Equations I-4, -5, and -6, the moment components, M_{G_x} , M_{G_y} , and M_{G_z} , are determined by transforming the gun recoil moment from gun to body axis coordinates.

The nonlinear aerodynamic derivatives used by the airframe equations of motion are represented by tabular data. The stability coefficients, or their derivatives, are tabulated as functions of the actual values of Mach number, angle of attack, and in some cases control surface deflections or sideslip angle. Since the duration of a digital aerial weapon delivery simulation is usually less than 10 seconds, the altitude of the aircraft usually varies no more than 10,000 ft. Therefore, the tables were not constructed as functions of altitude.

The dimensionless total aerodynamic force coefficients in Equations I-1, -2, and -3 are the drag coefficient, C_D , the lift coefficient, C_L , and the side

force coefficient, C_Y . The lift and drag coefficients are written in the stability axis coordinate system described by Figure I-1. If the aerodynamic force derivatives to be used in the simulation are defined in another axis system, the derivatives must be transformed into the stability axis system by a method outside of the program. The aerodynamic derivatives of the total force coefficients also include the effects of an additional longitudinal control surface such as the canard, δ_C .

In terms of the stability derivatives the total drag coefficient is:

$$C_D = C_D(\alpha, M) + C_D(\delta_C) \quad (I-13)$$

The lift coefficient is written in terms of stability derivatives as:

$$C_L = C_L(\alpha, M) + C_L(\delta_C) - C_{Z_{\delta_s}}(M) \delta_s - \frac{C}{2v} (C_{Z_Q}(M) Q + C_{Z_{\dot{\alpha}}}(M) \dot{\alpha}) \quad (I-14)$$

The total sideforce coefficient defined in terms of wind axis aerodynamic derivatives is:

$$C_Y = C_Y(\alpha, M, \beta) + C_Y(\delta_C) + C_{Y_{\delta_r}} \delta_r + C_{Y_{\delta_a}}(\alpha, \delta_s, M) \delta_a + C_{Y_{\delta_D}} \delta_D + \frac{b}{2v} \{C_{Y_P}(\alpha, M) P + C_{Y_R}(\alpha, M) R\} \quad (I-15)$$

The dimensionless aerodynamic moment coefficients in Equations I-4, -5, and -6 are the roll moment coefficient, C_ℓ , the yaw moment coefficient, C_n , and the pitch moment coefficient, C_m . These dimensionless coefficients are defined in terms of body axis derivatives. If the aerodynamic moment derivatives to be used in the simulation are defined in the stability axis system, then the subroutine transforms these derivatives into the body axis coordinate system. The total roll aerodynamic moment coefficient is:

$$C_\ell = C_\ell(\alpha, M, \beta) + C_\ell(\delta_C) + C_{\ell_{\delta_a}}(\alpha, \delta_s, M) \delta_a + C_{\ell_{\delta_r}} \delta_r + C_{\ell_{\delta_D}} \delta_D + \frac{b}{2v} \{C_{\ell_P}(\alpha, M) P + C_{\ell_R}(\alpha, M) R\} \quad (I-16)$$

The total yaw aerodynamic moment coefficient is:

$$C_n = C_n(\alpha, M, \beta) + C_n(\delta_C) + C_{n_{\delta_a}}(\alpha, \delta_s, M) \delta_a + C_{n_{\delta_r}} \delta_r + C_{n_{\delta_D}} \delta_D + \frac{b}{2v} \{C_{n_P}(\alpha, M) P + C_{n_R}(\alpha, M) R\} \quad (I-17)$$

The total pitch aerodynamic moment coefficient is:

$$C_m = C_m(\alpha, M) + C_m(\delta_C) + C_{m\delta_S}(M) \delta_S + \frac{c}{2v} \{ C_{m\dot{\alpha}}(M) \dot{\alpha} + (C_{mQ}(M) + C_{mQ}(\delta_C)) Q \} \quad (I-18)$$

Simulation of advanced aircraft with differential tail control surfaces requires that flexibility effects due to rudder deflections be included in the rudder sideforce, rolling moment and yawing moment aerodynamic derivatives. These aerodynamic derivatives are:

$$C_{Y\delta_r} = C_{Y\delta_r(f)}(M) * C_{Y\delta_r}(\alpha, M, \beta) \quad (I-19)$$

$$C_{l\delta_r} = C_{l\delta_r(f)}(M) * C_{l\delta_r}(\alpha, \delta_r, M, \beta) \quad (I-20)$$

$$C_{n\delta_r} = C_{n\delta_r(f)}(M) * C_{n\delta_r}(\alpha, \delta_r, M, \beta) \quad (I-21)$$

If the aircraft being simulated does not require the rudder flexibility effects, then $C_{Y\delta_r(f)}$, $C_{l\delta_r(f)}$, and $C_{n\delta_r(f)}$ are set to unity.

The differential tail effects due to tail boom flexibility for the differential tail sideforce, rolling moment, and yawing moment aerodynamic derivatives are:

$$C_{Y\delta_D} = C_{Y\delta_D(TF)}(M) * C_{Y\delta_D}(\alpha, \delta_S, M) + C_{Y\delta_D(F)}(M, \delta_S, \alpha) \quad (I-22)$$

$$C_{l\delta_D} = C_{l\delta_D(TF)}(M) * C_{l\delta_D}(\alpha, \delta_S, M) + C_{l\delta_D(F)}(M, \delta_S, \alpha) \quad (I-23)$$

$$C_{n\delta_D} = C_{n\delta_D(TF)}(M) * C_{n\delta_D}(\alpha, \delta_S, M) + C_{n\delta_D(F)}(M, \delta_S, \alpha) \quad (I-24)$$

If the aircraft being simulated does not require the differential tail flexibility effects then $C_{Y\delta_D(TF)}$, $C_{l\delta_D(TF)}$, and $C_{n\delta_D(TF)}$ are set to unity and $C_{Y\delta_D(F)}$, $C_{l\delta_D(F)}$, and $C_{n\delta_D(F)}$ are set to zero.

If the components of aerodynamic sideforce, rolling moment, and yawing moment due to spoiler deflections are to be included, then the effectiveness of the aileron, $C_{\delta_a}^*$, and the effectiveness of the spoiler, $C_{\delta_{sp}}$, must be combined by the following formula, external to the program:

$$C_{\delta_a} = C_{\delta_a}^* + k C_{\delta_{sp}} \quad (I-25)$$

where k is the ratio of the maximum spoiler deflection to the maximum aileron deflection.

Wind gust is applied to the airplane equations of motion through the aerodynamic terms only. This is accomplished by modifying the independent variables of angle of attack and sideslip angle by wind gust when they are used to find the aerodynamic derivatives in table lookups.

Advanced aircraft simulations requiring variation of the aircraft's weight, center of gravity, and inertia characteristics can be accomplished without reprogramming the aerodynamic data. When a center of gravity different than that referenced by the tabular aerodynamic moment data is specified, the following equations transform the aerodynamic moment derivatives corresponding to the desired center of gravity location.

$$C_m = C_m + C_L \Delta_{CG} \quad (I-26)$$

$$C_{m_{\delta_s}} = C_{m_{\delta_s}} - C_{Z_{\delta_s}} \Delta_{CG} \quad (I-27)$$

$$C_{n_p} = C_{n_p} + \Delta_{CG} \frac{c}{b} C_{Y_p} \quad (I-28)$$

$$C_{n_r} = C_{n_r} + \Delta_{CG} \frac{c}{b} C_{Y_r} \quad (I-29)$$

$$C_{n_{\beta}} = C_{n_{\beta}} + \Delta_{CG} \frac{c}{b} C_{Y_{\beta}} \quad (I-30)$$

$$C_{n_{\delta_a}} = C_{n_{\delta_a}} + \Delta_{CG} \frac{c}{b} C_{Y_{\delta_a}} \quad (I-31)$$

$$C_{n_{\delta_r}} = C_{n_{\delta_r}} + \Delta_{CG} \frac{c}{b} C_{Y_{\delta_r}} \quad (I-32)$$

$$C_{n_{\delta_D}} = C_{n_{\delta_D}} + \Delta_{CG} \frac{c}{b} C_{Y_{\delta_D}} \quad (I-33)$$

where $\Delta_{CG} = (\text{CG location}) - (\text{table reference CG location})$.

The effect of the center of gravity shift on the tail length ratio is also simulated. The aerodynamic tail length is the distance from the center of pressure on the wing to the center of pressure on the horizontal tail. The tail length ratio is described by:

$$\Delta_{TL} = \frac{T.L. - c \text{ (C.G. location)}}{T.L. - c \text{ (table reference C.G. location)}} \quad (I-34)$$

where the center of gravity location is specified as a percentage of the mean aerodynamic chord. The effects on the coefficients are described by the equations

$$C_{m_{\delta_s}} = C_{m_{\delta_s}} \Delta_{TL} \quad (I-35)$$

$$C_{m_Q} = C_{m_Q} \Delta_{TL} \quad (I-36)$$

$$C_{m_{\dot{\alpha}}} = C_{m_{\dot{\alpha}}} \Delta_{TL} \quad (I-37)$$

The simulation of the aircraft's acceleration at any body location is formulated by

$$\bar{a}_p = \bar{a}_{cg} + \bar{a}_r \quad (I-38)$$

where the body axis components of \bar{a}_{cg} , the acceleration of the aircraft's center of gravity, are simulated by:

$$a_{cgx} = [T \cos \delta_e + \bar{q}S (C_L \sin \alpha - C_D \cos \alpha)]/m \quad (I-39)$$

$$a_{cgy} = \bar{q}S C_Y/m \quad (I-40)$$

$$a_{cgz} = [-T \sin \delta_e - \bar{q}S (C_L \cos \alpha + C_D \sin \alpha)]/m \quad (I-41)$$

The body axis components of \bar{a}_r , the acceleration of the (x_r, y_r, z_r) location of the aircraft relative to the center of gravity due to the angular velocities and accelerations are simulated by:

$$\begin{bmatrix} a_{rx} \\ a_{ry} \\ a_{rz} \end{bmatrix} = \begin{bmatrix} (+Q^2 + R^2) (-\dot{R} + PQ) & (\dot{Q} + PR) \\ (\dot{R} + PQ) & -(R^2 + P^2) & (-\dot{P} + QR) \\ (-\dot{Q} + RP) & (\dot{P} + QR) & -(P^2 + Q^2) \end{bmatrix} \begin{bmatrix} x_r \\ y_r \\ z_r \end{bmatrix} \quad (I-42)$$

The normal acceleration, measured by an accelerometer at any aircraft location relative to the center of gravity and oriented at angle α_n relative to the z body axis, is simulated in terms of the body axis components of \bar{a}_p by:

$$g_n = -\frac{1}{g} (a_{pz} \cos \alpha_n + a_{px} \sin \alpha_n) \quad (I-43)$$

The lateral acceleration equation is simulated as a_{py} . The angular orientation of the normal accelerometer with respect to the body axes is shown in Figure I-1.

I.2 Flight Control System Model

The flight control system model for the air-to-air TAWDS(AA) program can be used to mathematically describe the flight control laws developed in the Tactical Weapon Delivery (TWeaD) Program (References I-1 - I-5), the Survivable Flight Control System (SFCS) Program (References I-6 - I-8), and the Multimode Program (References I-9 - I-10), as well as the flight control systems of current high performance fighter and attack aircraft. The structure of the TAWDS(AA) model also allows for decoupling design techniques to enable the mechanization of longitudinal direct force modes for precise attitude or flight path control. The TAWDS(AA) program includes not only feedback control laws but also interconnects, which couple pilot command inputs.

The flexibility of the model is shown by Figures I-2 and I-3. The generic model can simulate (1) pertinent control system characteristics and flight control laws and (2) various types of existing and advanced flight control systems. Capabilities include pitch, roll, and yaw axes series servo authorities; pitch, roll, and yaw axes feedback control laws; and integrated control system mechanization.

The air-to-air generic flight control system model, illustrated in Figures I-2 and I-3, can be used to mathematically describe both electrical and mechanical mechanizations. The electrical command signals are processed by flight control compensation networks, along with the feedback signals from air data systems and rate gyros and accelerometers. These processed signals are transmitted to command the hydraulically actuated servos which mechanically drive the hydraulic control surface actuators. The pilot's mechanical inputs are linked directly to the control surface actuators.

Pitch control can be provided by one or two longitudinal control surfaces, the elevator, and, optionally, horizontal canard surfaces. The canard is used for direct force control, gust alleviation, or drag alleviation. Roll control is provided by two lateral control surfaces and directional control by the rudder. The primary lateral control is augmented either through two lateral control surfaces such as ailerons and spoilers, whose respective deflections have a constant ratio to each other, or through the differential deflection of an all movable horizontal stabilator.

APPENDIX I REFERENCES

- I-1 Carleton, D. L., et al, "Development and Evaluation of the TWead II Flight Control Augmentation System," FTC-TD-72-1, November 1970.
- I-2 Carleton, D. L. and Powell, C. W., "Limited Air-to-Air Tracking and Qualitative Flying Qualities Evaluation of Selected Flight Control System Configurations in the F-4C/E Aircraft," FTC-TD-71-4, August 1971.
- I-3 Rubertus, D.P., "TWead Control Augmentation System," National Aerospace Electronics Conference, Dayton, Ohio, 15-17 May 1972.
- I-4 Richard, R. R., et al, "Stability and Control Evaluation of an F-4C Aircraft with a High Gain Adaptive Control Augmentation System," FTC-SD-71-17, June 1971.
- I-5 Orwat, J. C., et al, "Weapon Delivery Evaluation of an F-4C Aircraft with a High Gain Adaptive Control Augmentation System," FTC-TR-71-35, August 1971.
- I-6 Kisslinger, Robert L. and Wendl, Michael J., "Survivable Flight Control System, Interim Report No. 1 - Studies, Analyses and Approach, Supplement 1 - Supplement for Control Criteria Studies," Technical Report AFFDL-TR-71-20, May 1971.
- I-7 Hooker, D. S., Kisslinger, R. L., et al, "Survivable Flight Control System Final Report," Technical Report AFFDL-TR-73-105, December 1973.
- I-8 Ettinger, R. C., Majoros, R. L., and Powell, C. W., "Air Force Evaluation of the Fly-by-Wire Portion of the Survivable Flight Control System Advanced Development Program," FTC-TR-73-32.
- I-9 Quinlivan, R. P., "Multimode Flight Control Definition Study for Precision Weapon Delivery," Technical Report AFFDL-TR-71-39, June 1971.
- I-10 Quinlivan, R. P., "Multimode Flight Control Definition Study," Technical Report AFFDL-TR-72-55, June 1972.

APPENDIX II
WEAPON FIRE CONTROL SYSTEMS

In the TAWDS programs, weapon fire control systems were modeled for the air-to-air gunnery and air-to-ground bombing and gunnery tasks. The generic sight systems considered are listed in Figure II-1, and represent the basic characteristics of sights used on operational or near-operational fighter aircraft. Target tracking data with the gunnery sights was used in developing the pilot models described in Section 4. For air-to-ground bombing, the FIP (Future Impact Point) sight was selected because (1) unlike the Continuously Computed Impact Point (CCIP) sight, it can be used to determine the pilot's precision tracking characteristics during a bombing pass, (2) it represents a particular solution based on a desired bomb release altitude of the CCIP bomb sight, (3) it can be extended to model a dive-toss type of bomb sight, and (4) it or similar bomb sights will likely be used on fighter aircraft in the near future.

A simplified approach, referred to as the modified vacuum trajectory method, was used in computing the weapon impact for the air-to-ground CCIP and FIP sights. This approach, described in Reference II-1 or in Appendix IV of this report, uses an empirical equation, with the constants evaluated by using weapon delivery tables. However, this approach avoids the need for integrating the nonlinear differential equations that describe the weapon's trajectory and impact point, and thus represents a practical approach for an airborne delivery computer.

The error sources and the equations used to compute the sensitivities of the dynamic errors for the stochastic program are presented in Reference II-1 or in Appendix III of this report.

II.1 Air-to-Air Gunnery Sights

Air-to-air gun fire control sights can be divided into two major classes, Director and Disturbed Reticle sights. These two generic sights are described in Reference II-2. Some of the more familiar Disturbed Reticle implementations are (1) Lead Computing Optical Sight System (LCOSS), (2) Damped Predictive Tracer Sight, and (3) Honest Tracer Line or Hot Line Sight. The Hot Line Sight differs from the others in the lack of damping. Due to the widespread use of LCOSS sights, and their close dynamic relationship to damped predictive tracer type sights, a generic LCOSS sight was configured, along with a Director sight, for the TAWDS(AA) program analysis.

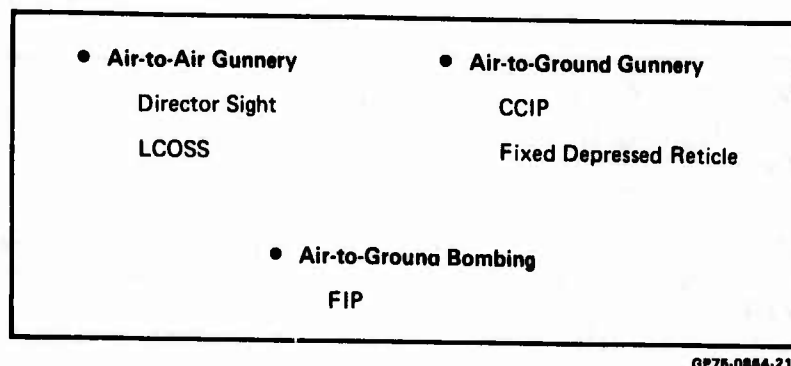


Figure II -1. Generic Sight Systems for Weapon Delivery Tasks

II.1.1 Bullet Time-of-Flight Computation for Air-to-Air Gunsight -

Figure II-2 presents the basic principles of computing the bullet time-of-flight used in the lead angle computations for air-to-air gunsights. This computation avoids the complexity of integrating a bullet to target range, and is applicable to an airborne computer. It is based on equating an approximate equation for predicted future target range, D_{FT} , and predicted future bullet range, D_{FB} , and then solving simultaneously for the bullet time-of-flight, T_F . The resulting quadratic equation is solved by using the quadratic formula, with the smaller root giving the value of T_F .

The ballistic fit equation used to predict future bullet range uses a ballistic coefficient, K_B , which accounts for range shortening due to drag and makes results more consistent with standard 20mm ballistic tables.

In programming the equations shown in Figure II-2, a check in computing T_F is required to accommodate "beam type" attack conditions (target aspect of 90 degrees). In this case, the attacker airspeed is approximately the negative of the range rate, reducing the quadratic equation for T_F to a linear equation.

II.1.2 The LCOSS Sight - The LCOSS sight model programmed in the TAWDS(AA) computer program contains the basic characteristics associated with advanced LCOSS or Damped Predictive Tracer Sights described in References II-2 and II-3. These characteristics include the use of (1) ownship body rates, (2) ownship load factor as an estimate of target acceleration, and (3) attacker angle of attack and airspeed to account for ballistic curvature. Each of these inputs

Geometry, $D_{FT} = R + (\dot{R} + V_A) T_F$	(1)	
Ballistic Fit, $D_{FB} = \frac{(V_A + V_M) T_F}{1 + K_D T_F}$	(2)	
Equation (1) and (2),		
$R + (\dot{R} + V_A) T_F = \frac{(V_A + V_M) T_F}{1 + K_D T_F}$	(3)	
Solving (3) for T_F ,		
$(\dot{R} + V_A) K_D T_F^2 + (\dot{R} - V_M + K_D R) T_F + R = 0$	(4)	
Employing the Quadratic Formula,		
$T_F = \frac{-K_2 - \sqrt{K_2^2 - 4K_1 R}}{2K_1}$	(5)	
Where $K_1 = (\dot{R} + V_A) K_D$		
$K_2 = \dot{R} - V_M + K_D R$		
$K_D = K_B \sqrt{V_M^2 + V_A^2} \rho / \rho_0$		

D_{FT}	- Predicted Future Target Range
D_{FB}	- Predicted Future Bullet Range
R	- Present Range
\dot{R}	- Present Range Rate
T_F	- Bullet Time-of-Flight
V_A	- Attacker Velocity
V_M	- Bullet Muzzle Velocity
K_D	- Ballistic Drag Coefficient
ρ / ρ_0	- Attacker Relative Air Density
K_B	- Ballistic Constant (0.00614 for 20 mm bullet)

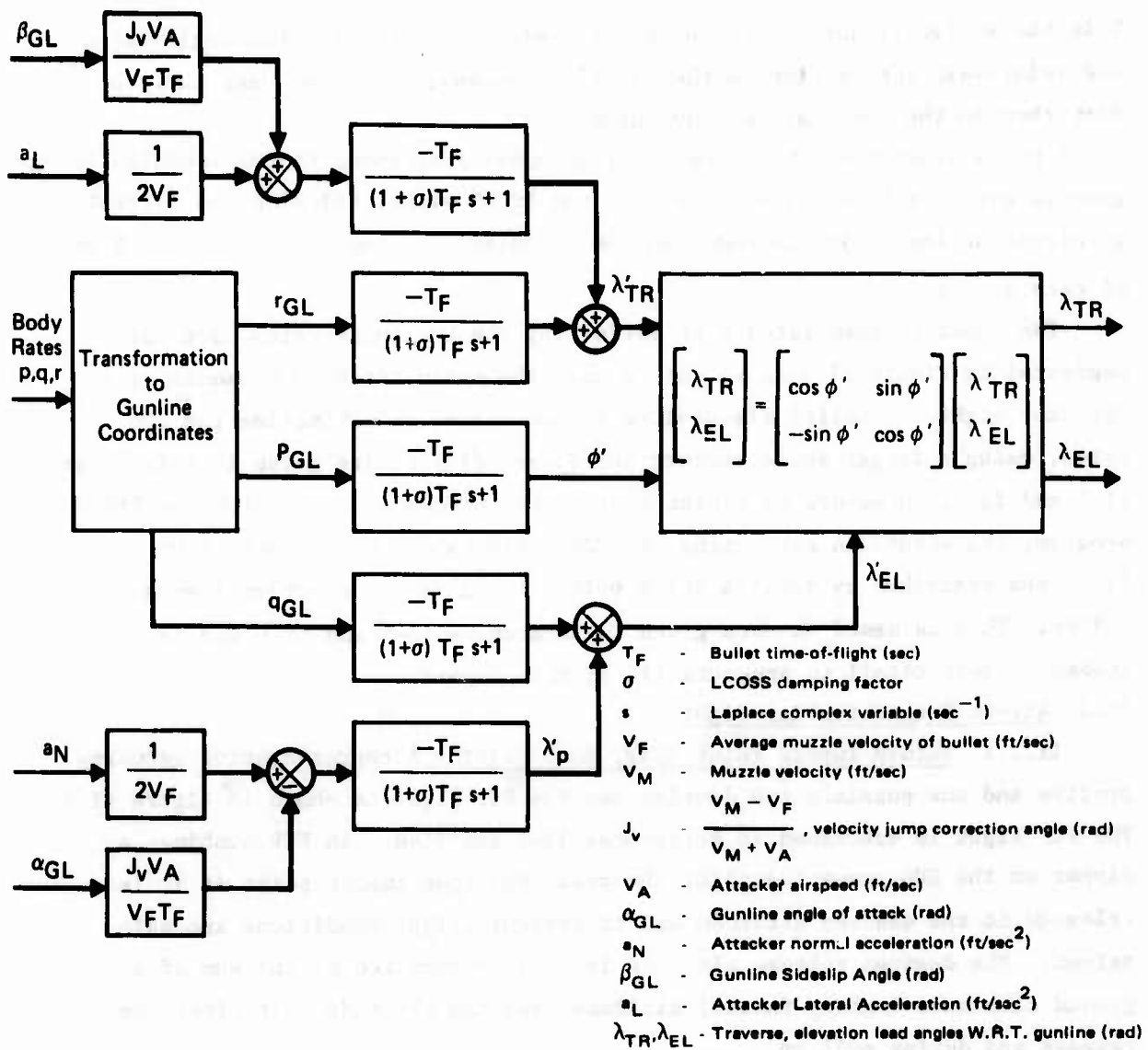
GP75-0864-206

Figure II-2. Basic Principles of the Time-of-Flight Computation Used in LCOSS and Director Sights

is damped by the time constant, $(1+\sigma)T_F$, as shown in Figure II-3, which describes the dynamics of the LCOSS sight model in block diagram form. This model does not explicitly include the two-degree-of-freedom gyro generally associated with an LCOSS sight, but the basic gyro dynamics are accounted for by the time constant $(1+\sigma)T_F$, and the roll angle transformation used in obtaining the lead angles.

Although they are generally not used in disturbed reticle type sights, the model includes sideslip and lateral acceleration inputs which are multiplied by a gain (or switch) of magnitude of 0 or 1 in the TAWDS(AA) program. These inputs are included in TAWDS(AA) so this sight model will be compatible with aircraft whose control law mechanization allows for sideslip.

II.1.3 The Director Sight - The primary difference in a Director sight is the use of Line-Of-Sight (LOS) angle rates instead of ownship body rates.



GP75-0864-207

Figure II-3. Functional Flow Diagram of Generic Lead Computing Optical Sight System (LCOSS)

This has a significant effect on loop dynamics. Because the LOS angle rates are relatively insensitive to the pilot's commands, it is not necessary to damp them in the same way as body rates.

A block diagram of the Director sight model programmed in the TAWDS(AA) program is given in Figure II-4. As with the LCOSS sight, sideslip and lateral acceleration inputs are included in the TAWDS(AA) program (multiplied by a gain of zero or one).

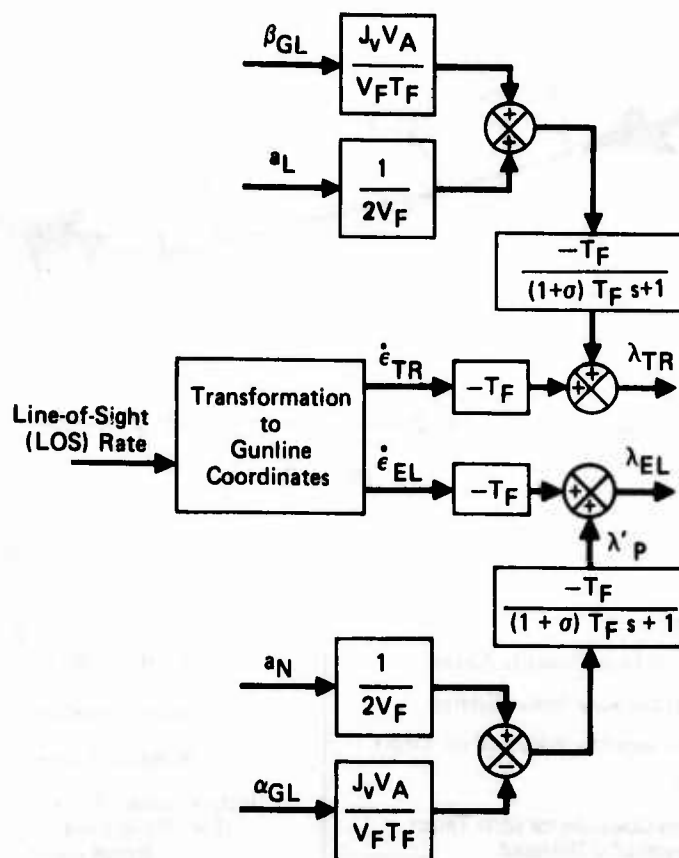
The dynamics associated with estimating the LOS angle rates have been neglected in Figure II-4 so as not to mask the basic tracking dynamics of a Director sight. Detailed discussions on approaches to estimating the LOS rates, using a target angle tracker and Kalman filter, are given in References II-4 and II-5. However, in making Monte Carlo stochastic runs with the TAWDS(AA) program, the errors in estimating the LOS angle rates are assumed to be correlated and described by passing white noise through a second-order low-pass filter. This is based on data given in References II-5 and II-6 and is described in more detail in Appendix III of this report.

II.2 Air-to-Ground Bombing Sight

II.2.1 Future Impact Point (FIP) Bomb Sight - A representative geometry profile and one possible HUD display for the FIP sight is shown in Figure II-5. The FIP sight is described in References II-7 and II-8. In FIP bombing, a pipper on the HUD shows the pilot the predicted bomb impact point if it is released at the desired altitude and if present flight conditions are maintained. The desired release altitude is usually computed as the sum of a ground clearance (safety factor) altitude, and the altitude lost after bomb release and during pull up.

The FIP bombing system can be considered a particular solution to the CCIP bombing system. The pilot's task is to steer the aircraft to keep the FIP pipper on the target until the bomb release altitude is reached. As a cue to the time-to-go to release, a cross is displayed to show the bomb's instantaneous (present) impact point. This point, which is called the Displayed Impact Point (DIP), is based on the CCIP bombing equations. The angular difference between the FIP pipper and the DIP cross is proportional to range-to-go, and hence provides the time-to-go to release cue. With an automatic release mode, the bomb is automatically released when the DIP cross passes through the FIP reticle (with bomb enable button depressed).

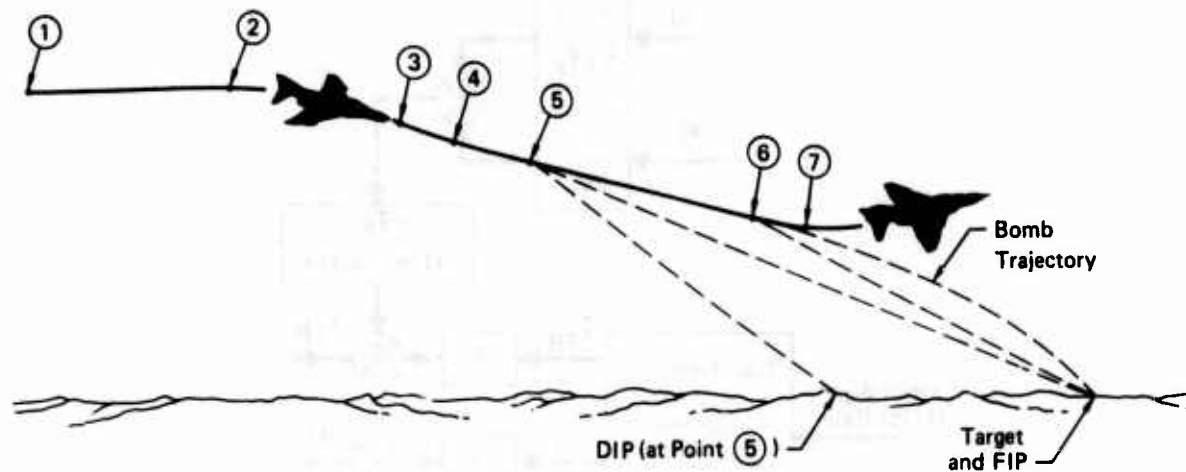
In implementing the FIP mode, slant range measurements are made along the Line-Of-Sight to the FIP pipper. Aircraft altitude relative to the future



- $\dot{\epsilon}_{TR}, \dot{\epsilon}_{EL}$ - Traverse, elevation LOS rates in gunline coordinates (rad/sec)
- V_F - Average muzzle velocity of bullet (ft/sec)
- V_M - Muzzle velocity (ft/sec)
- J_V - $\frac{V_M - V_F}{V_M + V_A}$, velocity jump correction angle (rad)
- V_A - Attacker airspeed (ft/sec)
- T_F - Bullet time-of-flight (sec)
- α_{GL} - Gunline angle of attack (rad)
- a_N - Attacker normal acceleration (ft/sec²)
- β_{GL} - Gunline sideslip angle (rad)
- a_L - Attacker lateral acceleration (ft/sec²)
- $\lambda_{TR}, \lambda_{EL}$ - Traverse, elevation lead angles W.R.T. gunline (rad)

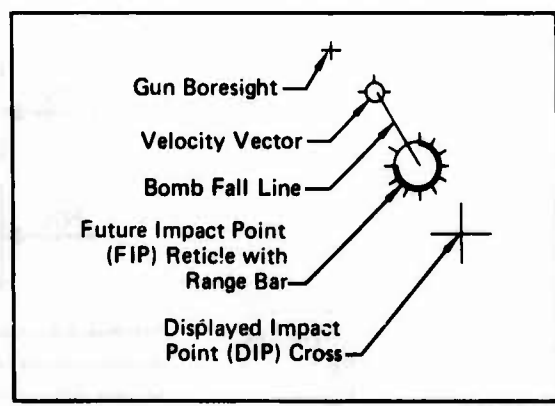
Figure II -4. Functional Flow Diagram of Director Sight

GP75-0864-209



Head-Up Display

- ① Target Detection
- ② Start of Turning Dive Towards Target
- ③ Air-to-Ground Delivery Mode Entered
- ④ Aircraft Maneuvered to Place FIP on Target
- ⑤ FIP on Target
- ⑥ DIP Moves into Coincidence with Target - Bombs Automatically Released
- ⑦ Start of Pullup Maneuver



GP75-0064-95

Figure II -5. Profile View of Representative FIP Bombing Attack

impact point is used in computing the elevation positioning angles of the FIP and DIP symbols on the HUD. For an uneven terrain, the DIP symbol represents the impact point in the horizontal plane containing the future impact point. This provides a stable vertical position for the FIP and DIP symbols.

II.2.2 FIP Bombing Sight Equations in TAWDS(AG) Program - The bomb component equations in TAWDS(AG) for the FIP bombing sight are summarized in Figure II-6. The components are along and orthogonal to the ground velocity vector. The effect of rack time delay, T_D , is included in the bomb equations, which references them to the point at which the release signal is given rather than to the actual release point.

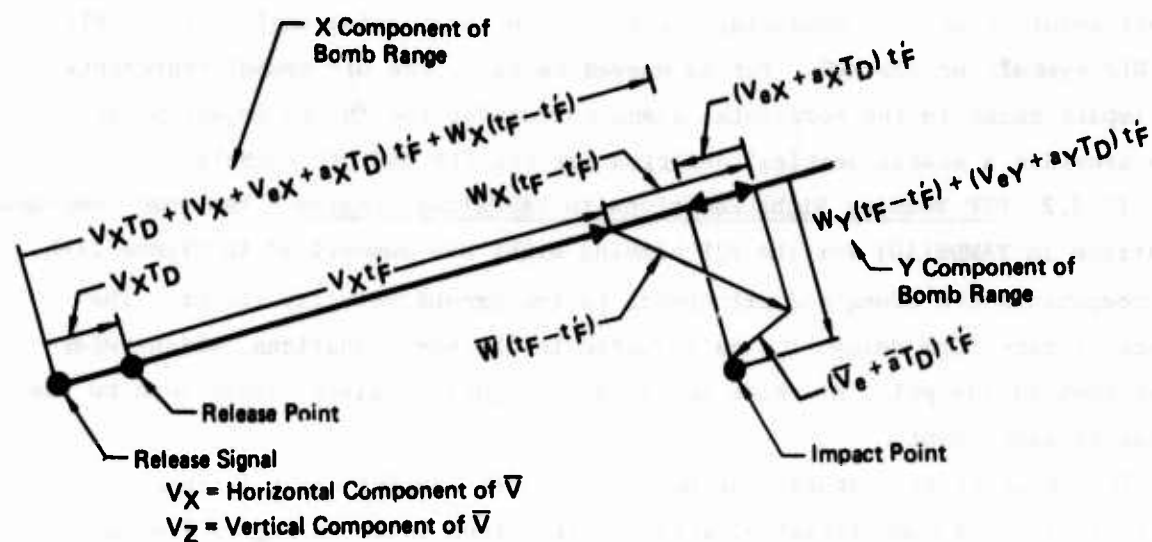
The sequence of computations used in the FIP bombing sight is shown in Figure II-7. The bomb impact equations differ from those in Figure II-6 by the time-to-go to release factor.

For the first computation cycle the value of the bomb retardation factor is set equal to one, since a gravity drop term for non-zero values of the aircraft's dive angle is not available at the start of computations. The bomb retardation factor converges to the correct value after several computational cycles.

In the computational sequence, the expression for the bomb's time-of-fall in air mass (assuming zero wind) is computed, using the quadratic solution for the vertical equations of the modified vacuum trajectory. The altitude used in this computation is the desired bomb release altitude with respect to the target. It is the sum of three components: (1) desired ground clearance (safety factor), (2) altitude lost during pull up, and (3) altitude lost between bomb release and start of pull up. The gravity drop term is then obtained and the bomb retardation factor is updated. Finally, the horizontal components of bomb range, as determined by the two horizontal equations, are determined, along with present altitude above target, for positioning the FIP reticle on the HUD.

Because the bomb retardation factor is the only parameter used from the previous cycle, and its value changes slowly, the equations converge quickly and maintain a highly accurate dynamic solution. As a result, only one pass through the cycle is required.

The altitude lost during pull up is a function primarily of dive angle and velocity. Figure II-8 gives curves for the actual altitude lost by an F-4 aircraft during a 4G pull up. (Similar data is also available for other



$$\begin{aligned}
 h_R &= V_z T_D + (V_z + V_{eZ} + a_z T_D) t_f + g C_B t_f^2 / 2 \\
 X_B &= V_x T_D + (V_x + V_{eX} + a_x T_D) t_f + W_x (t_f - t_f) \\
 Y_B &= (V_{eY} + a_y T_D) t_f + W_y (t_f - t_f)
 \end{aligned}
 \left. \vphantom{\begin{aligned} h_R \\ X_B \\ Y_B \end{aligned}} \right\} \begin{array}{l} \text{Complete} \\ \text{Modified Vacuum} \\ \text{Trajectory} \\ \text{Equations} \end{array}$$

- a - Aircraft acceleration during T_D
- g - Acceleration of gravity ($\approx 32.174 \text{ ft/sec}^2$)
- C_B - Bomb retardation factor
- h_R - Bomb release altitude relative to impact point
- T_D - Bomb rack release time delay
- t_f - Actual bomb time-of-fall
- t_f - Bomb time-of-fall in air mass (assuming zero wind)
- \bar{V} - Aircraft ground track velocity vector
- V_e - Bomb ejection velocity vector
- W - Horizontal wind velocity vector
- x_B - Bomb ground range along \bar{V}
- y_B - Bomb ground range orthogonal to \bar{V}
- Subscript x - Horizontal component of vector along \bar{V}
- Subscript y - Horizontal component of vector orthogonal to \bar{V}
- Subscript z - Vertical component of vector

GP78-0864-55

Figure II -6. Summary of Bomb Component Equations at Bomb Release Signal in Ground Track Velocity Coordinates

$C_B = 1$ [First Cycle Only]
 $h_R = h_{SF} + h_L + h_{\Delta} + V_Z T_D$
 $t'_F = \frac{-(V_Z + V_{eZ} + a_Z T_D) + \sqrt{(V_Z + V_{eZ} + a_Z T_D)^2 + 2g C_B (h_R - V_Z T_D)}}{g C_B}$ (From Vertical Trajectory Equation with $h_R = h$)

$D_g = \frac{1}{2} g C_B t'^2_F$
 $C_B = 1 + K_1 D_g^{K_2} V_A^{K_3} (\rho_T / \rho_0)$
 $t_F - t'_F = (K_4 C_B^{K_5} - 1) t'_F$

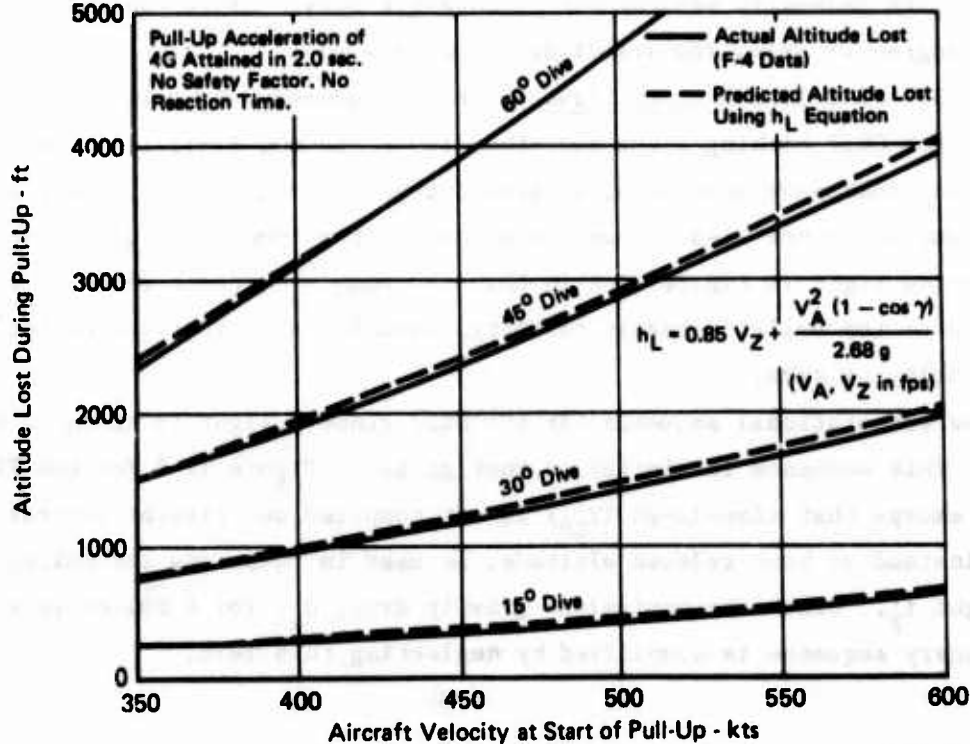
$T_{GO} = \frac{h - D_g - (V_E t'_F / \cos \theta_A)}{V_Z} - \frac{(V_X + V_{EX}) t'_F}{V_X} - T_D$
 $X_B = V_X T_D + (V_X + V_{eX} + a_X T_D) t'_F + W_X (t_F - t'_F) + V_X T_{GO}$
 $Y_B = (V_{eY} + a_Y T_D) t'_F + W_Y (t_F - t'_F)$

h, X_B, Y_B are Then Transformed Through Drift Angle, δ , Pitch, θ_A , and Roll, ϕ , and Converted to Corresponding Angles for Positioning the FIP Reticle of the HUD.

ρ_T / ρ_0	- Target Relative Air Density
D_g	- Equivalent Gravity Drop
K_1, \dots, K_5	- Constants Computed from Bomb Tables
θ_A	- Aircraft Pitch Angle
h	- Present Aircraft Altitude
h_{SF}	- Safety Factor or Ground Clearance Altitude
h_L	- Altitude Lost During Pullup
h_{Δ}	- Altitude Increment from Bomb Release to Start of Pullup
T_{GO}	- Time-to-Go to Bomb Release

GP75-0864-83

Figure II -7. Sequence of Computations for FIP Bombing Sight



GP75-0864-84

Figure II -8. Estimating Altitude Lost During Dive Recovery for 4G Pullup

G values.) The dashed curves show the results of the simplified mathematical equation used in the TAWDS(AG) program.

II.3 Air-to-Ground Sights

For the air-to-ground gunnery weapon delivery task, the Fixed Depressed Reticle and CCIP sights are included in the TAWDS(AG) program.

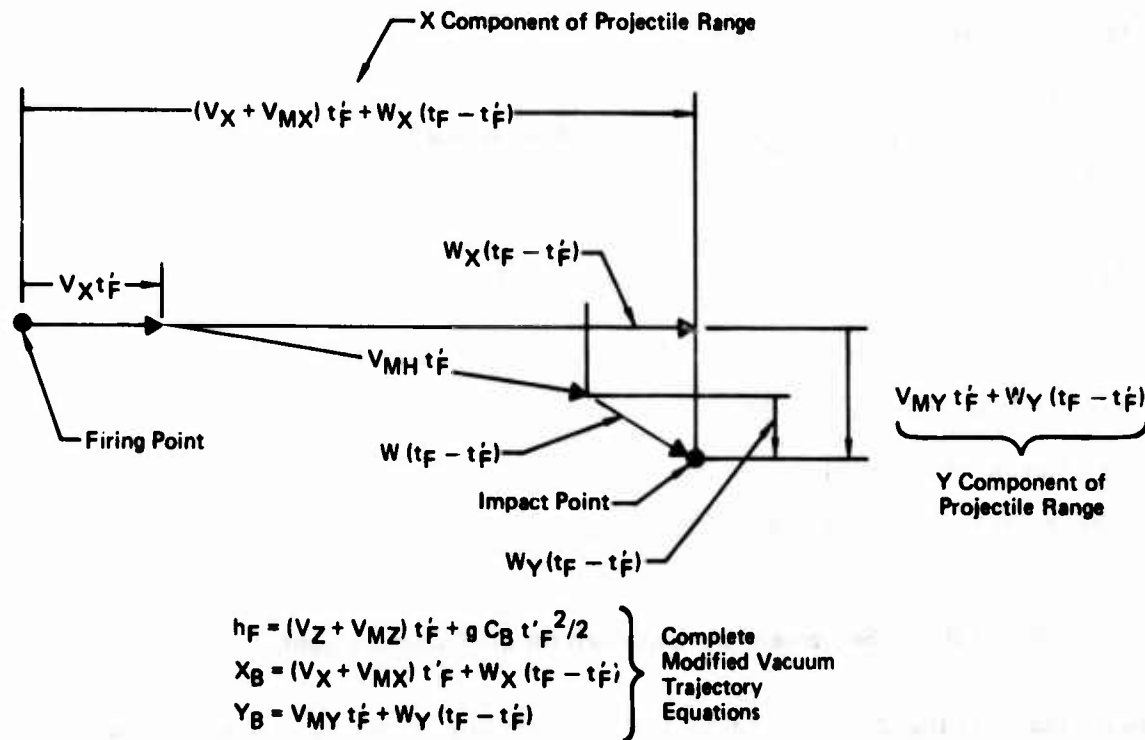
II.3.1 The Fixed Depressed Reticle Gunnery Sight - For the Fixed Depressed Reticle sight, the pilot chooses a set of nominal firing conditions, namely airspeed, dive angle, and altitude or range. The following information is displayed to the pilot: (1) airspeed, (2) pitch angle, (3) radar range or altitude, and (4) angle of attack.

For the Fixed Depressed Reticle sight, there are two basic options in the TAWDS(AG) program. In one option, the pilot chooses a nominal firing altitude and uses the altitude display. In the other, the pilot chooses a nominal firing range. The pilot can estimate target range by comparing the projected mil area of the target to that of the pipper. If radar range is displayed to the pilot, however, it is assumed that the radar is slaved to the pipper.

Note that the dive angle is not directly displayed in some current fighter aircraft. Theoretically, it can be calculated by monitoring both the pitch and angle-of-attack displays. However, because of the heavy workload at this time, pilots generally monitor the pitch angle only. Since the angle of attack is one degree or less, the resulting error is small.

II.3.2 The CCIP Gunnery Sight - The CCIP gunnery sight is essentially the same as the CCIP bombing sight described in References II-1, II-7, and II-8. The bullet component equations, in ground track velocity coordinates, are summarized in Figure II-9. These equations differ from those given for the FIP bombing sight in Figure II-6 in that the bomb's ejection velocity is replaced with the bullet's muzzle velocity, assuming also that the bullet's firing delay is zero.

The computational sequence for the CCIP gunnery sight is given in Figure II-10. This sequence is similar to that given in Figure II-7 for the FIP sight, except that time-to-go (T_{GO}) is not computed and present aircraft altitude, instead of bomb release altitude, is used in computing the bullet time-of-flight t'_F . Since the equivalent gravity drop, D_g , for a bullet is small, the gunnery sequence is simplified by neglecting this term.



- C_B - Bullet retardation factor
- g - Acceleration of gravity ($\approx 32.174 \text{ ft/sec}^2$)
- h_F - Firing altitude relative to impact point
- t_F - Actual bullet time-of-flight
- t'_F - Bullet time-of-flight in air/mass (assuming zero wind)
- \vec{V} - Aircraft ground track velocity vector
- \vec{V}_M - Muzzle velocity vector
- \vec{W} - Horizontal wind velocity vector
- X_B - Bullet ground range along \vec{V}
- Y_B - Bullet ground range orthogonal to \vec{V}
- Subscript X - Horizontal component of vector along \vec{V}
- Subscript Y - Horizontal component of vector orthogonal to \vec{V}
- Subscript Z - Vertical component of vector

GP75-0064-53

Figure II -9. Summary of Bullet Component Equations in Ground Track Velocity Coordinates

II.4 Other Sight System Considerations

Dive-Toss Bombing and Air-to-Ground Rocketry can also be incorporated in the TAWDS(AG) program.

II.4.1 Dive-Toss Bombing Sight - The FIP bombing sight program can be extended to include dive-toss delivery. References II-1, II-7, and II-8 describe the dive-toss bombing sight and how it can be interfaced with the FIP sight. The FIP bombing sight equations would be modified as follows. Instead of designating the target with the airspeed or ground track velocity vector, as is normally done in dive-toss implementations, the FIP pipper would be used. The computed bomb impact point would be determined by using present aircraft

$$C_B = 1 \text{ [First Cycle Only]}$$

$$h_F = h_B = h$$

$$t_{\dot{F}} = \frac{-(V_Z + V_{MZ}) + \left[(V_Z + V_{MZ})^2 + 2g C_B h \right]^{1/2}}{g C_B} \quad \text{(From Vertical Trajectory Equation with } h_F = h)$$

$$C_B = 1 + K_1 t_{\dot{F}}^{K_2} (\rho_T / \rho_0)^{K_3} \quad \rho_T / \rho_0 - \text{Target Relative Air Density}$$

$$t_F - t_{\dot{F}} = (K_4 C_B^{K_5} - 1) t_{\dot{F}} \quad K_1, \dots, K_5 - \text{Constants Computed from Bullet Tables}$$

$$X_B = (V_X + V_{MX}) t_{\dot{F}} + W_X (t_F - t_{\dot{F}})$$

$$Y_B = V_{MY} t_{\dot{F}} + W_Y (t_F - t_{\dot{F}})$$

h, X_B, Y_B are Then Transformed Through Drift Angle, δ ; Pitch, θ_A ; and Roll, ϕ ; and Converted to Corresponding Angles for Positioning the CCIP Symbol of the HUD.

GP75-0884-52

Figure II-10. Sequence of Computations for CCIP Gunnery Sight

altitude and setting T_{GO} to zero in the FIP bombing sight equations, Figure II-7. Bomb release occurs automatically (if the bomb enable switch is depressed by pilot) during the pull up maneuver when the computed bomb range equals (or exceeds) the computed target range.

The pilot performs a wings-level, constant load factor, pull up while nulling the traverse impact error, until automatic bomb release. The display of the traverse impact error will vary with the aircraft. When the pilot maintains his ground track velocity vector on a displayed vertical line, the bomb traverse impact error will be zero.

II.4.2 Air-to-Ground Rocketry Sights - Since air-to-ground rocketry sights are usually quite similar to air-to-ground gunnery sights, there is no difficulty in adding the rocket sights described in Reference II-1 to the TAWDS (AG) program. For the Fixed Depressed Reticle sight, the rocket manual would be used to determine the reticle position on the HUD. For the CCIP sight, the rocket's velocity at burnout, V_R , would be used in the CCIP gunnery sequence given in Figure II-10 and, along with the rocket trajectory tables, in computing the ballistic retardation factor, C_B .

APPENDIX II

REFERENCES

- II-1. Berger, J. B., et al., "Flight Control Requirements for Weapon Delivery, Interim Report for Period June 1973 - May 1974," Technical Report AFFDL-TR-74-119.
- II-2. Berg, R. L., Sears, M. M., and Zirkle, G. W., "Air-to-Air Fire Control Exposition, Phase I (EXPO I)," AFAL-TR-72-122, April 1972.
- II-3. Berg, R. L. and Sears, M. M., "Air-to-Air Fire Control Exposition, Phase III (EXPO III)," AFAL-TR-73-287, September 1973.
- II-4. Murphy, W. J., Simmons, D. E., and Schneider, J. R., "Advanced Air-to-Air Gun Fire Control System Definition Study (Unclassified Title)," AFAL-TR-73-211, August 1973.
- II-5. Berg, R. L., Murphy, W. J., and Simmons, D. E., "Advanced Gun Fire Control System (AGFCS), Design Study (Phase II)," AFAL-TR-74, April 1974.
- II-6. Corrigan, J. D., "F-15A/GAU-7/A Gun Attack Mode Error Budget and Accuracy Analysis Plan (Unclassified Title)," Report MDC A2226 (Contract F33657-72-C-0637) February 1974.
- II 7. "Data and Support for the USAF Moving Base Air-to-Ground Simulation of the Vector Lift Fighter," MDC Report A2733, 9 May 1974.
- II-8. "Advanced Fighter Technology Integration, Near Term Demonstrator (Phase I), (Simulation Data Package)", MDC A3301, submitted to AFFDL/PTC, 1 April 1975.

APPENDIX III

ERROR SOURCES AND SENSITIVITIES FOR WEAPON DELIVERY SIGHTS

The source errors, the stationary sensitivity equations, and the dynamic tracking error equations given in Reference III-1 for air-to-ground gunnery are extended to bombing weapon delivery in this Appendix. The derivations of these equations are the same as described in Reference III-1. For completeness, the source errors for gunnery and the associated equations are also included. In addition, the error sources used in simulating the LCOSS and Director air-to-air gunnery sights are tabulated. The symbols used are listed in Section III.3.

III.1 Air-to-Air Gunnery

For air-to-air gunnery the Monte Carlo method is used in determining the bullet miss statistics instead of the covariance method used in air-to-ground weapon delivery. While the covariance method uses linearized perturbation equations, the Monte Carlo method uses non-linear equations. The bullet miss statistics are computed by making multiple runs, with different error values being added to selected variables on each run.

The most significant error sources are listed in Figure III-1. Aircraft body rates and linear accelerations are not included, because error magnitudes generally assumed in their measurements are so small they would have negligible effect on bullet miss statistics. Most of the error sources affect pipper computation and positioning. However, errors in the muzzle velocity and gunline attitude are used only in integrating the bullet; their nominal values are used in the pipper computation.

Each of the error sources in Figure III-1 is assumed to act as a bias during one run of a Monte Carlo case, except for the LOS rate errors. The Director sight uses LOS rates for computing the lead angle. As described in References III-2 and III-3, LOS rates are estimated by using a target tracking sensor (e.g. angle tracking radar or electro-optical sensor) and a Kalman filter. In the TAWDS(AA) program, correct LOS rates are computed and then second order correlated noise is added to represent expected general error characteristics. This approach was taken for three reasons. First, the formulation of the Kalman filter and the associated parameter values is directly related to the tracking sensor used. Secondly, a detailed description of the sensor noise characteristics is not available at present. And thirdly, only preliminary investigations, without flight test, have been conducted in modeling the tracking sensors and the Kalman filter, and further research may result in significant modifications to present models.

Airspeed	Range
Body Angle of Attack	Range Rate
Body Sideslip	HUD Display and Alignment Angles
Relative Air Density	Gun Alignment Angles W.R.T. Body
Line-of-Sight Rates*	Muzzle Velocity

* Does not apply to LCOSS Sight

GP75-0864-92

Figure III-1. Summary of Error Sources for Air-to-Air LCOSS and Director Sights

As a result of data given in References III-2, III-3, and III-4, the radar and electro-optical sensors appear to have second order noise characteristics. This form of error on the LOS rate estimates can be expected also because the Kalman filter, or other types of data filters, have difficulty in reducing correlated measurement noise.

In the TAWDS(AA) program, errors in the LOS rates (ΔW) are modeled by passing white Gaussian noise through a second-order low-pass filter of the form

$$\Delta W = \frac{K \omega_m^2}{s^2 + 2\zeta_m \omega_m s + \omega_m^2} N(0,1) \quad (\text{III-1})$$

where s is Laplace transform variable,

ω_m is the low pass filter bandwidth in rad/sec,

ζ_m is the low pass filter damping ratio,

$N(0,1)$ is the Gaussian noise of zero mean and standard deviation of 1,

K is a gain parameter to give the desired magnitude to ΔW .

Equation (III-1) is discretized using the state transition matrix approach given in Reference III-5. Since ζ_m and ω_m do not appear to vary significantly between the elevation and traverse axes, the same values of these parameters are used in both axes in the TAWDS(AA) program.

After discretization, K is given by

$$K = \sigma \sqrt{\frac{4\zeta_m}{\omega_m}} \sqrt{\Delta t} \quad (\text{III-2})$$

In this equation, the factor $\sqrt{4\zeta_m/\omega_m}$ represents the reciprocal of the gain when passing white noise through a second order filter (see Reference III-5). Δt

is the discretization or integration interval. The factor $\sqrt{\Delta t}$ is needed since discretizing the continuous Gaussian noise process $N(0,1)$ results in a gain of $1/\sqrt{\Delta t}$ (see Reference III-6). The variable σ is the desired standard deviation of ΔW .

Since the sensor noise characteristics are generally a function of range, as described in References III-2, III-3, and III-4, σ is computed in the TAWDS(AA) program by

$$\sigma = \frac{1500}{R} \sigma' \quad (\text{III-3})$$

where R is the range and σ' is the standard deviation at $R = 1500$ feet. This results in σ decreasing as target range increases, which is characteristic of target tracking sensors. Different values of σ in the traverse and elevation axes can be used in the TAWDS(AA) program.

III.2 Air-to-Ground Error Sources and Sensitivities

The error sources and sensitivities presented in this section include both along-track and cross-track errors. The "error sense" is taken as the computed value minus the actual value. This results in a positive along-track error when the actual impact point falls ahead of the nominal. A cross-track error, ΔY , is taken as positive when the actual impact point falls to the right (as would be seen by the pilot) of the nominal.

° Air-to-Ground Bombing - The along-track and cross-track error sources for the FIP bombing sight are given in Figure III-2. They include both errors that exist at bomb release and those associated with target position. The stationary along-track and cross-track error sensitivity equations corresponding to these error sources are shown in Figures III-3 and III-4.

The elevation and traverse dynamic tracking error equations for the FIP bomb sight are presented in Figure III-5. These dynamic equations are obtained by determining perturbations in the tracking error rate equations which are based on the difference between the pipper and the Line-Of-Sight rates.

It should be noted that the elevation axis equations are simplified by using a pseudostate, ϵ'_{EL} , which is the difference between the elevation tracking error (ϵ_{EL}) and the pipper elevation angle (θ_p), instead of the tracking error. Thus the elevation tracking error is the sum of perturbations in ϵ'_{EL} and θ_p . The perturbation equation for θ_p is given in Figure III-5.

Along-Track Error Source	
Target Position* Radar Range Measurement Radar Positioning A. Boresight Alignment B. Off-Boresight Positioning C. Radome Refraction Pitch Angle Error A. INS Boresight Alignment B. Pitch Angle Measurement Pipper Positioning A. Pilot Aiming B. Boresight Alignment C. Off-Boresight Positioning D. Windscreen Refraction	Weapon Release Along-Track (Inertial) Velocity Vertical (Inertial) Velocity True Airspeed Ejection Velocity Magnitude Rack Release Time Delay Bomb Dispersion

Cross-Track Error Source	
Target Position* Heading Angle Error A. INS Boresight Alignment B. Heading Angle Measurement Pipper Positioning A. Pilot Aiming B. Boresight Alignment C. Off-Boresight Positioning D. Windscreen Refraction	Weapon Release Cross-Track (Inertial) Velocity Sideslip Bomb Dispersion

* At Pilot Release Command for FIP Sight

GP75-0084-51

Figure III -2. Summary of Along-Track and Cross-Track Error Sources for FIP Bombing Sight

The error sources and sensitivity equations given in Figures III-2, III-3, and III-4 are the same as those given in Reference III-7 for the CCIP bombing sight, since the computed bomb impact points are the same at the desired bomb release altitude. The FIP elevation axis dynamic tracking error equations in Figure III-5 have been modified from those given in Reference III-7 for the CCIP bombing sight to account for the time-to-go to bomb release (T_{GO}) and bomb release altitude parameters. The traverse equations are not modified because these parameters are not used in computing the cross-track bomb impact point. In the TAWDS(AG) program, the north-east-down and the

Target Position*	Weapon Release
Radar Range Measurement $(\Delta X =) \frac{\sin(\theta_I - \theta_P)}{\sin \theta_I} \Delta R_{AT}$	Along-Track (Inertial) Velocity $-(T_D + t_F) \Delta V_X$
Radar Elevation Positioning $-R_{AT} \frac{\sin(\theta_I - \theta_P)}{\sin \theta_I \tan \theta_P} \Delta \theta_R$	Vertical (Inertial) Velocity $[(T_D + t_F') \cot \theta_I - \tan \theta_V (t_F - t_F')] \Delta V_Z$
Pitch Angle $-R_{AT} \frac{\cos(\theta_I - \theta_P)}{\sin \theta_I} \Delta \theta_A$	True Airspeed $\left[\frac{\cot \theta_I K_3 (C_B - 1) D_g}{V_A C_B} + \sec \theta_V (t_F - t_F') \right] \Delta V_A$
Pipper Elevation Positioning $\frac{R_{AT}}{\sin \theta_P} \Delta \theta_P$	Ejection Velocity Magnitude $t_F' \frac{\cos(\theta_I - \theta_V)}{\sin \theta_I} \Delta V_E$
	Rack Release Time Delay $V_A \frac{\sin(\theta_I - \theta_V) - \dot{\theta}_V t_F' \cos(\theta_I - \theta_V)}{\sin \theta_I} \Delta T_R$
	Bomb Dispersion $\frac{(V_{BR} + V_{BI})}{2 \sin \theta_I} t_F' \Delta \theta_{DIS}$

* At pilot release command

GP75-0964-43

Figure III-3. Summary of Along-Track Error Sensitivity Equations for FIP Bombing Sight ground-track-heading coordinates are the same, since no steady state winds are assumed.

Reference III-1 describes the approach used in computing the dynamic tracking error equations in Figure III-5. As an example of this approach, the computation of ΔT_{GO} is outlined. The equation for T_{GO} is

$$T_{GO} = \frac{h - 1/2 g C_B (t_F')^2 - V_E t_F' / \cos \theta_A}{w \cos \theta_A - u \sin \theta_A} - t_F' \quad (III-4)$$

assuming $V_{EX} \approx 0$ and $T_D \approx 0$. Then the perturbation of T_{GO} can be written as

$$\Delta T_{GO} = \frac{\partial T_{GO}}{\partial u} \Delta u + \frac{\partial T_{GO}}{\partial w} \Delta w + \frac{\partial T_{GO}}{\partial \theta_A} \Delta \theta_A + \frac{\partial T_{GO}}{\partial h} \Delta h + \frac{\partial T_{GO}}{\partial t_F'} \Delta t_F' + \frac{\partial T_{GO}}{\partial C_B} \Delta C_B \quad (III-5)$$

Target Position*	Weapon Release
Heading Angle $(\Delta Y =) - V_x t_F \Delta \psi_H$	Cross-Track (Inertial) Velocity $-t_F \Delta V_y$
Pipper Position $R_{AT} \Delta \psi_P$	Sideslip $V_A (t_F - t'_F) \Delta \beta_A$
	Bomb Dispersion $\frac{(V_{BR} + V_{BI})}{2} t'_F \Delta \psi_{Dis}$

* At pilot release command

GP75-0864-73

Figure III-4. Summary of Cross-Track Error Sensitivity Equations for FIP Bombing Sight

The computation of these partial derivatives from Equation (III-4) is straight forward.

Since it is desired to express ΔT_{GO} as a function of the state variables Δu , Δw , $\Delta \theta_A$, and Δh , the approach used to compute $\Delta t'_F$ and ΔC_B as a function of these variables is as follows. Starting with:

$$C_B = 1 + K_1 (D_g)^{K_2} V_A^{K_3}, \quad (III-6)$$

ΔC_B is computed as:

$$\Delta C_B = \frac{2K_2 (C_B - 1) \Delta t'_F}{t'_F} \quad (III-7)$$

where $\partial C_B / \partial V_A$ is small and neglected. This leaves $\Delta t'_F$ to be computed as a function of the desired state variables. The equation for t'_F is:

$$t'_F = \frac{-V_Z + \sqrt{V_Z^2 + 2gC_B h_R}}{gC_B} \quad (III-8)$$

Elevation Axis Dynamic Tracking Error Model

$$\Delta \dot{\epsilon}'_{EL} = G_{\epsilon'_{EL}} \Delta \epsilon'_{EL} + G_R \Delta R_{AT} + G_U \Delta u + G_W \Delta w + G_q \Delta q$$

where $\epsilon'_{EL} = \epsilon_{EL} - \theta_P$, $\Delta \epsilon_{EL} = \Delta \epsilon'_{EL} + \Delta \theta_P$

$$G_{\epsilon'_{EL}} = [u \cos(\alpha - \epsilon'_{EL})] / R_{AT}$$

$$G_R = [u \sin(\alpha - \epsilon'_{EL})] / R_{AT}^2$$

$$G_U = -[\sin(\alpha - \epsilon'_{EL}) - \alpha \cos(\alpha - \epsilon'_{EL})] / R_{AT}$$

$$G_W = -[\cos(\alpha - \epsilon'_{EL})] / R_{AT}$$

$$G_q = 1.0$$

$$\Delta \theta_P = G_U \Delta u + G_W \Delta w + G_{\theta_A} \Delta \theta_A + G_{TGO} \Delta TGO$$

where $G_U = (A \sin \theta_A - B \tan \theta_P + AC) \cos^2 \theta_P$

$$G_W = -(A \cos \theta_A + B + AD) \cos^2 \theta_P$$

$$G_{\theta_A} = [D_g (\sin \theta_A + \tan \theta_P \cos \theta_A) / b + Ad + V_A AD] \cos^2 \theta_P$$

$$G_{TGO} = -[(w + u \tan \theta_P) / b] \cos^2 \theta_P$$

$$A = [D_g (a \sin \theta_A - b \cos \theta_A) (1 + 2K_2 - \frac{2K_2}{C_B}) + TGO (wb + ua)] / (c + g C_B t'_F b^2)$$

$$B = (TGO + t'_F) / b$$

$$C = (2V_A (1 - \cos \gamma) / (k_2 g) - k_1 \sin \gamma) / t'_F$$

$$D = (V_A \sin \gamma / (k_2 g) - k_1 \cos \gamma) / t'_F$$

$$a = -(w + V_E) (TGO + t'_F) - D_g \cos \theta_A$$

$$c = -u \sin \theta_A + (w + V_E) \cos \theta_A$$

$$b = u (TGO + t'_F) - D_g \sin \theta_A$$

$$d = u \cos \theta_A + (w + V_E) \sin \theta_A$$

and $\Delta TGO = F_U \Delta u + F_W \Delta w + F_{\theta_A} \Delta \theta_A + \Delta h$

where $F_U = ((TGO + t'_F) \sin \theta_A - A_2 (\sin \theta_A + C)) / (c + g C_B t'_F) / (w \cos \theta_A - u \sin \theta_A)$

$$F_W = -(TGO + t'_F) \cos \theta_A + A_2 (\cos \theta_A + D) / (c + g C_B t'_F) / (w \cos \theta_A - u \sin \theta_A)$$

$$F_{\theta_A} = (A_1 - A_2 (d + D)) / (c + g C_B t'_F) / (w \cos \theta_A - u \sin \theta_A)$$

$$A_1 = -V_E t'_F \tan \theta_A \sec \theta_A + (TGO - t'_F) (w \sin \theta_A + u \cos \theta_A)$$

$$A_2 = D_g + h_R - V_E t'_F \tan \theta_A \sin \theta_A + 2D_g K_2 (C_B - 1) / C_B$$

OP78-0064-72

Figure III -5. Dynamic Tracking Error Model for FIP Bombing Sight

Traverse Axis Dynamic Tracking Error Model	
$\Delta \dot{\epsilon}_{TR} = G_{\epsilon_{TR}} \Delta \epsilon_{TR} + \Delta \dot{\beta}_A + G_{\phi} \Delta \phi + G_{\dot{\phi}} \Delta \dot{\phi} + G_p \Delta p + G_r \Delta r$	
where	$G_{\epsilon_{TR}} = u/R_{AT}$
	$G_{\phi} = -u D_0 \cos \theta_A \cos \phi / R_{AT}^2$
	$G_{\dot{\phi}} = D_0 \cos \theta_A \cos \phi / R_{AT}$
	$G_p = \sin \theta_p$
	$G_r = \cos \theta_p$

GP75-0864-50

Figure III -5. Dynamic Tracking Error Model For FIP Bombing Sight (Concluded)

where:

$$V_Z = (w + V_E) \cos \theta_A - u \sin \theta_A \quad (\text{III-9})$$

$$h_R = -V_A k_1 \sin \gamma + \frac{V_A^2 (1 - \cos \gamma)}{k_2 g} + h_{SF} + h_{\Delta} \quad (\text{III-10})$$

In these equations, h_{SF} and h_{Δ} are assumed to be constant and $\gamma = \theta_A - \alpha$. Then taking perturbations of Equations (III-8) to (III-10) and collecting terms as a function of the state variables and substituting in Equation (III-3), gives the equation for ΔT_{GO} in Figure III-5. When determining perturbations for Equations (III-8) through (III-10), it is assumed that $\Delta V_A \approx \Delta u$, $\Delta \gamma \approx \Delta \theta_A$, and $\Delta \alpha \approx \Delta w / V_A$.

o Air-to-Ground Gunnery - Figures III-6 and III-7 present a list of error sources for the air-to-ground Fixed Depressed Reticle and CCIP gunnery sights respectively. The associated stationary along-track and cross-track sensitivity equations are given in Figures III-8 and III-9. The Fixed Depressed Reticle sight sensitivities are given for both the nominal firing altitude and range options described in Reference III-7 or Appendix II of this report.

The dynamic tracking error sensitivity equations are presented in Figure III-10 for the Fixed Depressed Reticle sight and in Figure III-11 for the CCIP

Along-Track Error Source	
<p>Airspeed</p> <ul style="list-style-type: none"> A. Airspeed Measurement B. Airspeed Display C. Pilot Airspeed Matching <p>Along-Track Wind</p> <p>Angle-of-Attack Variation</p> <p>Aircraft Weight Estimation</p> <p>Pilot Timing</p> <p>Muzzle Velocity</p> <p>Gun Elevation Boresight</p>	<p>Pitch Angle</p> <ul style="list-style-type: none"> A. Sensor Boresight B. Pitch Angle Measurement C. Pitch Angle Display D. Pilot Pitch Angle Matching <p>Pipper Elevation Positioning</p> <ul style="list-style-type: none"> A. Pipper Boresight B. Off-Boresight Positioning C. Pilot Aiming D. Windscreen Refraction <p>Altitude Measurement and Display</p>

Cross-Track Error Source
<p>Cross-Track Wind</p> <p>Sideslip Angle</p> <p>Bank Angle</p> <p>Pipper Azimuth Positioning</p> <ul style="list-style-type: none"> A. Pipper Boresight B. Off-Boresight Positioning C. Pilot Aiming D. Windscreen Refraction <p>Gun Azimuth Boresight</p>

GP75-0864-49

Figure III-6. Summary of Error Sources for Fixed Depressed Reticule Gun Sight

Along-Track Error Source	
Along-Track (Inertial) Velocity	Pipper Elevation Positioning
Vertical (Inertial) Velocity	A. Pipper Boresight
Airspeed	B. Off-Boresight Positioning
Pitch Angle	C. Pilot Aiming
A. INS Boresight	D. Windscreen Refraction
B. Pitch Angle Measurement	Radar Range Measurement
Muzzle Velocity	Radar Elevation Positioning
Gun Elevation Boresight	A. Radar Boresight
	B. Off-Boresight Positioning
	C. Radome Refraction

Cross-Track Error Source
Cross-Track (Inertial) Velocity
Heading Angle
A. INS Boresight
B. Heading Angle Measurement
Sideslip Angle
Pipper Azimuth Positioning
A. Pipper Boresight
B. Off-Boresight Positioning
C. Pilot Aiming
D. Windscreen Refraction
Gun Azimuth Boresight

GP76-0084-47

Figure III -7. Summary of Error Sources for CCIP Gunnery Sight

Error Source	Error Sensitivity	
	Fixed Depressed Reticle Sight*	CCIP Sight
• Along-Track (Inertial) Velocity	-	$(\Delta X) - t_F \Delta V_X$
• Vertical (Inertial) Velocity	-	$[t_F \cot \theta_1 - \tan \theta_V (t_F - t_F)] \Delta V_Z$
• True Air Speed	$-[2\alpha_W \cos(\theta_1 - \theta_D) + \sin(\theta_1 - \theta_D)] \frac{t_F}{\sin \theta_1} \Delta V_A$	$\sec \theta_V (t_F - t_F) \Delta V_A$
• Pitch Angle	$-\left[\alpha_W \tan \theta_A V_A \frac{\cos(\theta_1 - \theta_D)}{\sin \theta_1} t_F \right.$ $\left. + R_{AT} \frac{\sin(\theta_1 - \theta_p)}{\sin \theta_1 \tan \theta_p} \right] \Delta \theta_A \text{ (Altitude Option)}$ $-\alpha_W \tan \theta_A V_A \frac{\cos(\theta_1 - \theta_D)}{\sin \theta_1} t_F \Delta \theta_A \text{ (Range Option)}$	$\left[\frac{V_M \cos(\theta_1 - \theta_{GL}) t_F}{\sin \theta_1} - R_{AT} \frac{\cos(\theta_1 - \theta_p)}{\sin \theta_1} \right] \Delta \theta_A$
• Pipper Elevation Positioning	(Same as CCIP)	$\frac{R_{AT}}{\sin \theta_p} \Delta \theta_p$
• Altitude	$\frac{\sin(\theta_1 - \theta_p)}{\sin \theta_1 \sin \theta_p} \Delta h_{AT} \text{ (Altitude Option Only)}$	-
• Range	(Same as CCIP - Radar Range Option Only)	$\frac{\sin(\theta_1 - \theta_p)}{\sin \theta_1} \Delta R_{AT}$
• Radar Elevation Positioning	(Same as CCIP - Radar Range Option Only)	$\frac{-R_{AT} \sin(\theta_1 - \theta_p)}{\sin \theta_1 \tan \theta_p} \Delta \theta_R$
• Muzzle Velocity	(Same as CCIP)	$\frac{-\sin(\theta_1 - \theta_{GL})}{\sin \theta_1} t_F \Delta V_M$
• Gun Elevation Boresight	(Same as CCIP)	$-V_M \frac{\cos(\theta_1 - \theta_{GL})}{\sin \theta_1} t_F \Delta \theta_{GB}$
• Along-Track Wind	$t_F W_X$	-
• Aircraft Weight Estimation	$V_A \frac{\alpha_W \cos(\theta_1 - \theta_D)}{W_A \sin \theta_1} t_F \Delta W_A$	-
• Pilot Timing	$V_A \frac{\sin(\theta_1 - \theta_p)}{\sin \theta_1} \Delta T_p$	-
• Angle-of-Attack	$V_A \frac{\cos(\theta_1 - \theta_D)}{\sin \theta_1} t_F \Delta \alpha$	-

* Fixed Depressed Reticle sensitivities apply to both the altitude and range options unless otherwise specified.

OP78-0064-48

Figure III -8. Summary of Along-Track Error Sensitivity Equations for Air-to-Ground Gunnery

Error Source	Error Sensitivity	
	Fixed Depressed Reticle Sight*	CCIP Sight
• Cross-Track (Inertial) Velocity	-	$(\Delta Y =) -t_F \Delta V_Y$
• Heading Angle	-	$-V_X t_F \Delta \psi_H$
• Sideslip Angle	$V_A t_F \Delta \beta_A$	$V_A (t_F - t_{F'}) \Delta \beta_A$
• Pipper Azimuth Positioning	(Same as CCIP)	$R_{AT} \Delta \psi_P$
• Gun Azimuth Boresight	(Same as CCIP)	$-V_M t_{F'} \Delta \psi_{GB}$
• Bank Angle	$[\sigma_{PG} - \frac{V_A}{V_A + V_M} \alpha_{GL}] R_{AT} \Delta \beta_A$	-
• Cross-Track Wind	$t_F W_Y$	-

* Fixed Depressed Reticle sensitivities apply to both the altitude and range options

GP78-0064-64

Figure III -9. Summary of Cross-Track Error Sensitivity Equations for Air-to-Ground Gunnery

Elevation Axis Dynamic Tracking Error Model	Traverse Axis Dynamic Tracking Error Model
$\Delta \epsilon_{EL} = G_{\epsilon_{EL}} \Delta \epsilon_{EL} + G_R \Delta R_{AT} + G_U \Delta u + G_W \Delta w + G_q \Delta q$	$\Delta \epsilon_{TR} = G_{\epsilon_{TR}} \Delta \epsilon_{TR} + G_\beta \Delta \beta_A + G_p \Delta p + G_r \Delta r + G_\phi \Delta \phi$
Where $G_{\epsilon_{EL}} = (u \cos \Delta_{EL} - w \sin \Delta_{EL}) / R_{AT}$	Where $G_{\epsilon_{TR}} = (u \cos \Delta_{TR}) / R_{AT}$
$G_R = (u \sin \Delta_{EL} + w \cos \Delta_{EL}) / R_{AT}^2$	$G_\beta = (u \cos \Delta_{TR}) / R_{AT}$
$G_U = -(\sin \Delta_{EL}) / R_{AT}$	$G_p = \sin \theta_p$
$G_W = -(\cos \Delta_{EL}) / R_{AT}$	$G_r = \cos \theta_p$
$G_q = 1.0$	$G_\phi = 0.0$
$\Delta_{EL} = (\theta_p - \epsilon_{EL})$	$\Delta_{TR} = (\beta_A + \epsilon_{TR})$

GP78-0064-65

Figure III -10. Dynamic Tracking Error Models for Fixed Depressed Reticle Gunnery Sight

Elevation Axis Dynamic Tracking Error Model

$$\Delta \epsilon'_{EL} = G_{\epsilon'_{EL}} \Delta \epsilon_{EL} + G_R \Delta R_{AT} + G_U \Delta u + G_W \Delta w + G_Q \Delta q$$

where $\epsilon'_{EL} = \epsilon_{EL} - \theta_p$, $\Delta \epsilon_{EL} = \Delta \epsilon'_{EL} + \Delta \theta_p$

$$G_{\epsilon'_{EL}} = [u \cos(\alpha - \epsilon'_{EL})] / R_{AT}$$

$$G_R = [u \sin(\alpha - \epsilon'_{EL})] / R_{AT}^2$$

$$G_U = -[\sin(\alpha - \epsilon'_{EL}) - \alpha \cos(\alpha - \epsilon'_{EL})] / R_{AT}$$

$$G_W = -[\cos(\alpha - \epsilon'_{EL})] / R_{AT}$$

$$G_Q = 1.0$$

$$\Delta \theta_p = G_U \Delta u + G_W \Delta w + G_{\theta_A} \Delta \theta_A + G_h \Delta h$$

where $G_U = (A \sin \theta_A - B \tan \theta_p) \cos^2 \theta_p$

$$G_W = -(A \cos \theta_A + B) \cos^2 \theta_p$$

$$G_{\theta_A} = [D_g (\sin \theta_A + \tan \theta_p \cos \theta_A) / b + Ad] \cos^2 \theta_p$$

$$G_h = \cos^2 \theta_p A / t'F$$

$$A = D_g (a \sin \theta_A - b \cos \theta_A) \left(1 + K_2 - \frac{K_2}{C_B}\right) / ((c + g C_B t'F) b^2)$$

$$B = t'F / b$$

$$a = -a't'F - D_g \cos \theta_A \qquad a' = w - V_m \sin \Delta \alpha_{GL}$$

$$b = b't'F - D_g \sin \theta_A \qquad b' = u + V_m \cos \Delta \alpha_{GL}$$

$$c = -b' \sin \theta_A + a' \cos \theta_A \qquad d = b' \cos \theta_A + a' \sin \theta_A$$

GP74-0488-5

Traverse Axis Dynamic Tracking Error Model

$$\Delta \epsilon_{TR} = G_{\epsilon_{TR}} \Delta \epsilon_{TR} + G_{\beta} \Delta \beta_A + G_{\dot{\beta}} \Delta \dot{\beta}_A + G_{\phi} \Delta \phi + G_{\dot{\phi}} \Delta \dot{\phi} + G_p \Delta p + G_r \Delta r$$

where $G_{\epsilon_{TR}} = u / R_{AT}$

$$G_{\dot{\phi}} = D_g \cos \theta_A \cos \phi / R_{AT}$$

$$G_{\beta} = u V_m / ((u + V_m) R_{AT})$$

$$G_p = \sin \theta_p$$

$$G_{\dot{\beta}} = u / (u + V_m)$$

$$G_r = \cos \theta_p$$

$$G_{\phi} = -u D_g \cos \theta_A \cos \phi / R_{AT}^2$$

GP75-0864-45

Figure III -11. Dynamic Tracking Error Models for CCIP Gunnery Sight

gunnery sight. These equations are obtained by taking perturbations in the tracking error rate equations, which are based on the difference between the pipper and the Line-Of-Sight rates. For the Fixed Depressed Reticule sight, the pipper rates are equal to the body rates, since the pipper is fixed in the HUD during a gunnery pass.

The elevation axis equations given in Figure III-10 for a Fixed Depressed Reticule sight have been modified from those given in References III-1 and III-7. This modification is based on writing the Line-Of-Sight rate equation (ω_{LOS}) as a function of the correct body airspeed components u and w (i.e., $u = V_A \cos \alpha$ and $w = V_A \sin \alpha$).

III.3 List of Mathematical Symbols for Air-to-Ground Weapon Delivery

<u>Symbol</u>	<u>Definition</u>
B_A	Aircraft bank angle (rad)
C_B	Weapon retardation factor used in modified vacuum trajectory equations
D_g	Equivalent gravity drop or pass distance of weapon (ft)
g	Acceleration of gravity ($\approx 32.174 \text{ ft/sec}^2$)
h, h_{AT}	Aircraft altitude relative to target (ft)
h_L	Altitude lost during pull up after bomb release
h_R	Desired bomb release altitude relative to target (ft)
h_{SF}	Safety factor or ground clearance altitude
h_Δ	Altitude increment from bomb release to start of pull up
K_1, K_2, K_3	Constants in C_B equation
k_1, k_2	Constants used in computing altitude lost during pull up
p, q, r	Body roll, pitch, yaw rates (rad/sec)
R_{AT}	Target range (ft)
T_D	Bomb rack release time delay (sec)
t_F	Weapon time-of-flight to impact point (sec)
t'_F	Weapon time-of-flight in airmass (assumes zero wind)
T_{GO}	Time-to-go to desired bomb release altitude (sec)
u, v, w	Aircraft airspeed components in body coordinates (ft/sec)
V_A	Aircraft airspeed (ft/sec)
V_{BR}	Bomb velocity at release (ft/sec)
V_{BI}	Weapon impact velocity (ft/sec)
V_E	Bomb ejection velocity (ft/sec)
V_M	Muzzle velocity (ft/sec)
V_X, V_Y	Orthogonal horizontal components of aircraft ground track velocity vector, (ft/sec)

SymbolDefinition

V_Z	Vertical component of aircraft ground track velocity vector, positive down (ft/sec)
W_A	Aircraft weight (lb)
W_X, W_Y	Wind velocity along and orthogonal to ground track velocity vector (ft/sec)

Note: The error sensitivity equations presented in Figures III-3, III-4, III-8, and III-9 were derived in References III-7 and III-1 assuming pitch angles were positive down, whereas the dynamic tracking error equations in Figures III-5, III-10, and III-11 were derived assuming that pitch angles were positive up. These angles are denoted below by *. In the TAWDS(AG) program, all equations are programmed assuming these angles are positive up.

SymbolDefinition

α	Aircraft body angle of attack (rad)
α_{GL}	Gunline angle of attack (rad)
α_W	Aircraft wing angle of attack (rad)
β_A	Aircraft sideslip angle (rad)
$\epsilon_{TR}, \epsilon_{EL}$	Traverse, elevation tracking error (rad)
ϵ'_{EL}	Pseudostate used in CCIP and FIP elevation dynamic tracking error model (rad)
θ_A	Aircraft (waterline) pitch angle (rad)*
γ, θ_D	Air mass flight path angle (dive angle) (rad)*
θ_{DIS}	Bomb dispersion in pitch (rad)
θ_{GB}	Gun pitch angle W.R.T. body (rad)
θ_{GL}	Gunline pitch angle (rad)*
θ_I	Weapon impact angle (nominally positive, rad)
θ_P	Pipper pitch angle (rad)*
θ_R	Radar pitch angle (rad)*
θ_V	Inertial flight path angle (dive angle) (rad)*
σ_{PG}	Pipper depression angle W.R.T. gunline, positive down (rad)
ϕ	Body roll angle (rad)
ψ_{DIS}	Bomb dispersion in traverse (rad)
ψ_{GB}	Gun yaw angle W.R.T. body (rad)
ψ_H	Aircraft heading angle (rad)
ψ_P	Pipper azimuth angle W.R.T. body symmetry plane (rad)

APPENDIX III
REFERENCES

- III-1. Williams, A.H., Landy, R.J., and Murphy, W.J., "Aerial Gunnery Methodology, Volume II - Air-to-Ground Gunnery," AFATL-TR-72-218, Volume II, November 1972.
- III-2. Murphy, W.J., Simmons, D.E., and Schneider, J.R., "Advanced Air-to-Air Gun Fire Control System Definition Study (Unclassified Title)," AFAL-TR-73-211, August 1973.
- III-3. Berg, R.L., Murphy, W.J., and Simmons, D.E., "Advanced Gun Fire Control System (AGFCS), Design Study (Phase II)," AFAL-TR-74, April 1974.
- III-4. Corrigan, J.D., "F-15A/GAU-7/A Gun Attack Mode Error Budget and Accuracy Analysis Plan (Unclassified Title)," Report MDC A2226 (Contract F33657-72-C-0637) February 1974.
- III-5. Bryson, A.E., Jr. and Ho, Y.C., "Applied Optimal Control," Blaisdell Publishing Co., 1969.
- III-6. Kuo, B.C., "Analysis and Synthesis of Sampled-Data Control Systems," Prentice-Hall, page 417, 1963.
- III-7. Berger, J.B., et al., "Flight Control Requirements for Weapon Delivery, Interim Report for Period June 1973 - May 1974," Technical Report AFFDL-TR-74-119.

APPENDIX IV
DEVELOPMENT OF MODIFIED VACUUM TRAJECTORY EQUATIONS

This appendix presents a simplified development of the modified vacuum trajectory equations used in the air-to-ground CCIP and FIP weapon delivery sights modeled in the air-to-ground TAWDS(AG) program. While bombing is discussed specifically, the basic approach is also applicable to gunnery and rockets. A more extensive description of this approach is given in Reference IV-1, as applied to gunnery.

The advantage of this approach is the relatively simple computations required to determine the weapon impact point, in comparison to integrating the weapon's nonlinear differential equations of motion. Acceptable accuracy is achieved over a large part of the air-to-ground weapon delivery envelope. However, since the approach utilizes the weapon delivery tables, the accuracies can only be as precise as the tables themselves. Representative data indicating the accuracy of the technique are given in this appendix.

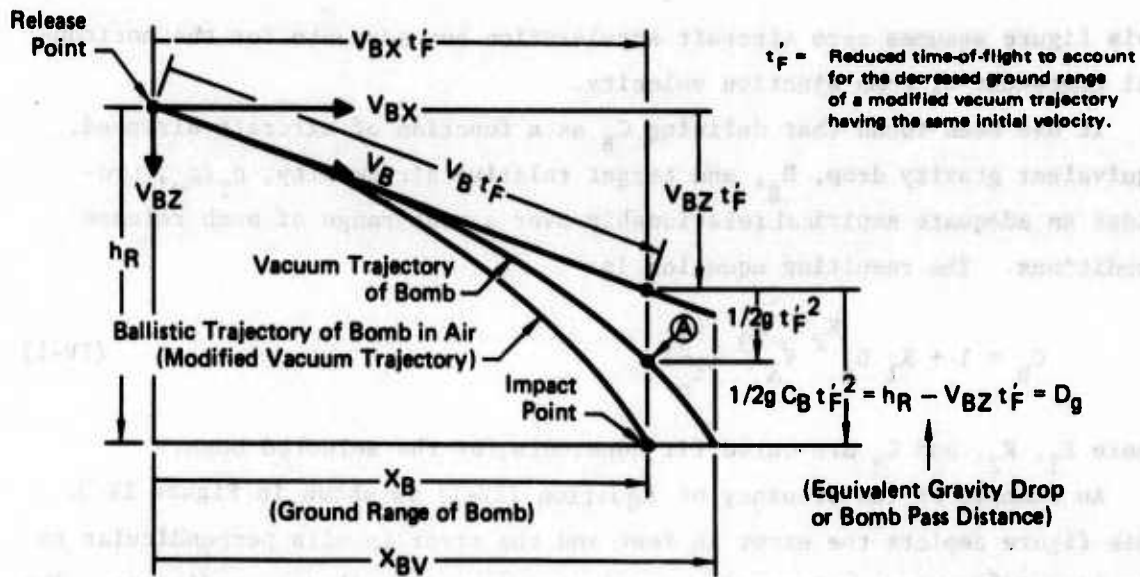
IV.1 Modified Vacuum Trajectory Equations

Example bomb trajectories are shown in Figure IV-1, depicting bomb flight in air and in a vacuum. The effect of drag in air causes the bomb to fall short of the vacuum trajectory impact point. The drag also increases the time-of-fall of the bomb, since its effect opposes gravitational acceleration. The effect of wind is separately considered in Section IV.4.

In the modified vacuum trajectory approach, the decreased ground bomb range is associated with an equivalent (modified) vacuum trajectory. The modified trajectory has the same initial horizontal velocity, but a decreased time-of-fall, t'_F , to account for the decreased range. Then, in the vertical direction, this decreased time-of-fall is accounted for by increasing the gravitational acceleration by a ballistic factor. The ballistic factor, C_B , is referred to as the retardation factor because it yields the decreased, or retarded, ground range of the bomb.

IV.2 Description of C_B Equation

An exact value of C_B is derived from the weapon delivery tables for a specific set of release conditions. An example is shown in Figure IV-2.



$$\left. \begin{aligned} X_B &= V_{BX} t_F' \\ h_R &= V_{BZ} t_F' + g C_B t_F'^2 / 2 \end{aligned} \right\} \text{Modified Vacuum Trajectory Equations}$$

GP75-0084-44

Figure IV-1. Modified Vacuum Trajectory Equations

- Obtain a Set of Corresponding Values of the Following Parameters from Bomb Tables:
 - h_R - Release Altitude
 - γ - Dive Angle
 - V_A - Aircraft True Airspeed
 - V_e - Bomb Ejection Velocity
 - X_B - Ground Range of Bomb
- Obtain Reduced Time of Fall, t_F' , From the Horizontal Modified Vacuum Trajectory Equation:

$$t_F' = \frac{X_B}{V_{BX}} \quad \text{Where } V_{BX} = V_A \cos \gamma - V_e \sin \gamma$$
- Obtain C_B from the Vertical Modified Vacuum Trajectory Equation:

$$C_B = (h_R - V_{BZ} t_F') \frac{2}{g t_F'^2} \quad \text{Where } V_{BZ} = V_A \sin \gamma + V_e \cos \gamma$$
- Elimination of t_F' from Above Equations Yields the Single Equation:

$$C_B = \left(h_R - \frac{V_{BZ} X_B}{V_{BX}} \right) \frac{2 V_{BX}^2}{g X_B^2}$$

GP75-0084-06

Figure IV-2. Derivation of Bomb Retardation Factor from Bomb Tables

This figure assumes zero aircraft acceleration but accounts for the horizontal component of bomb ejection velocity.

It has been found that defining C_B as a function of aircraft airspeed, equivalent gravity drop, D_g , and target relative air density, ρ_T/ρ_O , provides an adequate empirical relationship over a wide range of bomb release conditions. The resulting equation is:

$$C_B = 1 + K_1 D_g^{K_2} V_A^{K_3} \left(\frac{\rho_T}{\rho_O}\right) \quad (IV-1)$$

where K_1 , K_2 , and K_3 are curve fit constants for the selected bomb.

An example of the accuracy of Equation (IV-1) is shown in Figure IV-3. This figure depicts the error in feet and the error in mils perpendicular to the Line-Of-Sight at release for a selected range of release conditions. The error in bomb ground range, ΔX_B , is computed by comparison with the actual bomb range, X_B , obtained from ballistic tables. Figure IV-4 presents the accuracy with which ground range for a 20mm bullet against a sea-level target can be predicted.

The variation in bomb ground range with target altitude above sea level is small for low drag bombs. Impact point accuracy can be improved, however, by accounting for the air density at target altitude in the calculation of C_B . This is illustrated in Figure IV-5. While the original error is less than one mil, accounting for the air density reduces the error by a factor of five to ten.

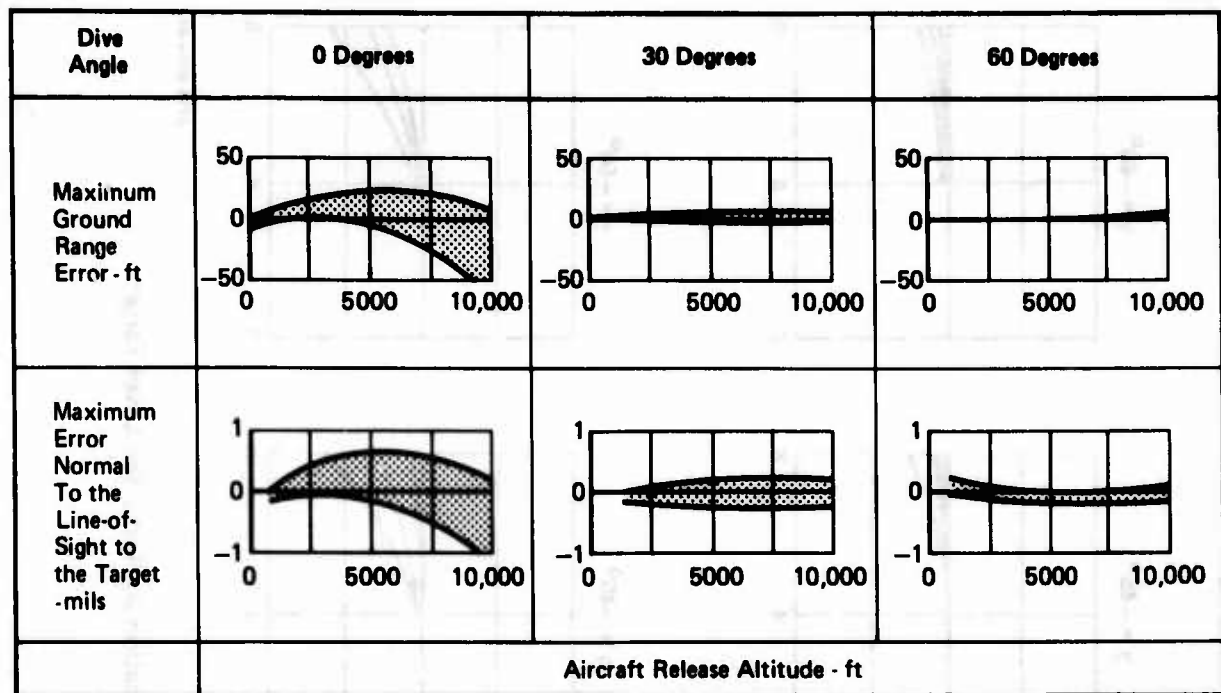
Data for the 20mm bullet is shown in graphical form in Figure IV-6. This figure shows that neglecting air density causes only small errors at firing ranges less than 4000 feet. However, Figure IV-7 shows that accounting for target altitude, as in Equation (IV-1), can significantly reduce the predicted bullet error at greater ranges.

IV.3 Computation of Actual Time-of-Fall

The actual weapon time-of-fall (or time-of-flight), t_F , can be related to the reduced time-of-fall t'_F and C_B by the equation:

$$t_F = K_4 C_B^{K_5} t'_F \quad (IV-2)$$

As will be shown in the next section, t_F is only used to compensate for the effect of wind over the interval $(t_F - t'_F)$, and thus great accuracy is not required.



GP78-0864-87

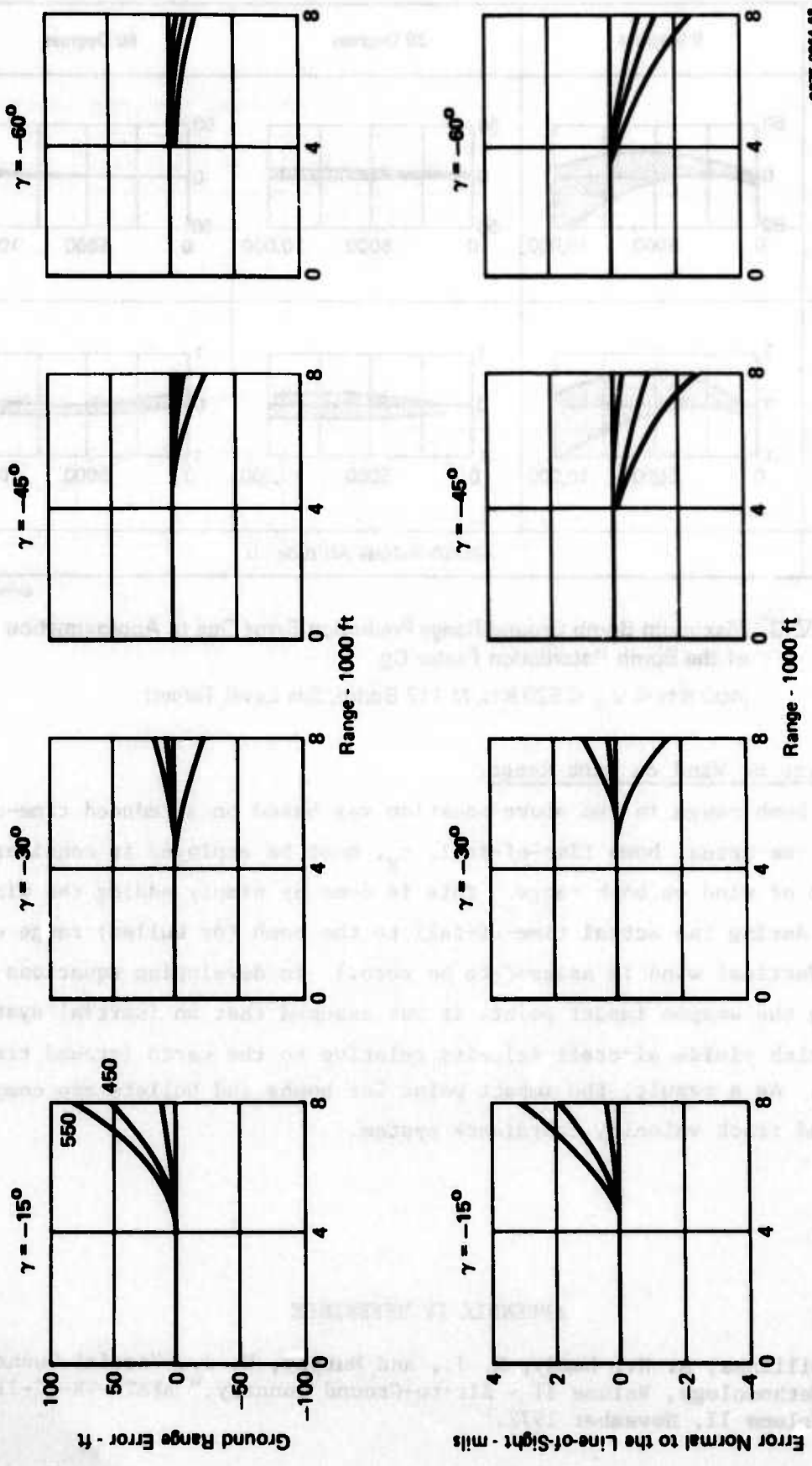
Figure IV-3. Maximum Bomb Ground Range Prediction Error Due to Approximation of the Bomb Retardation Factor C_B
 (400 Kts $< V_A < 520$ Kts, M-117 Bomb, Sea Level Target)

IV.4 Effect of Wind on Bomb Range

While bomb range in the above equation was based on a reduced time-of-fall, t'_F , the actual bomb time-of-fall, t_F , must be employed in considering the effect of wind on bomb range. This is done by simply adding the wind component during the actual time-of-fall to the bomb (or bullet) range equations. (Vertical wind is assumed to be zero.) In developing equations predicting the weapon impact point, it was assumed that an inertial system is used which yields aircraft velocity relative to the earth (ground track velocity). As a result, the impact point for bombs and bullets are computed in a ground track velocity coordinate system.

APPENDIX IV REFERENCE

- IV-1. Williams, A. H., Landy, R. J., and Murphy, W. J., "Aerial Gunnery Methodology, Volume II - Air-to-Ground Gunnery," AFATL-TR-72-218, Volume II, November 1972.



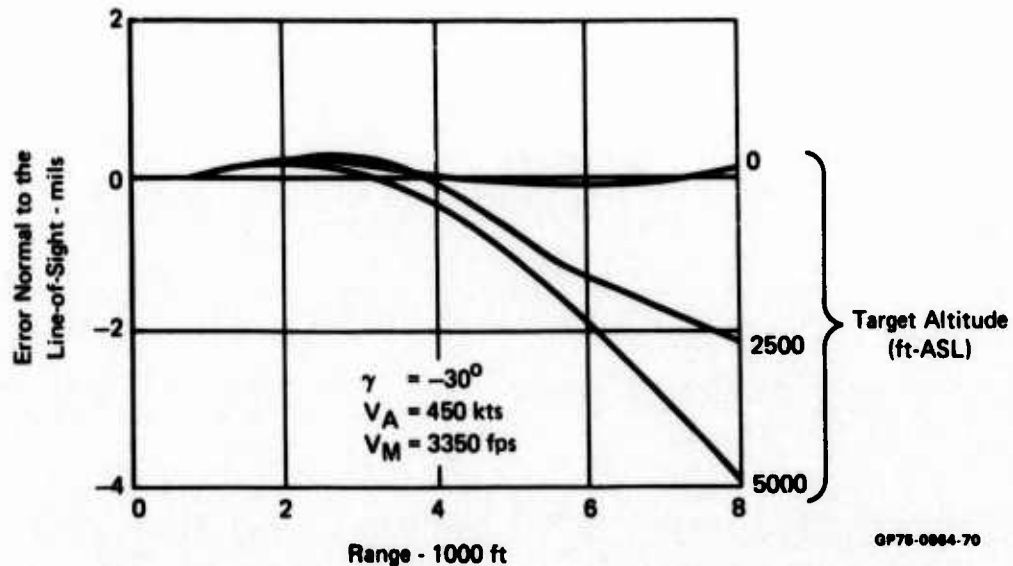
0775-0064-88

Figure IV -4. Bullet Ground Range Error Due to CB Approximation Against a Sea Level Target

True Airspeed (kts)	Altitude Above Target (ft)	Target At Sea Level	Target is at Some Altitude Above Sea Level					
			Bomb Ground Range (ft)	Altitude Above Sea Level (ft)	Bomb Ground Range (ft)	Error in Bomb Ground Range		
		No Compensation				ρ_T/ρ_0 Compensation		
		(ft)				(mils)	(ft)	(mils)
400	1000	5,109	6000	5,122	13	0.48	2	0.07
500	1000	6,366	6000	6,385	19	0.46	2	0.05
500	2000	9,015	5000	9,046	31	0.72	2	0.05
400	3000	8,870	4000	8,895	25	0.85	3	0.10
400	4000	10,233	3000	10,257	24	0.80	2	0.07
400	5000	11,429	2000	11,449	20	0.64	2	0.06

GP75-0864-69

Figure IV-5. Variation in Bomb Ground Range with Altitude of Target Above Sea Level (500 Lb MK-82 GP Bomb, 7 Ft/Sec Ejection Velocity, Level Release)



GP75-0864-70

Figure IV-6. Bullet Impact Error Due to C_B Approximation Without Target Altitude Compensation

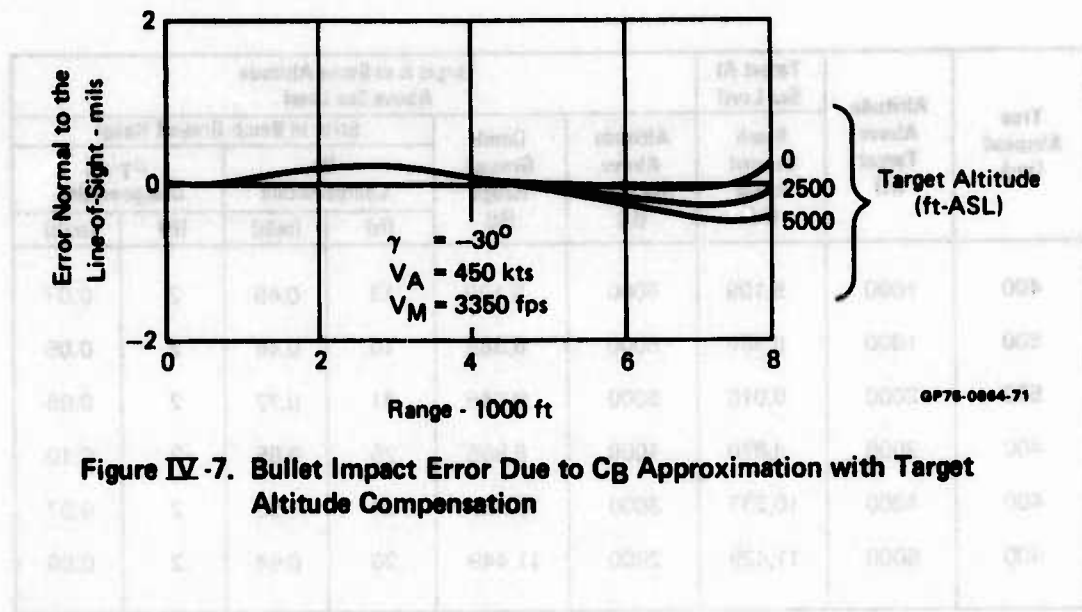


Figure IV-7. Bullet Impact Error Due to Cg Approximation with Target Altitude Compensation

Figure IV-8. Variation in Bomb Ground Range with Altitude of Target Above Sea Level

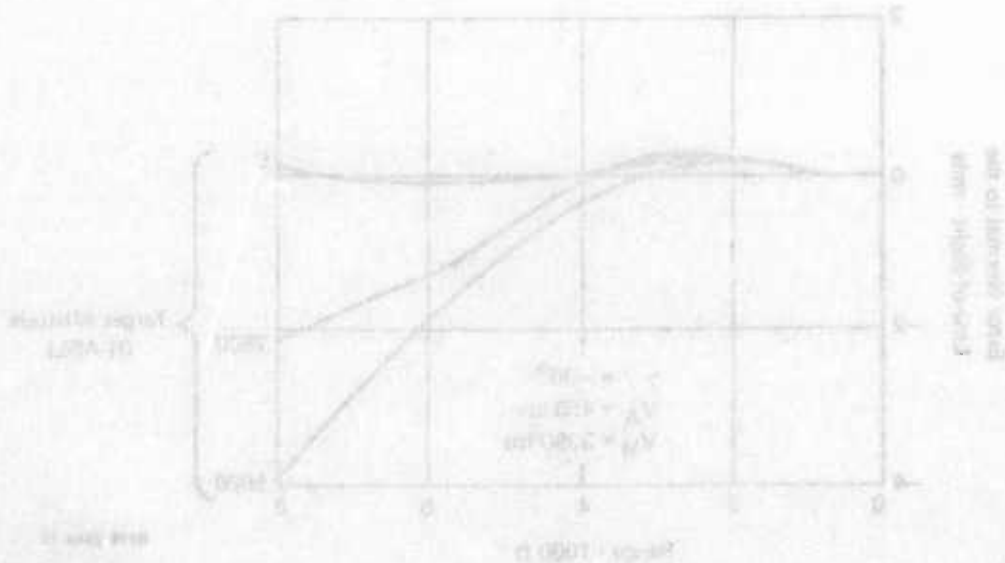


Figure IV-8. Variation in Bomb Ground Range with Altitude of Target Above Sea Level

APPENDIX V

AIR-TO-GROUND DYNAMIC FORMULATION FOR THE TAWDS(AG) PROGRAM

The air-to-ground TAWDS(AG) program uses linear state equations to implement the covariance method. These equations are obtained by perturbing non-linear noninal equations.

Equations V-1 through V-22 present the longitudinal linear equations.

Δu - forward velocity perturbation, body axis system:

$$\begin{aligned} \Delta \dot{u} = & X_u \Delta u + X_w \Delta w + (-g \cos \theta_N) \Delta \theta \\ & + X_h \Delta h + X_w w_g + (F_{Gx}/m) \\ & + WSE(1) + DGE(1) \end{aligned} \quad (V-1)$$

Δw - vertical velocity perturbation, body axis system:

$$\begin{aligned} \Delta \dot{w} = & Z_u \Delta u + Z_w \Delta w + (-g \sin \theta_N) \Delta \theta \\ & + (U_N + Z_q) \Delta q + Z_h \Delta h + Z_w w_g \\ & + Z_\delta \Delta \delta_e + (F_{Gz}/m) + WSE(2) \\ & + DGE(2) \end{aligned} \quad (V-2)$$

$\Delta \theta$ - pitch angle perturbation:

$$\Delta \dot{\theta} = q \quad (V-3)$$

Δq - pitch rate perturbation:

$$\begin{aligned} \Delta \dot{q} = & ((M_u/U_N) + M_w Z_u) \Delta u + (M_w + M_w Z_w) \Delta w \\ & + (-M_w g \sin \theta_N) \Delta \theta + (M_q + M_w (U_N + Z_q)) \Delta q \\ & + ((M_h/U_N) + M_w Z_h) \Delta h + ((-M_w U_N/L) (\sqrt{3} - 1)) w_1 \\ & + (M_w - M_w ((U_N/L) - Z_w)) w_g + (M_\delta + M_w Z_\delta) \Delta \delta_e \\ & + (M_w \sqrt{3U_N/L}) |w_g| + (M_w (F_{Gz}/m) + (M_{Gy}/I_{yy})) \\ & + WSE(4) + DGE(4) \end{aligned} \quad (V-4)$$

ΔR - range perturbation:

$$\Delta \dot{R} = (-1) \Delta u \quad (V-5)$$

Δh - altitude perturbation:

$$\Delta \dot{h} = \sin \theta_N \Delta u + (-\cos \theta_N) \Delta w + (U_N \cos \theta_N + W_N \sin \theta_N) \Delta \theta \quad (V-6)$$

$\Delta \epsilon_E$ - elevation tracking error perturbation:

$$\dot{\Delta \epsilon}_E = G_u(t) \Delta u + G_w(t) \Delta w + G_q(t) \Delta q + G_R(t) \Delta R + G_{\epsilon_E}(t) \Delta \epsilon_E \quad (V-7)$$

w_1 - vertical Dryden wind gust internal state:

$$\dot{w}_1 = (-U_N/L) w_1 + \sqrt{U_N/L} |w_g| \quad (V-8)$$

w_g - vertical Dryden wind gust state:

$$\dot{w}_g = ((-U_N/L)(\sqrt{3}-1)) w_1 + (-U_N/L) w_g + \sqrt{3U_N/L} |w_g| \quad (V-9)$$

$\Delta \delta_{e_1}$ - longitudinal stick force prefilter perturbation:

$$\Delta \dot{Y}_{\delta_{e_1}} = (1/\tau_o) (-\Delta Y_{\delta_{e_1}} + K_o (\Delta F_{P4} + P_{reml})) \quad (V-10a)$$

$$\Delta \delta_{e_1} = \Delta Y_{\delta_{e_1}} \quad (V-10b)$$

$\Delta \delta_{e_2}$ - first compensator perturbation:

$$\Delta \dot{Y}_{\delta_{e_2}} = K_6 K_F (K_{FB} \Delta \delta_{e_5} - K_{NL1} \Delta \delta_{e_1}) \quad (V-11a)$$

$$\Delta \delta_{e_2} = K_F (K_{FB} \Delta \delta_{e_5} - K_{NL1} \Delta \delta_{e_1}) + \Delta Y_{\delta_{e_2}} \quad (V-11b)$$

$\Delta \delta_{e_3}$ - second compensator perturbation:

$$\Delta \dot{Y}_{\delta_{e_3}} = (1/\tau_9) (-K_9 \Delta Y_{\delta_{e_3}} + (K_7 \tau_9 - K_9 \tau_7) (1/\tau_9) \Delta \delta_{e_2}) \quad (V-12a)$$

$$\Delta \delta_{e_3} = (\tau_7/\tau_9) \Delta \delta_{e_2} + \Delta Y_{\delta_{e_3}} \quad (V-12b)$$

$\Delta \delta_{e_4}$ - third compensator perturbation:

$$\Delta \dot{Y}_{\delta_{e_4}} = (1/\tau_{10}) (-K_{10} \Delta Y_{\delta_{e_4}} + (K_8 \tau_{10} - K_{10} \tau_8) (1/\tau_{10}) \Delta \delta_{e_3}) \quad (V-13a)$$

$$\Delta \delta_{e_4} = (\tau_8/\tau_{10}) \Delta \delta_{e_3} + \Delta Y_{\delta_{e_4}} \quad (V-13b)$$

$\Delta \delta_{e_5}$ - feedback filter perturbation:

$$\Delta \dot{Y}_{\delta_{e_5}} = (1/\tau_{27}) (-K_{27} \Delta Y_{\delta_{e_5}} + (K_{26} \tau_{27} - K_{27} \tau_{26}) (1/\tau_{27}) (\Delta \delta_{e_6} + \Delta \delta_{e_7})) \quad (V-14a)$$

$$\Delta \delta_{e_5} = (\tau_{26}/\tau_{27}) (\Delta \delta_{e_6} + \Delta \delta_{e_7}) + \Delta Y_{\delta_{e_5}} \quad (V-14b)$$

$\Delta\delta_{e6}$ - the normal acceleration filter perturbation:

$$\begin{aligned} \dot{\Delta Y}_{\delta_{e6}} &= (1/\tau_{13})(-K_{13}\Delta Y_{\delta_{e6}} + (K_{12}\tau_{13} - K_{13}\tau_{12}) \\ &\quad (K_{NZ1}/\tau_{13})(\Delta n_{Z_{cgs}} + K_{\theta}^*/g \Delta\ddot{\theta})) \end{aligned} \quad (V-15a)$$

$$\Delta\delta_{e6} = (\tau_{12}/\tau_{13})K_{NZ1}(\Delta n_{Z_{cgs}} + K_{\theta}^* \Delta\ddot{\theta}) + \Delta Y_{\delta_{e6}} \quad (V-15b)$$

$\Delta\delta_{e7}$ - the pitch rate filter perturbations:

$$\begin{aligned} \dot{\Delta Y}_{\delta_{e7}} &= (1/\tau_{17})(-K_{17}\Delta Y_{\delta_{e7}} + (K_{16}\tau_{17} - K_{17}\tau_{16}) \\ &\quad (K_{\theta}^*/\tau_{17}) \Delta\dot{\theta}) \end{aligned} \quad (V-16a)$$

$$\Delta\delta_{e7} = (\tau_{16}/\tau_{17}) K_{\theta}^* \Delta\dot{\theta} + \Delta Y_{\delta_{e7}} \quad (V-16b)$$

$\Delta\delta_e$ - the stabilator perturbation:

$$\dot{\Delta\delta}_e = (1/\tau_{11})(-\Delta\delta_e + \Delta\delta_{e4}) - K_{NLI} K_M (\Delta F_{P4} + P_{rem1}) \quad (V-17)$$

ΔF_{P1} - perturbed state for pilot model A:

$$\dot{\Delta Y}_{FP1} = (1/D_{E11})(-D_{E12}\Delta Y_{FP1} + (1/D_{E11})(D_{E10}D_{E11} - D_{E12}D_{E9})\Delta F_{P2}) \quad (V-18a)$$

$$\Delta F_{P1} = (D_{E9}/D_{E11}) \Delta F_{P2} + \Delta Y_{FP1} \quad (V-18b)$$

ΔF_{P2} - perturbed state for pilot model A:

$$\dot{\Delta Y}_{FP2} = (1/D_{E7})(-D_{E8}\Delta Y_{FP2} + (1/D_{E7})(D_{E6}D_{E7} - D_{E8}D_{E5}) \Delta F_{P3}) \quad (V-19a)$$

$$\Delta F_{P2} = (D_{E5}/D_{E7}) \Delta F_{P3} + \Delta Y_{FP2} \quad (V-19b)$$

Equations V-18a, -18b, -19a, and -19b are different for pilot model B.

Instead of states ΔY_{FP1} and ΔY_{FP2} , the states DUMD and DUM are used:

DUMD - intermediate perturbed state for pilot model B:

$$\dot{DUMD} = (1/D_{E7})(\Delta F_{P3} - D_{E11} DUMD - D_{E12} DUM) \quad (V-18c)$$

DUM - intermediate perturbed state for pilot model B:

$$\dot{DUM} = DUMD \quad (V-19c)$$

then for pilot model B, Equation (V-18b) becomes

$$\Delta F_{P1} = D_{E5} \dot{DUMD} + D_{E9} DUMD + D_{E10} DUM \quad (V-18d)$$

ΔF_{P3} - perturbed state for either pilot model:

$$\dot{\Delta F_{P3}} = (1/D_{E3})(-D_{E4} \Delta Y_{FP3} + (K_{PE}/D_{E3})(D_{E2} D_{E3} - D_{E4} D_{E1}) \Delta \epsilon_E) \quad (V-20a)$$

$$\Delta F_{P3} = K_{PE} (D_{E1}/D_{E3}) \Delta \epsilon_E + \Delta Y_{FP3} \quad (V-20b)$$

ΔF_{P4} - pilot model integrator state perturbation:

$$\dot{\Delta F_{P4}} = (1/D_{E_{INT}}) \Delta F_{P1} \quad (V-21)$$

P_{rem1} - elevation pilot model remnant

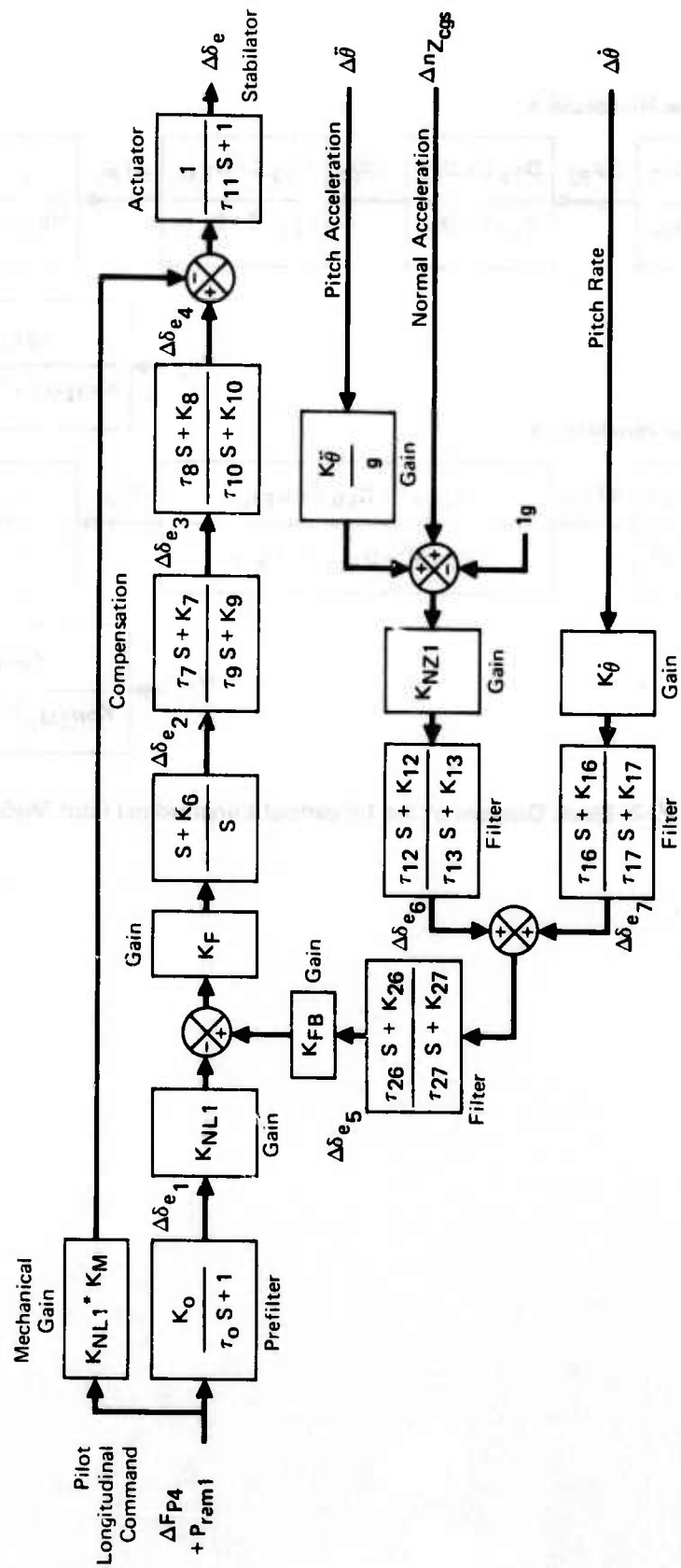
$$\dot{P}_{rem1} = (1/K_{PREM2})(-K_{PREM3} P_{rem1} + K_{PREM1} w_{n2}) \quad (V-22)$$

Figure V-1 is a block diagram of the longitudinal control system. It includes the name of each filter output and its internal state name (if there is one). Equations V-10 through V-17 relate to this figure. Figure V-2 is a block diagram of longitudinal pilot models A and B. Similarly to Figure V-1, this figure corresponds to equations V-18 through V-22.

Equations V-23 through V-44 present the lateral-directional linear differential equations.

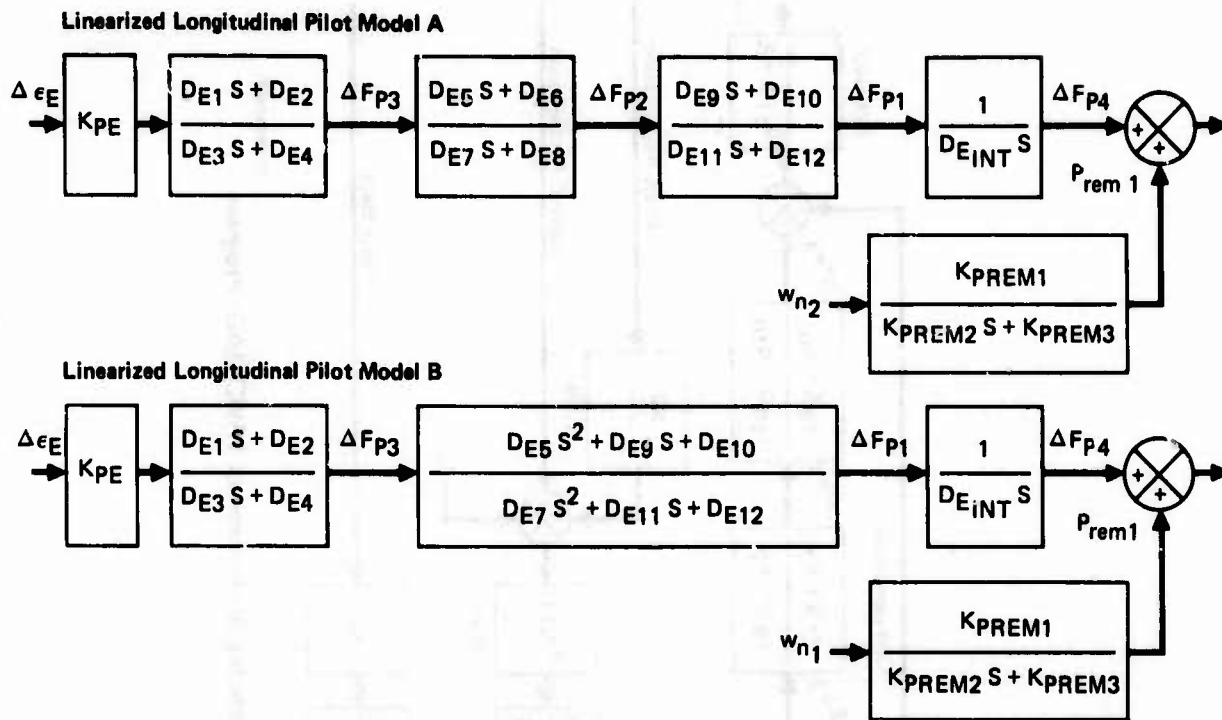
$\Delta \beta$ - sideslip angle perturbation:

$$\begin{aligned} \dot{\Delta \beta} = & Y_{\beta} \Delta \beta + Y_p \Delta p + Y_r \Delta r + (g/U_N) \Delta \phi + (Y_{\beta}/U_N) v_g \\ & + Y_{\delta_a} \Delta \delta_a + Y_{\delta_r} \Delta \delta_r \end{aligned} \quad (V-23)$$



GP75-0864-77

Figure V-1. Generic Longitudinal Flight Control System for Air-to-Ground TAWDS(AG) Program



GP78-0864-217

Figure V-2. Block Diagram of the Linearized Longitudinal Pilot Models

Δp - roll rate perturbation:

$$\begin{aligned} \Delta \dot{p} = & L_{\beta} \Delta \beta + L_p \Delta p + L_r \Delta r + (L_{\beta}/U_N) v_g + L_{\delta_a} \Delta \delta_a \\ & + L_{\delta_r} \Delta \delta_r + (M_{Gx}/I_{xx}) \end{aligned} \quad (V-24)$$

Δr - yaw rate perturbation:

$$\begin{aligned} \Delta \dot{r} = & N_{\beta} \Delta \beta + N_p \Delta p + N_r \Delta r + (N_{\beta}/U_N) v_g + N_{\delta_a} \Delta \delta_a \\ & + N_{\delta_r} \Delta \delta_r + (M_{Gz}/I_{zz}) \end{aligned} \quad (V-25)$$

$\Delta \phi$ - roll angle perturbation:

$$\Delta \dot{\phi} = \Delta p \quad (V-26)$$

$\Delta \epsilon_T$ - traverse tracking error perturbation:

$$\Delta \dot{\epsilon}_T = G_{\beta}(t) \Delta \beta + G_p(t) \Delta p + G_r(t) \Delta r + G_{\epsilon_T}(t) \Delta \epsilon_T + G_{\phi}(t) \Delta \phi \quad (V-27)$$

v_1 - lateral Dryden wind gust internal state:

$$\dot{v}_1 = (-U_N/L) v_1 + \sqrt{U_N/L} |v_g| \quad (V-28)$$

v_g - lateral Dryden wind gust state:

$$\begin{aligned} \dot{v}_g = & (-U_N/L) (\sqrt{3} - 1) v_1 + (-U_N/L) v_g \\ & + \sqrt{3U_N/L} |v_g| \end{aligned} \quad (V-29)$$

$\Delta \delta_{a_1}$ - lateral stick force prefilter perturbation:

$$\Delta \dot{\delta}_{a_1} = (1/\tau_1) (-\Delta \delta_{a_1} + K_1 (\Delta F_{CS1} + P_{rem2} + K_{PPHI} \Delta \phi)) \quad (V-30)$$

$\Delta \delta_a$ - aileron perturbation:

$$\begin{aligned} \dot{\Delta\delta}_a &= (1/\tau_8)(-\Delta\delta_a + K_{NL1} \Delta\delta_{a1} \\ &+ K_{NL1} K_{MC1} (\Delta F_{CS1} + P_{rem2} + K_{PPhi} \Delta\phi) \\ &- K_p \Delta p - K_\phi \Delta\phi - K_{RA} \Delta r) \end{aligned} \quad (V-31)$$

$\Delta\delta_{a2}$ - the aileron - rudder - interconnect (ARI) filter perturbation:

$$\begin{aligned} \dot{\Delta Y}_{\delta_{a2}} &= (1/\tau_{10})(-K_{10} \Delta Y_{\delta_{a2}} ((K_9 \tau_{10} - K_{10} \tau_9)/\tau_{10})(K_{ARI1} (\Delta F_{CS1} + P_{rem2} \\ &+ K_{PPhi} \Delta\phi) + K_{ARI2} (K_{NL1} \Delta\delta_{a1} + K_{NL1} K_{MC1} (\Delta F_{CS1} + P_{rem2} \\ &+ K_{PPhi} \Delta\phi) - K_p \Delta p - K_\phi \Delta\phi - K_{RA} \Delta r))) \end{aligned} \quad (V-32a)$$

$$\begin{aligned} \Delta\delta_{a2} &= \Delta Y_{\delta_{a2}} + (\tau_9/\tau_{10})(K_{ARI1} (\Delta F_{CS1} + P_{rem2} + K_{PPhi} \Delta\phi) \\ &+ K_{ARI2} (K_{NL1} \Delta\delta_{a1} + K_{NL1} K_{MC1} (\Delta F_{CS1} + P_{rem2} + K_{PPhi} \Delta\phi) \\ &- K_p \Delta p - K_\phi \Delta\phi - K_{RA} \Delta r)) \end{aligned} \quad (V-32b)$$

$\Delta\delta_{r1}$ - rudder force prefilter perturbation:

$$\dot{\Delta\delta}_{r1} = (1/\tau_{16})(-\Delta\delta_{r1} + K_{16} (\Delta F_{R1} + P_{rem3})) \quad (V-33)$$

$\Delta\delta_{r2}$ - angular rate feedback filter perturbation:

$$\begin{aligned} \dot{\Delta Y}_{\delta_{r2}} &= (1/\tau_{13})(-K_{13} \Delta Y_{\delta_{r2}} + ((K_{12} \tau_{13} - K_{13} \tau_{12})/\tau_{13})(K_\beta \Delta\beta \\ &+ K_\beta \dot{\Delta\beta} + K_{Pl\alpha} \Delta p + K_r \Delta r - K_{gV} (g/V_N) \cos\phi_N \cos\theta_N \Delta\phi)) \end{aligned} \quad (V-34a)$$

$$\begin{aligned} \Delta\delta_{r2} &= \Delta Y_{\delta_{r2}} + (\tau_{12}/\tau_{13})(K_\beta \Delta\beta + K_\beta \dot{\Delta\beta} + K_{Pl\alpha} \Delta p \\ &+ K_r \Delta r - K_{gV} (g/V_N) \sin\phi_N \cos\theta_N) \end{aligned} \quad (V-34b)$$

where: $\phi_N = 0.0$

$\Delta\delta_{r_3}$ - lateral acceleration filter perturbation:

$$\begin{aligned} \dot{\Delta Y}_{\delta_{r_3}} = & (1/\tau_{15})(-K_{15}\Delta Y_{\delta_{r_3}} + ((K_{14}\tau_{15} - K_{15}\tau_{14})/\tau_{15}) \\ & (V_N Y_{\beta} \Delta\beta + V_N Y_p \Delta p + V_N(Y_r+1)\Delta r + V_N Y_{\delta_a} \\ & + V_N Y_{\delta_r} + Y_{\beta} v_g + c g_x(N_{\beta} \Delta\beta + N_p \Delta p + N_r \Delta r \\ & + N_{\delta_a} \Delta\delta_a + N_{\delta_r} \Delta\delta_r + (N_{\beta}/U_N) v_g) - c g_z(L_{\beta} \Delta\beta \\ & + L_p \Delta p + L_r \Delta r + L_{\delta_a} \Delta\delta_a + L_{\delta_r} \Delta\delta_r + (L_{\beta}/U_N) v_g))) \end{aligned} \quad (V-35a)$$

$$\begin{aligned} \Delta\delta_{r_3} = & \Delta Y_{\delta_{r_3}} + (\tau_{14}/\tau_{15})(V_N Y_{\beta} \Delta\beta \\ & + V_N Y_p \Delta p + V_N(Y_r+1)\Delta r + V_N Y_{\delta_a} \\ & + V_N Y_{\delta_r} + Y_{\beta} v_g + c g_x(N_{\beta} \Delta\beta + N_p \Delta p + N_r \Delta r \\ & + N_{\delta_a} \Delta\delta_a + N_{\delta_r} \Delta\delta_r + (N_{\beta}/U_N) v_g) - c g_z \\ & (L_{\beta} \Delta\beta + L_p \Delta p + L_r \Delta r + L_{\delta_a} \Delta\delta_a \\ & + L_{\delta_r} \Delta\delta_r + (L_{\beta}/U_N) v_g)) \end{aligned} \quad (V-35b)$$

$\Delta\delta_r$ - the rudder perturbation:

$$\begin{aligned} \dot{\Delta\delta}_r = & (1/\tau_{23})(-\Delta\delta_r + K_{FLX} \\ & (K_{rr} \Delta\delta_{r_2} + K_{ay} \Delta\delta_{r_3} - K_{NL2} \Delta\delta_{r_1} - \Delta\delta_{a_2} \\ & - K_{NL2} K_{MR} (\Delta F_{R1} + P_{rem3}))) \end{aligned} \quad (V-36)$$

ΔF_{CS1} - perturbed lateral pilot model state:

$$\begin{aligned} \dot{\Delta Y}_{F_{CS1}} &= (1/D_{T11})(-D_{T12}\Delta Y_{F_{CS1}} \\ &+ ((D_{T10}D_{T11} - D_{T12}D_{T9})/D_{T11})\Delta F_{CS2} \end{aligned} \quad (V-37a)$$

$$\Delta F_{CS1} = (D_{T9}/D_{T11})\Delta F_{CS2} + \Delta Y_{F_{CS1}} \quad (V-37b)$$

ΔF_{CS2} - perturbed lateral pilot model state:

$$\begin{aligned} \dot{\Delta Y}_{F_{CS2}} &= (1/D_{T7})(-D_{T8}\Delta Y_{F_{CS2}} \\ &+ ((D_{T6}D_{T7} - D_{T8}D_{T5})/D_{T7})\Delta F_{CS3} \end{aligned} \quad (V-38a)$$

$$\Delta F_{CS2} = (D_{T5}/D_{T7})\Delta F_{CS3} + \Delta Y_{F_{CS2}} \quad (V-38b)$$

ΔF_{CS3} - perturbed lateral pilot model state:

$$\begin{aligned} \dot{\Delta Y}_{F_{CS3}} &= (1/D_{T3})(-D_{T4}\Delta Y_{F_{CS3}} \\ &+ (K_{PT}/D_{T3})(D_{T2}D_{T3} - D_{T4}D_{T1})\Delta \epsilon_T \end{aligned} \quad (V-39a)$$

$$\Delta F_{CS3} = K_{PT}(D_{T1}/D_{T3})\Delta \epsilon_T + \Delta Y_{F_{CS3}} \quad (V-39b)$$

P_{rem2} - lateral pilot model remnant:

$$\dot{P}_{rem2} = (1/K_{PREM5})(-K_{PREM6}P_{rem2} + K_{PREM4}w_{n4}) \quad (V-40)$$

ΔF_{R1} - perturbed directional pilot model state:

$$\begin{aligned} \dot{\Delta Y}_{FR1} &= (1/D_{T23})(-D_{T24}\Delta Y_{FR1} \\ &+ ((D_{T22}D_{T23} - D_{T24}D_{T21})/D_{T23})\Delta F_{R2} \end{aligned} \quad (V-41a)$$

$$\Delta F_{R1} = (D_{T21}/D_{T23})\Delta F_{R2} + \Delta Y_{FR1} \quad (V-41b)$$

ΔF_{R2} - perturbed directional pilot model state:

$$\begin{aligned} \dot{\Delta Y}_{FR2} &= (1/D_{T19}) (-D_{T20} \Delta Y_{FR2} \\ &\quad + ((D_{T18}^D D_{T19} - D_{T20}^D D_{T17})/D_{T19}) \Delta F_{R3} \end{aligned} \quad (V-42a)$$

$$\Delta F_{R2} = (D_{T17}/D_{T19}) \Delta F_{R3} + \Delta Y_{FR2} \quad (V-42b)$$

ΔF_{R3} - perturbed directional pilot model state:

$$\begin{aligned} \dot{\Delta Y}_{FR3} &= (1/D_{T15}) (-D_{T16} \Delta Y_{FR3} \\ &\quad + (K_{RT}/D_{T15}) (D_{T14}^D D_{T15} - D_{T16}^D D_{T13}) \Delta \epsilon_T \end{aligned} \quad (V-43a)$$

$$\Delta F_{R3} = K_{RT} (D_{T13}/D_{T15}) \Delta \epsilon_T + \Delta Y_{FR3} \quad (V-43b)$$

P_{rem3} - directional pilot model remnant:

$$P_{rem3} = (1/K_{PREM8}) (-K_{PREM9} P_{rem3} + K_{PREM7} w_{n6}) \quad (V-44)$$

Figure V-3 is a block diagram of the lateral-directional control system and Figures V-4 and V-5 are block diagrams of the lateral and the directional pilot models. Equations V-30 through V-44 relate to these figures.

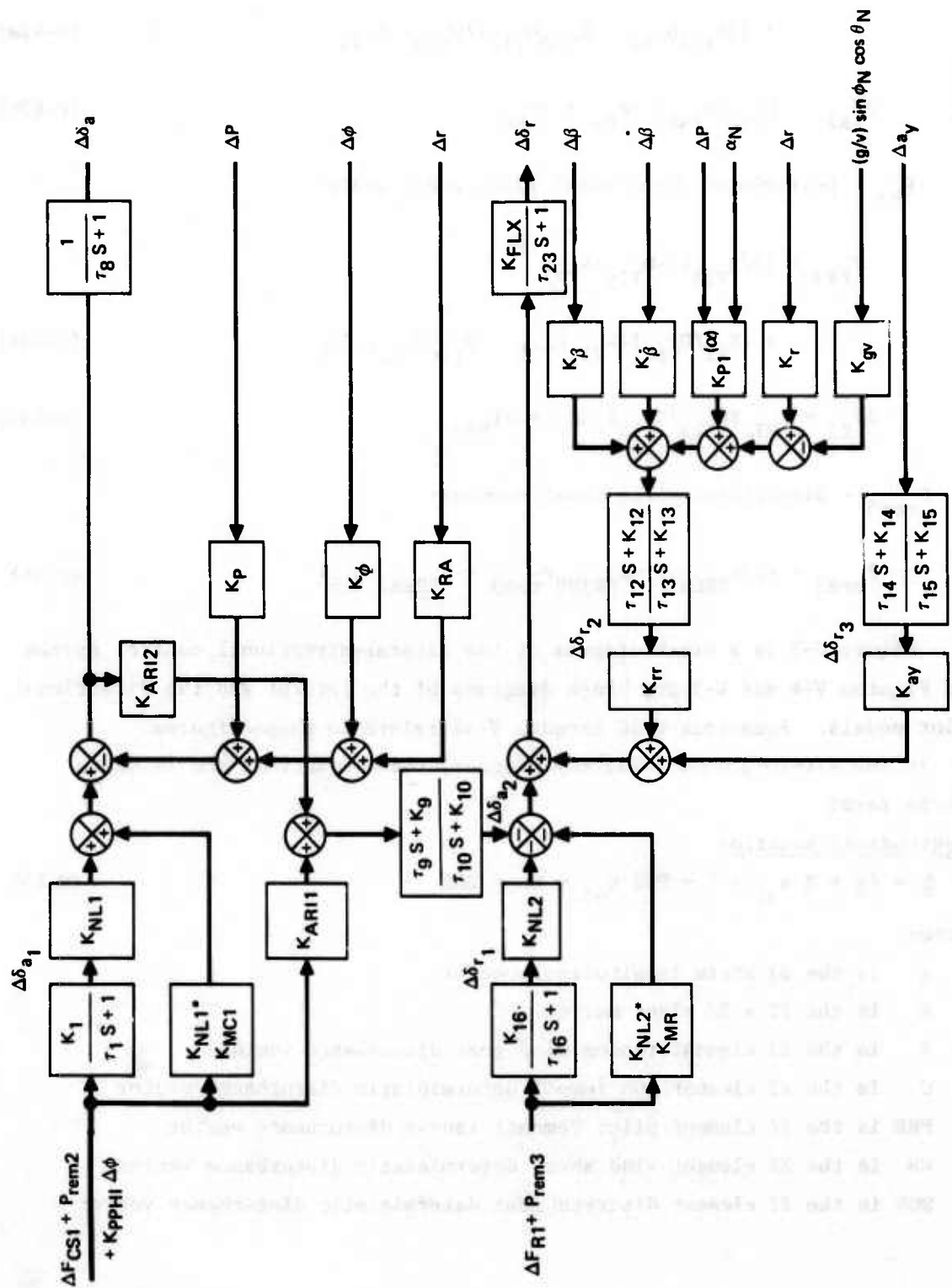
In the air-to-ground TAWDS(AG) program, these equations are in state matrix form:

Longitudinal Equation

$$\dot{\underline{x}} = \underline{A} \underline{x} + \underline{B} w_{n1} + \underline{C} + \underline{PRE} w_{n3} + \underline{WS} + \underline{DGE} \quad (V-45)$$

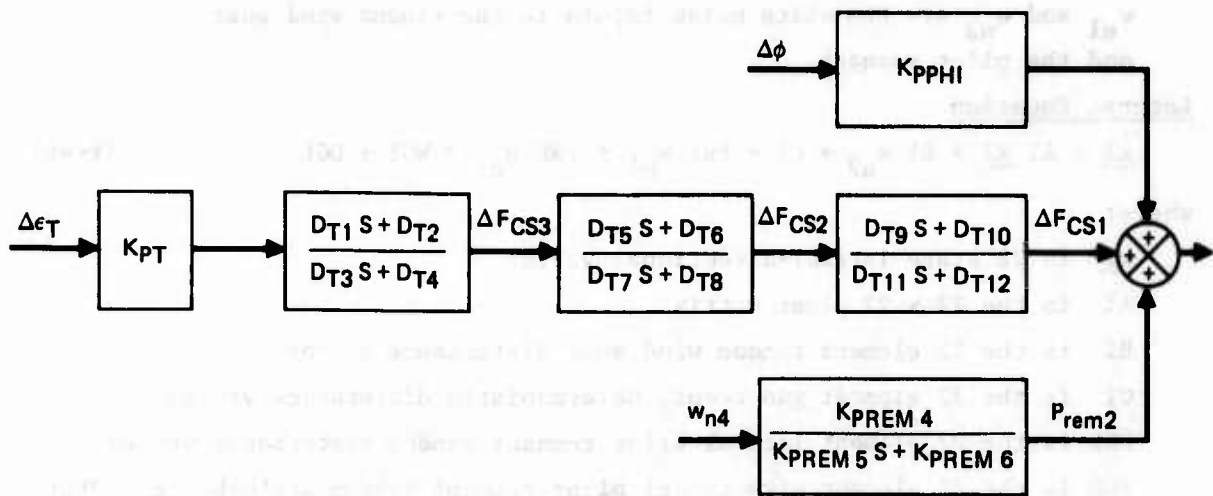
where:

- \underline{x} is the 22 state longitudinal vector
- \underline{A} is the 22 x 22 plant matrix
- \underline{B} is the 22 element random wind gust disturbance vector
- \underline{C} is the 22 element gun recoil deterministic disturbance vector
- \underline{PRE} is the 22 element pilot remnant random disturbance vector
- \underline{WS} is the 22 element wind shear deterministic disturbance vector
- \underline{DGE} is the 22 element discrete gust deterministic disturbance vector



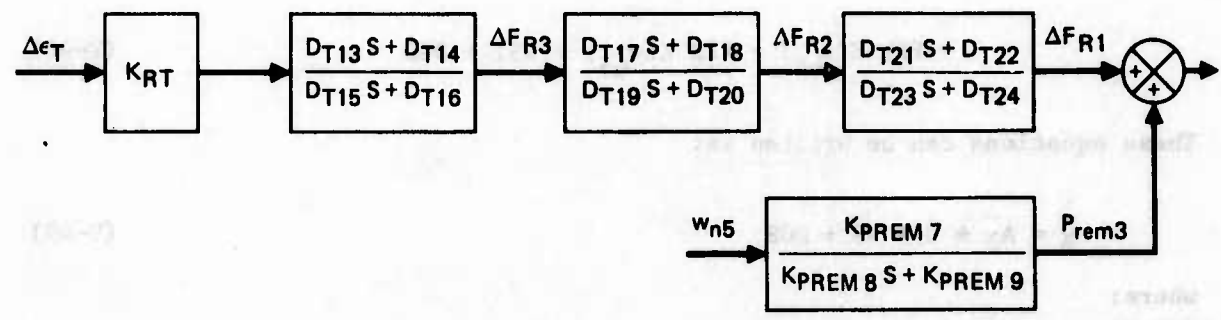
GP75-0884-212

Figure V-3. Block Diagram of the Linearized Lateral-Directional Flight Control System



GP78-0864-219

Figure V-4. Block Diagram of the Linearized Lateral Pilot Model



GP78-0864-219

Figure V-5. Block Diagram of the Linearized Directional Pilot Model

w_{n1} and w_{n3} are the white noise inputs to the random wind gust and the pilot remnant.

Lateral Equation

$$\dot{\underline{x}}_1 = A_1 \underline{x}_1 + B_1 w_{n2} + C_1 + PRL w_{n4} + PRD w_{n5} + WS_1 + DGL \quad (V-46)$$

where:

- \underline{x}_1 is 22 state lateral-directional vector
- A_1 is the 22 x 22 plant matrix
- B_1 is the 22 element random wind gust disturbance vector
- C_1 is the 22 element gun recoil deterministic disturbance vector
- PRL is the 22 element lateral pilot remnant random disturbance vector
- PRD is the 22 element directional pilot remnant random disturbance vector
- WS₁ is the 22 element wind shear deterministic disturbance vector
- DGL is the 22 element discrete gust deterministic disturbance vector
- w_{n2} , w_{n4} , and w_{n5} are the white noise inputs to the random wind gust and the pilot remnants.

The equations actually programmed in TAWDS(AG) are the mean and the covariance equations. These are derived from the state equations. Taking the expected value of Equation V-45 and V-46, the mean state differential equations are:

$$E\{\dot{\underline{x}}\} = A E\{\underline{x}\} + B E\{w_{n1}\} + C + PRE E\{w_{n3}\} + WS + DGE \quad (V-47)$$

$$E\{\dot{\underline{x}}_1\} = A_1 E\{\underline{x}_1\} + B_1 E\{w_{n2}\} + C_1 + PRL E\{w_{n4}\} + PRD E\{w_{n5}\} + WS_1 + DGL \quad (V-48)$$

These equations can be written as:

$$\dot{\underline{x}} = \underline{A} \underline{x} + C + WS + DGE \quad (V-49)$$

where:

- $E\{\underline{x}\} = \underline{\bar{x}}$, the mean state vector
- $E\{w_{n1}\} = 0$, assuming zero mean wind gusts
- $E\{w_{n3}\} = 0$, assuming zero mean pilot remnant

and

$$\dot{\underline{x}}_1 = A_1 \underline{x}_1 + C_1 + WS_1 + DGL \quad (V-50)$$

where:

$$E\{\underline{x}_1\} = \overline{\underline{x}_1}, \text{ the mean state vector}$$

$$E\{w_{n2}\} = 0, \text{ assuming zero mean wind gusts}$$

$$E\{w_{n4}\} = 0, \text{ assuming zero mean lateral pilot remnant}$$

$$E\{w_{n5}\} = 0, \text{ assuming zero mean directional pilot remnant}$$

Defining:

$$\Sigma = E\{(\underline{x} - \overline{\underline{x}})(\underline{x} - \overline{\underline{x}})^T\} \quad (V-51)$$

$$\Sigma_1 = E\{(\underline{x}_1 - \overline{\underline{x}_1})(\underline{x}_1 - \overline{\underline{x}_1})^T\} \quad (V-52)$$

the covariance differential equations are

$$\dot{\Sigma} = A\Sigma + \Sigma A^T + B Q_w B^T + (PRE) Q_e (PRE)^T \quad (V-53)$$

$$\begin{aligned} \dot{\Sigma}_1 = & A_1 \Sigma_1 + \Sigma_1 A_1^T + B_1 Q_{1w} B_1^T \\ & + (PRL) Q_{1\ell} (PRL)^T + (PRD) Q_{1d} (PRD)^T \end{aligned} \quad (V-54)$$

where:

$$Q_w = E\{w_{n1} w_{n1}^T\}$$

$$Q_e = E\{w_{n3} w_{n3}^T\}$$

$$Q_{1w} = E\{w_{n2} w_{n2}^T\}$$

$$Q_{1\ell} = E\{w_{n4} w_{n4}^T\}$$

$$Q_{1d} = E\{w_{n5} w_{n5}^T\}$$

For more information on the covariance method, see the Interim Report (Reference V-1).

REFERENCES

- V-1. Berger, J. B., et al., "Flight Control Requirements for Weapon Delivery, Interim Report for Period June 1973-May 1974," Technical Report AFFDL-TR-74-119.

APPENDIX VI

BURST STATISTICS FOR AIR-TO-GROUND WEAPON DELIVERY

This Appendix presents the equation formulation for the calculation of ensemble burst statistics for the air-to-ground gunnery task. Application of these statistical computations to the air-to-ground bombing task is discussed.

For the air-to-ground gunnery task each firing pass consists of a single burst, and the same number of rounds are fired for each burst. Consequently, the burst statistics derived in Reference VI-1 are calculated as follows:

- Ensemble Mean Impact Error: $E[b] = \bar{b}$

$$\bar{b} = \frac{1}{n} \sum_{i=1}^n m(i) \quad (VI-1)$$

- Burst Mean Impact Error Variance: $E[(b - \bar{b})^2]$

$$E[(b - \bar{b})^2] = \frac{1}{n} \sum_{i=1}^n \sigma_s^2(i) + \frac{1}{n^2} \sum_{i=1}^n \sum_{j=1}^n \rho_d(i,j) \sigma_d(i) \sigma_d(j) \quad (VI-2)$$

- Impact Error Variance within a Burst: $E[\frac{1}{n} \sum_{i=1}^n (a(i) - b)^2]$

$$E[\frac{1}{n} \sum_{i=1}^n (a(i) - b)^2] = \frac{1}{n} \sum_{i=1}^n (\sigma_s^2(i) + \sigma_d^2(i) + m^2(i)) - b^2 - E[(b - \bar{b})^2] \quad (VI-3)$$

where:

$m(i)$ = Mean Impact Error (for the i^{th} round)

$\sigma_s^2(i)$ = Impact Error Variance Due to Stationary Source Errors

$\sigma_d^2(i)$ = Impact Error Variance Due to Dynamic Source Errors

$\rho_d(i,j)$ = Dynamic Individual Round-to-Round Correlation

Coefficient for Rounds i and j

$a(i)$ = Impact error of i^{th} round of the burst

The variables required to compute the ensemble burst statistics are summarized as follows:

- Mean Aim Error Due to Stationary and Dynamic Source Errors
- Aim Error Variance from the Mean Due to Stationary Source Errors
- Aim Error Variance from the Mean Due to Dynamic Source Errors
- Dynamic Individual Weapon-to-Weapon Correlation Coefficient

The stochastic procedure originally developed to compute these four required variables for the air-to-ground gunnery task has been extended for air-to-ground bombing. The methods used in computing these variables are presented in terms of the gunnery problem.

VI.1 Mean Aim Error Due to Stationary and Dynamic Source Errors - The major contributors to air-to-ground gunnery impact errors are flight profile and system mechanization source errors. All of these source errors may be considered to have stationary components; that is, on any particular gunnery pass a random bias error may exist in some or all of these sources. It is assumed herein that, over an ensemble of aircraft, the mean of each of the stationary source errors is zero. However, there remains a stationary mean error for each pass, due both to sight mechanization errors and to the tracking error of the aircraft gunnery profile. The effects of these errors are time-varying; but they are categorized as stationary because their effects are fixed (deterministic) for each individual pass. They are computed simply by firing bullets and numerically integrating them down to the target plane, normal to the line-of-sight, where the impact error is computed.

The nominal attack gunnery profile can be arbitrarily chosen. Its associated time-varying parameters (such as range, velocity, pilot parameters, etc.) are then used to generate the elements of the system dynamics matrices of the linear perturbation model. Ultimately, the complete dynamics of the pilot, airframe, flight control system, and tracking geometry are described in the model by a set of interacting, nonlinear differential equations.

The approach taken to determine the impact error due to dynamic source errors such as wind gust, wind shear, pilot remnant, and weapon release force, is to linearize the dynamic equations of motion about the nominal gunnery profile. Thus, the dynamics of the airframe and tracking geometry are described by differential equations which have the following general form:

$$\dot{x}(t) = A(t) x(t) + B(t) u_v(t) + C(t) u_c(t) \quad (\text{VI-4})$$

where:

x = state variable vector

u_v = stochastic (variable) disturbance vector, assumed to be white noise

u_c = deterministic (constant) disturbance vector

These differential equations which describe the air-to-ground, wings level gunnery task, are separated into two sets of uncoupled linear differential equations, one for the longitudinal aircraft and elevation tracking state vector, and the other for the lateral-directional aircraft and traverse tracking state vector.

The mean vectors and covariance matrices associated with the elevation and traverse channels of the air-to-ground attack system linear dynamic model can be obtained directly from Equation (VI-4). Taking the expected value, the mean state variable differential equation is:

$$\dot{\bar{x}}(t) = A(t) \bar{x}(t) + C(t) u_c(t) \quad (\text{VI-5})$$

$E[x(t)] = \bar{x}(t)$, the mean state vector,

$E[u_v(t)] = 0$, assuming zero mean stochastic disturbance

$E[u_c(t)] = u_c(t)$

Only a few elements of the mean state vectors constitute dynamic source errors; that is, errors which reflect directly into the impact error. By separating the impact error into an along-track (elevation) and a cross-track (traverse) component, the individual error sources affecting the performance of each sight mechanization have been examined and their individual effects on the impact error components have been determined. The amount of change in impact error per unit change in each individual error source, with all other changes in error sources set to zero, is defined as impact error sensitivity.

Using these sensitivities, the total effect of the dynamic source errors on the impact error can be expressed in vector-matrix notation as,

$$\epsilon_{id}(t) = S(t) \epsilon_{sd}(t) \quad (\text{VI-6})$$

where:

$\epsilon_{id}(t)$ = the impact error vector due to dynamic source errors

$\epsilon_{sd}(t)$ = the dynamic source error vector (n x 1)

$S(t)$ - the impact error sensitivity matrix (2 x n)

The mean impact error can be obtained from Equation (VI-6) as:

$$m_{id}(t) = S(t) m_{sd}(t) \quad (\text{VI-7})$$

where:

$m_{id}(t)$ = the dynamic source error contribution to the mean impact error vector (2 x 1)

$m_{sd}(t)$ = the mean dynamic source error vector (n x 1)

The total mean impact error is computed as the sum of the mean impact error due to the stationary source errors and the mean impact error due to dynamic source errors:

$$m_i(t) = m_{is}(t) + m_{id}(t) \quad (\text{VI-8})$$

where:

$m_{is}(t)$ = the stationary source error contribution to the mean impact error vector (2 x 1).

VI.2 Impact Error Variances Due to Stationary Source Errors -

By definition, the impact error variance due to stationary source errors is:

$$\Sigma_{is}(t) = S(t) \Sigma_{ss} S^T(t) \quad (\text{VI-9})$$

where:

$\Sigma_{is}(t)$ = the stationary source error contribution to the impact error covariance matrix (2 x 2)

$S(t)$ = the impact error sensitivity matrix (2 x n)

Σ_{ss} = the stationary source error covariance matrix (n x n).

VI.3 Impact Error Variances Due to Dynamic Source Errors - By definition, the covariance matrix of the state variables defining the weapon delivery task is:

$$\Sigma_x = E [\tilde{x} \tilde{x}^T] \quad (\text{VI-10})$$

where: $\tilde{x} \triangleq x - \bar{x}$. (For convenience, the notation for time (t) has been omitted. It should be noted, however, that these variables are all time dependent.) Therefore, the differential covariance matrix is:

$$\begin{aligned} d\Sigma_x &= E[(\tilde{x} + d\tilde{x})(\tilde{x} + d\tilde{x})^T] - E[\tilde{x} \tilde{x}^T] \\ &= E[d\tilde{x} \tilde{x}^T + \tilde{x} d\tilde{x}^T + d\tilde{x} d\tilde{x}^T] \end{aligned} \quad (\text{VI-11})$$

where $d\tilde{x}$ is defined as:

$$d\tilde{x} = A(t) \tilde{x} dt + B(t) u_v(t) dt \quad (\text{VI-12})$$

and the variance of the white noise process is:

$$Q(t) = E[u_v(t) u_v^T(t)] \quad (\text{VI-13})$$

Substituting Equations (VI-12) and (VI-13) into Equation (VI-11), the differential covariance matrix can be expressed in differential equation form as:

$$\dot{\Sigma}_x(t) = A(t) \Sigma_x(t) + \Sigma_x(t) A^T(t) + B(t) Q(t) B^T(t) \quad (\text{VI-14})$$

As in the case of the stationary source errors, the contribution of the dynamic source errors to the total impact error variance can be determined from the dynamic source error covariance matrix and the impact error sensitivity matrix; that is,

$$\Sigma_{id}(t) = S(t) \Sigma_{sd}(t) S^T(t) \quad (\text{VI-15})$$

where:

$\Sigma_{id}(t)$ = the dynamic source error contribution to the impact error (dispersion) covariance (2 x 2)

$\Sigma_{sd}(t)$ = the dynamic source error covariance matrix (n x n).

VI.4 Dynamic Round-to-Round Correlation Coefficients - Calculation of the ensemble burst statistics defined by Equations (VI-2) and (VI-3) requires the correlation coefficient, $\rho_d(i,j)$, which measures the statistical correlation between all rounds i and j within the burst. In this subsection the technique for computing the dynamic round-to-round correlation coefficients for every pair of rounds in the burst is presented.

By definition, the dynamic round-to-round correlation coefficient is determined by the relation:

$$\rho_d(t_i, t_j) = \frac{\sigma_d^2(t_i, t_j)}{\sigma_d(t_i) \sigma_d(t_j)} \quad (\text{VI-16})$$

where:

$\sigma_d^2(t_i, t_j)$ = the dynamic source error contribution to the covariance between a round fired at time t_i and a round fired at time t_j ,

$\sigma_d(t_i), \sigma_d(t_j)$ = the dynamic source error contribution to the aim error variance at time t_i and t_j , respectively.

For the air-to-ground bombing mode where one bomb may be released, t_i equals t_j and the round-to-round correlation coefficient is unity.

The correlation matrix can be defined as:

$$\Sigma_x(t, t_j) = E[\tilde{x}(t) \tilde{x}^T(t_j)] \quad (\text{VI-17})$$

where $\tilde{x} = x - \bar{x}$.

The equation for \tilde{x} is:

$$\dot{\tilde{x}}(t) = A(t) \tilde{x}(t) + B(t) u_v(t) \quad (\text{VI-18})$$

so that:

$$\Sigma_x(t_i, t_j) = \Phi(t_i, t_j) \Sigma_x(t_j) \quad (\text{VI-19})$$

It can be shown that the correlation matrix satisfies the following differential equation:

$$\dot{\Sigma}_x(t, t_j) = A(t) \Sigma_x(t, t_j) \quad (VI-20)$$

This notation is chosen to emphasize that time t_j is fixed and that the running variable of integration is time t . The correlation matrices are propagated to the ground to get the correlation of impact errors on ground. The following 2 x 2 correlation matrices are obtained by using the sensitivities matrices in the following transformation:

$$\Sigma_{\theta_E \theta_T}(t, t_j) = S(t, t) \Sigma_x(t, t) S^T(t, t_j) \quad (VI-21)$$

APPENDIX VI REFERENCES

- VI-1. Williams, A.H., Landy, R.J., and Murphy, W.J., "Aerial Gunnery Methodology, Volume II - Air-to-Ground Gunnery," AFATL-TR-72-218, Volume II, November, 1972.

APPENDIX VII

DESCRIPTION OF FREQUENCY RESPONSE ANALYSIS COMPUTER PROGRAMS

VII.1 PROGRAM DESCRIPTIONS

The frequency response used to measure the pilot's describing function characteristics was obtained by using two programs listed in Reference VII-1: (1) the Time Series Spectrum Estimation Program (BMD03T) and (2) the Multiple Time Series Spectral Analysis Program (BMD04T). Two basic modifications to these programs were made: (1) the data printout was modified to reflect the data output desired in analyzing the pilot's transfer function characteristics and (2) the scale factor used in computing the autocorrelation coefficients was modified so that the sum of these coefficients equals the variance, independent of the output frequency increment selected. These programs utilize the Fast Fourier Transform. The theoretical background and description of their computational procedures are described in References VII-2 and VII-3.

VII.2 DATA RECORD LENGTH

For all cases, the data records were analyzed over the time interval from 5 to 20 seconds. This time interval was selected as the maximum interval for the weapon delivery encounters in which the data was considered to be approximately stationary, for statistical analysis. Each data record was first detrended by removing any bias and linear slope with time from the original data, and the "cosine taper" data window described in these references was applied to each detrended data record. Since an integration interval of .05 second was used, each data record contained 301 points. The modified data records were then increased to 512 points by adding zeros, because the Fast Fourier Transform algorithm requires a data record length which is an integral power of two (2^m).

VII.3 SELECTION OF DISCRETE FREQUENCIES

With the Fast Fourier Transform, amplitude and phase values are computed at frequencies:

$$f_k = \frac{k}{N \Delta t}, \quad k = 0, 1, \dots, N/2 \quad (\text{VII-1})$$

where N is the number of points in the data record (512) and Δt is the data time interval increment ($=.05$ seconds). However, the statistical error (or confidence band) in the resulting amplitude and phase estimates at these frequencies is as large as the estimates. In this case, the error is considered a chi-square variable with two degrees of freedom (d.f.). The statistical

error can be reduced by increasing d.f., which is accomplished by averaging j neighboring estimates, resulting in smoothed estimates with $2j$ d.f. However, since averaging reduces the frequency resolution of the estimates, a compromise value for j has to be selected. In analyzing the Manned Air Combat Simulation data, a value of $j=8$ was selected, resulting in 16 d.f. for 512 data points, or ≈ 9.41 d.f. for the data record of 301 data points. Then, ignoring the zero frequency increment, amplitude and phase estimates were printed out at the discrete frequency points

$$f_k = .176 + .312(k-1), k=1,2,\dots,32 \quad (\text{VII-2})$$

where a maximum value of $k=32$ is the number of frequency increments (bands) used, a consequence of selecting $j=8$.

VII.4 COMPUTATION OF CONFIDENCE BANDS AND COHERENCES

The confidence bands (r_k and $\Delta\phi_k$) on the gain (amplitude) and phase estimates at frequency f_k are computed by Program BMD04T, as described in Reference VII-1. The constant $C=1$ was selected in the equation for r_k on page 574 of this reference, which results in approximately "1 σ " ($\approx 68\%$) confidence bands for the gain and phase estimates. When the confidence band r_k is as large or larger than the gain estimate, $\Delta\phi_k$ is plotted as ± 200 degrees.

The multiple coherence function ($\gamma_{F_1}^2$) computed by Program BMD04T is the same as described in References VII-2 and VII-3. The function $(1 - \gamma_{F_1}^2) G_{F_1}$, where G_{F_1} is the spectrum of the output F_1 , gives the remnant spectrum for F_1 . This means that $\gamma_{F_1}^2$ gives the fraction of the output of F_1 's spectrum that can be linearly related to the inputs at the frequencies f_k given by Equation (VII-2) above. Since the elevation and traverse tracking errors are usually weakly correlated, $\gamma_{F_{LON}}^2$ is a good approximation to the degree of linearity between the elevation tracking error and the pilot's longitudinal force command, and $\gamma_{F_{LAT}}^2$ is a good approximation to the degree of linearity between the traverse tracking error and the pilot's lateral force command.

The confidence band r_k on the longitudinal gain estimate is proportional to the expression

$$r_k \propto \frac{(1 - \gamma_{F_{LON}}^2) G_{F_{LON}}}{(1 - \gamma_{\epsilon_{EL} \cdot \epsilon_{TR}}^2) G_{\epsilon_{EL}}} \quad (\text{VII-3})$$

where $G_{F_{LON}}$ and $G_{\epsilon_{EL}}$ are the spectrum at frequency f_k of longitudinal stick force

command (F_{LON} , the output) and elevation tracking error (ϵ_{EL} , the input), $\gamma_{F_{LON}}^2$ is multiple coherence for F_{LON} , and $\gamma_{\epsilon_{EL} \cdot \epsilon_{TR}}^2$ is multiple coherence between the elevation and traverse tracking errors. Similar expressions are computed for the lateral and directional gain estimates. Since the tracking error inputs are usually weakly correlated, $\gamma_{\epsilon_{EL} \cdot \epsilon_{TR}}^2$ will be around .25 or less most of the time. As a result r_k will vary in the following way: (1) r_k will become larger as $\gamma_{F_{LON}}^2$ decreases, which will be the most evident because $\gamma_{F_{LON}}^2$ is plotted below the longitudinal gain and phase estimates (and likewise for the lateral and directional gain and phase estimates); and (2) r_k will vary directly as the ratio of "output remnant over input spectrum" varies, since $(1 - \gamma_{F_{LON}}^2)G_{F_{LON}}$ is the output remnant.

APPENDIX VII REFERENCES

- VII-1. BMD (Biomedical Computer Programs), W. J. Dixon, Editor, Health Sciences Computing Facility, Department of Biomathematics, School of Medicine, Univ. of California at Los Angeles, Univ. of California Press, Jan 1, 1973
- VII-2. Otnes, R.K., and Enochson, L., "Digital Time Series Analysis", John Wiley and Sons, 1972.
- VII-3. Bendat, J.S. and Piersol, A.G., "Random Data: Analysis and Measurement Procedures", John Wiley & Sons, 1971.